AD NUMBER
AD378362
CLASSIFICATION CHANGES
TO: unclassified
FROM: confidential
LIMITATION CHANGES
TO: Approved for public release, distribution unlimited
FROM: Distribution: Further dissemination only as directed by Federal Aviation Administration, Office of Supersonic Transport Development, Washington, DC, 20553, Sep 1966, or higher DoD authority.
AUTHORITY
FAA ltr, 10 Oct 1972; FAA ltr, 10 Oct 1972

SECURITY MARKING

The classified or limited status of this report applies to each page, unless otherwise marked.
Separate page printouts MUST be marked accordingly.

NOTICES

When Government drawings, specifications, or other data are used for any purpose other than in connection with a definitely related Government procurement operation, the United States Government thereby incurs no responsibility nor any obligation whatsoever; and the fact that the Government may have formulated, furnished, or in any way supplied the said drawings, specifications, or other data, is not to be regarded by implication or otherwise as in any manner licensing the holder or any other person or corporation, or conveying any rights or permission to manufacture, use, or sell any patented invention that may in any way be related thereto.

All distribution of this document is controlled. In addition to security requirements which apply to this document and must be met, it may be further distributed by the holder only with specific prior approval of:

Director of Supersonic Transport Development
Federal Aviation Agency
Washington, D. C. 20553

The distribution of this report is limited because it contains technology identifiable with items excluded from export by the Department of State (U. S. Export Control Act of 1949, as amended).

PWA FP 66-100
SEPTEMBER 1966
C28-6C 2360. 9 B

(6) ~~UNCLASSIFIED TITLE~~

ENGINE PROPOSAL
FOR PHASE III OF THE
SUPERSONIC TRANSPORT DEVELOPMENT PROGRAM.

VOLUME III
TECHNICAL / ENGINE

REPORT A.

ENGINE PERFORMANCE (U).

(11) Sep 66

(12) 229p.

(14) PWA-FP-66-100-Vol-3A

(COMPETITIVE DATA)

(15) FA-SS-66-8

PREPARED FOR
FEDERAL AVIATION AGENCY
OFFICE OF SUPERSONIC TRANSPORT DEVELOPMENT
WASHINGTON, D. C.

Pratt & Whitney Aircraft DIVISION OF UNITED AIRCRAFT CORPORATION
FLORIDA RESEARCH AND DEVELOPMENT CENTER

CONTENTS

REPORT A
ENGINE PERFORMANCE INTRODUCTION

INTRODUCTION AND BACKGROUND

The Supersonic Transport engine is required to meet higher performance objectives than currently available engines can offer in order for the aircraft to be economically and operationally attractive. In addition, it must be designed to ensure long life and reliability and safety in operation. This report on Engine Performance defines the performance objectives of the JTF17 engine system and the aircraft requirements it is designed to meet. It presents descriptions of the engine and major components. Specific data are provided on the results of Phase II testing of the complete engine and the individual components. The actual weights of the engine and components are compared to estimated weights, and Pratt & Whitney Aircraft's system of weight control is explained.

Whether performance objectives are met will ultimately be proven in flight test and in airline operation of the Supersonic Transport. Pratt & Whitney Aircraft's record of meeting its performance objectives in other engine developments offers a clue to what may be expected in the JTF17 engine development program. Demonstrated specific fuel consumption is presented in figure 1 for comparison against the guarantees for various Pratt & Whitney Aircraft engines now in commercial service.

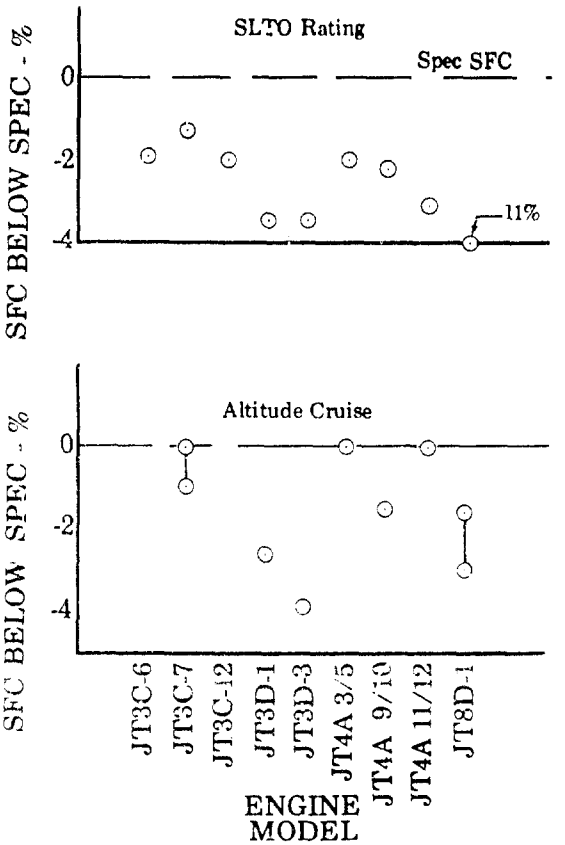

Figure 1. Comparison of Demonstrated Production Engine Performance to "When Ordered" Specification Rating

FD 17776
IIIA

A. PERFORMANCE OBJECTIVES AND REQUIREMENTS

1. JTF17 Performance Objectives

The JTF17 engine is designed to meet the high performance objectives defined in Engine Model Specifications 2698A and 2710 for the Lockheed and Boeing installations, respectively. The primary performance objectives are as follows:

a.	SLTO thrust	61,000 lb
b.	SLTO SFC	1.77 lb/hr/lb
c.	Cruise thrust	16,000 lb
d.	Cruise SFC	1.58 lb/hr/lb

(at Mach 2.7 and 65,000 ft altitude)

The engine has been designed to make efficient use of structure and materials and the weight objective is:

Basic Engine Weight 9860 lb (-21L); 9910 lb (-21B)

In addition, the engine has been designed to be reliable and safe, and ensure a long life in airline operation (50,000 hours). Other design objectives include superior growth potential, acceptable noise level (less than 116 PNdb at takeoff), versatility and maintainability to meet aircraft requirements, and, finally, minimum development risk.

2. Supersonic Transport Mission Requirements

To establish requirements, mission profiles (shown in figure 2) were generated based on JTF17 engine performance for typical aircraft L/D and gross weight, and appropriate ground overpressure criteria using mission requirements and average mission lengths (1455 statute miles for domestic flights and 1980 statute miles for international flights) defined by the economic ground rules contained in FAA Report SST 66-3. The international mission was selected for cruise life criteria, because a large percentage of the total flight time is at cruise. The domestic mission was selected for mission cycle criteria, because the shorter mission requires a greater number of cycles for a given airframe operating time. The criteria for hot-day and transient operation as a percentage of cruise hours were established by the airframe manufacturers and are defined by the engine model specifications. The selection of time percentages for reverse thrust, and the number of engine operating cycles from idle to SLTO power were based on expected service operating techniques and previous engine experience. The normal operating envelopes are shown in figures 3 and 4 and the reverse thrust envelopes in figures 5 and 6.

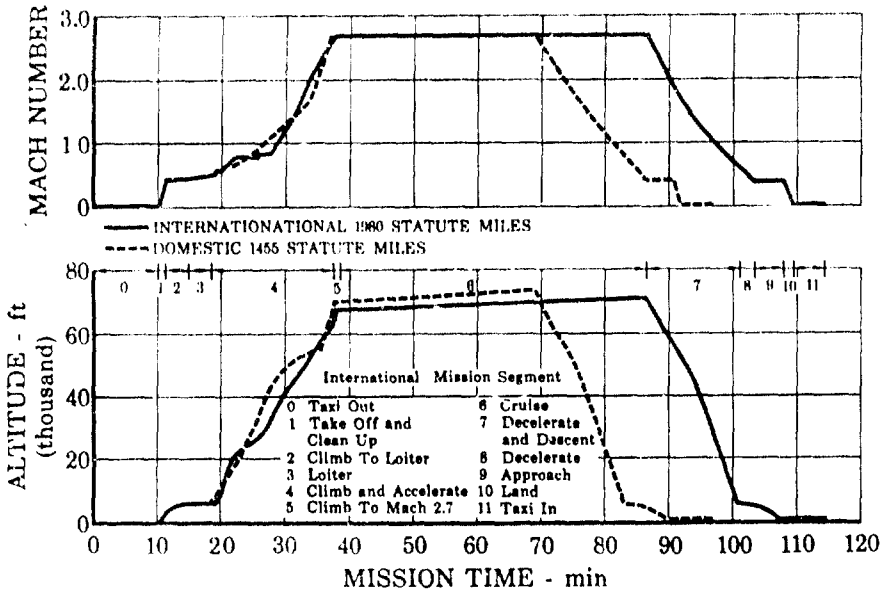

Figure 2. Average Mission Profiles

FD 16381
IIIA

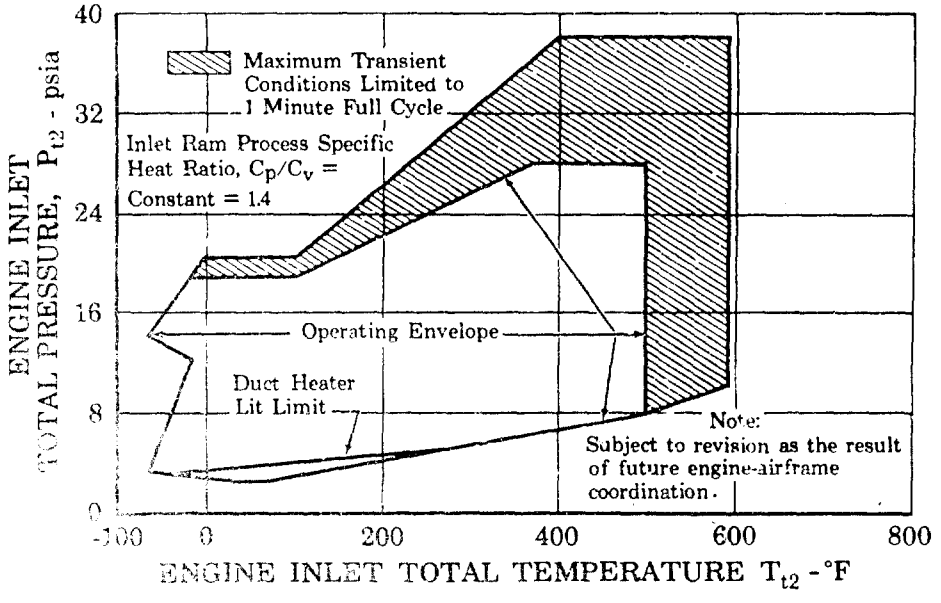

Figure 3. Engine Inlet Pressure vs Inlet Temperature

FD 16330
IIIA

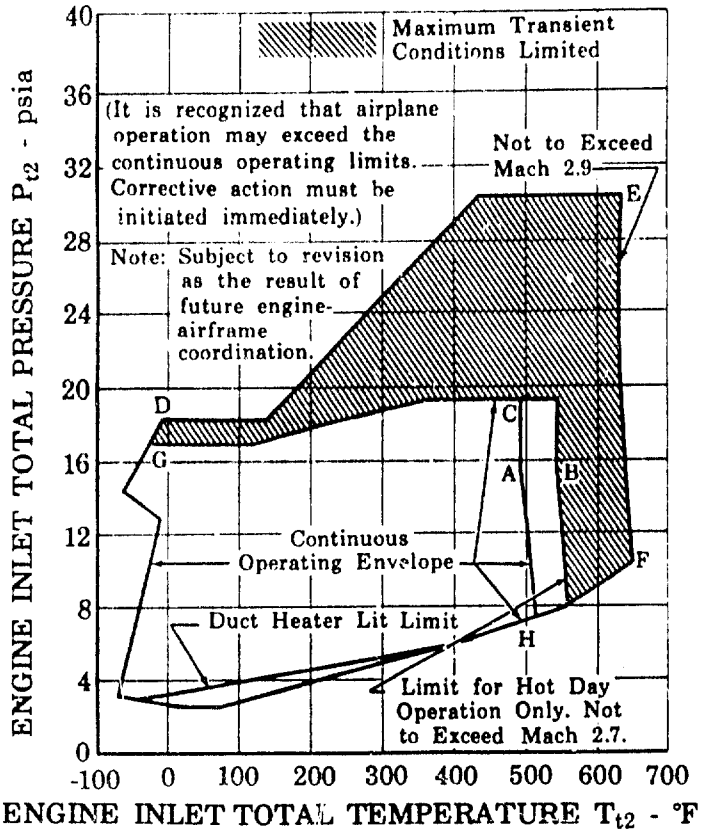

Figure 4. Engine Operating Envelope - Lockheed FD 17609 IIIA

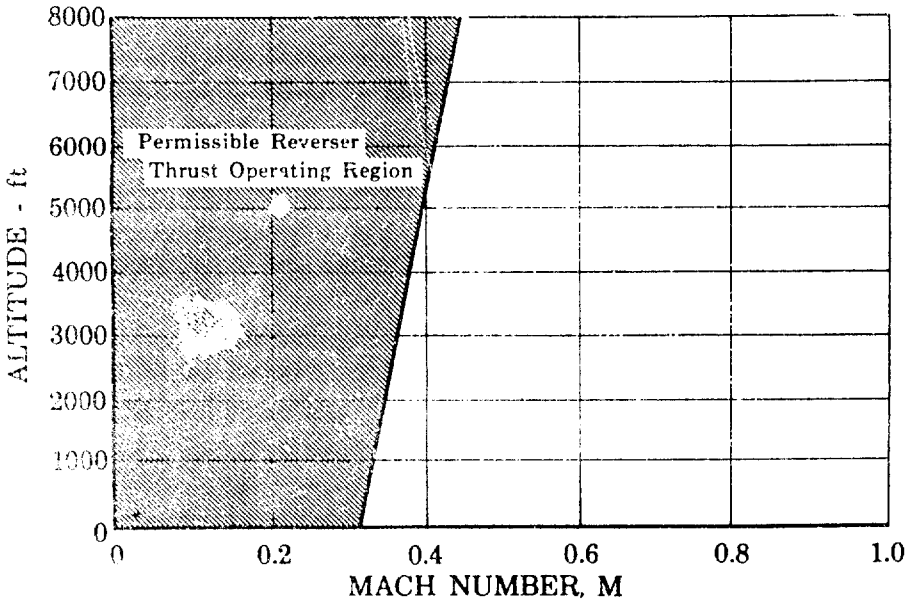

Figure 5. JTF17 Reverser Thrust Operation - Boeing FD 16332 IIIA

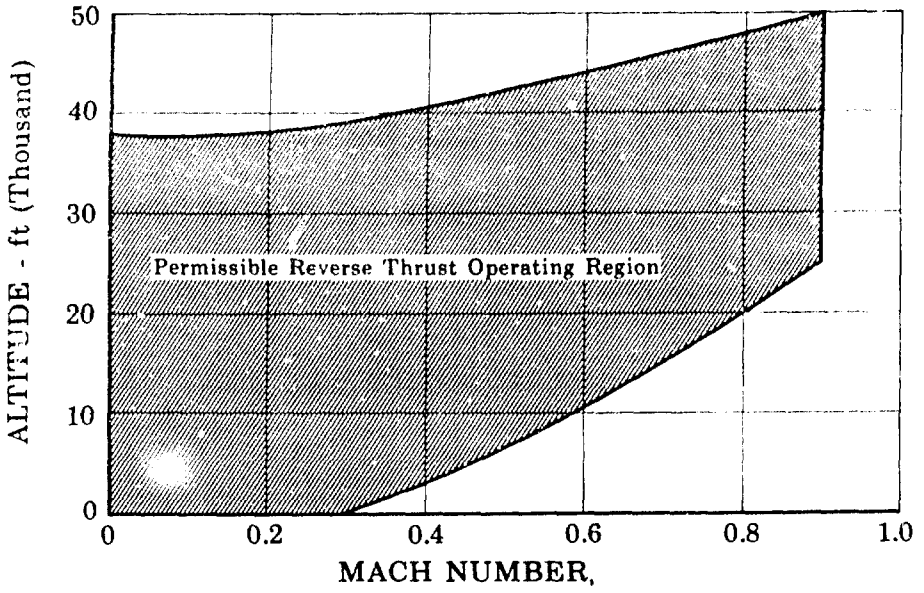

Figure 6. JTF17 Reverser Thrust Operation - Lockheed FD 16331 IIIA

B. PHASE II ACHIEVEMENTS

1. Cycle Selection

Early in Phase II, P&WA with the concurrence of both airframe manufacturers, selected the duct heating turbofan engine based on extensive cycle and mission analyses that showed the superiority of the turbofan engine in the areas of range/payload performance, safety, noise, inlet/engine compatibility, and growth potential. Detailed information is presented in Section I of this report on the results of the various analyses that were completed. For the supersonic transport basic mission at equal payloads the turbofan gives 170 statute miles greater range potential or, trading range for payload, 6300 pounds greater payload than the turbojet in the fixed wing aircraft. Similar advantages are shown in the swing-wing aircraft analysis.

2. Engine System Optimization and Testing

The engine system was optimized during Phase II to achieve maximum range/payload for a given gross takeoff weight with acceptable noise levels. Maximum turbine inlet and augmentor discharge temperatures were selected consistent with advanced design concepts to provide maximum efficiency and airflow. Pressure ratios and percent augmentation were established considering optimum mission performance and minimum weight in Phase II P&WA studies. Selection of a basic 650 lb/sec airflow size for the Phase II-C demonstrator engine was coordinated with the two airframe manufacturers. The 687 lb/sec airflow JTF17A-21 engine proposed for Phase III is substantially this same Phase II-C engine with a slight increase in fan blade length within the original engine envelope. The performance of the engine system proposed is completely described in the Engine Model Specifications. Digital computer cycle matching decks have

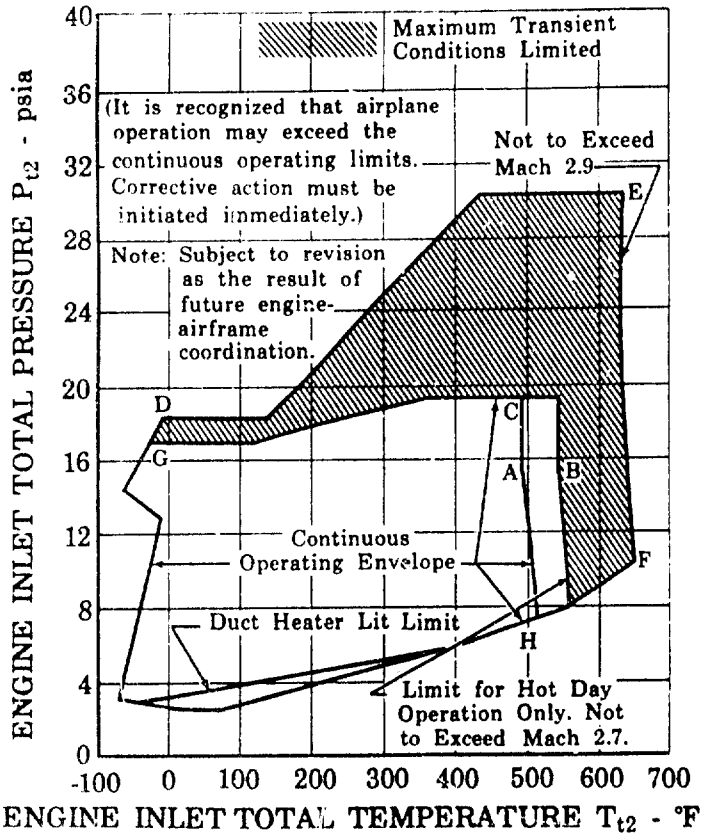

Figure 4. Engine Operating Envelope - Lockheed FD 17609 IIIA

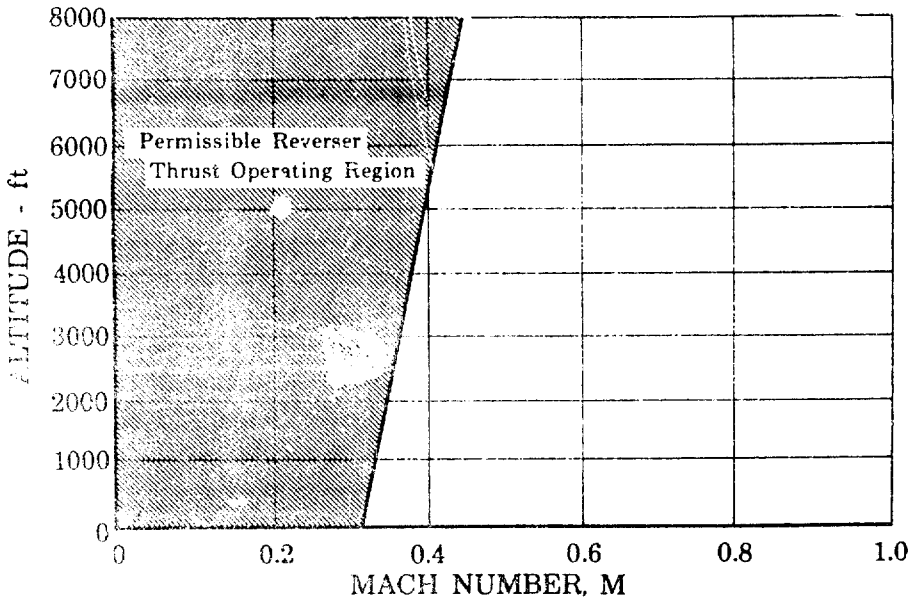

Figure 5. JT8D7 Reverser Thrust Operation - Boeing FD 16332 IIIA

life and resistance to foreign object damage than film cooling. Test data on both the high and low pressure turbine efficiencies have exceeded JTF17 design requirements.

d. Duct Heater

Duct heater performance is discussed in terms of pressure loss and combustion efficiency, including cooling data and ignition characteristics. Phase II-C tests have demonstrated the required SLTO performance of the full-scale annular duct heater. Cruise performance goals were approached. Excellent ignition characteristics were exhibited and the tests indicate that duct heater ignition should not affect fan and inlet stability. Condition of the duct heater parts was excellent after 45 hours of hot full-scale rig testing.

e. Exhaust System

Exhaust nozzle performance is presented along with the effects of geometry variation in blow-in-ejector doors, reverser-suppressor, and trailing edge flaps. Exhaust system models tested in Phase II-C exceeded subsonic and supersonic cruise performance goals for the prototype system and achieved the production engine goals. A model of the exhaust system in a simulated Lockheed wing installation has been tested in the wind tunnel. The performance data met design objectives.

4. Engine Weight

The weights of the engines specified in the Engine Model Specification and a breakdown of the component estimated weights are presented in Section IV of this report. That section also explains Pratt & Whitney Aircraft's system of weight prediction and control and an extensive weight reduction program, now underway, which will be extended through Phase III. The weights of the JTF17 production engines in the Engine Model Specifications are 9910 pounds and 9860 pounds for Boeing and Lockheed, respectively. Prototype weights are 3% higher. Actual weight of the first test engine was 50 pounds less than the estimated weight for that engine.

C. PLANS FOR PHASE III PERFORMANCE TESTING

Initial engine testing in Phase III will be conducted using the three JTF17 engines available from Phase II-C. These engines will be supplemented so that a total of 12 development JTF17 engines will be used for the Phase III test program. Altogether 8000 hours of engine testing are planned in Phase III. Included in this total are 845 hours of altitude performance testing and 625 hours of sea level performance testing.

Although all engine tests provide a certain amount of performance data, these tests will be specifically designed to determine basic engine and component performance and to evaluate the effect of engine changes on performance at simulated sea level environmental conditions with and without heated inlet air and at simulated subsonic, transonic, and supersonic flight conditions. The engine ground and flight test programs, as well as individual component test programs, planned for Phase III are presented in detail in Volume IV, Report E. A detail work plan for the design and development work to be performed in Phase III is presented in Volume V, Report H.

SECTION I
CYCLE SELECTION

A. SUMMARY

During Phase I, four cycles were compared for the supersonic transport. Two highly competitive cycles, the duct heating turbofan and the afterburning turbojet showed clear advantages over the other cycles, and comparisons of these two were continued into Phase II-C. Early in Phase II-C, P&WA, with the concurrence of both airframe manufacturers, selected the duct heating turbofan engine. This selection was based upon cycle and mission analyses conducted by P&WA and the airframe manufacturers, which showed the superiority of the turbofan engine in the areas of range/payload performance, safety, noise, inlet/engine compatibility, and growth potential.

For the design mission, assuming a 687 lb/sec turbofan and a 600 lb/sec turbojet of comparable technology, the turbofan gives 170 statute miles greater range or 6300 pounds greater payload for the fixed-wing aircraft and 160 more miles range or 6100 pounds greater payload for the swing-wing aircraft. Trip fuel consumption at representative international and domestic route ranges is 1 to 8% lower for the turbofan, which directly affects supersonic transport operating cost. For subsonic missions, trip fuel consumption is 22% lower for the turbofan than for the turbojet.

If emergency conditions require the aircraft to fly at subsonic speed after the midpoint of a 4000-statute-mile mission, the turbofan powered aircraft can complete the mission using only part of the fuel reserves established by the FAA economic model, with either three or four engine operation. The turbojet powered aircraft requires fuel reserves as much as 6600 pounds in excess of those set forth by the FAA economic model.

The turbofan cycle also provides lower temperature air for cooling the augmentor, 660°F compared to more than 1700°F for the turbojet. This results in (1) greater durability of the augmentor parts and (2) elimination of the spontaneous-ignition fire hazard that exists around the outside of the much hotter turbojet engine.

Noise studies also indicate that the turbofan-powered supersonic transport is superior to the turbojet-powered aircraft. The turbofan cycle permits transport compliance with the FAA-balanced field length requirement and airport and community noise objectives. With the turbojet cycle, compliance with these objectives would appear to be beyond the present knowledge of sound suppression.

The characteristics of the two-spool duct heating turbofan permit matching of engine and inlet airflow over a wide range of nonstandard conditions as well as during off-design operation of the inlet. The bypass ratio may be manually adjusted by the flight crew during cruise flight by varying the duct nozzle area to match inlet flow precisely with little or no speed change to either rotor. The turbojet can increase airflow only by increasing rotor speed, with an associated weight increase.

B. ENGINE REQUIREMENTS

The success of the supersonic transport requires that the propulsion cycle selection be based on considerations of range/payload performance, safety, noise, inlet/engine compatibility and growth.

1. Range/Payload Performance

Economic operation requires a powerplant that results in minimum operating costs when integrated with the airframe. Thus, minimum fuel consumption of the propulsion system is a prime prerequisite, not only for the design maximum range, but also for the shorter distance missions that will inevitably be flown.

Range and payload considerations impose stringent requirements on the powerplant. In selecting the cycle, the following factors must be considered:

1. Basic mission performance, including sonic boom constraints
2. Effect of nonstandard day ambient temperature
3. Effect of mission stage length
4. Variations from optimum in cruise altitude.

2. Safety Requirements

The primary safety factor to be considered in selecting a cycle for the SST engine is the ability to complete the mission under emergency or adverse conditions such as an in-flight engine shutdown, loss of cabin pressurization, extended loiter, and diversion to an alternative destination. A secondary safety consideration is the temperature of the outside of the engine. A hot engine exterior increases the probability of fire in the nacelle if a fuel leak occurs.

3. Engine Noise Objectives

Aircraft community and airport noise has become a major operational problem of jet transport operation. Public reaction to this noise has imposed serious limitations on aircraft operation even to the extent of curtailing certain operations or of requiring special noise abatement flight procedures. Unfortunately, these special antinoise requirements are not always compatible with economical aircraft operation, or tend to infringe upon safety procedures by altering climb-out and descent paths.

To avoid the above problems, the FAA has established the following airport and community noise criteria for the supersonic transport. These must be considered as minimum objectives, and great emphasis is to be placed on bettering them.

1. Airport (2500 ft sideline) 116 PNdb
2. Community (3 mile point) 105 PNdb
3. Approach (1 mile) 109 PNdb
4. Noise levels should progressively decrease as flight proceeds beyond the point of 2 above.

These noise objectives, coupled with the FAR takeoff runway length requirement, impose strict limitations on aircraft takeoff and subsequent climb. Thus, any noise advantage that may be realized through cycle selection must be considered and weighed heavily.

4. Inlet/Engine Compatibility

To meet the design objectives of the SST, it is mandatory that the inlet be operated in a highly efficient and stable manner. Of primary concern are ram pressure recovery, airflow distortion, flow stability, and minimum drag. To satisfy these requirements, the engine and inlet must be operated in a complementary fashion and with precise airflow matching at both design and off-design conditions. Because of the penalties associated with relatively small airflow mismatching, a method for rematching the inlet/engine in flight to achieve best performance is highly desirable. For instance, an airflow mismatch causing a loss of ram recovery of 1% will result in a range loss of approximately 23 statute miles.

Reasonable levels of inlet flow distortion should be accepted by the engine without loss of performance. Significantly higher distortion levels, as may be expected during acceleration or maneuvering flight, must be accepted by the engine without compressor stall or burner flameout.

5. Engine Growth Requirements

Engine growth is required in those categories that will result in supersonic transport economic growth. Because transport economic growth is realized primarily through increased takeoff gross weight and cruise Mach number, engine performance growth capabilities are required in sea level takeoff thrust, transonic thrust, cruise specific fuel consumption, and higher Mach numbers. These growth items should be attainable with minimum change in design, weight, cost, and without loss of engine safety and reliability.

C. BASIS FOR COMPARISON

1. Cycles Studied

Cycle studies were conducted initially with the evaluation of four cycles:

STF223	Afterburning Turbofan
STF219	Duct Heating Turbofan
STJ221, 226, 228	Nonaugmented Turbojets
STJ222, 225, 227	Afterburning Turbojets

The afterburning turbofan and the nonaugemented turbojet cycles were eliminated from the competition during the initial evaluation by the airframe companies, and detailed performance data for the two remaining powerplants were then supplied to the airframe contractors. Subsequent studies resulted in the selection, by both airframe contractors, of the STF219 duct heating turbofan engine (forerunner to the JTF17 engine) from among the two cycles submitted by Pratt & Whitney Aircraft. Details of the comparative performance of the two cycles are presented in the following sections.

CONFIDENTIAL

Phase II-A reports referencing these studies may be found in Final Contract Report, PWA 2397; Items 1, 2, 3, and 16.

2. Engine Performance

During Phase II-C, comparisons of the two engine cycles that originally appeared most promising, the duct heated turbofan and the augmented turbojet, were continued.

With two exceptions, the performance levels and weights of the JTF17A-21 turbofan and STJ227 turbojet represent the same level of technology and the same turbine and augmentor temperatures. To provide a comparison of the two cycles which is intentionally conservative relative to turbofan performance, the augmentor efficiency of the turbojet was arbitrarily increased 5% over data from existing hardware whereas the turbofan augmentor efficiency represents current hardware. Similarly the weight of the turbojet was arbitrarily reduced 1000 lbs. below the value considered to be consistent with the turbofan weight.

The JTF17A-21 and STJ227 are sized to 687 lb/sec and 600 lb/sec sea level static airflow, respectively, for mission performance comparison with both the fixed-wing and swing-wing airplanes. Comparative performance is shown in table 1.

Table 1. General Performance Comparison

Sea Level Takeoff*	JTF17A-21	STJ227
Weight, Including Nozzle, lb	9860(-21L) 9910(-21B)	9900
Overall Pressure Ratio	12.96	9.26
Bypass Ratio	1.31	--
Fan Pressure Ratio	2.84	--
Corrected Airflow, lb/sec	687	600
Maximum Augmented Thrust, lb	61,000	68,000
Maximum Augmented TSFC, lb/hr/lb	1.77	1.80
Mach 1.2, 40,000 Feet*		
Maximum Augmented Thrust, lb	25,350	29,600
Maximum Augmented TSFC, lb/hr/lb	1.85	1.90
Mach 2.7, 65,000 Feet**		
Corrected Airflow, lb/sec	417	414
Typical Cruise Thrust, lb	16,000	16,000
Typical Cruise TSFC, lb/hr/lb	1.56	1.50

*Ram Recovery per MIL-E-5008B
Corrected Ejector Secondary Airflow = 0.02

**Ram Recovery = 0.892
Corrected Ejector Secondary Airflow = 0.02

CONFIDENTIAL

Typical subsonic fuel consumptions of the two engine cycles are shown in figure 1. The specific fuel consumption of the turbojet cycle is 16% higher than that of the turbofan cycle in the normal thrust range during subsonic operation. The normal mission requires subsonic operation (departure air maneuver, destination air maneuver, hold, cruise to alternative destination, etc.) to the extent that the superior subsonic performance of the turbofan has a strong influence on the total fuel consumption.

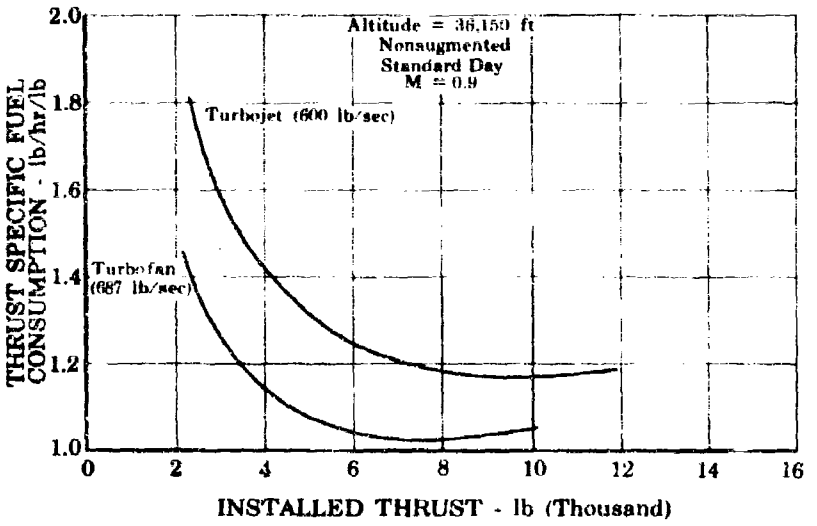

Figure 1. Installed Performance at M = 0.9 FD 16724
AI

Typical supersonic cruise characteristics of the two engine cycles are shown in figure 2. The specific fuel consumption of the turbojet cycle is about 4% lower than that of the turbofan. However, the much lower TSFC of the turbofan during subsonic operation more than offsets its slightly higher TSFC at cruise.

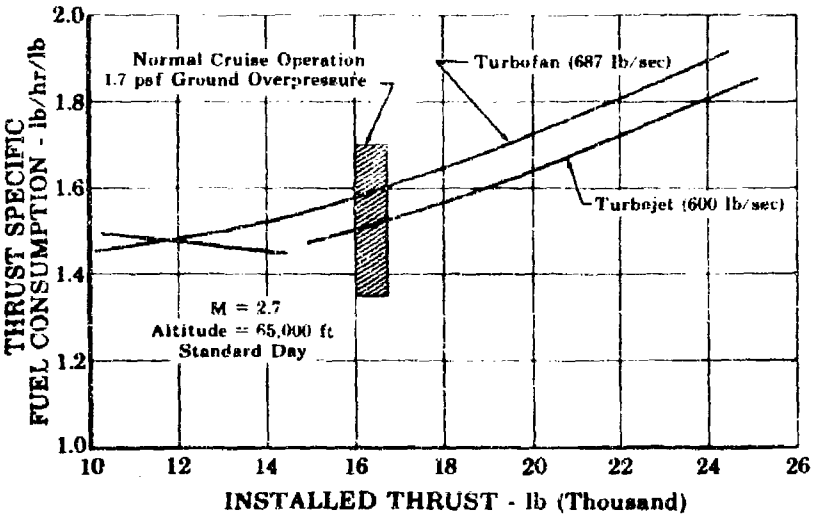

Figure 2. Installed Performance at M = 2.7 FD 16727
AI

3. Airplane Performance

The airplane aerodynamic performance used in these studies is representative of a 550,000-pound maximum takeoff gross weight fixed-wing supersonic transport and a 600,000-pound maximum takeoff gross weight swing-wing supersonic transport. The performance was generated from information obtained from the Lockheed California Company and The Boeing Company. The flight profiles and inlet performance levels are those defined by the airframe manufacturer.

D. CYCLE COMPARISON

1. Range/Payload Performance

a. Fixed-Wing Aircraft

For the supersonic transport design mission, at equal payloads, the turbofan has 170 statute miles greater range potential, or since range can be traded for payload, 6300 pounds greater payload than the turbojet in the fixed-wing airplane. The turbofan also burns less trip fuel than the turbojet at equal range and payload.

Figure 3 illustrates the variation in trip fuel consumption with range for the two engine cycles and shows the trip fuel advantage of the turbofan for all mission stage lengths. Figure 4 presents the ratio of the total fuel load (including reserves) of the turbojet to that of the turbofan as a function of range. This curve shows that the fuel load of the turbojet becomes increasingly larger than that of the turbofan as the range is reduced. Correspondingly, for a fixed takeoff gross weight, the payload potential of the turbofan is greater than that of the turbojet at the maximum range and becomes increasingly larger as shorter range missions are considered. The curves of figure 4 are terminated approximately at the maximum turbojet range with the indicated payload.

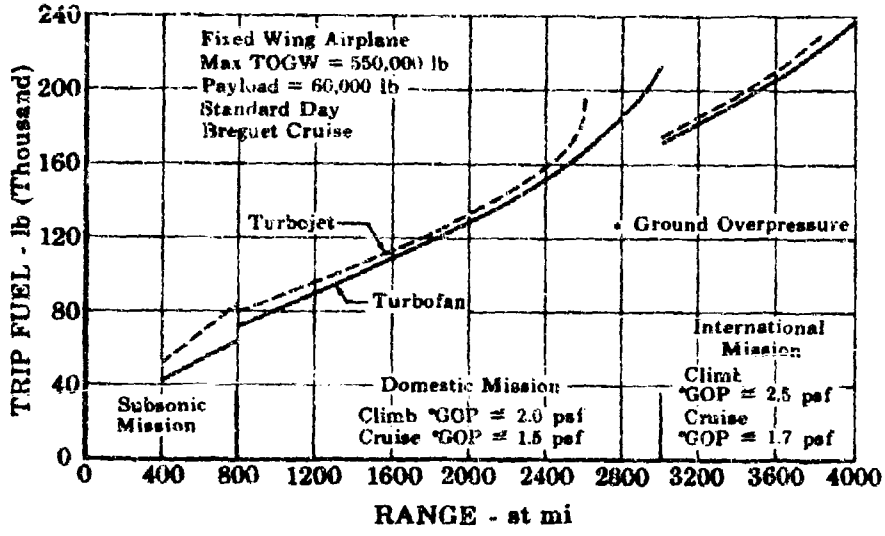

Figure 3. Range - Fuel Consumption

FD 16723
AI

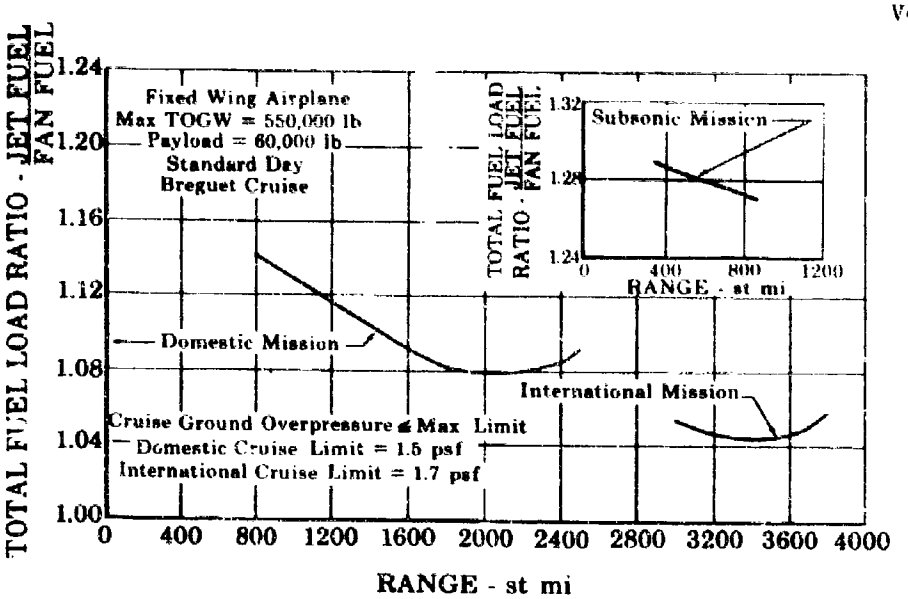

Figure 4. Turbojet - Turbofan Total Fuel Load Ratio

FD 16744
AI

The trip fuel consumption advantage of the turbofan over the turbojet is summarized in figure 5 as a function of stage length. For the fixed-wing airplane studied, the turbojet reaches its maximum range of 2500 statute miles for domestic ground overpressure limits and 3830 statute miles for international ground overpressure limits carrying the indicated payload. To extend the range beyond these values the turbojet-powered airplane must offload payload as indicated in figure 6.

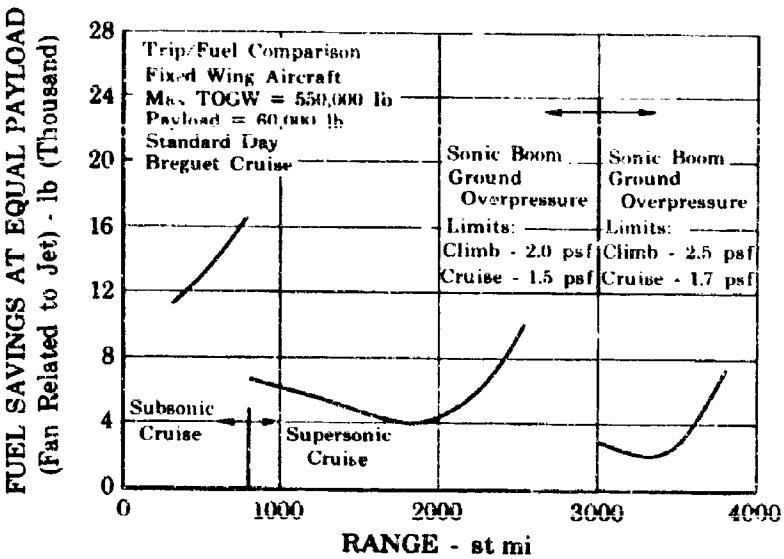

Figure 5. Trip/Fuel Comparison

FD 16728
AI

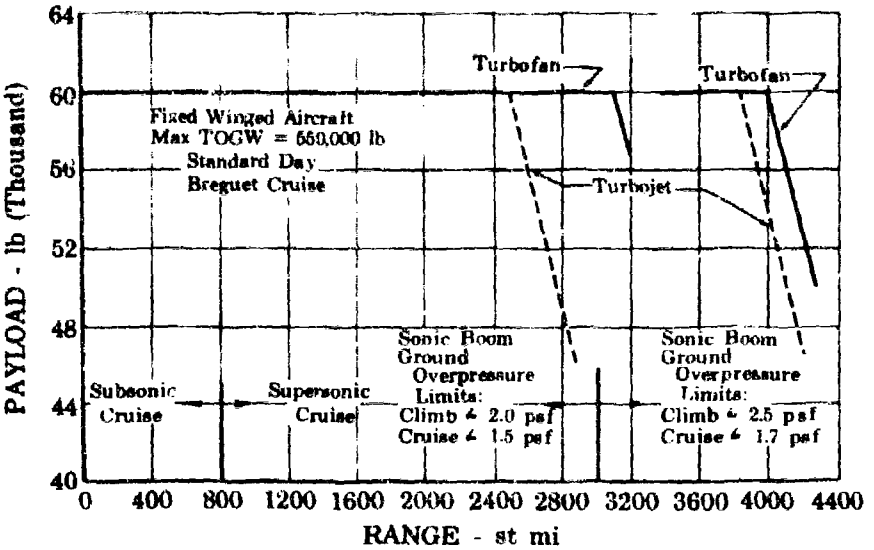

Figure 6. Range/Payload Comparison FD 17747 AI

b. Swing-Wing Aircraft

The comparison of performance between the turbofan and turbojet cycles for the swing-wing aircraft results in similar conclusions as were derived from the study of the fixed-wing aircraft. On the design mission the turbofan has an advantage of 160 statute miles in range or 6100 lb of payload. Figure 7 shows the variation in trip fuel consumption with range and figure 8 compares total fuel load. Figures 9 and 10 summarize the advantage of the turbofan with plots of trip fuel savings and payload differential relative to stage length. The curve shows that the turbofan-powered airplane studied can carry 18 more passengers than the turbojet from Washington, D. C. to Paris based on a tradeoff factor of 200 lb per passenger.

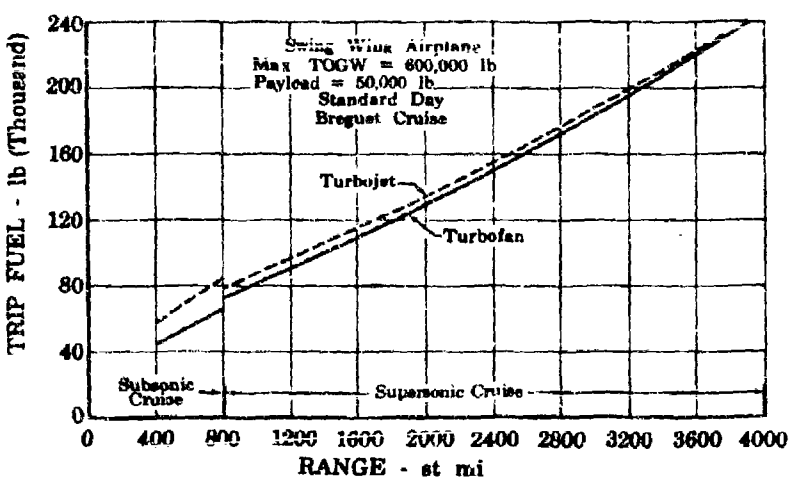

Figure 7. Range - Fuel Consumption FD 16741 AI

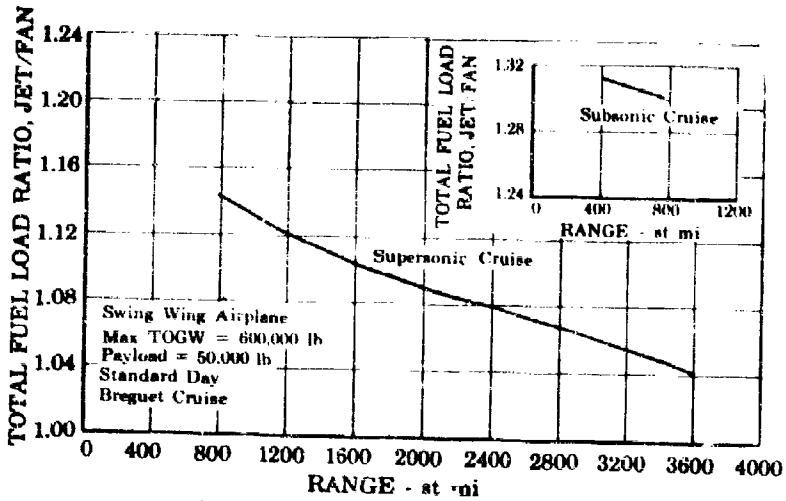

Figure 8. Turbojet - Turbofan Total Fuel Load Ratio

FD 16722
AI

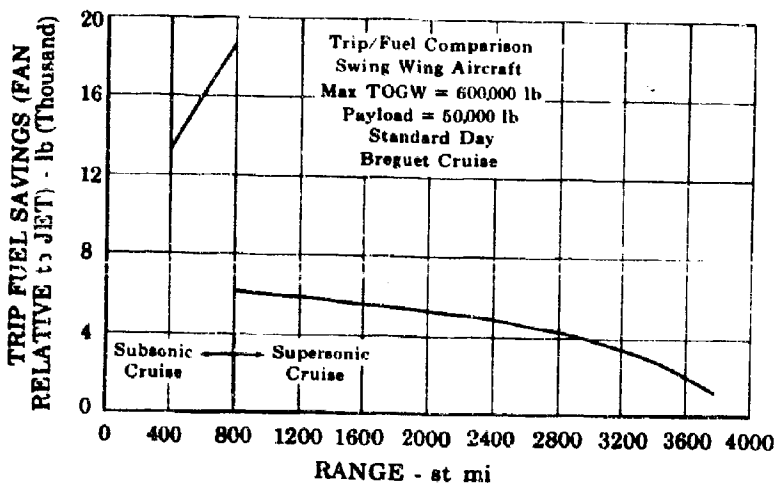

Figure 9. Trip/Fuel Comparison

X-15729
AI

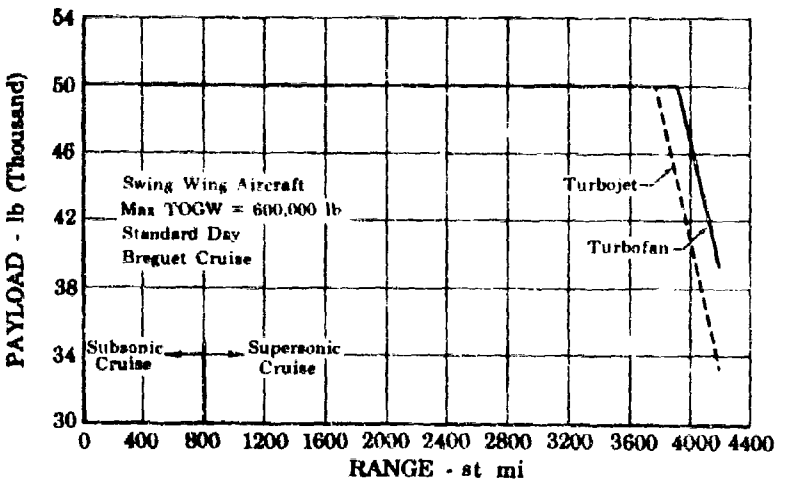

Figure 10. Range/Payload Comparison

FD 17749
AI

2. Safety

From a propulsion standpoint, the powerplant that provides the greater range during abnormal emergency operating conditions provides greater safety. Table 2 lists the resulting maximum ranges for emergency conditions existing from the midpoint (2000 statute miles) of the design range for the fixed-wing airplane, and indicates the percentage of reserve fuel that would be required to complete the mission. In all cases the turbofan engine is superior to the turbojet engine. When forced to fly at subsonic speeds with three engines, the turbojet is unable to complete 25% of the international flight stage lengths without using reserve fuel and must have an additional 6600 pounds of fuel, (off-loaded payload), to complete the 4000 statute mile flight. In comparison the turbofan-powered aircraft can complete 80% of the international flights without using fuel reserves and is able to complete the 4000-statute mile mission with the normal flight payload.

Maximum ranges for the swing-wing airplane, for emergency conditions existing from the midpoint of the design range, are listed in table 3. The turbofan cycle is superior to the turbojet cycle in all cases. When forced to fly at subsonic speeds on three engines the turbojet requires all of the fuel reserves to complete the design range mission as compared to 61% for the turbofan-powered aircraft. If forced to fly subsonically on four engines, the turbojet must burn 98% of the available fuel reserves. In this instance, the turbofan-powered airplane, using 54% of its fuel reserves, can complete the 4000-statute mile mission with 6100 pounds more payload.

Table 2. Emergency at 2000 Miles of a 4000-Mile Trip

Fixed-Wing Aircraft

Turbofan Payload = 60,000 lb
Turbojet Payload = 53,700 lb

	Fan	Jet
A. Continue Supersonic - Three (3) Engines		
Additional range without use of fuel reserves, statute miles	1,715	1,660
Total range without use of fuel reserves, statute miles	3,715	3,660
Fuel reserves required to complete trip, lb	12,500	15,400
Percent of fuel reserves used to complete trip	32	33
B. Continue Subsonic - Three (3) Engines		
Additional range without use of fuel reserves, statute miles	1,295	1,130
Total range without use of fuel reserves, statute miles	3,295	3,130
Fuel reserves required to complete trip, lb	37,300	Insufficient
Percent of fuel reserves used to complete trip	95	114
Payload reduction to provide sufficient fuel reserves, lb	0	6,600
C. Continue Subsonic - Four (4) Engines		
Additional range without use of fuel reserves, statute miles	1,405	1,175
Total range without use of fuel reserves, statute miles	3,405	3,175
Fuel reserves required to complete trip, lb	29,000	Insufficient
Percent of fuel reserves used to complete trip	74	105
Payload reduction to provide sufficient fuel reserves, lb	0	2,100

Table 3. Emergency at 2000 Miles of a 4000-Mile Trip

Swing-Wing Aircraft

Turbofan Payload = 46,850 lb
Turbojet Payload = 40,750 lb

	Fan	Jet
A. Continue Supersonic - Three (3) Engines		
Additional range without use of reserves, statute miles	1,675	1,670
Total range without use of reserves, statute miles	3,675	3,670
Fuel reserves required to complete trip, lb	15,350	15,350
Percent of fuel reserves to complete trip	42	35
B. Continue Subsonic - Three (3) Engines		
Additional range without use of reserves, statute miles	1,525	1,245
Total range without use of reserves, statute miles	3,525	3,245
Fuel reserves required to complete trip, lb	22,400	44,650
Percent of fuel reserves to complete trip	61	100
C. Continue Subsonic - Four (4) Engines		
Additional range without use of reserves, statute miles	1,565	1,250
Total range without use of reserves, statute miles	3,565	3,250
Fuel reserves required to complete trip, lb	14,750	44,050
Percent of fuel reserves to complete trip	54	98

An additional safety consideration is the temperature of the exterior of the engine. In the event of fuel leakage outside the engine, a hot engine exterior considerably increases the probability of fire. The turbofan engine has the advantage of lower temperature augmentor cooling air, approximately 660°F compared to more than 1700°F for the turbojet and thus has lower external metal temperatures. In addition to increased safety, the lower cooling air temperatures inherent in the turbofan cycle contribute significantly to longer engine component life. A detailed study of this safety feature is contained in PWA report PWA FR-1855.

In summary, the turbofan cycle is safer than the turbojet cycle both from the ability to complete the mission under adverse conditions and from spontaneous fire considerations.

3. Noise Considerations

A comparison of airport and community noise levels, and balanced field length, for swing-wing and fixed-wing aircraft, indicates substantially lower noise levels for the turbofan relative to the turbojet. The turbojet-powered aircraft cannot simultaneously meet balanced field length requirements and airport or community noise level objectives.

At airport approach both the turbofan- and turbojet-powered aircraft meet FAA noise objectives at low thrust level. At high approach thrust levels, both engine cycles exceed the FAA objectives but are substantially quieter than current jets. The turbofan, however, offers significantly greater potential for approach noise reductions due to the versatility of the cycle and the characteristics of the generated noise.

Figures 11 and 12 illustrate the variation in balanced field length and community noise with airport noise for the fixed-wing aircraft. The turbofan-powered aircraft meets the balanced field length requirement with airport noise levels as much as 1.8 PNdb below the airport noise limit. In comparison, the turbojet-powered aircraft, at takeoff power settings which allow compliance with the field length requirements, exceeds the airport noise limit by a minimum of 1.2 PNdb. A comparison of community noise levels indicates that neither the turbofan- nor turbojet-powered aircraft satisfies the 105 PNdb objective. However, the turbojet-powered aircraft community noise level is a minimum of 10 PNdb higher than the 105 PNdb objective. The turbofan-powered aircraft community noise level exceeds the objective by only 2.5 PNdb

For the swing-wing aircraft, a comparison of the turbofan and turbojet cycles indicates that, at balanced field lengths below the maximum requirement (figure 13) the turbofan-powered aircraft airport noise level is as much as 3.3 PNdb below the 116 PNdb objective, and the turbojet complies with the airport noise limit only at the maximum balanced field length. Community noise level (figure 14) of the turbofan-powered aircraft is as much as 4.4 PNdb below the objective, compared to the turbojet community noise level of at least 1.5 PNdb above the objective.

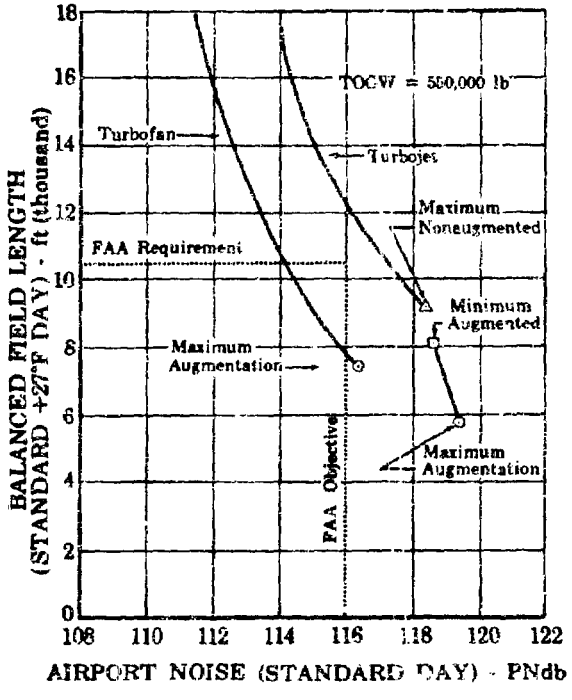

Figure 11. Airport Noise vs Balanced Field Length - Fixed-Wing Aircraft FD 16864 AI

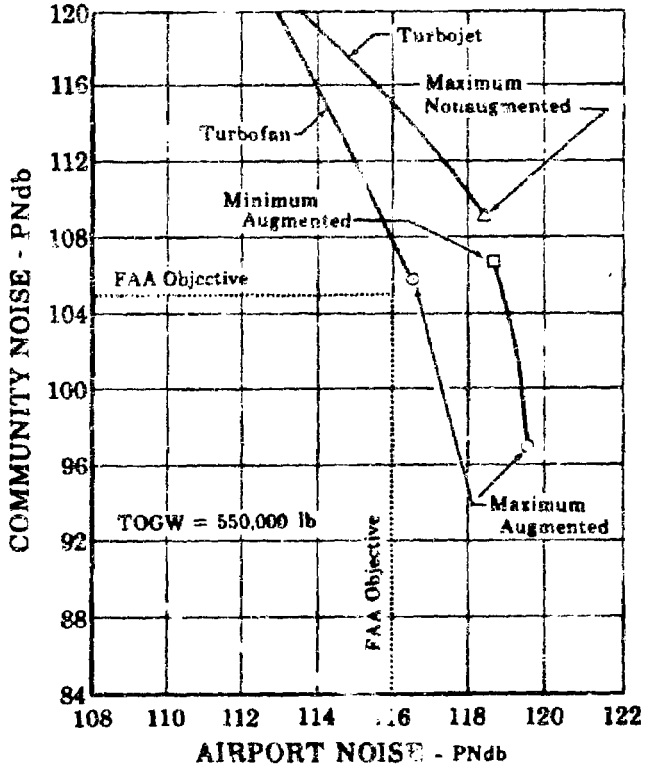

Figure 12. Airport Noise vs Community Noise - Fixed-Wing Aircraft FD 16865 AI

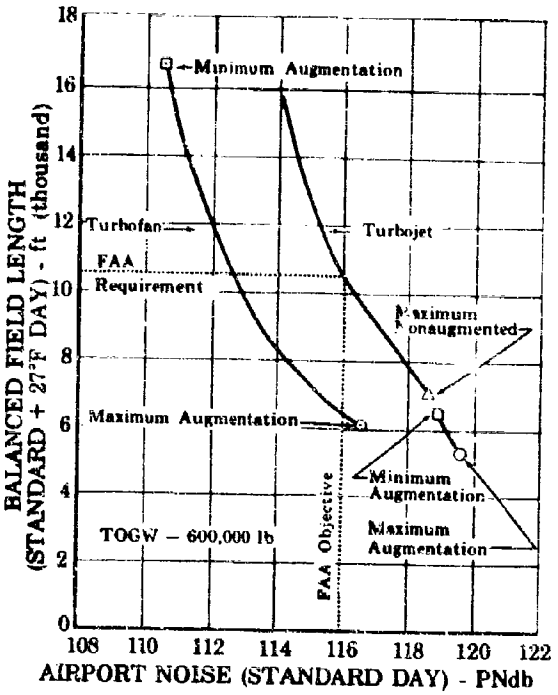

Figure 13. Airport Noise vs Balanced Field Length - Swing-Wing Aircraft

FD 16867
AI

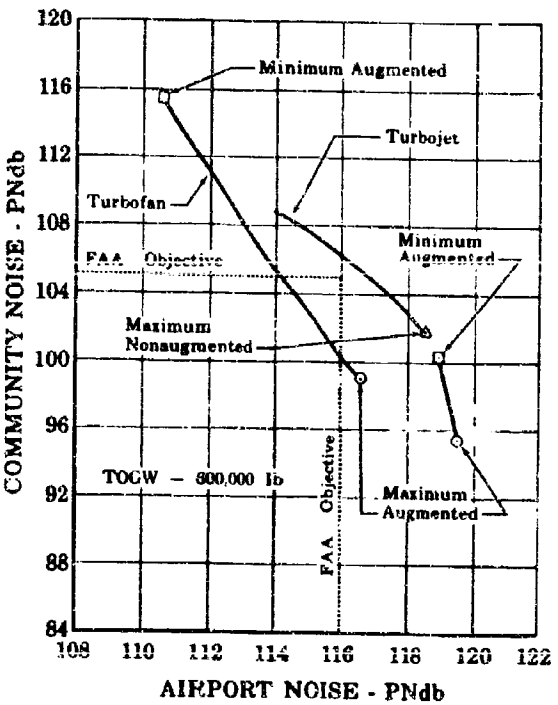

Figure 14. Airport Noise vs Community Noise - Swing-Wing Aircraft

FD 16866
AI

In the above comparison, equal noise attenuation was assumed for the fan and jet cycles, as follows:

	Fixed-Wing Aircraft	Swing-Wing Aircraft
Exhaust Noise Attenuation - Turbofan or Turbojet		
Maximum Augmented, PNdb	4	4
Minimum Augmented and Below, PNdb	3	3
Fan Noise Attenuation - Turbofan		
Approach, db/octave band	15	15
Community, db/octave band	6	3

A comparison of turbofan and turbojet noise on approach is shown in figure 15.

At low levels of approach thrust, the noise levels of both cycles do not exceed the 109 PNdb objective, although the turbojet shows an advantage over the turbofan (figure 15). As approach thrust level is increased, the perceived noise levels of the two cycles converge and show approximately equal noise.

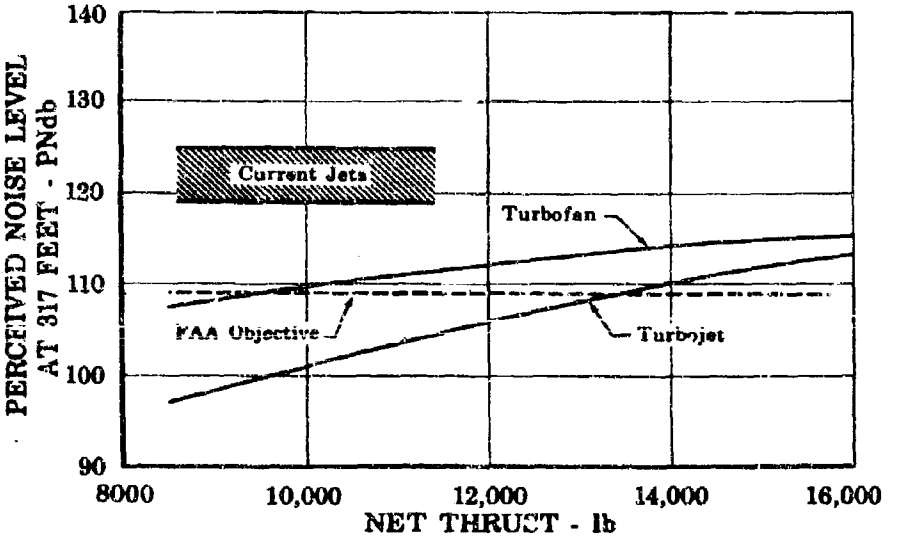

Figure 15. Perceived Noise, M = 0.21, Standard Day, at Airport Approach

FD 16925 AI

Because of cycle differences, the turbofan engine enjoys significantly greater potential for further noise attenuation than does the turbojet. The turbofan noise is a composite of exhaust noise, made up of two exhaust streams, and fan-generated noise. The turbojet noise is pure exhaust jet noise produced by a single stream. As a result, it is believed that future progress heavily favors the turbofan. Experimental evidence (Volume III, Report C) has indicated that the potential for fan noise

attenuation without performance compromise is great and it may be reasonably expected that future research and development in this area will lead to further attenuation of turbofan engine noise. Major gains in exhaust noise appear to be more difficult to realize, particularly without loss to performance, which in many cases can negate the gains made by attenuation. However, any exhaust gains made are equally applicable to both turbofan and turbojet cycles.

The turbofan enjoys a further advantage due to its cycle and the division of thrust between two streams. It is possible by proper cycle adjustment and operation to match the duct and jet exhaust streams such as to minimize noise at any given power level. These effects are not included in the above comparison since the corresponding engine requirements are not included in the current design. Gains of 1 to 2 PNdb may be realized by these techniques.

4. Range/Payload - Nonstandard Days

Figure 16 illustrates the effect of ambient temperature on thrust and thrust specific fuel consumption at the transonic flight condition, and indicates that neither cycle enjoys a significant advantage.

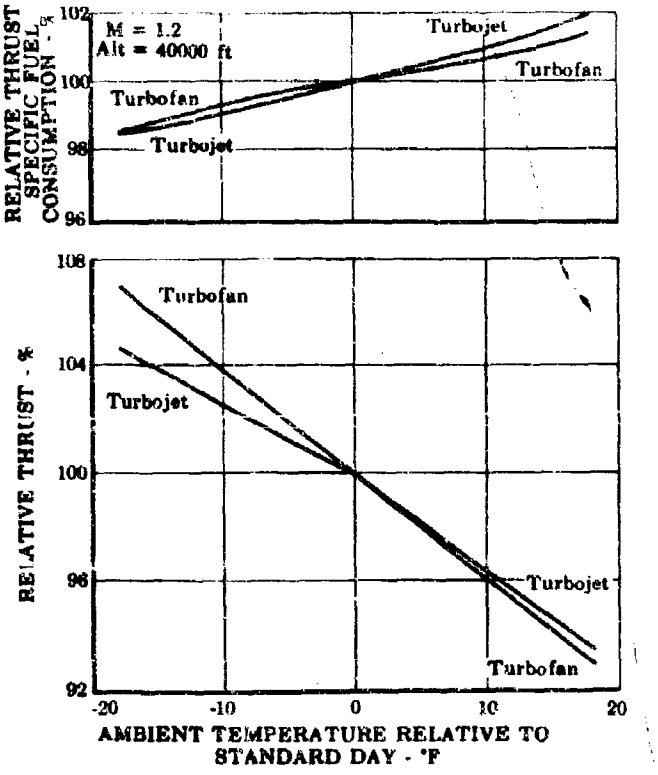

Figure 16. Ambient Temperature Effect on Engine Performance

FD 16742
AI

Figure 17 shows the effect of cruise ambient temperature on turbofan and turbojet payloads for the 4000-statute mile mission for the fixed-wing airplane. Because of the ability of the turbofan engine to match inlet airflow without changing rotor speed, the mass airflow change of the turbofan engine is considerably less than that of a turbojet engine on hotter than standard days. For this reason the increase in augmentation level required on a hot day is less for the turbofan than for the turbojet. Relative to the turbofan, the turbojet loses 3300 lb more payload on a + 18°F day.

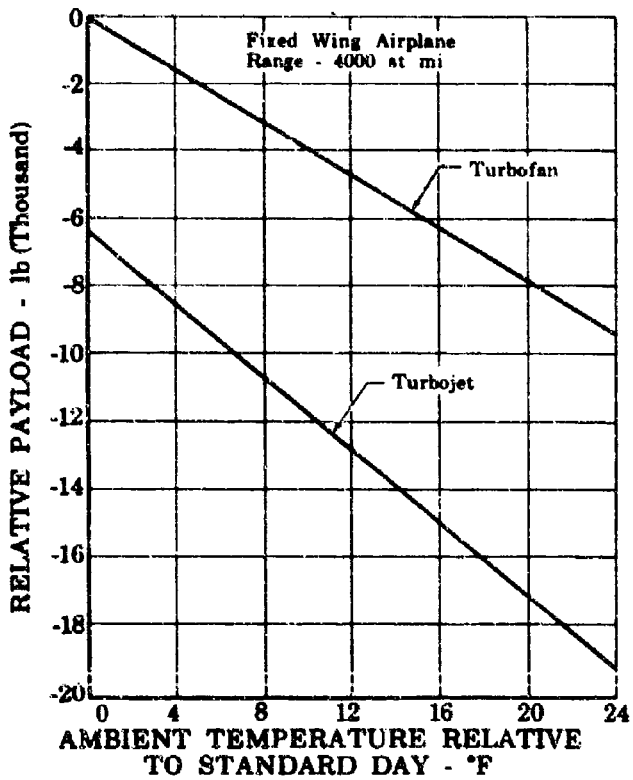

Figure 17. Cruise Ambient Temperature Effect on Payload - Fixed-Wing Aircraft FD 16731 AI

Figure 18 illustrates the effect of cruise ambient temperature on payload for the swing-wing airplane. The resultant loss in payload of the turbojet-powered airplane relative to the turbofan-powered airplane is 3900 lb on a + 18°F day.

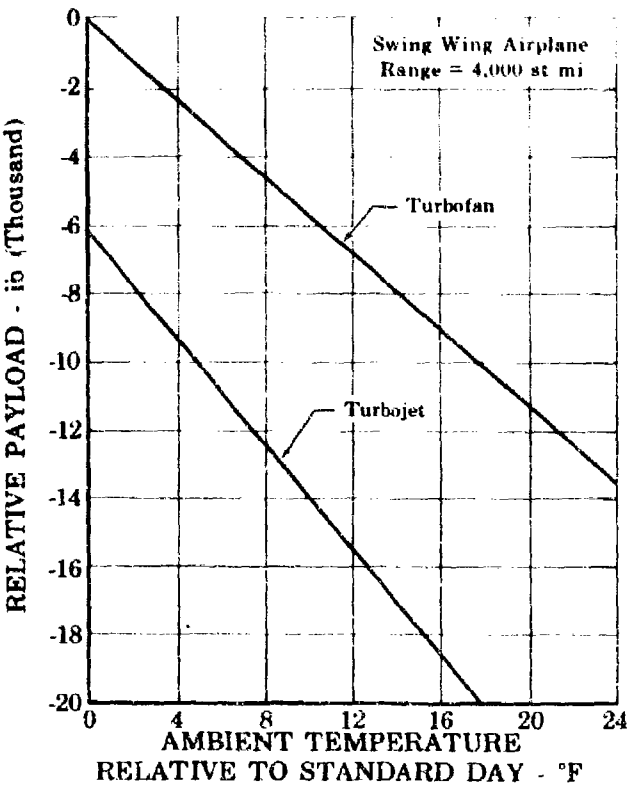

Figure 18. Cruise Ambient Temperature Effect on Payload - Swing-Wing Aircraft

FD 16743
AI

5. Engine-Inlet Airflow Match

Experience with high Mach number, high performance inlets has shown that many variables can affect the matching of inlet and engine airflow. These variables include control tolerances for both the inlet and engine, off-design angles of attack and yaw, changes in boundary bleed requirements for inlet stability, and inlet leakage. The loss in inlet ram recovery is about 1% for each 1% the inlet is undersize due to the above factors. If the inlet is effectively oversize, the excess air must be spilled or bypassed and results in additional aircraft drag.

The two-spool turbofan cycle offers a unique characteristic in correcting for the above mismatch problem. The engine airflow may be adjusted by the flight crew over approximately a 13% airflow range to maintain precise airflow matching of the engine to the inlet. This variation in airflow is attained at almost constant rotor speed and, therefore, entails no weight or structural penalties to the cycle. Airflow variations in the turbojet cycle may be accomplished only with significant changes in rotor speed and attendant large weight penalties.

Figure 19 illustrates the payload change resulting from a mismatch of inlet and engine airflow at cruise condition for the two engine cycles. The turbojet loses payload for either an oversized or undersized inlet. The small gain in turbofan payload with an oversized inlet is due to a small increase in cycle efficiency at the higher engine airflow.

Report D, Section II, should be referred to for a complete description of inlet/engine compatibility.

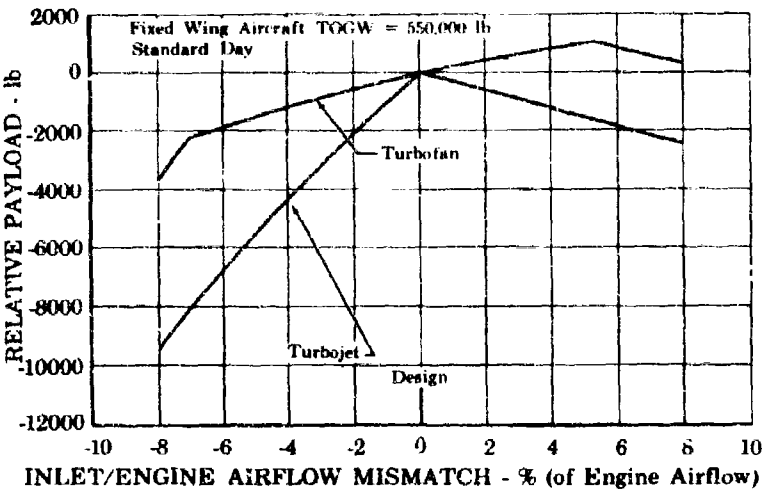

Figure 19. Effect of Inlet Mismatch on Payload FD 16725 AI

6. Effect of Begin Cruise Altitude

Figure 20 illustrates the effect of begin cruise altitude on range for the turbojet and turbofan cycles for a fixed-wing airplane. It is concluded that the cycles are equal with regard to range or payload penalty with altitude. The ground overpressure international flight limit is indicated.

Similar results were obtained for a swing-wing airplane

7. Growth Potential

Figure 21 illustrates the effect of design turbine inlet temperature on payload for the swing-wing aircraft. An increase in turbine inlet temperature of the augmented turbofan results in a gain in payload. An increase in design turbine inlet temperature, at constant engine airflow and cruise thrust, requires the turbojet to throttle back nonaugmented or to increase cruise altitude with a resulting decrease in aircraft L/D. In either case the turbojet cycle will not benefit from turbine inlet temperature increases above 2300°F. Similar results were obtained for the fixed-wing airplane.

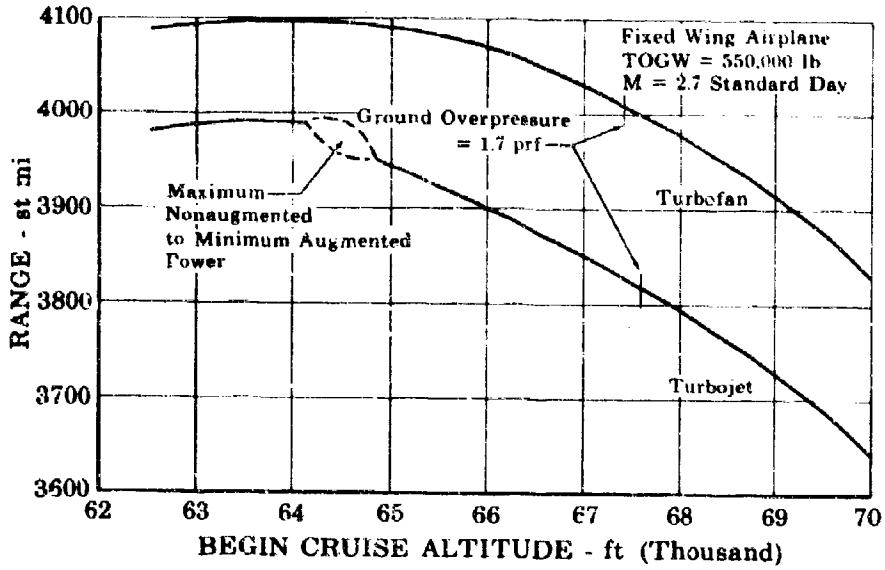

Figure 20. Begin Cruise Altitude

FD 16726
AI

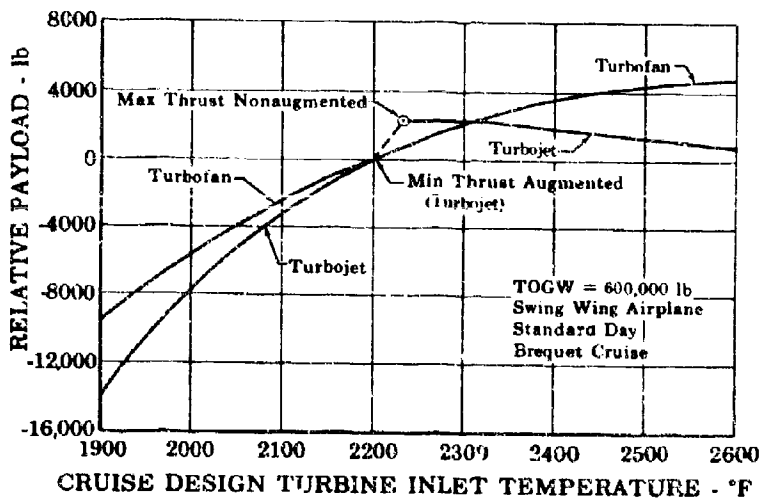

Figure 21. Effect of Design Turbine Inlet Temperature on Payload

FD 16760
AI

Figure 22 presents the effect of increasing flight Mach number on the two engine cycles. The turbofan cycle shows a distinct advantage over the turbojet in increased range or payload. The 90 mile difference in increased range at Mach 3 is equivalent to approximately 3000 lb in payload or 15 passengers.

Report G should be referred to for a complete description of engine growth potential.

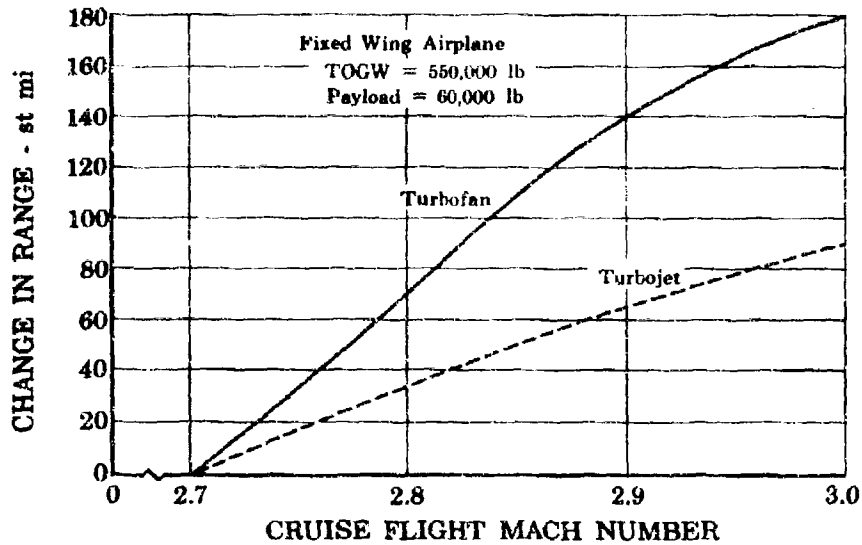

Figure 22. Cruise Mach No. Effect on Design Range — FD 16730 AI

8. Reduced Turbine Temperature

Our comparative study assumed that either engine would be developed for continuous cruise operation at a turbine temperature of 2200°F. Dependent on particular route structures and maintenance procedures, each airline will determine through sufficient operating experience the level of operating turbine inlet temperature yielding the greatest economic return. These economic considerations may dictate the desirability of operating aircraft on some routes at somewhat reduced cruise temperatures to achieve the proper balance between aircraft performance and parts life. Both the turbofan and turbojet engine cycles will result in a loss in aircraft performance as turbine temperature is reduced. Figure 21 shows the comparative performance in terms of aircraft payload. It will be noted that the loss resulting from the turbojet is significantly greater than that of the turbofan.

E. CONCLUSIONS

In summary, the turbofan engine cycle provides greater range/payload, greater safety, less noise, greater growth potential with increased Mach number and suffers less from off-design operation than the turbojet engine cycle. This is true for both fixed-wing and swing-wing aircraft and is primarily a result of the fan cycle versatility and ability to match a wide range of aircraft requirements without compromise to the basic cycle or design point performance.

SECTION II
SYSTEM PERFORMANCE

A. ENGINE SYSTEM

1. System Description

The JTF17 is a twin spool non-mixed turbofan engine with augmentation provided by fan duct heating. An overall view of the engine, as provided by a full-size mockup, is presented in figure 1. The basic components of the engine and its flow paths are shown schematically in figure 2. Major components and engine subsystems are described briefly in the following paragraphs; more complete description (with regard to performance) is provided in the referenced report section.

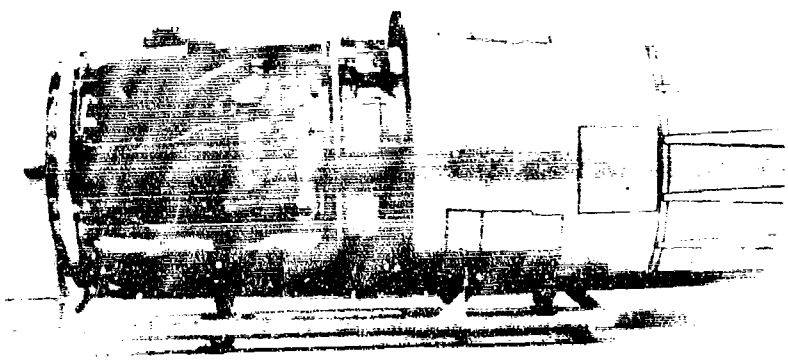

Figure 1. JTF17 Full-Scale Mockup FE 60735 AII

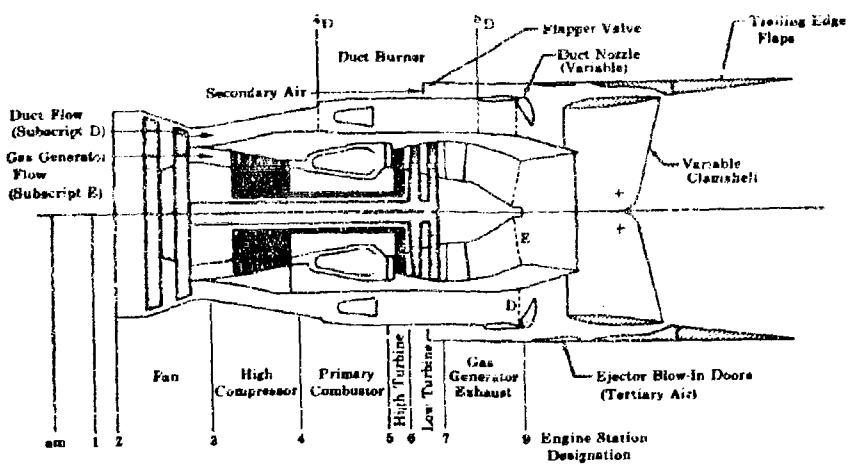

Figure 2. JTF17 Turbofan Engine Flow Schematic FD 16721 AII

a. Gas Generator

(1) Fan-Compressor (Reference Report A, Section III-A)

The fan-compressor of the JTF17 incorporates a total of eight stages. The first two stages constitute the fan and low pressure compressor; fan blading provides a duct pressure ratio of approximately 2.9 at sea level takeoff and 1.6 at supersonic cruise. The high pressure compressor is composed of six stages and, in combination with the low pressure compressor, provides an overall compression ratio of approximately 13 at sea level takeoff and 4.6 at supersonic cruise.

The two-stage fan is overhung, which eliminates conventional inlet guide vane structure. The orientation of all fan-compressor airfoils, except high rotor inlet guide vanes, is fixed. The high rotor inlet guide vanes are variable and can be rotated to a closed position to prevent airflow through the gas generator, and thus they provide aerodynamic braking for engine windmilling during flight.

Towershafts for engine and airframe accessory drives are geared from the high rotor, and a high pressure, high temperature air bleed for engine and airframe accessories is provided at the high pressure compressor discharge.

(2) Primary Combustor (Reference Report A, Section III-B)

The gas generator, or primary combustor is a unique, annular, ram-induction burner that provides low pressure losses, excellent temperature profiles, and high combustion efficiencies over a wide range of fuel/air ratios. By utilizing the ram-induction principle, it is possible to realize these benefits with a much shorter burner length than would be possible with more conventional designs.

(3) Turbine (Reference Report A, Section III-C)

The JTF17 incorporates a three-stage reaction turbine in which all airfoils except the 3rd-stage blades are convectively air cooled to permit operation at inlet temperatures up to 2300°F for takeoff and climb, and 2200°F for supersonic cruise. It was designed for minimum weight and utilizes a controlled vortex design to assure high efficiency.

The first turbine stage drives the high pressure compressor (from which all towershafts for engine and airframe accessory drives are geared). The second and third stages drive the fan.

The gas generator is provided with a fixed geometry convergent-divergent nozzle, which permits both high and low pressure turbines to operate at nearly constant expansion ratio over most of the engine operating range.

b. Augmentor (Reference Report A, Section III-D)

The duct augmentation system includes a two-zone combustion arrangement and a variable area exit nozzle in the fan duct. An annular ram-induction burner similar to that in the gas generator constitutes the first zone for combustion, which is utilized for augmentation at levels up to approximately 30%; Zone II fuel is introduced at the discharge of the annular burner where it unites with combustor bypass air and Zone I combustion gases. Total fuel/air ratio at full augmentation with both zones in operation is approximately 0.06.

The short length of the ram-induction burner permits use of a low divergence angle diffuser to minimize pressure losses in the fan duct, and its operating characteristics assure capability for smooth light-off and stable operation over the entire augmentation range.

The variable area convergent nozzle at the fan duct exit is modulated by the fuel control in accordance with a schedule based on duct fuel flow. Thus, augmentation level may be varied over a wide range without affecting the gas generator.

c. Exhaust System (Reference Report A, Section III-E, and Report C)

The JTF17 exhaust system combines a blow-in-door ejector and variable (rotating) clamshell to accomplish the reverser-suppressor function and to achieve the effective area changes necessary to control the expansion of the combined streams of exhaust gases from the gas generator and duct at all operating conditions.

The elements of the exhaust system can be identified in figure 2. These include the secondary air passage and flapper valve, tertiary air blow-in doors, variable clamshells, and pressure-actuated trailing edge flaps. The position shown in figure 2 is that for supersonic cruise. The clamshell is in the full open position, forming the initial divergent portion of the nozzle, and the trailing edge flaps, which form the nozzle exit, are also in the full open position for maximum expansion. Tertiary air doors are closed, and a small quantity of secondary air flows through the system to control the expansion of the gas generator and duct streams and to provide cooling for ejector surfaces.

The takeoff positioning of exhaust system elements is illustrated in figure 3. The trailing edge flaps are closed to minimum area due to pressure loading, and the clamshell sections are in a partially open position to admit tertiary air, which enters through the blow-in doors. The tertiary air, in combination with any available secondary airflow, serves to reduce overexpansion losses aerodynamically and to reduce noise. Introduction of the tertiary stream provides a buffer shroud of gas that (through mixing with the hot core gases from the gas generator and augmentor) provides a velocity gradient from the hot exhaust jet surface to the wall to attenuate the noise normally associated with an interface between a high velocity jet and quiescent air.

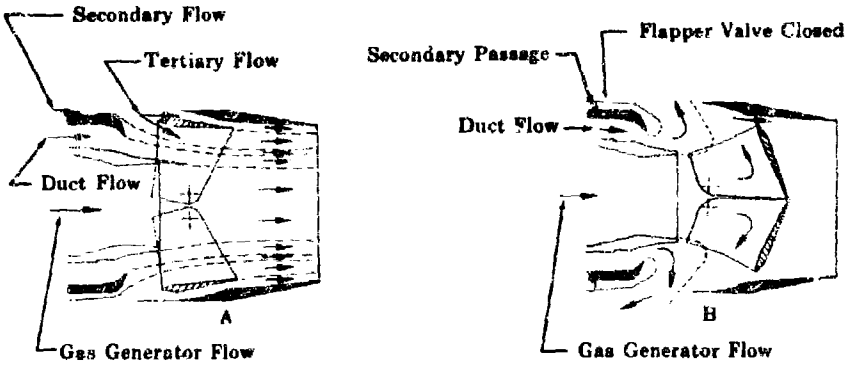

Figure 3. JTF17 Exhaust System Positions FD 16890
AII

To accomplish thrust reversal, the clamshell sections are rotated to the full closed position as shown in figure 3, deflecting the exhaust gases forward through the tertiary air doors at a mean angle of 20 degrees to the nozzle centerline. The flapper valve in the secondary air passage closes to prevent reingestion of exhaust gases.

d. Engine Controls and Accessories (Reference Report B, Section III)

The JTF17 engine control is a hydromechanical unit that incorporates both gas generator and duct heater controls in a unitized assembly. The control, gas generator fuel pump, engine hydraulic pump, and engine oil pump are driven mechanically by towershafts geared from the high compressor. The duct heater fuel is supplied by a compressor bleed air turbopump, similar to that of the J58 engine, rather than by a mechanically driven pump.

Dual input levers are provided for the control; a single power lever controls thrust modulation from full reverse to idle to maximum augmentation. The second, or fuel shutoff, lever provides for starting and stopping of fuel flow to the control and for aerodynamic windmill brake operation.

Ignition is provided by a capacitor discharge intermittent duty AC power system. Two fuel-cooled, hermetically-sealed, exciter packages, each containing two independent exciter circuits for one gas generator igniter and one duct heater igniter, are employed.

The operation of the engine control is described in Volume III, Report B, Section III.

2. System Optimization

In the discussion of cycle selection in Section I, it was made apparent that the duct augmented turbofan engine was selected because it provided maximum range and/or payload for the supersonic transport. Optimization

of the engine system, therefore, was directed toward achieving maximum range/payload for a given gross takeoff weight with acceptable noise levels, and the process was one of obtaining the best compromise between takeoff, climb, and subsonic performance, and supersonic cruise TSFC.

Maximum turbine inlet and augmentor discharge temperature consistent with the capability of advanced design concepts were selected to provide maximum efficiency and airflow. Pressure ratios and percent augmentation were established through an iterative process that recognized engine weight differences and considered total mission performance. Bypass and pressure ratios were established in studies conducted by Pratt & Whitney Aircraft under Phase II-A. Because of the interrelationship of engine size and aircraft performance, final selection of airflow was based upon studies made by airframe manufacturers using P&WA supplied engine data.

It can be inferred from the above comments on final airflow selection that engine system optimization must be closely related to the installation being considered. The JTF17 engine system provides a high degree of flexibility that will permit final "tuning" with a minimum of hardware change when ultimate mission profile and airframe configuration are established.

3. Engine Variations

a. Engine Models

Two models of the JTF17 engine, the JTF17A-21B, and the JTF17A-21L are proposed. The JTF17A-21B meets the specific requirements of the Boeing airframe, and the JTF17A-21L meets those of the Lockheed aircraft. The two engines are defined in Model Specifications No. 2710 and 2698, respectively. Because of the inherent versatility of the cycle, the same basic engine can be used for both applications; small differences in the airflow schedules at supersonic cruise conditions between the two installations are achieved by changes in fan duct flow that are adequately handled by the fuel control.

Although there are no differences in major components that affect performance, there are minor hardware differences between models necessitated by differences in installation requirement. These are mainly concerned with mounting provisions and thrust nozzle alignment (the exhaust nozzles of both engines are canted downward from the engine centerline by small, but different, angles), as reflected in the installation drawings (Drawing No. 2129601 for the JTF17A-21B and No. 2128101 for the JTF17A-21L). In addition, because of different aircraft red line dive speeds, the JTF17A-21B requires increased structural strength in casing sections; this does not, however, affect performance determination.

b. Prototype System

The approach that was followed in the design of the JTF17, and that will be continued in subsequent phases of the SST program, is to proceed directly toward the achievement of production engine design and performance objectives. Therefore, all system performance estimates are generated using component performance goals for type certified engines and there are no

separate performance objectives for the prototype system as such. However, any realistic appraisal must recognize that final objectives may not be realized in the development time span of the prototype construction phase. For this reason, tolerances of 3% on maximum thrust level and 5% on thrust specific fuel consumption have been established for the prototype. While it is not possible at this time to define precisely the variances existing in the prototype engines, experience would indicate that certain components will be less highly developed than others at the time of prototype delivery. Table 1 shows the estimated component performance levels required to meet minimum prototype performance compared to those of the JTF17 production engine.

B. SYSTEM PERFORMANCE

1. General

The performance characteristics and engine operating envelopes of the two models of the JTF17 are defined in the applicable model specifications. For typical flight profiles in either installation, the JTF17 operates with some level of augmentation for almost the entire mission; this is indicated by the representative curve in figure 4.

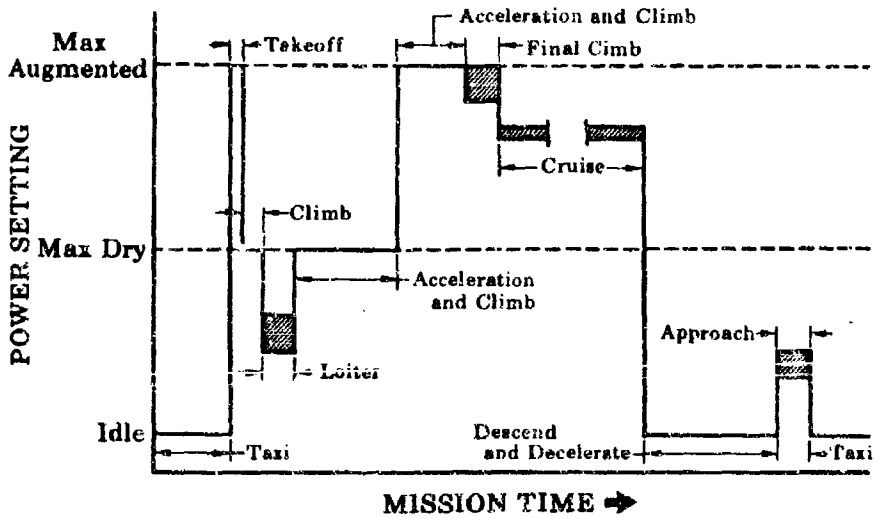

Figure 4. Engine Power Settings During Operational Mission — FD 16892 AII

Estimated maximum augmented thrust and maximum augmented thrust specific fuel consumption are presented in curve form as a function of Mach number for altitudes from sea level to 80,000 feet in the engine model specifications.

The engine model specifications are the basic performance and installation documents that provide user data. They include information on installation, specified ratings, performance, operating envelope, thrust transients, inlet pressure distortion limits, engine systems, fuel and oil requirements, limiting zone temperatures, power extraction, etc.

A definition of performance ratings may be found in the model specifications that are included as part of this proposal. It is believed that the system performance estimates provided in the model specification will provide

an adequate basis for determination of JTF17 installed engine capability. The following paragraphs are intended to provide a better understanding of the methods of performance determination and of the information contained in the specification.

Table 1. JTF17 Production and Prototype Engine Design Tables

Parameters	Units	Production		Prototype	
		Sea Level	Cruise	Sea Level	Cruise
Alt	ft	0.0	65000	0.0	65000
M		0.0	2.7	0.0	2.7
T_{t2}	°R	519	954	519	954
P_{t2}	psia	14.7	16.3	14.7	16.3
P_{t3}/P_{t2E}		2.68	1.58	2.60	1.56
P_{t3}/P_{t2D}		2.90	1.62	2.81	1.57
η_{FE}		0.888	0.898	0.850	0.860
η_{FD}		0.788	0.808	0.777	0.787
T_{t3E}	°R	709	1090	710	1100
T_{t3D}	°R	752	1120	747	1110
WAT2	lb/sec	687	417	687	417
WAT	lb/sec	687	341	687	341
BPR		1.30	1.88	1.37	1.98
N_1	rpm	6490	5620	6440	5550
$N_1/\sqrt{\theta T_2}$	rpm	6490	4140	6440	4090
ΔH_F	Btu/lb	51.6	39.3	51.2	38.5
WAD	lb/sec	388	222	398	226
WA_{3D}	lb/sec	158	182	167	190
$\Delta P/P_D$ cold		0.050	0.068	0.056	0.074
$\Delta P/P_D$ hot		0.058	0.015	0.071	0.018
WFD	lb/hr	81700	11900	83900	13000
TTD	°R	3630	2060	3600	2110
$\eta_{D/H}$		0.911	0.970	0.902	0.965
P_{td}/P_{am}		2.66	29.3	2.49	28.2
$F/A_{D/H}$		0.060	0.0153	0.060	0.0163
WAE	lb/sec	299	118	290	115
WAE3	lb/sec	130	98.3	130	96.3
P_{t4}/P_{t3}		4.84	2.32	4.73	2.81
P_{t4}/P_{t2}		13.0	4.38	12.3	4.38
η_c		0.859	0.868	0.820	0.810
T_{t4}	°R	1160	1510	1180	1530

CONFIDENTIAL

Table 1. JTF17 Production and Prototype Engine Design Tables (Continued)

Parameters	Units	Production		Prototype	
		Sea Level	Cruise	Sea Level	Cruise
8th-Stage Bleed	% WAE	0.8	0.68	0.8	0.68
Turbopump Bleed	% WAE	1.0	1.0	1.0	1.0
N_2	rpm	8220	8270	8230	8160
$N_2/\sqrt{\theta T_2}$	rpm	8220	6100	8230	6020
$N_2/\sqrt{\theta T_3}$	rpm	7030	5700	7030	5610
ΔH_{HPC}	Btu/lb	112	108	115	111
$\Delta P/PB$		0.057	0.070	0.061	0.079
η_B		0.990	0.990	0.986	0.986
F/A_B		0.0264	0.0192	0.0263	0.0190
WFP	lb/hr	26100	7560	25300	7270
P_{t5}	psia	180	70	170	65.8
T_{t5}	°R	2760	2660	2760	2660
TCA	% WAE	6.24	5.66	6.22	5.65
η_{th}		0.878	0.869	0.879	0.870
η_{tl}		0.893	0.880	0.892	0.877
P_{t7}	psia	32.3	12.5	28.9	11.2
T_{t7}	°R	1890	1840	1870	1820
$\Delta P/P_{7-9}$		0.017	0.017	0.025	0.025
P_{t9}	psia	31.7	12.3	28.2	10.9
T_{t9}	°R	1910	1850	1890	1830
P_{t9}/P_{am}		2.16	14.8	1.92	13.2
% Corr. Sec. Flow (Engine Face)		2.0	2.0	2.0	2.0
% Sec. Flow (Engine Face)		4.91	2.93	4.92	2.96
Secondary Flow (Engine Face)	lb/sec	33.7	10.0	33.8	10.1
CFP (Includes Effect of Turbopump Air in Secondary Stream)		0.982	1.0012	0.98	0.999

2. Steady-State Operation

Steady-state, forward thrust, system performance estimates (as well as estimates for other operating regimes) for the JTF17 engine have been generated using the latest available estimates, based on actual Phase II-C testing where possible, for major component performance. Sources of

CONFIDENTIAL

component performance data will be made evident in the discussion of the major items (combustors, turbine, fan-compressor, augmentor, and exhaust system) presented later in this report. The thermodynamics involved in system performance determination can be seen in sample calculations provided at the end of this section.

Digital computer cycle matching decks are used to obtain steady-state system performance estimates, and both digital and analog dynamic simulations are used to investigate transient performance. In the dynamic simulations, air inlet performance, inlet control, engine performance, engine control, and the complete fuel system are simulated so that the behavior of the system as a whole can be observed over the full range of flight conditions and so that effects of off-design conditions and malfunctions can be analyzed.

Because of the wide spectrum of flight conditions that must be considered, it is difficult to present engine data in sufficient detail in any convenient summary form to satisfy all requirements. Therefore, a digital computer cycle matching calculation deck that provides steady-state performance estimates for the entire range of engine operation from idle to maximum augmented thrust, and complete instructions for its use, are provided as a part of each model specification.

All performance estimates generated by the cycle matching deck are premised upon the use of fuel conforming to P&WA Specification PWA 522 (10 November 1964) at its minimum lower heating value of 18,400 Btu/lb. Ambient conditions used are in accordance with the U.S. Standard Atmosphere (Geometric), 1962, and inlet total pressure recovery is as defined by Specification MIL-E-5008B.

Estimates of engine performance under certain conditions are included in curve form in the applicable model specifications, and estimates for flight conditions of particular interest, determined using the specification matching decks, are presented in tabular form in report PWA FR-1986 for the JTF17A-21L and in report PWA FR-1987 for the JTF17A-21B; both reports will be made available to the evaluators on request.

"Uninstalled" engine performance is defined as the performance attainable with:

1. No power extraction or high compressor air bleed except that required for operation of engine accessories and controls
2. Allowance for effect of 2% temperature corrected secondary airflow to the reverser-suppressor.
3. Exhaust system effects (external boattail drag on trailing edge flaps when they are not in the full open position, and, where appropriate, drag resulting from induction of tertiary air through ejector blow-in doors) accounted for.*

*As will be made apparent in the description of the exhaust system in Section IIIE and in the sample calculations, this is accomplished by use of nozzle thrust coefficients determined in wind tunnel model tests. In the models, the exhaust nozzle centerline is parallel to and coincident with the engine centerline, so the canting of the aircraft installation is not duplicated. However, this will introduce no measurable error.

Performance estimate curves presented in the model specification are based on the above assumptions; the cycle matching decks provided as part of the specification, however, provide capability for determining the effects of power extraction and customer air bleed from the high compressor, so that the effects of these installation requirements can be evaluated where they are of interest. Performance estimates for operation with power extraction and air bleed are included in reports PWA FR-1986 and FR-1987.

Limits that define the estimated engine operating envelope are incorporated in the computer decks, and the calculation routine provides for printing of a notation in the event that any limit is exceeded. Operating limits are based upon design life considerations as outlined in Volume III, Report B. The continuous operating limits shown in figure 5 define the flight operating regions in which the engine may be operated continuously with no degradation of design life, and the transient limits shown indicate the range into which excursions of limited duration (one minute each occurrence) are possible without any deleterious effect. The total accumulated operating time in the transient region must, however, be limited to a maximum of 10 hours in each 10,000 hours of total engine operation.

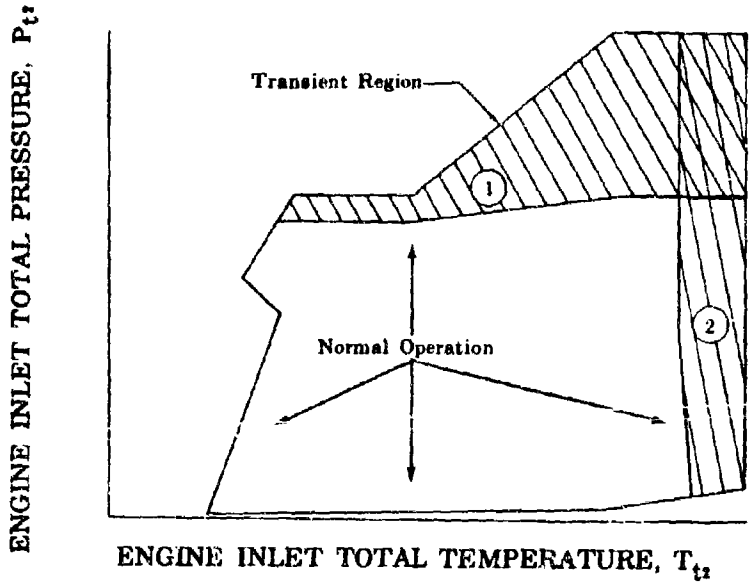

Figure 5. Representative Engine Operating Envelope — FD 16897 AII

Reasons for definition of the engine operating envelope can be visualized by reference to figure 5 and table 2. Representative flight limitations are presented in terms of engine inlet pressure and temperature in the illustration, and the transient region is divided into zones representing areas in which different types of limitations exist with regard to load and limiting stress. The loads, limiting stresses, and parts affected are defined in the table. A more detailed understanding of the limits on individual parts can be obtained from the discussions of mechanical design included in Volume III, Report B.

4. Reverse Thrust Operation

A brief description of the operation of the exhaust system to provide reverse thrust was given above and a detailed discussion is provided in Section III, Paragraph E of this report. Section 23.0 of the applicable model specification provides specific definition of requirements, and curves showing estimated operating envelope and maximum net reverse thrust (uninstalled) for standard and hot days, when reingestion of exhaust gases is not experienced, are provided. Because of structural limitations, maximum reverse thrust operation is limited to 1 minute; however, continuous reverser operation at idle on the ground is permitted.

Engine performance during reverse thrust operation is determined using normal cycle matching digital computer calculation techniques with the application of thrust coefficients for the reverser determined in wind tunnel tests of ejector nozzle models.

5. Starting

(a) Ground Starting

The estimated maximum ground starting time of the JTF17 engine is 30 seconds, assuming compliance with the requirements of Section 20.2 of the applicable model specification with regard to starter output, fuel temperature and pressure, electrical power, and engine inlet air pressure.

The required starter output, as defined by curve sheet number 30 in the model specification is determined by engine motoring characteristics and minimum firing speed (rotor speed at which ignition is possible). Because adequate theoretical techniques for establishing motoring torque and minimum ignition speeds are not available, it is customary to estimate these characteristics employing an analysis based largely upon use of data from existing engines having features that can be related. For estimates of JTF17 starting, experience with JT3D and JT8D engines was used as a basis.

A representative starting requirement (starter output) curve is presented in figure 6. The lower limit of the starter band represents the minimum torque required for rotor acceleration; the upper limit is set to assure structural integrity of the power takeoff. The basic starter band represents standard day requirements; a correction must be applied for nonstandard (low temperature) conditions. Reduced ambient temperature causes an increase in motoring torque because of the greater aerodynamic work required with increased air density and the higher fuel and oil viscosities. It is estimated that a reduction of ambient temperature from 0°F to -40°F will necessitate an increase in motoring torque of approximately 37% for the JTF17. If the minimum torque curve is complied with, the estimated maximum starter power for the JTF17 is 230 horsepower, even at reduced temperatures.

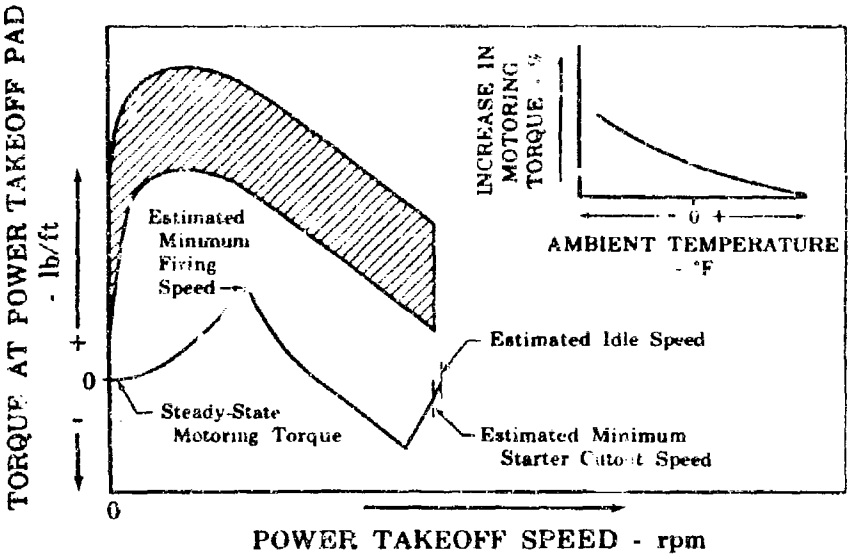

Figure 6. Representative Engine Starting Requirements — FD 16898 AII

Experimental definition of starting characteristics with the degree of accuracy necessary to verify the estimated starting requirements requires specific testing of engines incorporating special instrumentation. This is not within the scope of the Phase II effort; however, 47 starts have been accumulated to date on demonstrator engines and, as indicated in Table 3, enough of these have been accomplished in time periods in the range of 30 seconds to provide confidence that the estimated time can be attained consistently.

Table 3. Phase II-C Demonstration Engine Starting Times (Engine FX-162, Build 1)

Test No.	Air Pressure Supplied to Starter at Time Zero: Elapsed Time (Seconds) To Fuel Pressure Buildup	Light	Idle Thrust
4	8	23	36
7	5	22	33
8	6	25	34
10	7	15	26
11	6	24	30

(b) In-Flight Starting

In-flight starting of the JTF17 engine is possible without assistance over a wide range of flight conditions (assuming that the normal operating envelope is observed) as indicated by the windmilling restart envelopes in the engine model specifications for the two engine models. The critical region for starting is the low Mach number limit, because this defines the minimum combustor pressure considered adequate for ignition. The lower limit for restarting of the JTF17 was established from analysis of JTF17 combustor rig data and by JT3D, JT8D, and J58 engine experience.

The minimum starting limit line was established to provide windmilling combustor pressures varying from approximately 7.5 to 15 psia. The 7.5 psia minimum is believed to be adequate based upon past experience with other engine models. Minimum burner pressure for ignition has not yet been investigated in JTF17 primary combustor test rigs, but successful lights have been achieved at pressures as low as 9 psia, and there was no indication that this was a lower limit.

Estimated windmilling combustor pressures and airflows, and gas generator fuel flows and fuel/air ratios for various flight conditions along the minimum in-flight starting limit are presented in table 4. Note in the table that fuel/air ratios are typically on the order of 0.01. In testing of JTF17 primary combustor rigs, ignition has been demonstrated consistently at fuel/air ratios of 0.005, so no problems are anticipated in maintaining a combustible mixture.

Table 4. Gas Generator Combustor Parameters for In-Flight (Windmill) Starting

Mach No.	Altitude, ft	High Rotor Speed, rpm	Primary Burner Pressure, psia	Primary Fuel Flow, lb/hr	Primary Combustor Airflow, lb/sec	Primary Fuel/Air Ratio
2.5	80,000	6320	12	1200	30	0.01
1.9	69,000	5150	8	1200	25	0.01
1.4	52,000	4600	8	1200	25	0.01
1.0	36,000	3670	9	1300	30	0.01
0.7	23,000	2440	11	1200	30	0.01
0.6	14,000	2180	14	1400	30	0.01

Manual sequencing of controls for in-flight starting is not critical. The airflow rates during windmilling operation preclude critical accumulation of fuel, and although the igniters and their exciters are intermittent duty cycle devices, they can be operated continuously for relatively long periods (up to 10 minutes for the gas generator igniter).

Recommended control sequencing (refer to Volume III, Report B, Section III for a more complete description of control and ignition system operation) is as follows:

1. Position the thrust control lever in the idle detent.
2. Move gas generator and augmentor ignition switches to "ON." This actuates the gas generator exciters that fire the igniters and arms the augmentor exciters.)
3. Move fuel cutoff lever to "FUEL ON" position. (Movement of the fuel cutoff lever to the on position assures that the aerodynamic brake is off, and causes the gas generator fuel dump valve to close and fuel to be introduced to the gas generator fuel nozzles).
4. Position thrust control lever for desired operating level after ignition.
5. Dependent upon operating procedures for flight regime, return ignition switches to "OFF" position.

6. Acceleration

Pratt & Whitney Aircraft has made extensive use of dynamic simulation in studies of the JTF17 engine in order to investigate control requirements, control performance, and inlet-engine compatibility. Control considerations are treated in Volume III, Report B, and inlet compatibility is discussed in Volume III, Report D. Dynamic simulations were also used to establish engine acceleration performance; this is discussed below.

The fan duct augmentor contributes to rapid thrust increase when excursions to augmented levels are made. The augmentor operating level does not affect gas generator discharge conditions significantly, and therefore the duct combustor can be lit at an appropriate point defined by high rotor speed while the low rotor is still accelerating. This capability minimizes elapsed time differences between accelerations to maximum dry and maximum augmented thrust.

The annular ram-induction combustor used in the fan duct provides particularly soft augmentor light-off. During demonstrator engine testing in the Phase II-C, 24 augmentor lights have been accomplished to date. Ignition has been recorded at augmentor fuel/air ratios of less than 0.002; the resulting thrust increase is approximately 2.5% of maximum augmented, which would not be perceptible to passengers, and the resulting pressure perturbation is small enough to assure that fan and inlet operation will not be affected.

The guaranteed engine response (standard day) for power lever movements between idle and 75% maximum nonaugmented, 95% maximum nonaugmented rating, and maximum augmented rating to 95% full reverse are given in Section 8 of the applicable model specification, and the relationship of high rotor speed vs time is shown on curve sheet 34. Estimated elapsed time for acceleration from idle at sea level and from a typical approach condition 0.21 Mach number at 325 feet, to 95% maximum nonaugmented and maximum augmented ratings (power lever movement in one second or less) for standard and nonstandard conditions are presented in table 5. Thrust

vs time curves for the various accelerations are shown in figures 7 through 9. Because acceleration characteristics are primarily dependent upon high compressor rotor performance, there are no differences between engine models.

Table 5. JTF17 Estimated Acceleration Response

Flight Condition	Atmosphere	Power Lever Movement	Estimated Elapsed Time to 95% Selected F_n (Seconds)
Sea Level Static	STD	Idle to Max Nonaugmented	5.4
	STD +27°F		5.7
	STD -18°F		4.8
Sea Level Static	STD	Idle to Max Augmented	5.5
	STD +27°F		6.0
	STD -18°F		5.0
Approach	STD	Approach setting to Max	2.3
	STD +27°F	Nonaugmented	2.3
	STD -18°F		2.3
Approach	STD	Approach setting to Max	2.5
	STD +27°F	Augmented	2.5
	STD -18°F		2.5

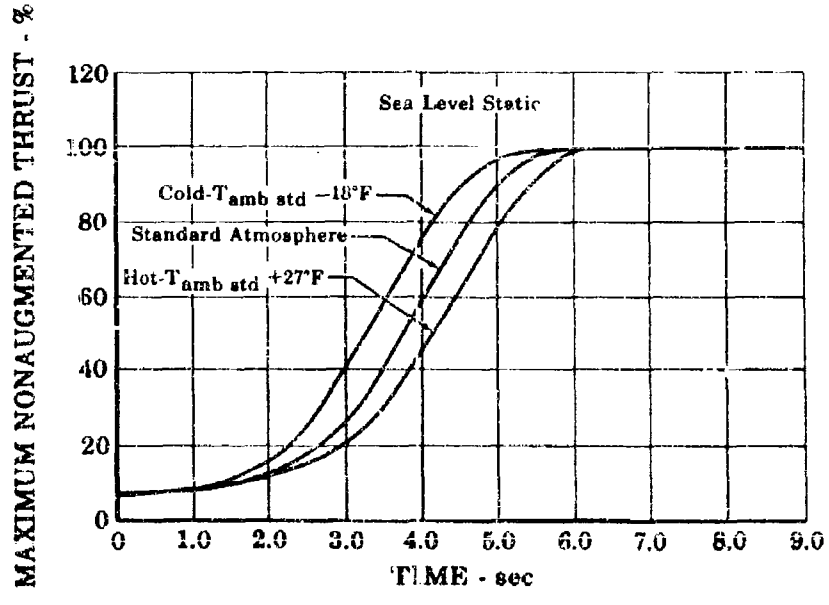

Figure 7. Estimated Engine Acceleration Idle to Maximum Nonaugmented Power

FD 16872
AII

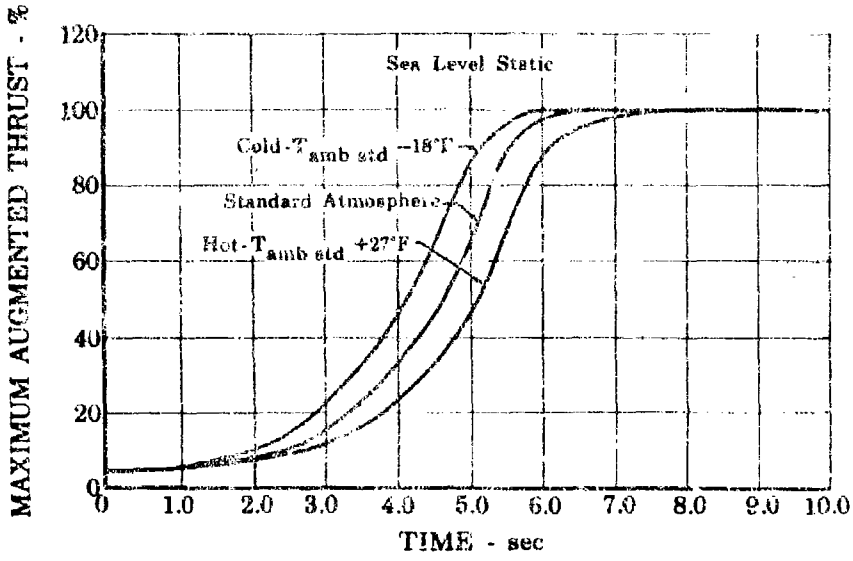

Figure 8. Estimated Engine Acceleration Idle to Maximum Augmented Power — FD 16871 AII

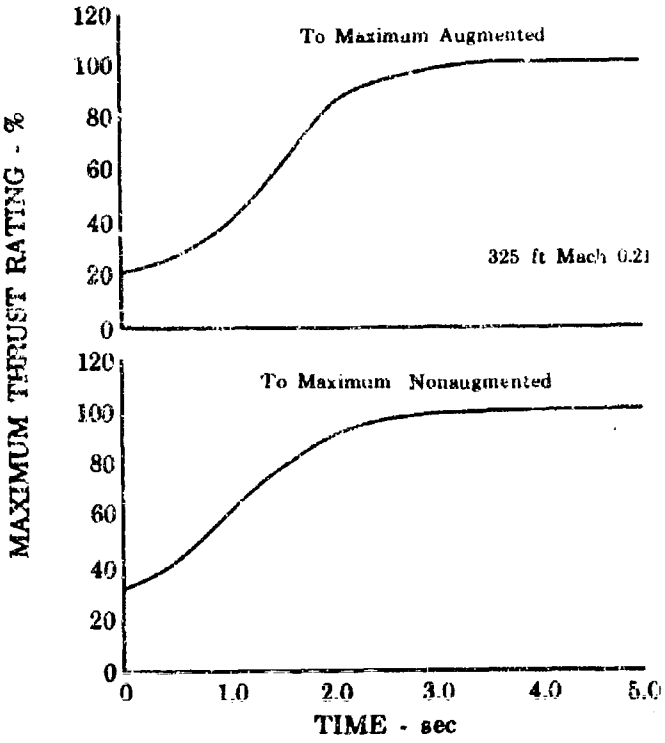

Figure 9. JTF17 Turbofan Engine Accelerations from Approach Flight Condition — FD 16900 AII

C. SAMPLE CALCULATIONS

Sample calculations illustrating the procedures used for estimation of JTF17 system performance are presented in table 6. Calculations for the maximum augmented sea level takeoff condition for both the JTF17A-21B and the JTF17A-21L, and for a typical cruise condition of the JTF17A-21L (Mach 2.7 at 65,000 ft) are included.

The table provides definition of parameters by both description and symbol, and indicates assumptions and sources of input information. Engine station designations are shown in figure 2. The conventions established for station designation in other P&WA twin spool engines have been generally adhered to, and subscripts E and D have been used to differentiate between gas generator (engine) and duct flows.

D. DEMONSTRATOR ENGINE PERFORMANCE SUMMARY

Four engine calibrations at sea level and one partial engine calibration at altitude have been accomplished. The total engine running time to date is 74.83 hours, with 19.5 hours above 2000°F turbine inlet temperature, 0.59 hours at 2300°F T.I.T., and 1.65 hours at Mach 2.7. The results of the sea level calibrations are shown below.

Engine	161-1	162-1	161-3	161-4
Thrust, lb	24,350	36,080	38,750	47,590
Turbine Inlet Temperature, °F	1780	2060	2100	2335

The rated turbine inlet temperature and design airflow have both been achieved.

Prior to engine testing, rig tests showed that the high compressor had a low surge line and that the turbine areas required to match the engine components correctly were larger than the maximum class available. The first three engine calibrations required both low turbine temperature and bleed in order to prevent surge in addition to the largest turbine class available.

Engine 161-4 incorporated surge line fixes developed in build 5 of the compressor rig. This engine was operated at rated turbine temperature to give 47,590 lb thrust. The high rotor speed was 7% low. Rematching of the turbine to increase high rotor speed at rated temperature will further increase thrust.

On 22 July, 2.07 hours of heated inlet testing, 1.65 hours of which were at an inlet condition simulating Mach 2.7 cruise at 65,000 feet, were conducted without duct heating. At these conditions the maximum turbine inlet temperature was 2170°F. If this altitude gas generator performance is combined with full-scale duct heater rig data it is estimated that the duct heater lit TSFC will be within 5% of engine ratings at cruise thrust level.

Table 6. JTF17 Cycle Calculation

	Calculation	Symbol	Units	SLTO
1	ALTITUDE	ALT	ft	0
2	MACH NUMBER	M		0
3	AMBIENT TEMPERATURE	T_{AM}	°R	519
4	AMBIENT PRESSURE	P_{AM}	psia	14.7
5	ENGINE INLET TOTAL TEMPERATURE	T_{T2}	°R	519
6	INLET RAM RECOVERY	P_{T2}/P_{T2}'		1.0
7	ENGINE INLET TOTAL PRESSURE	P_{T2}	psia	14.7
8	NORMALIZED INLET PRESSURE	δ_{T2}		1.0
9	NORMALIZED INLET TEMPERATURE	θ_{T2}		1.0
10	ENGINE INLET CORRECTED AIRFLOW	W_{AT2}	lb/sec	687
11	ENGINE INLET AIRFLOW	W_{AT}	lb/sec	687
12	FAN COMPRESSOR CORRECTED ROTOR SPEED	$N_1/\sqrt{\theta_{T2}}$	rpm	6490
13	FAN COMPRESSOR ROTOR SPEED	N_1	rpm	6490
14	ID FAN COMPRESSOR PRESSURE RATIO	P_{T3E}/P_{T2}		2.68
15	ID FAN COMPRESSOR EFFICIENCY	η_{C1E}		0.888
16	OD FAN COMPRESSOR PRESSURE RATIO	P_{T3D}/P_{T2}		2.90
17	REYNOLDS CORRECTION FACTOR	$\Delta\eta$		0
18	CORRECTED OD FAN COMPRESSOR EFFICIENCY	η_{C1D}		0.788
19	ID FAN DISCHARGE IDEAL TOTAL TEMPERATURE	$T_{T3E\ IDEAL}$	°R	687
20	ID FAN DISCHARGE TOTAL TEMPERATURE	T_{T3E}	°R	709
21	OD FAN DISCHARGE IDEAL TOTAL TEMPERATURE	$T_{T3D\ IDEAL}$	°R	703
22	OD FAN DISCHARGE TOTAL TEMPERATURE	T_{T3D}	°R	752
23	BYPASS RATIO	BPR		1.30
24	HIGH COMPRESSOR INLET AIRFLOW	W_{AE}	lb/sec	299
25	DUCT INLET AIRFLOW	W_{AD}	lb/sec	388
26	ID FAN DISCHARGE ENTHALPY	h_{T3E}	Btu/lb	170
27	OD FAN DISCHARGE ENTHALPY	h_{T3D}	Btu/lb	180
28	FAN POWER		Btu/sec	35500
29	ID FAN DISCHARGE PRESSURE	P_{T3E}	psia	39.4
30	ID FAN DISCHARGE NORMALIZED PRESSURE	δ_{T3E}		2.68
31	ID FAN DISCHARGE NORMALIZED TEMPERATURE	θ_{T3E}		1.37
32	OD FAN DISCHARGE PRESSURE	P_{T3D}	psia	42.7
33	OD FAN DISCHARGE NORMALIZED PRESSURE	δ_{T3D}		2.90
34	OD FAN DISCHARGE NORMALIZED TEMPERATURE	θ_{T3D}		1.45
35	AVERAGE FAN PRESSURE RATIO	P_{T3D}/P_{T2}		2.80
36	HIGH COMPRESSOR INLET CORRECTED AIRFLOW	W_{AE3}	lb/sec	130
37	HIGH COMPRESSOR PRESSURE RATIO	P_{T4}/P_{T3E}		4.84
38	HIGH COMPRESSOR SURGE PRESSURE RATIO	$(P_{T4}/P_{T3})_{SURGE}$		5.34
39	REYNOLD'S CORRECTION FACTOR	$\Delta\eta_{C2}$		0
40	HIGH COMPRESSOR EFFICIENCY	η_{C2}		0.859
41	HIGH COMP. DISCHARGE IDEAL TOTAL TEMP.	$T_{T4\ IDEAL}$	°R	1098
42	HIGH COMPRESSOR DISCHARGE TOTAL TEMP.	T_{T4E}	°R	1160
43	HIGH COMPRESSOR DISCHARGE TOTAL ENTHALPY	h_{T4}	Btu/lb	282
44	HIGH COMPRESSOR POWER		Btu/sec	33500
45	HIGH COMPRESSOR CORRECTED ROTOR SPEED	$N_2/\sqrt{\theta_{T3}}$	rpm	7030
46	HIGH COMPRESSOR ROTOR SPEED	N_2	rpm	8220
47	HIGH COMPRESSOR DISCHARGE PRESSURE	P_{T4E}	psia	191
48	TURBINE COOLING AIR	TCA/W_{AE}		0.0624

F17 Cycle Calculation

Symbol	Units	SLTO	Cruise	Source
	ft	0	65000	
		0	2.7	
	°R	519	390	1962 GEOMETRIC ATM
	psia	14.7	0.83	1962 GEOMETRIC ATM
	°R	519	954	f(M)
$_{T_2'}$		1.0	0.847	MIL-E-5008B
	psia	14.7	16.3	f(M, $P_{T_2}/P_{T_2'}$)
		1.0	1.11	f(P_{T_2})
		1.0	1.84	f(T_{T_2})
	lb/sec	687	417	AIRFLOW SCHEDULE f(T_{T_2})
	lb/sec	687	341	f(W_{AT_2}, θ_{T_2}, δ_{T_2})
$\overline{\theta}_{T_2}$	rpm	6490	4140	ID FAN MAP
	rpm	6490	5620	f($N/\sqrt{\overline{\theta}_{T_2}}$, $\sqrt{\theta}_{T_2}$)
P_{T_2}		2.68	1.58	ID FAN MAP
		0.888	0.898	ID FAN MAP
P_{T_2}		2.90	1.62	OD FAN MAP
		0	−0.004	f(REYNOLDS NUMBER)
		0.788	0.808	OD FAN MAP AND REYNOLDS CORR.
IDEAL	°R	687	1081	K AND K GAS TABLES f(P_{T3E}/P_{T_2}, T_{T_2})
	°R	709	1090	f($\eta_{C_{1E}}$, $T_{T3E\ IDEAL}$, T_{T_2})
IDEAL	°R	703	1090	K AND K GAS TABLES f(P_{T3D}/P_{T_2}, T_{T_2})
	°R	752	1120	f(η_{C1D}, $T_{T3D\ IDEAL}$, T_{T_2})
		1.30	1.88	
	lb/sec	299	118	f(BPR, W_{AT})
	lb/sec	388	222	f(BPR, W_{AT})
	Btu/lb	170	265	K AND K GAS TABLES f(T_{T3E})
	Btu/lb	180	271	K AND K GAS TABLES f(T_{T3D})
	Btu/sec	35500	15400	f(h_{T3E}, h_{T3D}, h_{T_2}, W_{AD}, W_{AE})
	psia	39.4	25.7	f(P_{T3E}/P_{T_2}, P_{T_2})
		2.68	1.75	f(P_{T3E})
		1.37	2.11	f(T_{T3E})
	psia	42.7	26.4	f(P_{T3D}/P_{T_2}, P_{T_2})
		2.90	1.79	f(P_{T3D})
		1.45	2.16	f(T_{T3D})
P_{T_2}		2.80	1.61	f(P_{T3E}/P_{T_2}, P_{T3D}/P_{T_2}, W_{AD}, W_{AE})
	lb/sec	130	98.3	HIGH COMPRESSOR MAP
P_{T3E}		4.84	2.92	HIGH COMPRESSOR MAP
$P_{T3)\ SURGE}$		5.34	3.51	HIGH COMPRESSOR MAP
		0	0.012	f(REYNOLD'S NUMBER)
		0.859	0.868	COMPRESSOR MAP, ($\Delta\eta_{C_2}$)
IDEAL	°R	1098	1458	K AND K GAS TABLES, f(P_{T_4}/P_{T_3}, T_{T3E})
	°R	1100	1510	f(η_{C_2}, $T_{T_4\ IDEAL}$, T_{T3E})
	Btu/lb	282	372	f(T_{T4})
	Btu/sec	33500	12700	f(h_{T4}, h_{T3E}, W_{AE})
$\overline{\theta}_{T_3}$	rpm	7030	5700	HIGH COMPRESSOR MAP
	rpm	8220	8270	f($N_2/\sqrt{\theta_{T_3}}$, θ_{T_3})
	psia	19.	75	f(P_{T_4}/P_{T3E}, P_{T3E})
W_{AE}		0.0624	0.0566	

2

Table 6. JTF17 Cycle Calculation (Continued)

	Calculation	Symbol	Units	SLTO
49	EIGHTH STAGE SEAL LEAKAGE	$8_{8SI}\ W_{AE}$		0.008
50	BLEED AIR TO DRIVE TURBOPUMP	$TBL\ W_{AE}$		0.01
51	PRIMARY COMBUSTOR AIRFLOW	W_{AP}	lb/sec	275
52	PRIMARY COMBUSTOR FUEL FLOW	W_{FB}	lb/hr	26100
53	PRIMARY COMBUSTOR GAS FLOW	W_{g5}	lb/sec	282
54	PRIMARY COMBUSTOR PRESSURE LOSS	$1\text{-}P_5/P_4$		0.057
55	PRIMARY COMBUSTOR DISCHARGE PRESSURE	P_{T5}	psia	180
56	PRIMARY COMBUSTOR EFFICIENCY	η_B		0.990
57	PRIMARY COMBUSTOR FUEL AIR RATIO	F/A_B		0.0264
58	IDEAL TEMPERATURE RISE	$\Delta T'$	°R	1610
59	PRIMARY COMBUSTOR TEMPERATURE RISE	ΔT	°R	1600
60	TURBINE INLET TEMPERATURE	T_{T5}	°R	2760
61	RATIO OF SPECIFIC HEATS	γ_5		1.29
62	GAS CONSTANT AT HIGH TURBINE INLET	R_5	$\frac{ft - lb_F}{lb_M - °R}$	53.5
62A	HIGH TURBINE EFFICIENCY	η_{HT}		0.878
63	HIGH TURBINE PRESSURE RATIO	P_{T5}/P_{T6}		2.14
64	HIGH TURBINE DISCHARGE TOTAL PRESSURE	P_{T6}	psia	84.1
65	HIGH TURBINE INLET AREA	A_5	ft²	1.11
66	HIGH TURBINE INLET GAS FLOW	W_{gLT}	lb/sec	293
67	LOW TURBINE INLET TEMPERATURE	T_{T6m}	°R	2324
68	LOW TURBINE EFFICIENCY	η_{LT}		0.893
69	LOW TURBINE PRESSURE RATIO	P_{T6}/P_{T7}		2.60
70	LOW TURBINE DISCHARGE PRESSURE	P_{T7}	psia	32.3
71	LOW TURBINE INLET AREA	A_6	ft²	2.27
72	GAS FLOW IN TAILPIPE	W_{gTP}	lb/sec	301
73	TAILPIPE TOTAL TEMPERATURE	T_{T7m}	°R	1890
74	IDEAL TEMP. RISE FOR HEAT RELEASE IN TAILPIPE	$\Delta T'_{TP}$	°R	1390
75	ACTUAL TEMPERATURE RISE	ΔT_{TP}	°R	19
76	TOTAL TEMPERATURE AFTER HEAT RELEASE	T_{T9}	°R	1910
77	TAILPIPE EXIT PRESSURE	P_{T9}	psia	31.7
78	RATIO OF SPECIFIC HEATS IN TAILPIPE	γ_9		1.31
79	GAS CONSTANT IN TAILPIPE	R_9	$\frac{ft - lb_F}{lb_M - °R}$	53.5
80	TAILPIPE FLOW PARAMETER	$\left(\frac{W\sqrt{T}}{P_A}\right)_9$		0.52
81	TAILPIPE JET AREA	A_{JE}	ft²	5.54
82	TAILPIPE PRESSURE RATIO	P_{T9}/P_{AM}		2.16
83	PLUG COOLING AIR	P_{CA}/W_{AD}		0.03
84	DUCT DIFFUSER AIRFLOW	W_{DUCT}	lb/sec	379
85	DUCT DIFFUSER PRESSURE LOSS	$1\text{-}P_4/P_{3D}$		0.05
86	TOTAL PRESSURE AT DUCT HEATER INLET	P_{T4D}	psia	40.5
87	TOTAL TEMPERATURE AT DUCT HEATER INLET	T_{T4D}	°R	7.55
88	DUCT FLOW PARAMETER	$\left(\frac{W\sqrt{T}}{P_A}\right)_{4D}$		0.129
89	DUCT DIFFUSER RATIO OF SPECIFIC HEATS	γ_{4D}		1.39
90	DUCT DIFFUSER MACH NUMBERS	M_{4D}		0.145
91	DUCT HEATER EFFICIENCY	η_D		0.911

17 Cycle Calculation (Continued)

Symbol	Units	SLTO	Cruise	Source
δ_{SSL} W_{AE}		0.008	0.0068	
TBL W_{AE}		0.01	0.01	
W_{AP}	lb/sec	275	109.7	$f(W_{AE}, T_{CA}, T_{BL}, \delta_{SSL})$
W_{FE}	lb/hr	26100	7560	
W_{B3}	lb/sec	282	111.7	$f(W_{AP}, W_{FE})$
$1-P_3/P_4$		0.057	0.070	
P_{T5}	psia	180	70	$f(P_{T4}, 1-P_3/P_4)$
η_B		0.990	0.990	PRIMARY COMBUSTOR SECTION
F/A$_R$		0.0264	0.0192	$f(W_{FE}, W_{AP})$
$\Delta T'$	°R	1610	1150	$f(F/A, T_{T4}, P_{T4})$
ΔT	°R	1600	1150	$f(\Delta T, \eta B)$
T_{T5}	°R	2760	2660	$f(\Delta T, T_{T4})$
γ_5		1.29	1.30	K AND K GAS TABLES $f(F/A, T_{T5})$
R_5	$ft-lb_F$ / $lb_M-°R$	53.5	53.4	f(F/A)
η_{TP}		0.878	0.869	
P_{T5}/P_{T6}		2.14	2.15	
P_{T6}	psia	84.1	32.4	
A_5	ft²	1.11	1.11	TURBINE SECTION
W_{gLT}	lb/sec	293	116	
T_{T6D}	°R	2324	2250	
η_{LT}		0.893	0.880	
P_{T6}/P_{T7}		2.60	2.60	
T_{T7}	psia	32.3	12.5	
A_6	ft²	2.27	2.27	
W_{gFP}	lb/sec	301	118.4	
T_{T7D}	°R	1890	1840	
$\Delta T'_{TP}$	°R	1390	1050	
ΔT_{TP}	°R	19	6	$f(\Delta T'_{TP}, \eta_B)$
T_{T9}	°R	1910	1850	$f(\Delta T_{TP}, T_{T7})$
P_{T9}	psia	31.7	12.3	
		1.31	1.32	K AND K GAS TABLES $f(F/A_{7M}, T_{T9})$
	$ft-lb_F$ / $lb_M-°R$	53.5	53.4	$f(F/A_{7M})$
$\left(\frac{W\sqrt{T}}{P_A}\right)_9$		0.52	0.52	$f(\gamma_9, R_9, P_{T9}, P_{AM})$
A_9	ft²	5.54	5.54	$f[(W\sqrt{T}/P_A)_9, W_{gTP}, P_{T9}, T_{T9}]$
P_{T9}/P_{AM}		2.16	14.8	$f(P_{T9}, P_{AM})$
W_{AD}/W_{AP}		0.03	0.03	
W_{DUCT}	lb/sec	879	216	$f(W_{AD}, \delta_{SSL}, P_{CA})$
P_4/P_{3D}		0.05	0.068	$f(W_{AD3})$
P_{3D}	psia	40.5	21.6	$f(1-P_4/P_{3D}, P_{T3D})$
T_{T4D}	°R	7.55	1120	$f(W_{AD}, P_{CA}, T_{T3D}, W_{AE}, \delta_{SSL}, T_{T4E})$
$\left(\frac{W\sqrt{T}}{P_A}\right)_{4D}$		0.129	0.145	$f(W_{DUCT}, T_{T4D}, P_{T3D}, A_{DUCT})$
γ_{4D}		1.39	1.37	$f(T_{T4D})$ K AND K GAS TABLES
A_{4D}		0.145	0.16	$f(\gamma_{4D}, (W\sqrt{T}/P_A)_{4D})$
		0.911	0.970	AUGMENTATION SECTION

2

Table 6. JTF17 Cycle Calculation (Continued)

	Calculation	Symbol	Units	SL
92	DUCT HEATER FUEL FLOW	W_{FD}	lb/hr	8
93	DUCT FUEL/AIR RATIO	F/A_D		0
94	IDEAL TEMPERATURE RISE IN DUCT HEATER	$\Delta T'_D$	°R	3
95	ACTUAL TEMPERATURE RISE IN DUCT HEATER	ΔT_D	°R	2
96	DUCT HEATER EXIT TEMPERATURE	T_{T5D}	°R	3
97	GAS CONSTANT IN DUCT	R_D	$\frac{ft-lb_F}{lb_M-°R}$	5
98	RATIO OF SPECIFIC HEAT AT D/H DISCHARGE	γ_{5D}		1
99	PRESSURE LOSS FOR DUCT HEATER	$1-P_{TD}/P_{4H}$		0.
100	DUCT EXIT PRESSURE	P_{TD}	psia	3
101	DUCT PRESSURE RATIO	P_{TD}/P_{AM}		2
102	DUCT EXIT TEMPERATURE	T_{TD}	°R	3
103	RATIO OF SPECIFIC HEATS AT DUCT EXIT	γ_D		1
104	DUCT FLOW PARAMETER	$\left(\frac{W\sqrt{T}}{P_A}\right)_D$		0.
105	GAS FLOW AT DUCT HEATER EXIT	W_{gD}	lb/sec	4
106	GAS FLOW AT DUCT EXIT	W_{gDTP}	lb/sec	4
107	DUCT JET AREA	A_{JD}	ft^2	8
108	GAMMA CORR. TO GAS GENERATOR GROSS THRUST	$F_g\gamma_g/F_g\gamma=1.4$		1.
109	GAS GENERATOR GROSS THRUST PARAMETER (γ=1.4)	$(F_g/W_g\sqrt{T_T})_E$		1.
110	GAS GENERATOR IDEAL GROSS THRUST γ=1.4	$F_{gE\ IDEAL}$	lb	19
111	GAS GENERATOR IDEAL GROSS THRUST	$F_{gE\ IDEAL}$	lb	20
112	GAMMA CORRECTION TO DUCT GROSS THRUST	$F_g\gamma_D/F_g\gamma=1.4$		1.
113	DUCT GROSS THRUST PARAMETER ($\gamma = 1.4$)	$(F_g/W_g\sqrt{T_T})_D$		1.
114	DUCT IDEAL GROSS THRUST ($\gamma = 1.4$)	$F_{gD\ IDEAL\ \gamma=1.4}$	lb	41
115	DUCT IDEAL GROSS THRUST	$F_{gD\ IDEAL}$	lb	42
116	TOTAL IDEAL GROSS THRUST	$F_{gT\ IDEAL}$	lb	62
117	SECONDARY-TO-PRIMARY AIRFLOW RATIO	W_s/W_{AD}		0.0
118	GROSS THRUST COEFFICIENT FOR 2% CORRECTED SECONDARY RATIO	C_F		0.9
119	GROSS THRUST COEFFICIENT FOR INCLUDING EFFECT OF TURBOPUMP AIR	C_F		0.9
120	TOTAL GROSS THRUST	F_{gT}	lb	61
121	RAM DRAG	F_r	lb	
122	NET THRUST	F_{SN}	lb	61
123	TOTAL FUEL FLOW	W_{FT}	lb/hr	107
124	THRUST SPECIFIC FUEL CONSUMPTION	$TSFC_n$	lb/hr/lb	1.

cle Calculation (Continued)

ymbol	Units	SLTO	Cruise	Source
	lb/hr	81700	11900	
		0.060	0.0153	$f(W_{FD}, W_{DUCT})$
	°R	3300	990	$f(F, A_D, T_{T4D}, P_{T4D})$
	°R	2960	970	$f(\Delta T', \eta_D)$
	°R	3720	2090	$f(\Delta T_D, T_{T4D})$
	$ft-lb_F$ / $lb_M-°R$	53.6	53.4	$f(F/A_D)$
		1.25	1.32	$f(F/A_D, T_{T5D})$ K AND K GAS TABLES
P_{4H}		0.058	0.015	RAYLEIGH LOSSES
	psia	38.2	24.2	$f(1-P_{TD}, P_{4H}, P_{TJ})$
AM		2.66	29.3	$f(P_{TD}, P_{AM})$
	°R	3630	2060	$f(P_{TD}, T_{T3D}, T_{T3D}, W_{DUCT})$
		1.26	1.32	$f(F/A_D, T_{TD})$ K AND K GAS TABLES
$\Gamma]_D$		0.51	0.52	$f(P_{TD}, P_{AM}, \gamma_D, R_D)$
	lb/sec	402	220	$f(W_{FD}, W_{DUCT})$
	lb/sec	414	226	$f(W_{gD}, PCA)$
	ft^2	8.64	5.67	$f[(W\sqrt{T}/A_D)_D, W_{SLOTD}, T_{TD}, P_{TD}]$
$_D\gamma=1.4$		1.009	1.02	$f(\gamma_0, P_{T9}/P_{AM})$
$_8\sqrt{T_T})_8$		1.510	2.50	$f(P_{T9}/P_{AM})$
AL	lb	19850	12700	
AL	lb	20100	13000	
$\gamma=1.4$		1.02	1.027	$f(\gamma_D, P_{TD}/P_{AM})$
$\sqrt{T_T})_D$		1.67	2.68	$f(P_{TD}/P_{AM})$
AL $\gamma=1.4$	lb	41700	27500	
AL	lb	42500	28300	
AL	lb	62500	41300	$f(F_{FD\ IDEAL}, F_{gT\ IDEAL})$
AD		0.0491	0.0293	NOZZLE SECTION
		0.980	0.999	NOZZLE SECTION
		0.982	1.0012	NOZZLE SECTION
	lb	61300	41300	$f(F_{gT\ IDEAL})$
	lb	0	28500	
	lb	61300	12800	$f(F_{GR}, F_R)$
	lb/hr	107900	19500	$f(W_{FD}, W_{FE})$
	lb/hr/lb	1.8	1.52	$f(W_{FT}, F_{NR})$

2

A. FAN/COMPRESSOR

1. Summary

The selection of the compressor components of the JTF17 engine was strongly influenced by two considerations of importance to the supersonic transport mission. First, to achieve the economic goals of the SST, the compressor components (and engine) must use the most advanced propulsion technology. Secondly, along with optimization of performance, the engine must have the lowest possible degree of development risk and the highest degree of reliability and maintainability. Development risk was minimized by basing the component efficiency to be achieved on the levels already achieved in commercial engines or on data from existing test rigs. Compressor design features which enhance reliability and maintainability were evolved from airline and Mach 3 (plus) J58 engine experience.

The design of the fan/compressor takes advantage of the natural distortion attenuation which arises because the low speed fan rotor is followed directly by the high compressor operating at higher speed. This arrangement, which eliminates the low pressure compressor stages usually following the fan, provides a twofold benefit in that the high speed rotor has good distortion attenuating characteristics by virtue of its relatively high speed and also because it induces incremental velocities at the fan roots which automatically tend to balance the effects of distortion. Matching of the fan elements to produce a distortion attenuating characteristic, even at cruise, has provided the basic distortion tolerance required for high Mach number operation.

Although only a small amount of development work has thus far been undertaken in this early phase of the program, it is notable that a substantial portion of the goals for the production engine have already been achieved.

Both the fan and high compressor have proved to have the flow capacity to meet design requirements including the high flow transonic operating point. High cruise efficiencies, important to the mission economics, have been demonstrated. The high pressure compressor rig is within 1.3% of cruise production goals and already exceeds the prototype requirements at the required surge margin. Fan cruise efficiencies (Build 7) have been demonstrated within 1% of the production engine goal and exceed the prototype requirement at the necessary surge margin.

Testing has indicated high pressure compressor efficiency at sea level take off (SLTO) to be essentially at the prototype level but higher surge margin is needed. These data have shown the problem to be premature root stalling. Preliminary tests, both single stage and of the multistage high compressor, have substantiated the effectiveness of the corrective redesign.

The fan duct efficiency at SLTO is within 1% of the prototype goal and 2% of the production engine value. Improvements in both engine side efficiency and fan surge margin at SLTO are required and it is shown that

CONFIDENTIAL

both may be met by adaptation of the JTF14 fan design which is very similar and has already demonstrated the required performance improvements.

It is noted that all efficiencies are actual rig values and no accounting has been made for losses due to the extensive rig instrumentation or variable vanes. These loss-producing test rig features are not a part of the engine configuration.

2. Fan

a. Fan Design Considerations

Since the fan is an important component in setting the engine envelope, the selection of specific flow (airflow per unit first rotor annulus area) is of major importance. High specific flow, however, while minimizing fan diameter increases the axial Mach number and leads, in general, to lower efficiency. Experience with other P&WA fans, particularly commercial fan engines, was used to provide a balance between these factors (figure 1) and minimize the development risk. These data indicate that the efficiency, herein normalized with the respective values for each compressor at a specific flow of 40 lb/sec ft^2, decays rapidly as the specific flow exceeds 42-43 lb/sec ft^2. Three of the most significant operating points in the mission for which the engine is intended are indicated on this experience curve: (1) SLTO, (2) Transonic (Max flow), and (3) Mach 2.7 cruise. The wide difference between the cruise and maximum (transonic) specific flow is readily evident in this figure and is characteristic of high Mach number operation. (These diverse requirements will be discussed in more detail in the fan/compressor design section of Report B.) The design point was selected to provide the high efficiency needed at cruise without forcing the efficiency during transonic operation onto the sharply falling portion of the band at high specific flows. It can be seen that the JTF17 falls in approximate center of the experience band.

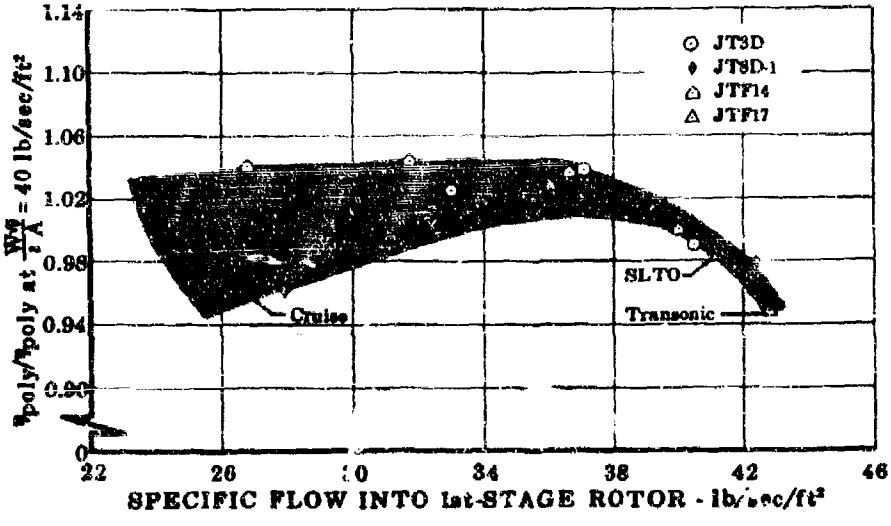

Figure 1. Specific Flow Comparisons

FD 16958
AIIIA

CONFIDENTIAL

The design point efficiency and pressure ratio were primarily based on P&WA experience with the high performance fan designed for the JTF14 engine and used as the basis of the JT9D fan destined for the Boeing 747 aircraft. A 0.6 scale model of this fan had been tested, hence actual data could be used and an unusually high degree of confidence placed in the design goals. Further, since this fan represented a significant increase in tip speed and loading over the earlier commercial engines, it also included advances in technology necessary to maintain attractive economics for the supersonic transport. For comparison purposes the following table presents data from the JTF14 fan tests closely corresponding to the SLTO design point of the JTF17 fan.

COMPARISON OF FAN OPERATION

	JTF14 Rig Data	JTF17 SLTO Design Point
Average Rotor Pressure Ratio	1.72	1.74
Tip Speed	1630 ft/sec	1690 ft/sec
Specific Flow	40.2 lb/sec ft^2	41.2 lb/sec ft^2
Avg. Rotor Adiabatic Efficiency	86.2%	84.8%
Avg. Rotor Adiabatic Efficiency Duct Side	84.8%*	81.2%
Avg. Rotor Adiabatic Efficiency Engine Side	91.4%*	91.1%

*JTF14 data reduced to the 1.30 bypass ratio of the JTF17. Actual values of these efficiencies are higher for the JTF14 bypass ratio.

It should be noted that the JTF14 data are for an early build of an experimental fan rather than a fan which has undergone extensive development. The efficiencies shown for the JTF17 design are for the developed version of this fan. It may be noted that the JTF17 design rotor efficiency goals have been conservatively made less than the already demonstrated efficiency of the JTF14 rig.

The specific flow of the JTF17 fan was increased from that of the Phase II-C design value of 40.1 lb/sec ft^2 (approximately equal to JTF14) as was the tip speed because testing of the Phase II-C fan rig proved that the high flow, high tip speed performance of this fan exceeded expectations. These data are discussed in later paragraphs of this section.

The JTF14 is also undergoing development, in a slightly modified form, and will be used in the JT9D engine. The similarities of these two fans provide a significant benefit to both development programs because of the interchange of information possible.

The JTF17 production engine fan performance goals are shown on the compressor maps in figures 2 and 3. Figure 2 indicates total fan airflow vs duct side fan pressure ratio and efficiency and figure 3 indicates engine side airflow vs engine side fan pressure ratio and efficiency. The requirements of the prototype engine fan differ from those of the production engine primarily in that the efficiency goals are relaxed at no change in fan total flow. The respective design efficiency goals are noted in the following table for Cruise and SLTO operation.

CONFIDENTIAL

JTF17 Fan Design

	Prototype Engine		Production Engine	
	Cruise	SLTO	Cruise	SLTO
Duct Side Efficiency	78.7%	77.7%	80.8%	78.8%
Engine Side Efficiency	86.0%	85.0%	89.8%	88.8%

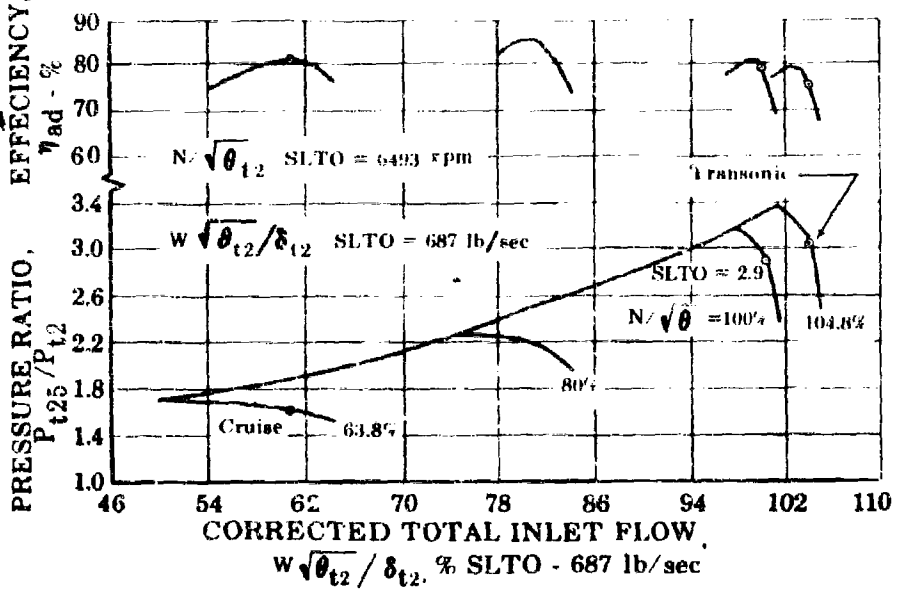

Figure 2. JTF17 Fan Characteristics - Duct Side FD 16959 AIIIA

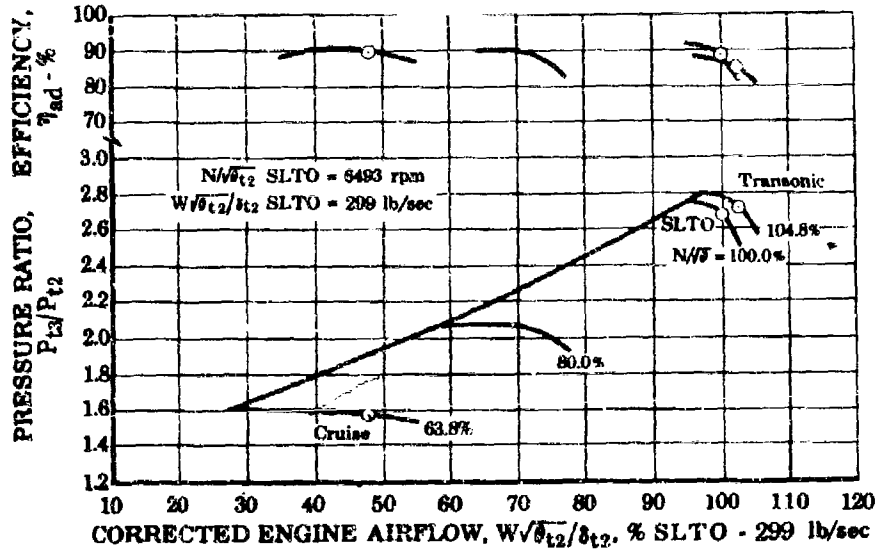

Figure 3. JTF17 Fan Characteristics - Engine Side FD 16960 AIIIA

CONFIDENTIAL

b. Inlet Distortion Considerations

The fundamental internal aerodynamics of a fan stage and a turbojet compressor stage are identical; the distinction being indicative of the engine cycle rather than any basic aerodynamic difference within the turbomachinery. As a consequence, the distortion tolerance and performance characteristics of both fan and jet stages are similar and any differences between the distortion tolerance of the turbofan and turbojet engine arise from the influence of the cycle on the matching of the stages. The JTF17 benefits in this respect both because of the versatility associated with the dual discharge of the fan and because the two-rotor arrangement permits a rotor speed differential to exist between the fan and compressor. These factors are discussed in the following paragraphs.

An inherent advantage of the fan cycle arises because of the fan's dual discharge flow path. The bypass ratio (duct flow/engine flow) increases from 1.3 at SLTO operation to 1.88 at cruise. The differential in bypass ratio is analogous to interstage compressor bleed in that both enable the total flow in the front stages to be increased, preventing stall in these stages and improving distortion tolerance. The turbo-fan, however, utilizes this flow in the propulsion cycle while conventional compressor bleed is not beneficially recovered.

The dual nature of the discharge also provides a benefit when consideration is given to the effect of perturbations, generated within the engine, on the operation of the front stages. In the case of a turbojet, a flow perturbation due to a factor such as a primary fuel flow transient will effect the flow in the front stages on a one-to-one basis as dictated by mass flow continuity in the single flow path. The same perturbation in a turbofan primary burner will similarly effect the high pressure compressor. However, the flow through the front stages (fan) will change by a much lower percentage because the engine side flow represents less than one half of the total flow through the fan. Since a smaller surge margin is thus needed to insure against instability triggered internally, a greater amount is available to provide inlet distortion tolerance. The duct side of the fan, by virtue of its higher rotational velocity, provides a high degree of distortion attenuation and is a stabilizing influence on both internally and externally generated perturbations.

A third advantage attributable to the dual discharge flow path of a fan engine is the ability to maintain a higher pressure ratio at the tip (duct side) than at the root (engine side). This permits the high work potential of the tip to be realized without a commensurate increase at the root which would force it to operate close to stall and reduce its distortion tolerance. This aspect of distortion tolerance is discussed more extensively in succeeding paragraphs of this section.

CONFIDENTIAL

The effect of these advantages of the fan cycle on the distortion tolerance is shown in figure 4 by comparison of several operational fan and jet engines. The index used to depict distortion sensitivity is the ratio of distortion tolerance to surge margin. Distortion tolerance is defined as the value of the parameter $(P_{t\ avg} - P_{t\ min})/(P_{t\ avg})$ that will make the surge line and operating line coincident at a given percent of the design airflow. Since engines may be matched with different surge margins, the distortion tolerance is divided (normalized) with the surge margin. The resultant parameter may be viewed as the distortion that will lower the surge margin by one unit. The jet engines represented are the J57, used in the F-101, and the J75 engine powering the F-105 aircraft. The fan engines are the TF30-P1 used in the F-111 and the JT8D and TF33 powering the Boeing 727 and B-52H aircraft. As indicated by the shaded bands of this figure, the turbofan engines have a greater distortion tolerance parameter by a considerable margin; almost 2 to 1. These data, which were obtained by impressing the same severe distortion pattern (180-degree low pressure, 180-degree high pressure) on the various engines, are a particularly valid comparison because these compressors were designed using similar methods and criteria; the major difference is the engine cycle. The absolute value of the distortion tolerance parameter is dependent upon, and controlled by, the matching of the fan/compressor stages, particularly the initial stages of the engine. As is discussed in later paragraphs of this section, these stages may be matched to increase or decrease the distortion tolerance, as needed to tailor the compressor to both the inlet and aircraft mission. The proper balance between inlet generated distortion and engine distortion tolerance must be determined by economic and safety considerations during the early phases of compatibility testing. The above data for turbofan and turbojet engines reflect the comparative advantage of the turbofan cycle when similar design criteria are employed, rather than an absolute limit for either cycle.

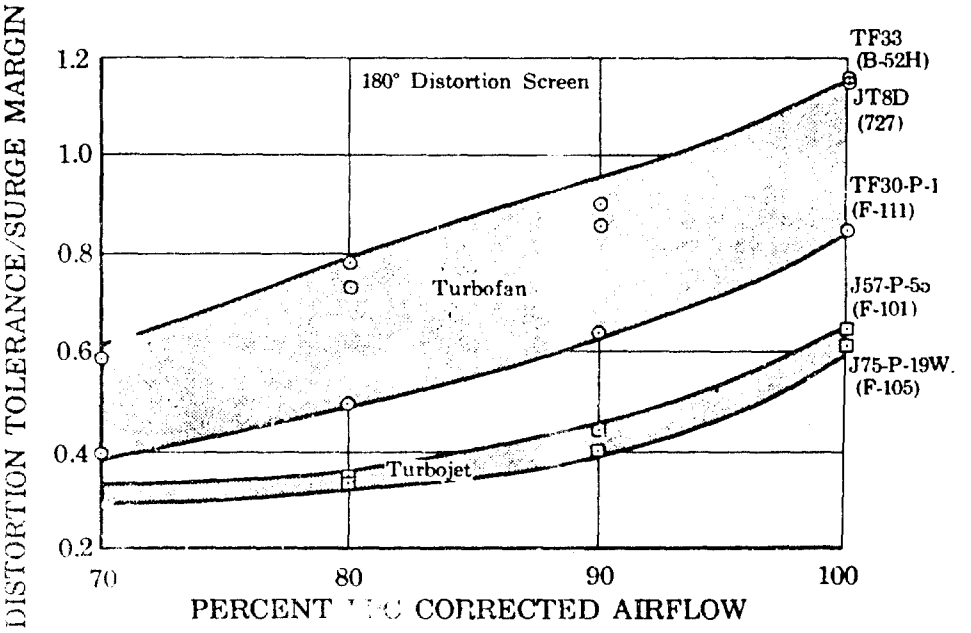

Figure 4. Comparative Effect of Inlet Distortion on Turbofan and Turbojet Engines

FD 17918
AIIIA

The design and stage matching of a fan/compressor for either a turbofan or turbojet engine requires the proper balance between performance and distortion tolerance to be achieved and consequently often involves the introduction of measures which compromise performance. The particular fan/compressor rotor arrangement selected for the JTF17 provides a unique feature which increases distortion tolerance without compromising performance.

This feature is the placement of only the fan on the low pressure (N_1) rotor. This differs from the arrangement used on current turbofan engines for low (subsonic) Mach number aircraft. These engines require a higher cycle pressure ratio for good fuel consumption and consequently have low pressure compressor stages as well as fan stages on the low pressure rotor. At high Mach numbers (above 2.0) the corrected rotor speed of any compressor is significantly reduced, tending to move the operating point of the initial stages toward stall and thus to reduce their distortion tolerance. As a result, the fan roots and front end stages of the low pressure compressor are prone to trigger the distortion induced surge. The JTF17 design has the high compressor immediately downstream of the fan with no intervening low pressure compressor stages. The high pressure compressor (HPC) rotates at 80% of its design corrected rotor speed at cruise flight conditions as opposed to the 65% at which the low pressure rotor rotates. At these higher corrected speeds the front stages of the HPC are naturally less sensitive to distortion and consequently reduce rather than trigger distortion induced instability. Furthermore, since the distortion attenuating stages of the high pressure compressor alter the static pressure field upstream to induce flow into regions of low total pressure (high distortion) the attenuating high compressor stages will, in the presence of inlet distortion passing through the fan, induce flow and thereby increase the distortion tolerance of the fan roots. In its gross effect, the high pressure compressor requires the fan to provide a specific value of exit corrected airflow. If distortion tends to force the fan root to lower airflow and higher pressure ratio, thus tending to cause surge, the high pressure compressor automatically induces more flow by dropping the static pressure and provides the compensating mechanism needed to keep the fan stable.

As has been described in the previous paragraphs, it is the front stages which must be particularly designed to provide good distortion tolerance. During the design phase, only the most general and incomplete knowledge of the type and extent of the expected inlet distortion is available. It is consequently not practical to undertake a detailed and sophisticated treatment of the problem; however, since it is inevitable that a supersonic inlet will produce a distorted exit profile, the design must include a basic bias toward inlet distortion tolerance.

As development proceeds with the selection of an airframe contractor and further definition of the inlet design, more extensive information on the distortion will become available making it possible to start fan component testing with simulated distortions. Detailed measurements taken

during compatibility tests (ref: Inlet/Engine Compatibility, Report E) will then make it possible to determine if modifications are needed to provide additional tolerance to accommodate the particular distortion pattern encountered. This phase of the testing is particularly important since it provides data early during Phase III when the design is relatively fluid. In addition to the obvious benefit of providing, if necessary, modifications to tailor the fan to the particular distortion of concern, it is also possible to reduce the margins in regions where the basic bias of the design to distortion has provided more tolerance than is necessary. In these regions the performance may be increased by elimination of the excessive tolerance margin.

Basic distortion tolerance is built into the design by consideration of the effect of distortion on the matching of the compressor stages. During passage of a compressor blade through a region of low total pressure the inlet velocity will be reduced and the angle of attack relative to the blade increased, tending to stall the blade. The natural effect of the more highly loaded blade will be to induce more flow and thus mitigate the effect of the low inlet total pressure; however, this tendency to maintain a constant inlet corrected flow is only a partially compensating reaction. As a result the blade must be expected to undergo reductions in the inlet velocity (flow) due to the low total pressure, tending to stall it as shown below in figure 5. The undistorted operating point for the stage is indicated as point "A" and the operating point while in the region of low total pressure by point "B".

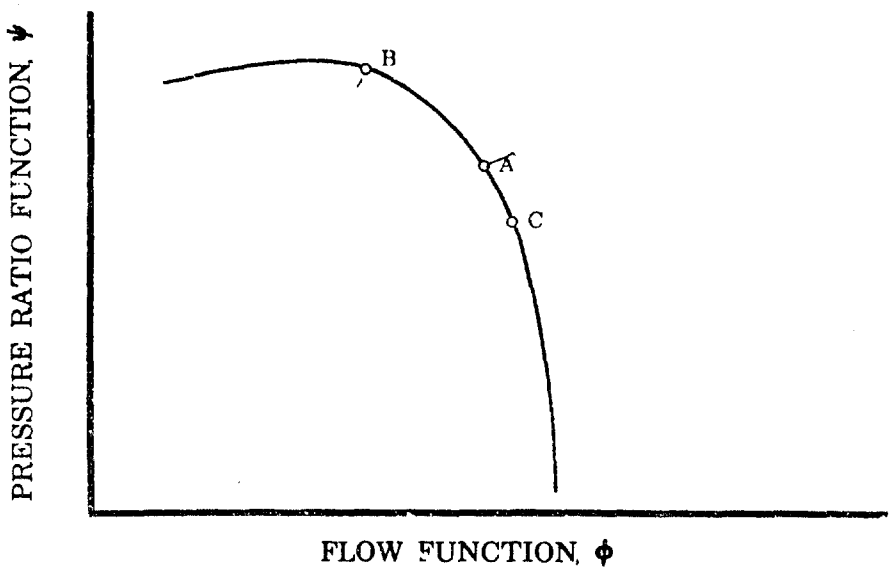

Figure 5. Stall Margin

FD 17529
AIIIA

Dependent upon the stabilizing influence of other parts of the compressor, such a shift in operating point may cause instability and surge. By designing the stage to operate at point "C" rather than "A" two desirable affects are achieved. First, the flow spread between the design operating point and the "surge" point is increased, allowing for a greater local inlet depression before the stage becomes unstable.

Secondly, the rate of change of pressure ratio with decreasing flow is increased. This means that the tendency for the compressor to locally induce flow into the region of low total pressure and to locally cause an increased pressure rise tending to make the flow leaving the stage in a less distorted pattern is enhanced. This effect often leads such a stage to be termed "distortion attenuating". The effect of achieving this condition as well as the opposite, "distortion amplifying", is shown in figure 6.

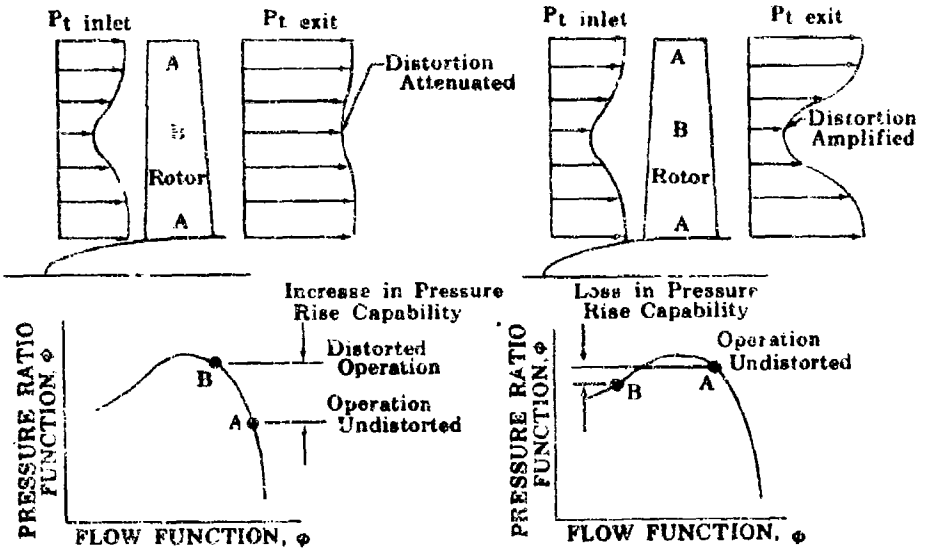

Figure 6. Distortion Attenuating and Amplifying Characteristics

FD 17528
AIIIA

Two cases are depicted in figure 6. On the left, a stage matched to be distortion attenuating; and on the right, one that will amplify the distortion. It is assumed that both are subjected to the identical distortion pattern, consisting of an inlet pressure depression at approximately midspan. The operating points representative of the sections outside and within the depression are depicted as A and B respectively. In the case on the left, the section of the blade within the depression (B) is seen to operate at a higher pressure ratio than those outside (A).

Thus, the total pressure profile leaving such a stage will be more uniform (less distorted) than that entering; hence, the term "distortion attenuating" is applied. If this stage were matched to point A in the right hand pressure ratio characteristic, the effect of the distortion would be to cause a lower pressure ratio (B) to be produced by the midspan section. The effect on the profile leaving would be to increase the inlet depression as shown, amplifying the distortion.

Provision for achievement of stage designs capable of "basic" distortion attenuation requires great care in high performance low hub-tip ratio compressors because of the large difference between the tip and root rotational velocities. This difference makes it relatively easy to provide the pressure ratio reserve needed for stability at the tip but tends

to prevent the attainment of this characteristic at the root. The concept of the "warped" fan, that is, the inclusion by P&WA of a fan cycle having a higher design pressure ratio on the duct side than on the gas generator side, makes possible a new means of satisfying the demands for high performance while maximizing the distortion attenuating characteristics of the entire blade. In this manner, the tip, running at high speeds, is allowed to produce the high pressure ratio for which it has ready capability with good attenuation. The root sections are not required to provide a balancing pressure ratio, for which they have poor capability, because the flow path is divided in the fan engine. The root, consequently, is matched to the lower pressure ratio, thus increasing its attenuating characteristic.

It may be noted from the foregoing discussion that the attenuating effect of a stage on inlet distortion is measured by the capacity of the stage to locally produce a compensating change in pressure ratio. The rate of change of the pressure ratio coefficient with the flow coefficient, $(-\partial\psi/\partial\phi)$ provides a ready index to the attenuation-amplification characteristic of the stage. A value of zero indicating no change in pressure ratio for a change in flow represents the neutral point, neither amplifying nor attenuating. Positive values indicate that a rise in pressure ratio accompanies a drop in flow, an attenuating characteristic, negative values indicate an amplifying characteristic. Figure 7 indicates the values of this index when applied to the JTF17 first rotor operating at cruise and SLTO. The positive values in all cases indicate the achievement of an attenuating characteristic.

Actual data from TF30 fan-low pressure compressor tests are presented in figure 8. It may be noted that the inlet distortion pattern is a severe circumferential one consisting of a 180-degree low pressure region. The nonuniformity at the fan discharge (duct side) is shown to be essentially a radial gradient, typical of a compressor discharge flow. The circumferential inlet distortion pattern is virtually completely attenuated. At the exit of the low pressure compressor the circumferential distortion has also been eliminated and the nonuniformity is the normal radial mode.

The distortion tolerance of a fan or compressor has often been judged using the undistorted surge margin as the criterion. Experience with many engines, including the J58 and TF30, has proved that this criterion is not completely adequate. The reason is that the distortion tolerance and surge margin of a multistage compressor may be controlled by differing portions of the compressor as the rotor speed, bleed rate, stator position, etc. are varied. As an example, if a compressor is being operated at a rotor speed at which the rear stages are most influential in causing the surge and the front stages are strongly distortion attenuating, inlet distortion will be eliminated or substantially reduced before reaching the sensitive stages and thus little change will be noted in the surge line. In a region of operation where the front stages are sensitive, the same amount of distortion may greatly lower the surge line.

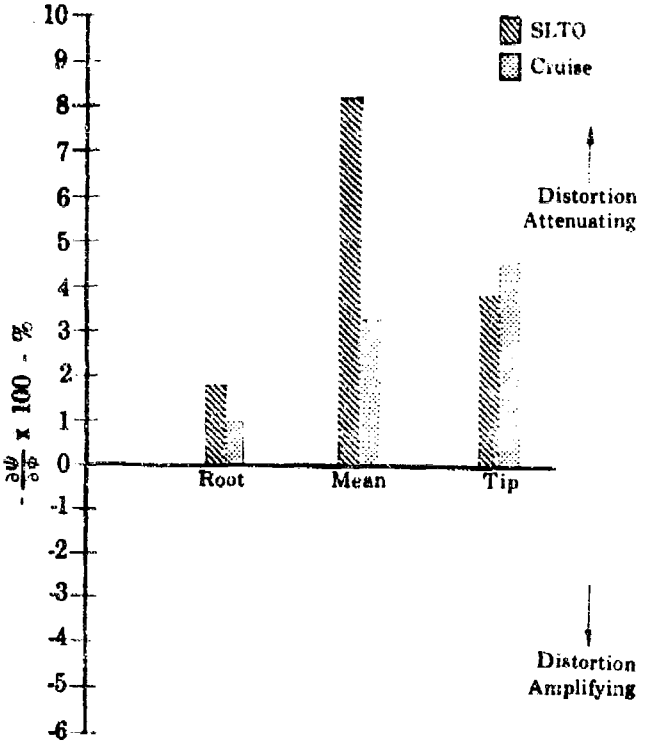

Figure 7. JTF17 Fan Distortion - Reaction Characteristics

FD 16961
AIIIA

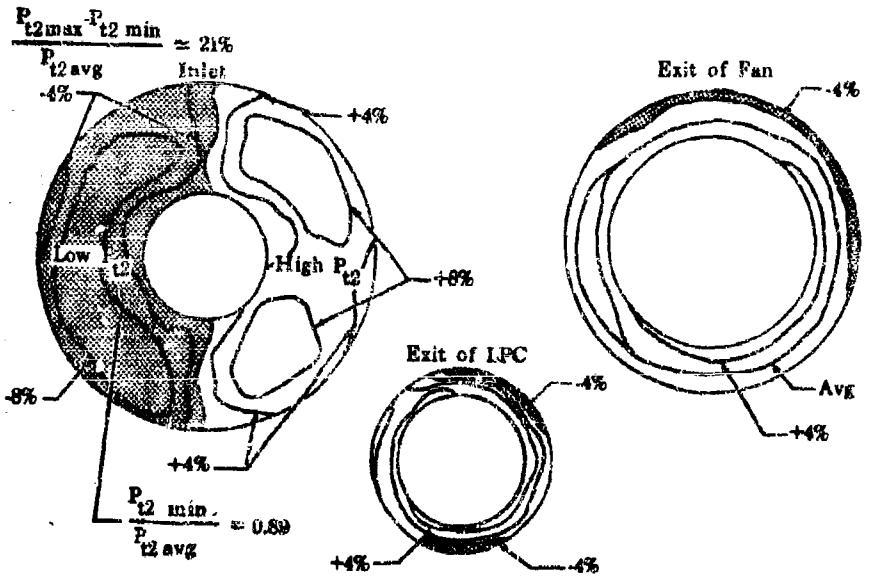

Figure 8. TF30 Turbofan Distortion Test of Fan/LPC Combination - 180-Degree Inlet Distortion Screen

FD 17855
AIIIA

CONFIDENTIAL

Generally, the overall effect of the distortion, which must be viewed within the context of its spacial and transient nature, is determined by how the low energy zones affect the sensitive regions of the compressor at each operating point. Introducing the distortion into a region of the compressor having great stability will produce only a small effect on the surge line; while when introduced into a less stable region, the same degree of distortion may exhibit a large adverse reaction on the compressor.

The usefulness of surge margin as an index of the allowable internally generated compressor perturbations is unchanged by distortion. However, the surge margin must be determined in the presence of the operational inlet distortion.

c. Phase II-C Fan Performance

During Phase II-C exploratory tests were conducted on a variety of 0.6 scale two stage transonic fans which are similar to the fan designed for the JTF17 engine. The purpose of this test program was to investigate the effects of critical geometric variables on the aerodynamics of this type of high performance fan and thereby to determine the development path which will require the least effort during Phase III. These exploratory tests included investigations of variables such as: stage work and radial work distribution, radial incidence angle distribution, splitter location and shape, shroud location and shape and blade solidity. Concurrently, the tests provided the assurance that the fan performance was acceptable for the demonstration engines run as part of the Phase II-C program.

The build 5 fan data are presented in this section since they are representative of the Phase II-C fan performance. The data are discussed relative to the design goals of the 650 lb/sec engine fan. These goals differ from those of the JTF17 engine since the latter were altered to reflect performance increases attainable through increases in airflow and pressure ratio at subsonic flight Mach numbers. Part of this increase is achieved by increasing the fan outside diameter without changing the case diameter. The remainder resulted from taking advantage of the excellent high specific flow performance noted during the Phase II-C testing. The principal objectives of the 650 lb/sec fan are tabulated below.

650 lb/sec Fan Objectives

	SLTO	Cruise
$W\sqrt{\theta_2}/\delta_2$ Total	650	392
Bypass Ratio	1.3	1.84
Duct Side Pressure Ratio	2.7	1.54
Engine Side Pressure Ratio	2.5	1.50
Duct Side Efficiency	81%	79%
Engine Side Efficiency	90%	89½%
Corrected Rotor Speed	6160 rpm	4000 rpm

The split discharge from the fan provides a degree of control freedom, not usually encountered in turbojet engines, that is directly related to the versatile high Mach number airflow scheduling available to the augmented turbofan. This feature also makes the presentation of fan data more complex.

The overall performance data for the fan are presented together with the respective 650 lb/sec goals (figures 9 and 10) in the form of compressor maps. These curves are similar to the higher airflow JTF17 compressor maps discussed previously and show:

(1) Total airflow versus the duct side fan pressure ratio and
(2) Engine side airflow versus engine side fan pressure ratio.

At the SLTO airflow and duct pressure ratio the required fan speed is noted to be 1% lower than the design estimate. The duct adiabatic compression efficiency is within 3 efficiency points of the goal and the 5% surge margin is ample for safe test stand engine operation. A large amount of operational experience with the J58 engine at the same (5%) SLTO surge margin has been accumulated. Matching the inner or engine section of the fan to the high pressure compressor SLTO design flow shows that a bypass ratio of 1.37 has been attained at an efficiency of 80%. This fan was tested with an exploratory splitter intended to increase the bypass ratio. The above value reflects this increase and indicates the relative ease with which this adjustment in flow split may be made.

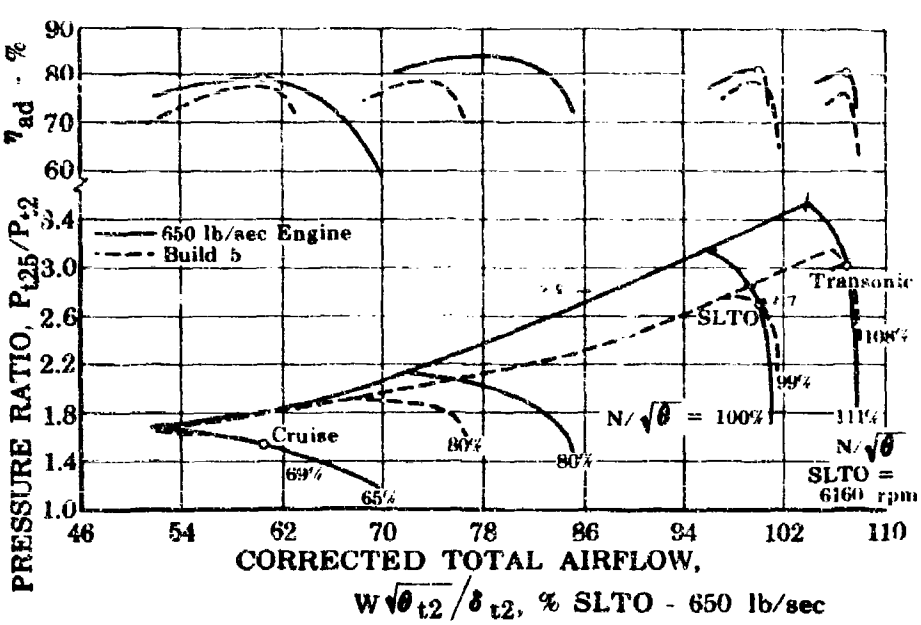

Figure 9. Fan Rig Build 5 Performance Relative to 650 lb/sec Engine Goals - Duct Side

FD 16972
AIIIA

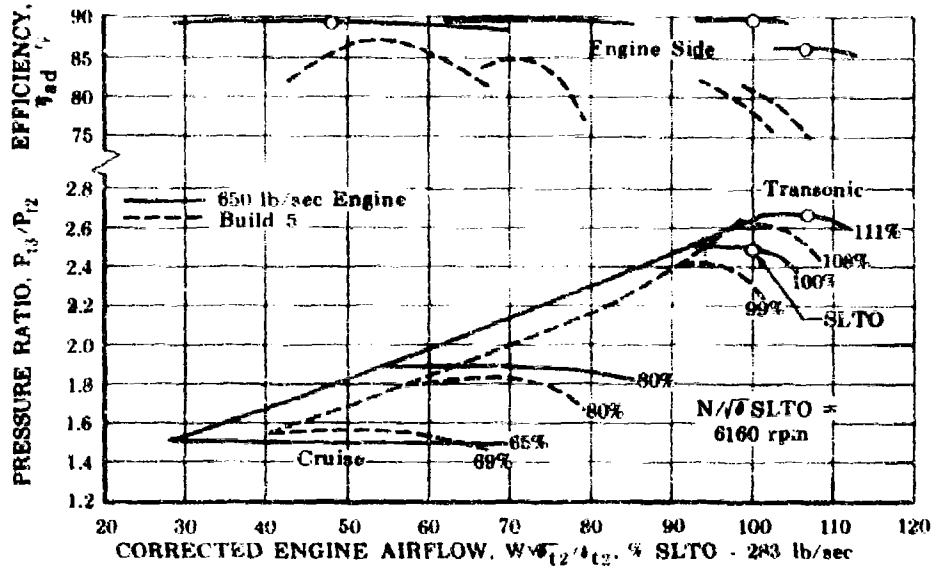

Figure 10 Fan Rig Build 5 Performance Relative to 650 lb/sec Engine Goal

FD 17537
AIIIA

At the cruise design airflow and duct side fan pressure ratio, the fan matched at a rotor speed 6% higher than the design estimate. The surge margin at this important point is almost identical with the design goal and the efficiency within 3-1/2 points of the production engine goal. The engine side of the fan matches to the high pressure compressor cruise design airflow at a pressure ratio 0.06 greater than design. The efficiency is 3½ points less than the cruise design point, however, excellent control of the cruise efficiency was demonstrated during testing of a later fan build (Build 7). This test (Build 7) was performed to explore the effect of lowering rotor incidence, particularly at the root, and peak efficiencies on both sides of the fan exceeded the cruise efficiency goal by over one point.

Operation at transonic flight Mach numbers is important because of the critical airframe drag. This fan demonstrated excellent high specific flow characteristics in that the required transonic flow and duct pressure ratio, the highest required for the mission, were achieved at a rotor speed 3% less than the design estimate. Furthermore, the efficiency at high specific flow exceeded the estimate based on the experience curve (figure 1) previously described. The latter data are presented together with the data from this test in figure 11. It may be noted that the efficiency of this build reaches a maximum at about 41 lb/sec ft^2, much higher than the other fans. Because of this characteristic and the favorable speed-flow characteristic already noted, the SLTO design specific flow of the JTF17 engine was increased from the 40.1 value of the Phase II-C design to 41.2. The 6% duct surge margin at this condition is also adequate for experimental purposes and perhaps for flight testing. As previously noted, operation of the J58 engine with 5% SLTO surge margin has proven satisfactory. The effect of inlet distortion on the surge line in this region is not expected to be large because the fan is operating with its greatest distortion attenuating capacity. In addition, the distortion produced by the inlet diffuser is expected to be near its minimum.

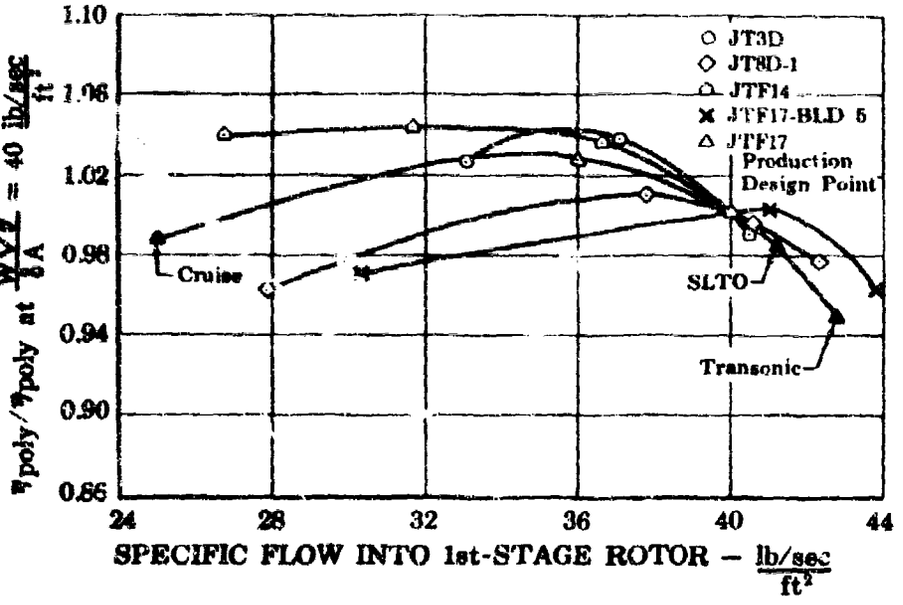

Figure 11. Specific Flow Comparisons

FD 16964
AIIIA

The excellent flow capacity of the fan is, in part, due to results of the exploratory tests conducted early (builds 1 and 2) in Phase II-C. These data showed that the cross-sectional shape and size of the shrouds had an important (4%) effect on the flow capacity.

The SLTO design speed stage performance of the individual two fan rotors is shown in figure 12 along with the 650 lb/sec engine SLTO design points. These data indicate that the first rotor pressure ratio characteristic closely matches the goal and does not exhibit a peaking tendency; however, its efficiency is approximately 4 points less than its goal. The second rotor pressure rise characteristic has exceeded the design point. The efficiency of this stage is seen to be at or slightly above its goal. Modifications to the first rotor to improve its performance will be discussed later in this section.

d. 650 lb/sec Fan Performance Relative to JTF17 Production Design

Although the 650 lb/sec fan design goals are not identical with those of the JTF17 production design, the performance already demonstrated does provide a useful base line. In this comparison, figure 13 and 14, the flow of the 0.6 scale fan rig tested during Phase II-C was scaled to the engine size (total fan airflow of the 687 lb/sec) in proportion with their respective first rotor annulus areas.

(1) Flow Rate

As has already been noted, the important SLTO and Transonic design specific flows for the JTF17 engine were set equal to the already demonstrated fan rig values. A high degree of confidence is thus placed on their achievement.

CONFIDENTIAL

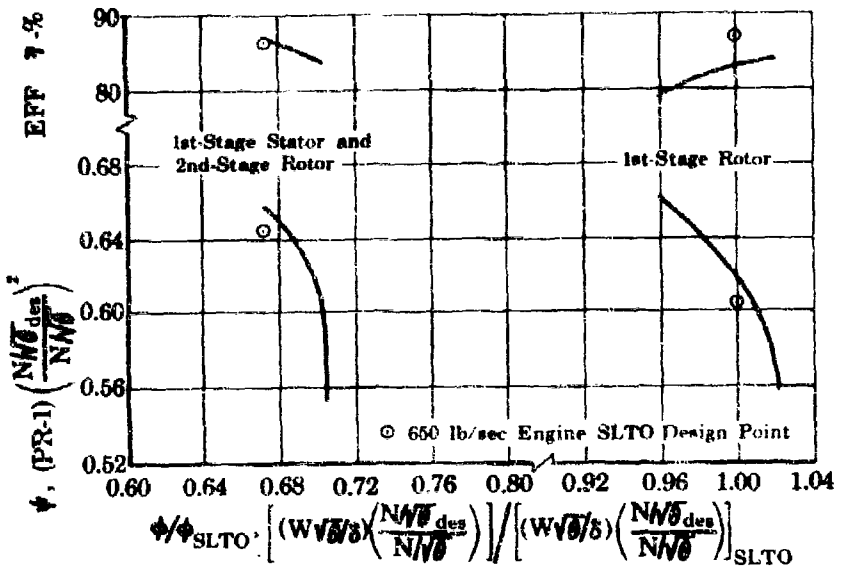

Figure 12. Fan Stage Performance - Build 5 FD 16965
AIIIA

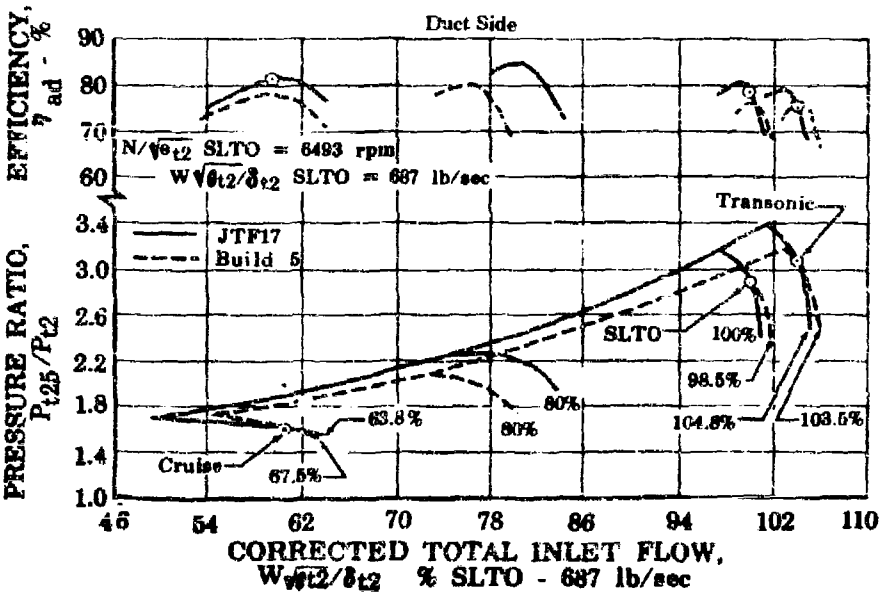

Figure 13. Fan Rig Build 5 Relative to JTF17 Goals FD 16966
AIIIA

CONFIDENTIAL

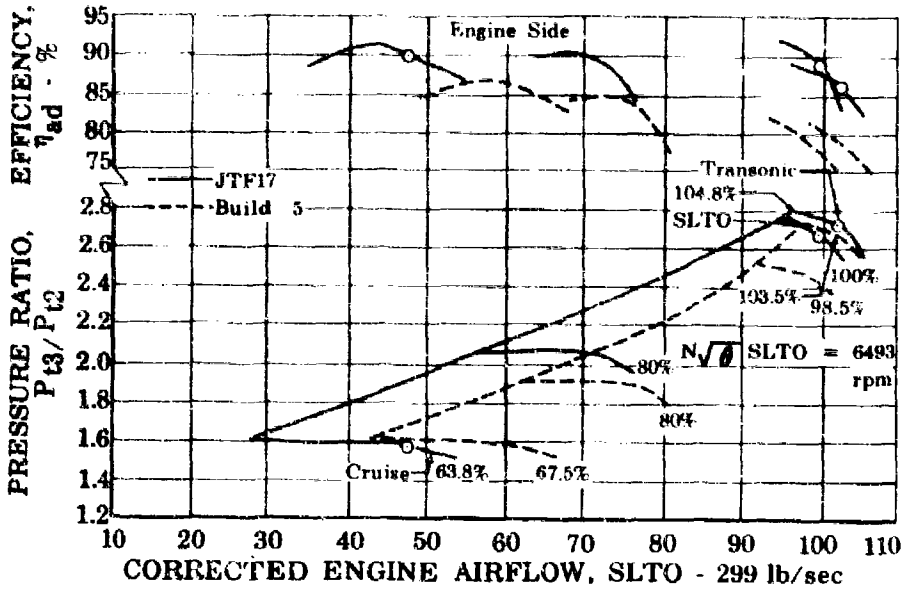

Figure 14. Fan Rig Build 5 Relative to JTF17 Goals FD 16967
AIIIA

(2) Bypass Ratio

The bypass ratio requirements of the engine are substantially unchanged from 650 lb/sec engine levels. As has been noted earlier, rig testing has shown that minor modifications to the fan flow splitter can provide substantial changes in bypass ratio. The already demonstrated variation of from approximately 1.2 to 1.4 brackets the engine SLTO design value of 1.3.

(3) Surge Pressure Ratio

The SLTO design point of the JTF17 fan differs from that of the 650 lb/sec fan in both speed and pressure ratio as shown in the following table:

Comparison of SLTO Fan Design Points

	Duct Side Pressure Ratio	Engine Side Pressure Ratio	Rotor Speed
650 lb/sec	2.7	2.5	6160
JTF17	2.90	2.68	6493

Scaling of the 650 lb/sec engine pressure rise to higher rotor speed using the ratio of the squares of the rotor speed yields the following comparison:

SLTO Fan Design Points at Normalized Rotor Speed

	Duct Side Pressure Ratio	Engine Side Pressure Ratio
650 lb/sec	2.88	2.66
JTF17	2.90	2.68

CONFIDENTIAL

It may be noted above that the major part of the required increase in pressure ratio is accounted for by the higher rotor speed.

It becomes apparent then, that a major consideration is the achievement of not only the increased fan work needed at SLTO design, but of the required duct surge pressure ratio (3.14). It has been shown (figure 12) that the first rotor has demonstrated greater pressure ratio capability relative to its design point than has the second stage. Further, increases in first rotor work have been demonstrated with two different rotors during tests of builds 3 and 7. These factors suggest that the desired duct surge pressure ratio may best be attained by increasing the loading of the first rotor. The pressure-flow characteristics of the build 5 fan are presented in figure 15 with the revised SLTO design points normalized to the rig speed.

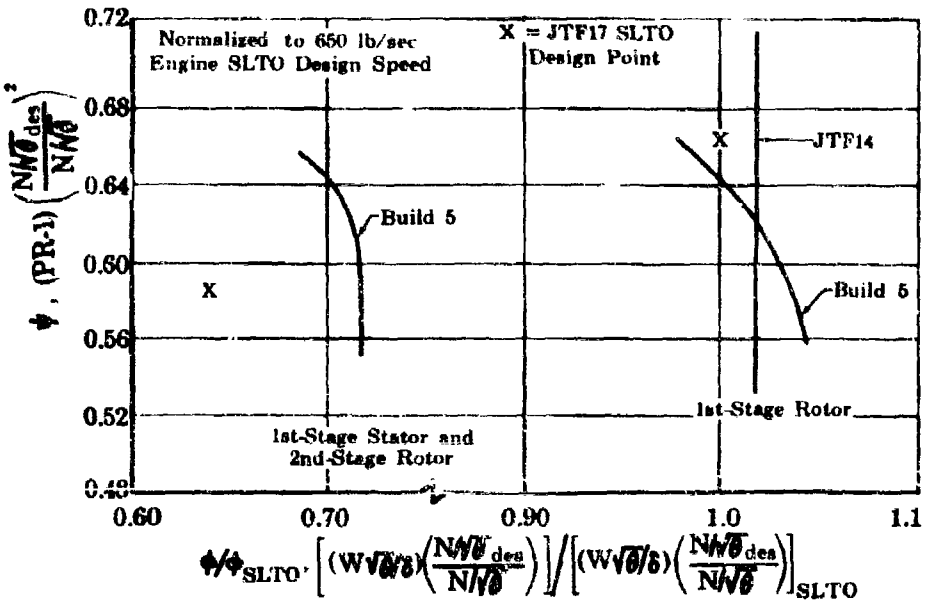

Figure 15. Fan Stage Performance Rig Build 5 and JTF14

FD 16968
AIIIA

As in the previous discussion where individual stage performance was compared with 650 lb/sec engine goals it is shown that the second stage (first stator-second rotor) has demonstrated the required design pressure ratio coefficient (0.585). Further, at the design pressure ratio, the stage has additional pressure ratio to provide surge margin for the fan. The flow capacity is larger than required as evident by the rightward displacement of the data from the design point. The first stage lacks the needed surge margin and actually has a peak pressure rise (ψ) slightly less than design. The JTF14 first rotor actual test data, also shown, on the scale of the JTF17 (in figure 15) does have the ability to attain the design point with additional capacity to provide surge margin.

The similarities in the operational requirements of these two rotors have already been noted (ref. Section III, Part A.2.a).

CONFIDENTIAL

The duct surge pressure ratio has been estimated for a fan combining the characteristics of these two available elements; namely, the JTF14 first rotor and the existing second stage. Since the bypass ratio of the JTF14 was very different from that of the JTF17 it was necessary to account for this in reducing the radial pressure ratio data of the JTF14. The resultant duct side pressure ratio characteristic is shown in figure 16 along with the duct side characteristic of the build 5 second stage (including the fan exit guide vane). The characteristics have been matched to the JTF17 production engine design flow and to each other. The duct speed line and surge point mathematically generated from these stage data is shown on a portion (SLTO) of the JTF17 design map in figure 17. It is shown that these two experimental stages have combined to provide the characteristics needed to achieve the SLTO design pressure ratio of 2.90 with the required surge margin.

It has been shown that the surge margin of the build 5 fan at cruise was almost identical with the design goal. The small increase in surge margin desired for the JTF17 design is expected to accompany the modifications discussed above in connection with the attainment of the SLTO surge margin.

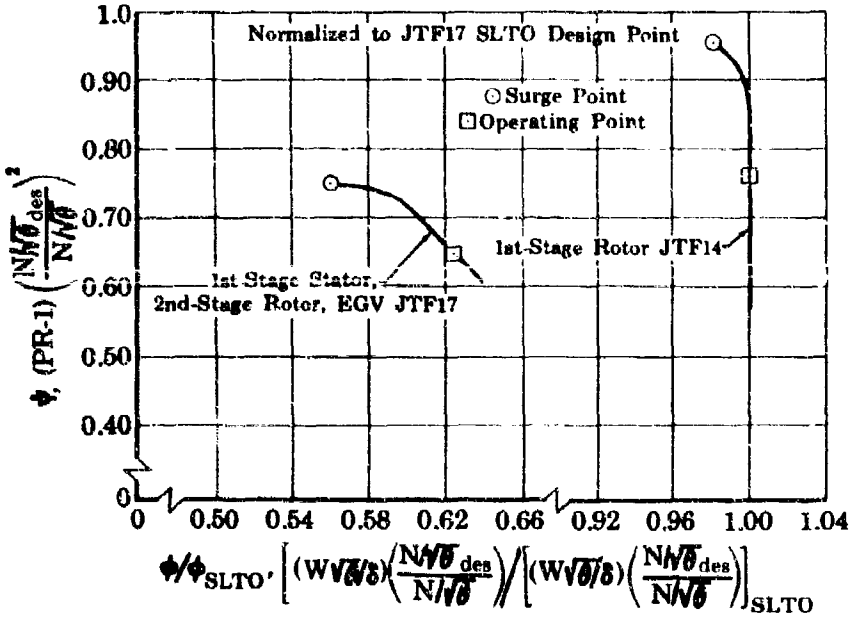

Figure 16. Fan Stage Characteristics - Duct

FD 16969
AIIIA

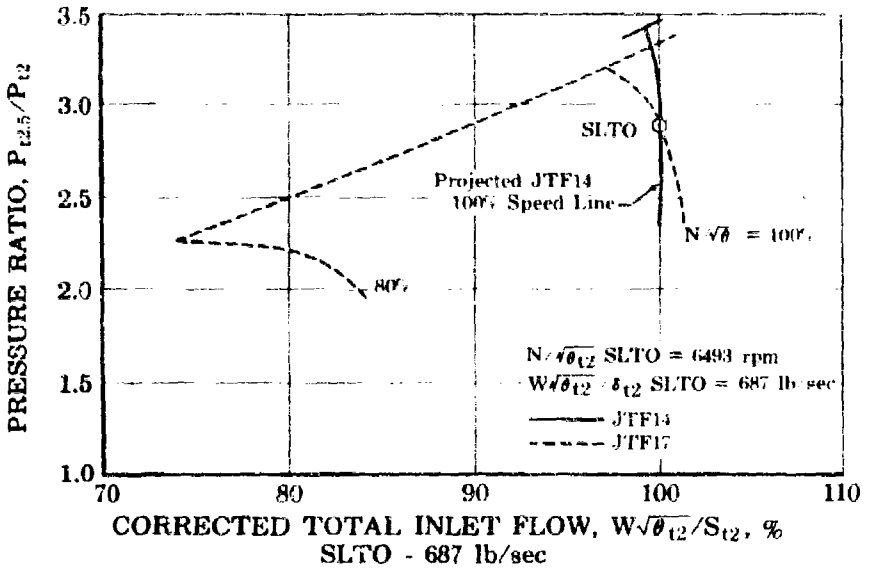

Figure 17. JTF17 Goals and Projected JTF14 Speed Line

FD 16970
AIIIA

(4) Efficiency

Build 5 of the fan rig has demonstrated the duct efficiency required for the production engine within 2% at SLTO and slightly exceeds that of the transonic operating point. High root efficiency has also been obtained from the JTF14 fan rotor which is similar to the JTF17 with the principal exception of the gap/chord ratio. This similarity has been noted earlier in this section and pertinent design criteria, including the efficiency data, tabulated for comparative purposes.

Because of the excellent demonstrated performance of the JTF14 fan, an experimental rotor for the JTF17 has been designed using the same principles. Investigation of the performance of this rotor is expected to begin late in Phase II-C or early in Phase III.

Throughout any discussion of fan (or compressor) rig performance it must be remembered that the rig and engine are not identical machinery. The rigs are heavily instrumented and have added structural members. The fan rig from which these data were generated contains in addition to twelve structural inlet vanes (not part of the engine design), 6 inlet pitot-static probes, 78 kiel type total pressure and temperature instruments on the vane leading edges which increase losses. Further inefficiency is generated by the variable vanes in both stages (64 first stators, 77 second stators, and 154 fan exit guide vanes) which cannot have the engine type airfoil at either their roots or tips because of the necessary clearance to allow movement and expansion. No accounting has been included for these factors although experience has shown engine-rig differences in the range of 1.7 to 4.5 percent in efficiency. The exact value can only be determined by testing of the aerodynamically clean engine configuration.

The cruise efficiency, highly important in obtaining low TSFC, has been found to be sensitive to the rotor incidence angle, based on tests of the 7th fan build. This build included rotors with overcambered leading edges, particularly at the root. This efficiency rise is shown in figure 18 relative to the production engine design. As shown on figure 18 the cruise efficiency was to within 1% of the goals and the peak efficiency actually exceeded the JTF17 goals.

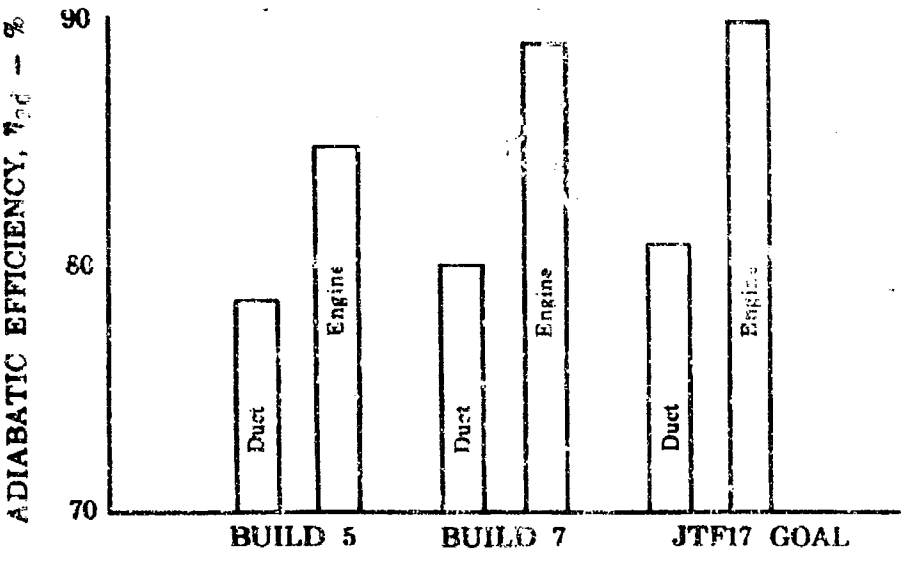

Figure 18. Comparison of Fan Rig Cruise Efficiency and JTF17 Production Engine Goals FD 16972 AIIIA

e. Prototype Fan Performance

The flow of the fan rig described exceeds the goal of both the prototype and production engines. The fan duct efficiency is within 1% of that required for the prototype engine at both cruise and SLTO. The demonstrated engine section efficiency at SLTO is approximately 3 points less than the goal and at cruise the efficiency is approximately 1-1/2% low. Both these efficiencies as well as the required SLTO surge margin are to be achieved primarily through modifications of the first rotor to bring its performance to the levels already demonstrated in the JTF14 engine fan. Modified versions of the 650 lb/sec fan have demonstrated both duct and engine cruise efficiencies exceeding the prototype requirements by approximately 1 and 3 points, respectively.

f. Conclusions (Fan)

Performance data obtained during Phase II-C have already demonstrated the flow needed for both production and prototype fan engines, including the maximum requirement at the transonic operating point. At the latter point the fan duct efficiency slightly exceeds the production engine goal while at the SLTO point it is within 2% of the goal and within 1% of the requirement of the prototype engine. The cruise efficiency requires 3% improvement to reach its ultimate goal but is now within 1% of the prototype requirement.

Engine side fan efficiency must be raised 3 points at SLTO and 1½ points at cruise to attain prototype requirements. Rig tests have demonstrated that leading edge modifications raise cruise efficiency, both duct and engine, to within 1% of the production engine level and several points above the prototype level.

Additional root efficiency has been demonstrated by the JTF14 fan which has also demonstrated the high pressure ratio required to produce the surge margin of the JTF17 design. This type of fan has been included in the fan development program.

Accomplishment of the production engine fan performance goals is expected from the above changes and elimination of rig configuration extra structural vanes, large quantities of instrumentation, and variable stators.

3. HIGH PRESSURE COMPRESSOR

a. High Pressure Compressor Design Point

The geometry selection of a high pressure compressor is more strongly influenced by efficiency, weight, and length and less by specific flow considerations than is the fan. This arises because the compressor is not as influential as the fan in the determination of the engine envelope and thus the specific flow may be lower. The high pressure compressor also need not be designed to accept as great a circumferential pressure distortion as the fan since it benefits from the distortion attenuation provided by the fan and the mixing which occurs within the passage between the fan and high compressor face. Data from TF30 engine fan tests with inlet distortion amounting to 16.0% $\left(\frac{P_{t\ max} - P_{t\ min}}{P_{t\ avg}}\right)$ show that the circumferential distortion is reduced to 7.5% or less than half, upon leaving that portion of the fan feeding the high pressure compressor.

The high compressor distortion tolerance requirements are also reduced due to the twin spool compressor design employed in the JTF17. This arrangement enables the high compressor to be operated at a higher percentage of design corrected rotor speed than is possible if a single shaft were used. The natural result of the higher rotor speed operation is to provide strong distortion attenuation in the front of the high compressor, thus protecting the rear stages which are the ones controlling the surge line at high speeds. This strong distortion tolerance, inherent in a two-spool engine, is beneficial not only within the high compressor but also provides a stabilizing influence on the fan. This occurs because the high pressure compressor, operating at relatively higher rotor speed, requires a nearly constant volume flow from the fan and as a result, resists the tendency of distortion to locally force the fan root toward its surge line.

The establishment of realistic overall performance levels is insured by using other P&WA high pressure compressor performance data, particularly those of commercial engines, as a basis and by tempering these data in accordance with experience from military and research compressors. Presented in the following table are representative data from several of these high pressure compressors together with the design point for the JTF17 production engine compressor.

Engine	Specific Flow lb/sec ft^2	Avg. Stage Pressure Ratio	Polytropic Efficiency	Corrected Tip Speed
JT8D	39.9	1.216	88.4	1060
JT3D	32.9	1.176	87.5	1170
TF30	32.9	1.167	86.7	1170
J58[1]	38.0	1.26	86.5	1140
JTF17	36.5	1.30	88.7	1160

[1]Denotes seven high pressure stages of single spool compressor.

Consideration of these data readily reveals that the specific flow and tip speed are conservative and well within acceptable limits. The average pressure ratio is higher than the older commercial engines but is close to the 1.278 demonstrated with the JTF14 high pressure compressor.

The benefits of reduced weight, length, and number of blades, vanes, and disks make the reduction of compressor stage axial length and number of stages attractive. The chord length of the high compressor has been made less than older compressors to achieve these benefits. The resultant average span-chord ratio is presented in figure 17 with the design polytropic efficiency and relevant data for other compressors.

Since concurrent attainment of high efficiency and stage pressure ratio are the primary goals of the compressor development, selective increases in blade and vane chord may become necessary. The JTF17 design has, therefore, been provided with sufficient high compressor axial length to decrease the average span-chord ratio to 2.13 as indicated by the band in figure 19.

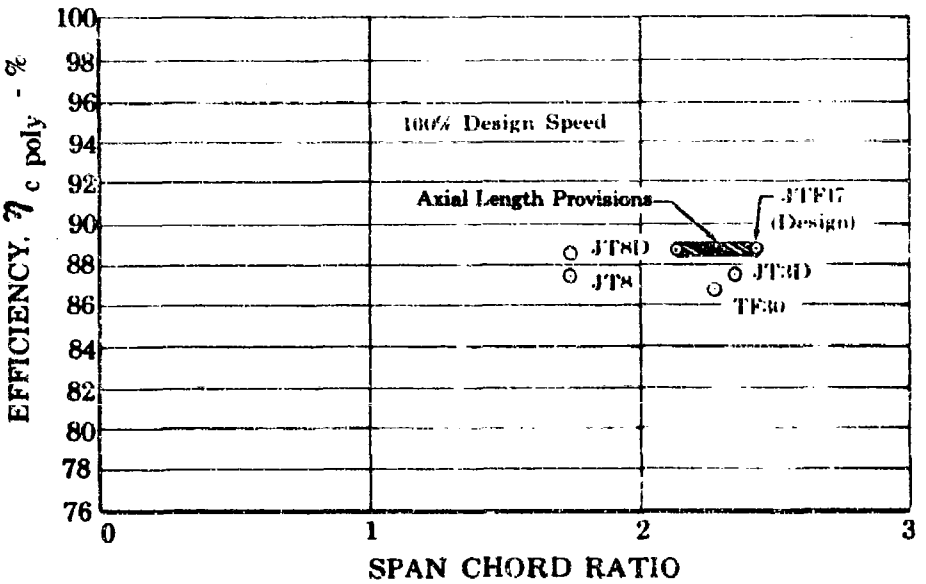

Figure 19. Polytropic Efficiency vs Span Chord Ratio for High Pressure Compressors

FD 16951
AIIIA

CONFIDENTIAL

The peak polytropic efficiencies of these compressors at rotor speeds equivalent to the JTF17 high compressor at the cruise operating point are tabulated below:

Engine	JT8D	JT3D	TF30	J58	JTF17
Cruise Polytropic Eff.	88.3	88.0	86.7	88.2	88.7

As in the case of the SLTO design point, the efficiency of the JTF17 is closely (0.4%) the same as that of the JT8D HPC.

The performance map for the production JTF17 engine high compressor is presented in figure 20 including the effect of the variable inlet guide vanes on the characteristics. Noted on the map are the points corresponding to take-off and cruise at standard conditions. The surge margins at these two operating points are 17% and 30% respectively, providing large margins for operating point perturbations and acceleration.

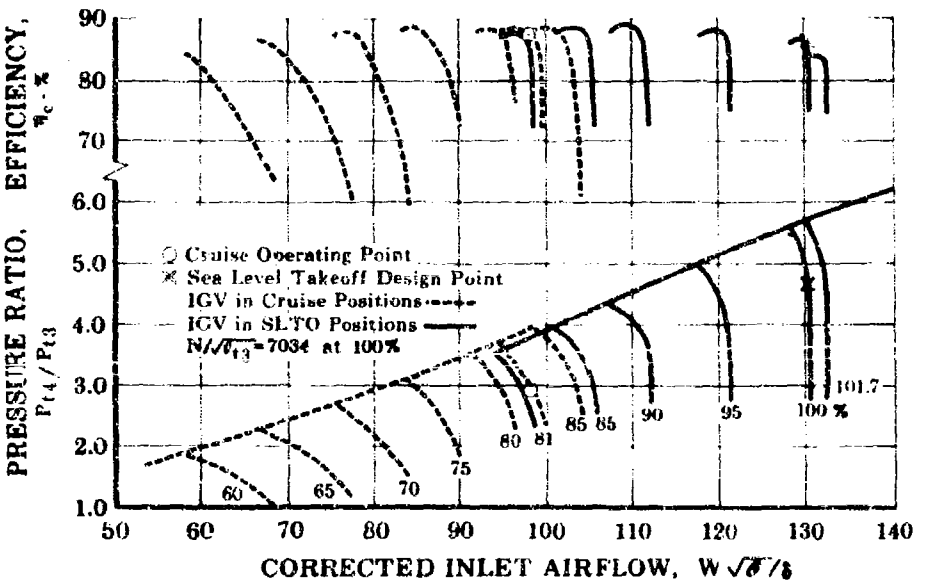

Figure 20. Estimated JTF17 High Pressure Compressor Performance FD 16952 AIIIA

The efficiency and pressure ratio expected of the prototype engine compressor are less than that of the production engine to account for progress during development. These differences are tabulated as follows:

	High Pressure Compressor			
	Prototype Engine		Production Engine	
	Cruise	SLTO	Cruise	SLTO
Efficiency	81.0%	82.0%	86.8%	85.9%
Pressure Ratio	2.81	4.73	2.92	4.84

CONFIDENTIAL

b. 650 lb/sec Engine HPC

Representative data for the full-scale high compressor tests during Phase II-C are presented in this section and are reviewed within the context of the requirements of the production and prototype engine.

The compressor tested during Phase II-C (650 lb/sec engine) was designed for a slightly lower pressure ratio (4.77) than is required for the JTF17 (4.84). In other respects the design goals are substantially the same. Since the unit was intended for development purposes an additional degree of versatility was provided by making both the third and seventh stators variable in addition to the inlet guide vane. The compressor was also heavily instrumented to provide the measurements necessary for internal compressor stage analysis.

The initial series of tests of the high pressure compressor rig consisted of five builds, starting with the "as-designed' compressor and ending with a test to determine the performance effects of stator modifications. In the following paragraphs: (1) the purpose of this test series is described and the major findings briefly noted, and (2) the results and conclusions of the last test, including the stage performance, are described in detail as being representative of current Phase II-C levels.

Testing of the first high compressor build "as-designed" was limited by high stresses and subsequent blade failures which was corrected in later builds by changing the scheduling of the variable vanes. It was determined that the middle stages of the compressor did not have the desired operating range and as a result the surge line of the compressor was not satisfactory. A strong tendency for the streamlines to shift toward the compressor OD in the middle stages was noted.

For the second test, the compressor was rebuilt with sealed blade roots to reduce recirculation, without provision for flow recirculation through the bore and into the gas path at the 3rd stage leading edge, and with aerodynamically more efficient struts in the intermediate case ahead of the compressor. The surge line, although slightly improved, was unsatisfactory for the reasons noted for the first build, although the radial flow distribution was somewhat improved.

The third test was conducted using the same configuration but simulating the fan discharge profile at the high compressor inlet. The profile had no measurable effect on the performance or surge line. It was also evident that the thermal efficiency of the compressor was quite good, particularly so early in its development.

Based on the previous tests, the 4th-test was conducted with the stator roots at the IGV, 3rd-, and 4th-stages (stage numbering convention: stages 1 and 2, fan; stages 3 through 8, HPC) locally overcambered to change the radial flow distribution. The stators of the fifth and sixth stages were overcambered to increase the work of the succeeding stages. The surge pressure ratio at design speed was increased by six percent. A marked increase in the root flow at the fifth stage was also evident, which is considered to be the primary reason for the improved overall surge pressure ratio.

The fifth (final) build of this test series differed from the fourth build in the third, fifth, and sixth stages. A new 3rd-stage blade having part span shrouds was introduced to reduce stresses in this rotor. The blade geometry was changed to compensate for the effect of the shroud. The roots of the fifth and sixth stators were overcambered similar to the first three stators to further influence the radial flow distribution. Overall performance data for this modified version of the initial design are presented in figure 21 for two combinations of the variable stator vanes.

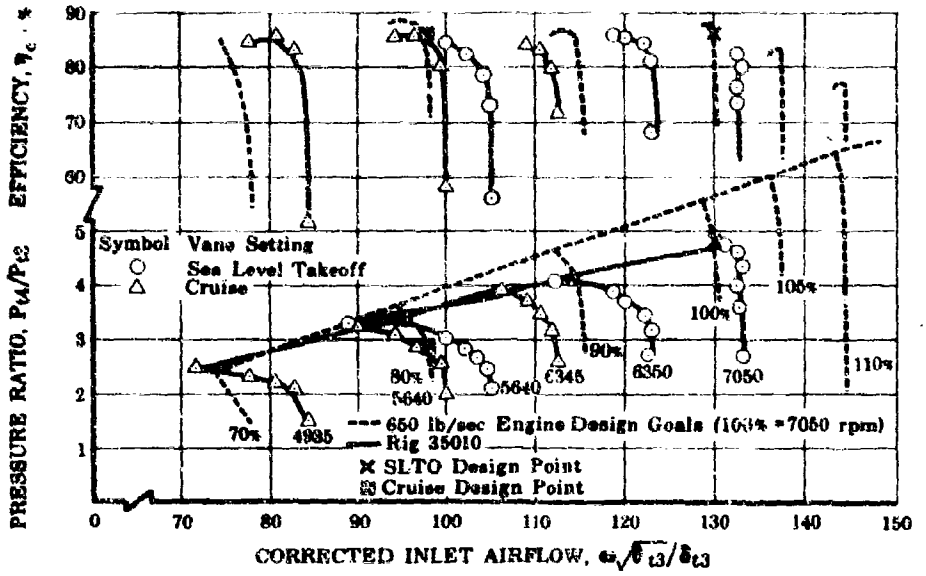

Figure 21. High Pressure Compressor With 650 lb/sec Engine Design Goals FD 16953 AIIIA

At the cruise operating point, the flow was equal to that required within 1%, and the surge line was virtually identical with the goal. The cruise efficiency at this stage of the development is 85.5% relative to a goal of 86%. The achievement of this efficiency is a major milestone.

The flow at the SLTO design speed exceeds that required by approximately 1 lb/sec. Earlier tests had shown even higher flows (build 4, 134 lb/sec) could be achieved by opening the variable IGV and third stator, if required. In spite of the numerous stator modifications which produce poor airfoil contours and also the high diffusion load they place on the rotor root leading edge, the compressor efficiency remained relatively high (81.8%). The combined achievement of both the design flow and an excellent efficiency for the initial compressor test confirm the soundness of the design.

The aerodynamic effect of the further stator overcamber and the shrouded 3rd-stage rotor was primarily to increase the surge pressure ratio to 4.75 at design speed, an increase of approximately 12% from the third build. This substantial increase in surge pressure ratio (0.5) at the SLTO speed is highly desirable and was a primary objective of the test. A more important result is that the test proved that the control of the flow in the

root region could produce immediate and dramatic increases in surge pressure ratio. This fact is the key to development of this compressor. The review of the stage performance which follows indicates the areas where the necessary improvement may be attained.

Extensive instrumentation within the stages of the high compressor rig has allowed detailed determination of the stage pressure rise and temperature rise characteristics. These stage data are presented in figure 22 for all high compressor stages in the form of curves of adiabatic stage efficiency (η_c) and pressure ratio coefficient (ψ) plotted against the flow coefficient (ϕ). For simplicity, only those data at the SLTO design speed are shown with the Phase II-C design goals for each stage.

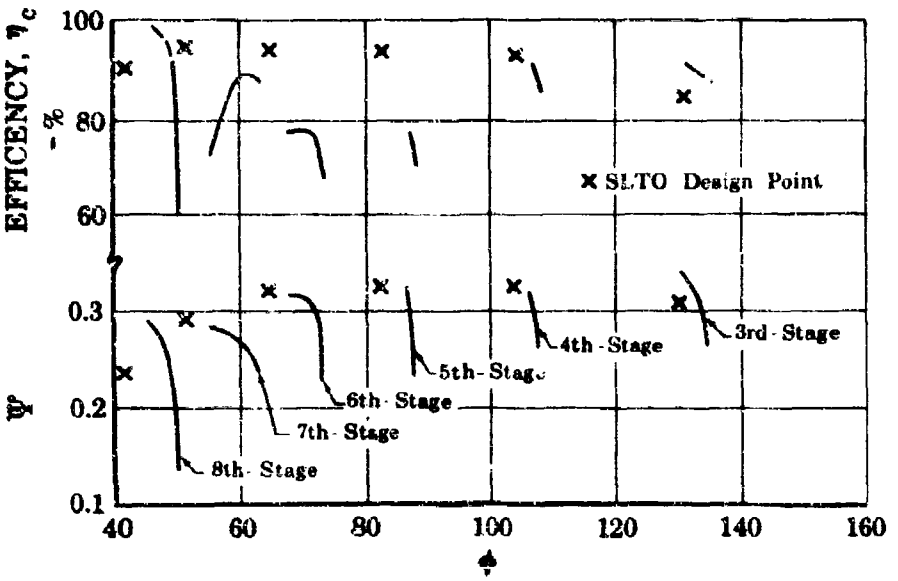

Figure 22. High Pressure Compressor Stage Characteristics at SLTO Speed

FD 16957
AIIIA

The pressure coefficient-flow coefficient data for the third stage demonstrate that the design point pressure ratio and flow have been readily achieved at an efficiency exceeding design expectation. The characteristics of the fourth stage are similar to the third and it has substantially achieved the design pressure ratio, flow, and efficiency. During testing the performance of these stages was modified through use of the variable stators showing that the flow could be altered as required.

Stages five through seven exhibit similar characteristics and may be considered together. These stages have maximum pressure ratio capability approximately equal to their design values and flow capacities significantly exceeding design. A portion of this excess flow capacity was introduced by the stator modifications primarily intended to improve surge pressure ratio. The pressure coefficient characteristic shows a stall tendency as noted in the sixth and seventh stages. Although the fifth stage characteristic does not exhibit this tendency it is believed to be latent. The earlier compressor builds did exhibit a stalling fifth stage which was suppressed by the stator modifications and resulted in the

CONFIDENTIAL

surge line improvement between the third and fifth builds. The stage efficiencies are less than required, particularly the fifth and sixth. The characteristics described are not uncommon to compressor stages of large span-chord ratio and are primarily the result of departures from two-dimensional flow along the root boundary. The JTF14 HPC which also had high span-chord ratio blading produced data pertinent to this problem leading to modifications of the design techniques to overcome the problem in the design of the JT9D HPC. These techniques which include higher root and tip work levels and negative design incidence angles have been included in the design of the JTF17 HPC and experimental parts are being procured for Phase II-C testing. The marked increase in surge pressure ratio of the Phase II-C compressor resulting from the increase in root boundary work introduced with the stator modifications further substantiates this technique. The efficiency of the compressor was not improved by these modifications and was in fact lowered considerably when compared at a constant pressure ratio. This result was expected since the modifications to the stators which involved cutting, bending, and welding of the aerodynamic surfaces produced inefficient stator airfoil contours and high diffusion loading at the rotor leading edge.

The eighth stage yielded good efficiencies and showed excellent pressure rise capability. The excess flow capacity of this stage is due to its being matched open using the variable seventh stator in order to be compatible with the previous stages. As these stages are developed to their goals, the eighth stage may be readily rematched to maximize surge pressure ratio.

The nature of the change in the stage characteristic resulting from the previously mentioned modification of the root work is shown in figure 23. In this figure the fifth stage data is used to show the result. It may be noted that the local increase in fourth stator root camber produced a large rise in the peak stage pressure ratio (Build 3 to Build 5). It is evident that relatively small changes at the root are capable of producing a greatly magnified effect on the stage performance by improving the radial matching of the stage. This amplifying effect of the local stator modification is seen in the relatively minor (1/2%) increase in maximum flow between the third and fifth build but the substantial (11%) increase in pressure rise coefficient resulting.

c. 650 lb/sec Engine HPC Relative to JTF17 Design

(1) Surge Margin

The preceding description of the performance of the high pressure compressor clearly indicates that the middle stages (5, 6, and 7) are preventing the achievement of the required surge pressure ratio at SLTO design speed. The data have further shown that premature stalling of the stage roots is causal and that corrective action, in the form of stator recamber, is effective. The latter tests do not represent the means by which permanent remedial action will be made for several reasons. Primary among these is the high loading that is placed on the rotor leading edge which leads to flow separation. The overcambered stators also result in enlargement of the stage flow capacity which mismatches the front stages, thereby reducing their pressure ratio. Both these factors contribute to lower efficiency.

CONFIDENTIAL

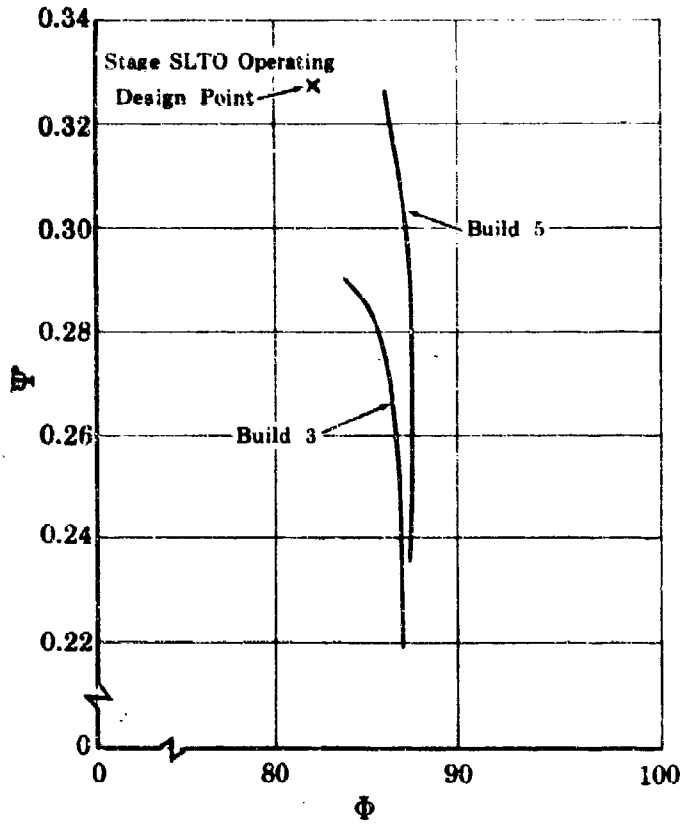

Figure 23. Effect of Stator Root Modification - Stage 5

FD 16954
AIIIA

These factors are not present when the adjustment is made to both rotors and stators. This allows the rotor root work to be increased without localizing the loading at the leading edge. The flow capacity is adjusted to the design goal by overcamber of the rotor and stator leading edges. Local overcamber at the root is required to lower incidence and raise efficiency by compensation for the spanwise flow encountered near the surge line. The increase in root work provides a bias toward higher root velocities and increases the pressure ratio at which an approximately two dimensional flow may be maintained. The effect of these changes is to allow the stages to realize their design operating range and avoid the premature stalling (figure 23) which has been noted during Phase II-C and with the JTF14 HPC.

Single stage compressor tests in support of this phase of development have been conducted with stages having loadings and geometry similar to the middle stages of the JTF17 HPC. Included among the stages tested was one having a rotor with the increased root work and the root leading edge overcamber discussed above. This stage, designated "A" in figure 24, produced a significantly higher root pressure ratio than the baseline stage, designated "B", and also had a greatly improved efficiency in the root region. Since the spanwise distribution of pressure ratio of the "A" stage is nearly constant in the inner portion of the annulus, as

CONFIDENTIAL

intended, it will provide a uniform flow profile for succeeding stages in this region. Thus, this type of stage is capable of maintaining an exit flow profile which is both uniform and similar to its inlet profile allowing such stages to be successfully "series connected". The data presented for the baseline stage (B) were similarly obtained with an inlet profile simulating the exit profile of this type of stage.

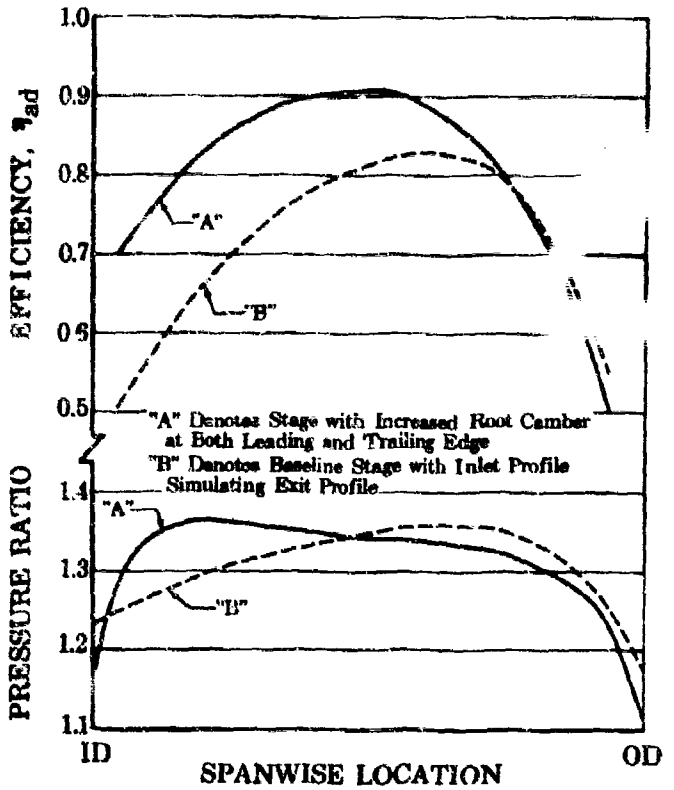

Figure 24. Single Stage Tests of Simulated JTF17 HPC Stage

FD 17854
AIIIA

This improved spanwise work distribution for these relatively high span-chord ratio stages was reflected in an increase in efficiency of approximately 7 points. Further improvements are possible by modification of the stator and the tip region of the rotor in the same manner.

It has been noted in the previous paragraphs describing the third and fourth stages that these stages have shown the capacity to reach and exceed their design points at good efficiency. The design of the JTF17 HPC takes advantage of this facet by increasing the work of these stages.

Provision has also been made in the design for increased blade and vane chord length since the span-chord ratio is known to influence stage operating range. The span-chord ratio of the 650 lb/sec compressor (2.67) was decreased to 2.43 for the JTF17 production engine design and space was provided for further decrease to 2.13 should development indicate longer chords are necessary.

CONFIDENTIAL

(2) Efficiency

The outlined corrective measures for the purpose of raising surge margin by prevention of premature root stalling, are also intended to improve SLTO efficiency. The coupling of these two factors is obvious since stalling of the root separates the flow and increases losses in both rotor and stator. The stage characteristics of figure 22, particularly those of the stalling sixth and seventh stages show how the stalling of the root, leading to the stage stall causes the efficiency to peak at a low value and, in the case of the seventh stage, to be sharply reduced.

The adiabatic efficiency of the third Phase II-C compressor build is shown in figure 25 together with the production engine goal at SLTO design speed and the efficiency of the compressor after stator modification (Build 5). It may be noted that while the third build, which was comprised essentially of the as-designed compressor tested in the presence of the fan discharge velocity profile, did not reach the required pressure ratio the efficiency data may be logically extrapolated to the production engine goal. In addition it must be remembered that this compressor differed from the production compressor in several ways, all of which lower efficiency and thus make the rig data appear pessimistic. One of these factors is the presence, in the rig, of variable stators in two stages (3 & 7) which are not part of the production engine design. Although variable stators are often used by P&WA during compressor development, it is recognized that they result in lower efficiency because of the clearance which must be provided at the walls to allow for thermal expansion and movement and the inability to provide an aerodynamically efficient wall due to mismatching of the bearing surfaces on the variable vanes and the case contours. Another large factor degrading compressor rig efficiency is the instrumentation needed to document internal performance. This compressor rig is equipped with 148 kiel type pressure and temperature measuring probes located along and protruding ahead of the vane leading edges; each constituting a disruptive influence to the airflow. In addition, 59 strain gages and their connections are cemented to the rotors and stators, further providing loss inducing mechanisms.

The sealing of the extended blade roots was found to be important in controlling the radial velocity distribution. This sealing was accomplished in the compressor rig by forcing a room temperature vulcanizing rubber into the gaps. This expedient but inefficient method is also believed to contribute to loss generation. Redesigned blade roots eliminate this problem on the production engines. Another difference between the rig and engine compressors results because the rig is run at ambient temperature, not heated to simulate engine operation. For this reason the tip clearances are enlarged and the I.D. flow path is not smooth. Both factors will tend to reduce efficiency and surge pressure ratio.

While it is difficult to assign an exact value to the efficiency degradation caused by the above factors experience (figure 26) has shown that engine compressors will run between 1½ to 4 points higher efficiency than their equivalent rig compressor.

CONFIDENTIAL

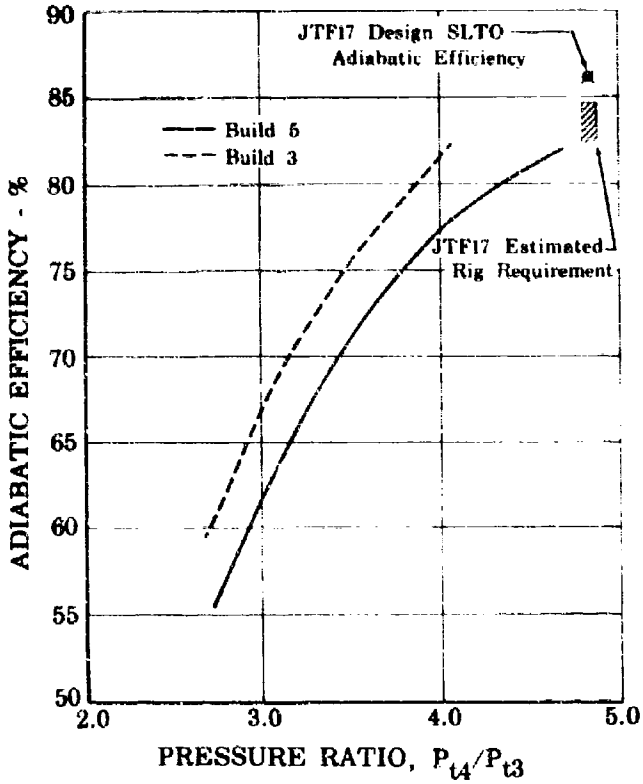

Figure 25. High Pressure Compressor Efficiency at SLTO Speed

FD 16955
AIIIA

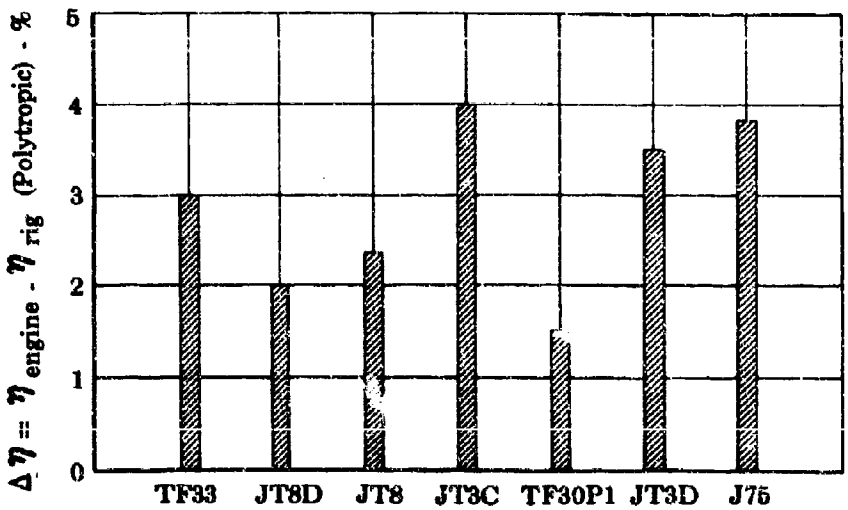

Figure 26. Difference Between Engine and Rig Efficiency

FD 16956
AIIIA

CONFIDENTIAL

Relating this information to the Phase II-C efficiency data of figure 25 by reducing the production engine design efficiency by these values it is shown that the maximum efficiency of the third and fifth builds is already at the lower limits of the band. Logical extrapolation of the build three data readily shows the attainability of the desired levels.

It is further evident that the stator modifications, while increasing the surge pressure ratio, were costly in efficiency, amounting to a loss of four points. As already described, a large part of this loss must be attributed to the manual reworking of these stators which produces poor aerodynamic surfaces. Even with these losses, the recorded efficiency is already closely at the lower end of the estimated acceptable rig efficiency band.

Additional assurance that the design efficiency goal of the JTF17 engine can be achieved arises from the knowledge that an increase of three to five percent in efficiency is usual during a development program.

d. Prototype Engine Goals

The requirements of the high pressure compressor for the prototype engine (FTS) are lower than those of the production engine as follows:

	Production	Prototype	Phase II-C Rig Results
Cruise	86.8%	81.0%	85.5%
SLTO	85.9%	82.0%	81.8%

The prototype cruise efficiency has already been greatly exceeded at the desired surge margin. The rig efficiency at SLTO is within 2/10 of 1% of the prototype engine goal. As has been previously described, the SLTO surge pressure ratio will be raised by the means already discussed. The speed-flow requirements of the prototype and production engines are the same, thus this requirement has already been satisfied for both compressors.

e. Conclusions (HPC)

The initial series of tests has demonstrated that the high pressure compressor rig can readily meet the flow requirements of both the prototype and production engines. The surge margin at cruise has been attained and the required prototype engine efficiency exceeded while the higher efficiency demanded for the production engine is only 1.3% above the value attained at this early stage.

The prototype engine SLTO efficiency has been demonstrated (-0.2% is within measurement error). Testing has indicated that the cause of the inadequate SLTO surge margin is stage mis-matching and premature root stalling. Higher root work at lower incidence angles is proposed to eliminate the problem and stator modifications to approximate the proposed changes have shown that the desired effect is achieved. By preventing root stall, these changes will also increase SLTO efficiency. Further increases in demonstrated efficiency are to be obtained by elimination of

CONFIDENTIAL

variable stators and the extensive instrumentation present in the compressor rig.

4. Transient Operation

The requisite fan and compressor surge margins during steady state and transient operation are maintained by the engine fuel control. The operation of the control and the schedules which determine the required fuel flow as a function of power setting are discussed in another section (Volume III, Report B, Section III). The effect of changes in engine power setting on the operation of the fan/compressor are discussed in the following paragraphs. For illustrative purposes, transients at two important flight conditions are considered: cruise, and sea level static. At both these conditions the effect of changes in power setting on augmented and non-augmented operation is included.

These transients at cruise are shown in figures 27 and 28 for the compressor and fan respectively. The path described by the operating point during a deceleration from maximum rated non-augmented to idle and back to maximum rated is presented in figure 27. Minimum surge margin occurs at idle speed during the acceleration where a value exceeding 11 percent is always maintained. The transient from maximum rated non-augmented power to maximum augmentation does not effect the compressor match point hence these points are coincident.

Fan operation (figure 28) from maximum rated non-augmented to idle and returning to maximum rated does not produce a significant departure from the equilibrium operating line, hence steady state, acceleration and deceleration occur along a single path. It is shown that the surge margin increases during this transient. Augmentor light-off is preceded by an increase in duct nozzle area and, since light-off is accomplished at a very low fuel-air ratio, (0.002) the transient is accompanied by an increase in surge margin rather than a decrease.

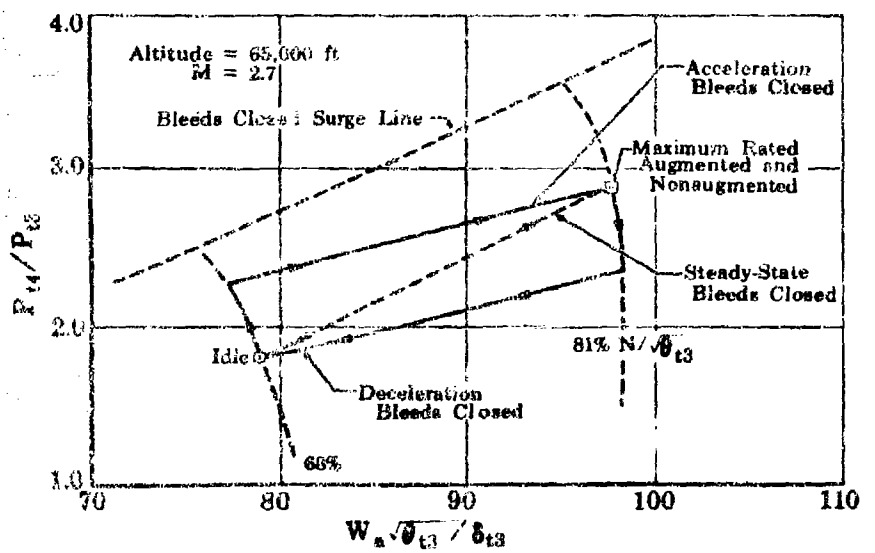

Figure 27. Cruise-Acceleration, Steady-State and Deceleration Operation of JTF17 Compressor

FD 17535
AIIIA

CONFIDENTIAL

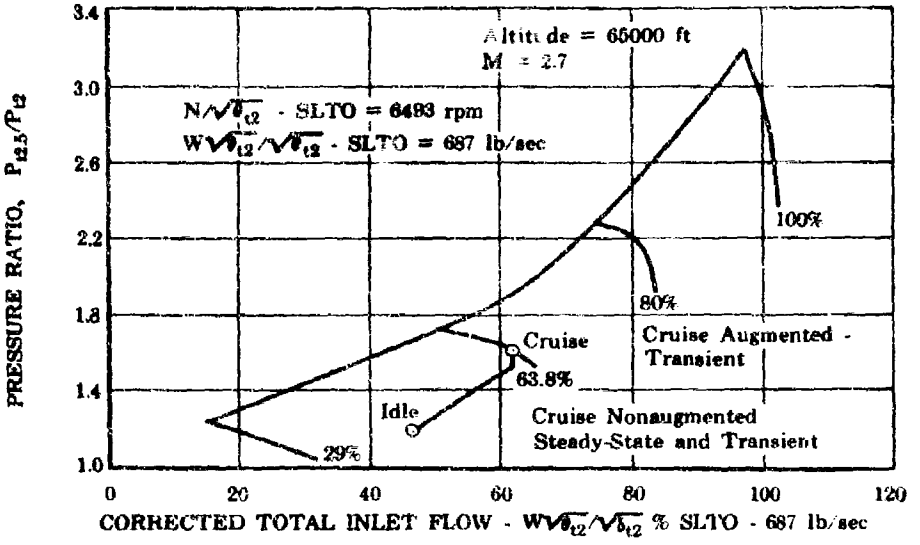

Figure 28. Cruise-Acceleration, Steady-State and Deceleration Operation of JTF17 Fan — FD 17534 AIIIA

Similarly, transient during sea level static operation are presented in figures 29 and 30. The maximum rated non-augmented to idle transient displays three modes of compressor operation encompassing both bleed and inlet guide vane operation. As at cruise the augmentor light does not affect the compressor match point and maximum rated non-augmented and augmented appear as a single point.

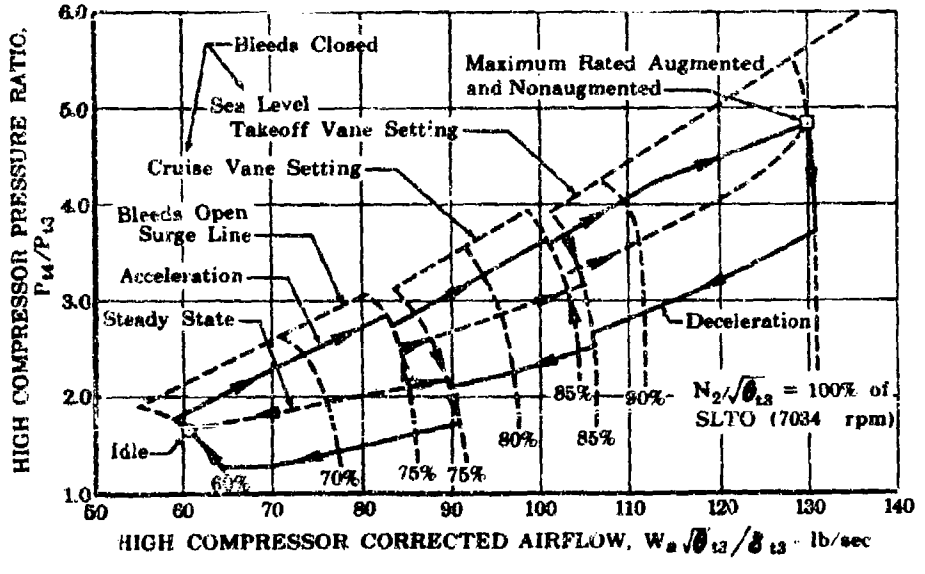

Figure 29. Sea-Level Static-Acceleration, Steady-State and Deceleration Operation of JTF17 Compressor — FD 17536 AIIIA

CONFIDENTIAL

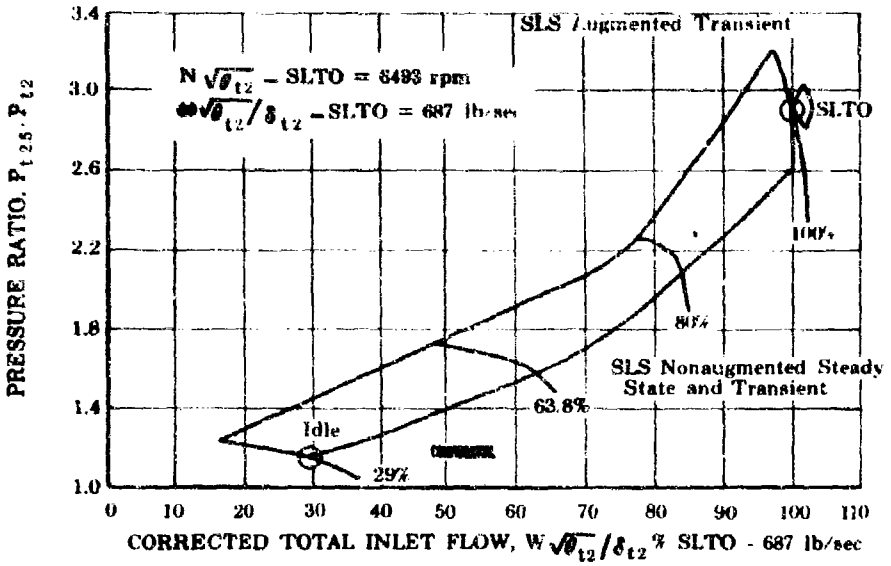

Figure 30. Sea-Level Static-Acceleration, Steady-State and Deceleration Operation of JTF17 Fan

FD 17538
AIIIA

Fan operation (figure 30) between idle and maximum rated non-augmented either steady state or transient (acceleration or deceleration) is along a single path as was shown at cruise. The change in duct pressure ratio which occurs at SLTO design airflow reflects the variation of duct nozzle position to control to this value of the total airflow. The transient accompanying augmentor light is also similar to that described at cruise in that duct burner ignition is preceded by opening of the nozzle to lower pressure ratio and increase surge margin, and ignition occurs at low (0.002) fuel-air ratio resulting in little variation in surge margin.

CONFIDENTIAL

B. PRIMARY COMBUSTOR

1. Introduction

The primary combustor incorporated in the Phase II-C experimental engine program uses the ram-induction concept. This concept has demonstrated excellent results, and is incorporated in the JTF17 prototype design. In principle, it employs the kinetic energy of the air directly to promote mixing rather than diffusing the air to a higher pressure and then re-accelerating it, as is done in more coventional burners. The ram-induction combustor development program has resulted in a short combustion section length without sacrificing important performance requirements. This section of the proposal will include: (1) a review of the primary combustor requirements, (2) a brief description of the annular ram-induction combustor selected, (3) a summary of the programs and results substantiating the performance of the primary combustor, and (4) the fuel nozzle description and development status. Unless specifically stated, the objectives, designs and performance of the production and prototype combustors are identical.

2. Primary Combustor Requirements

To achieve the overall engine performance required for an economically successful supersonic airplane and engine combination, each of the components must meet many requirements under all operating conditions. Requirements for the primary combustor include: (1) an exit temperature profile compatible with the turbine requirements, (2) high combustion efficiency, (3) low pressure drop, (4) short length, (5) large turndown ratio, (6) ability to accept airflow profile changes, and (7) durability.

3. Annular Ram-Induction Combustor Description

The ram-induction primary combustor uses a short, efficient diffuser of low area ratio to partially diffuse the air. The air, still at relatively high velocity, is then introduced to the combustor by turning vanes. With this approach, much of the pressure loss and length usually associated with the low velocity part of the engine diffuser are eliminated, and the high velocity provides efficient mixing. As shown in figure 1, the combustor is about 41 inches in diameter, 28.5 inches long, and has an average annular height of 7.3 inches. The design approach Mach number is 0.25, and the pressure drop, including that of the diffuser, is about 5.7% for the production engine and 6.1% for the prototype engine at SLTO.

The ram-induction combustor has been selected for its state-of-the-art advancements which make it possible to achieve the SST primary combustor requirements with the short length and resultant low weight that are unique to this concept.

4. Primary Combustor Background

Development of the ram-induction burner concept began at FRDC in 1963. The short combustion length and the uniform temperature distribution demonstrated by the early tests resulted in the decision to incorporate the ram-induction combustor in the JTF17 experimental engine. Development was continued on the JTF17 program with water table analogy tests and rig testing

for investigation of features affecting temperature distribution. The test rigs included a 120-degree sector of an annular combustor patterned after the JTF17 engine design, and a full-scale annular rig consisting of an adapted JT4 engine. The use of a JT4 engine permitted testing of the primary combustor at sea level temperature and pressure conditions. The JT4 engine program proceeded rapidly, and by January 1966 the objectives had been achieved, i.e., comparable performance to that experienced in current commercial JT4 engines and demonstration of the suitability for use in the experimental JTF17 engines.

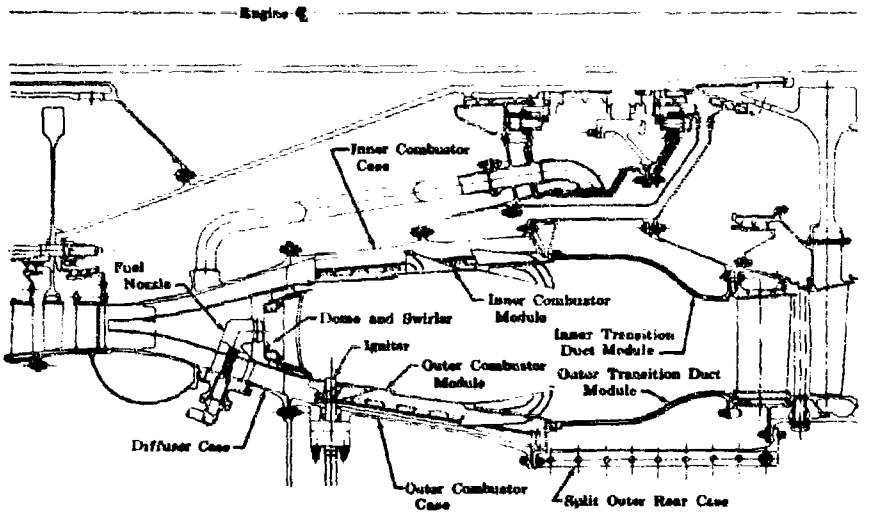

Figure 1. Primary Combustor Cross Section FD 16990 AIIIB

5. Primary Combustor Performance

The performance of the primary combustor annular ram-induction configuration has been demonstrated on a 120-degree segment rig, a modified JT4 engine, and the experimental JTF17 engines. The two-dimensional water table analogy has also been used as an aid to understanding the reactions to configuration changes. The expected burner performance and its substantiation are presented below in terms of temperature profile, combustion efficiency, pressure loss, volumetric heat release, turndown ratio, and tolerance of distorted air velocity profiles. Burner durability and the fuel injection system are also included.

a. Exit Temperature Profile

In the evaluation of the primary combustor exit temperature distribution patterns, several numerical parameters are used for comparison purposes. These are ΔTVR, d_{max}, and $d_{r\ max}$. ΔTVR is the ratio between the temperature rise at the highest individual point in the exit distribution and the average overall temperature rise, and is a useful parameter for early evaluation of data. However, it is not used as a final parameter as it compares measured data with an average temperature, and the desired turbine inlet profile is not a flat line and thus cannot be represented by a single average temperature. A new goal of 10% d_{max} has been established to

reflect a comparison with the desired turbine inlet profile. This new measure of temperature profile suitability, d_{max}, is the maximum positive difference between the measured temperature at any radial point and the desired circumferential average at the same radius at which the maximum positive difference occurs, expressed as a percentage of the desired temperature rise at the same point. For evaluation of the primary combustor temperature distribution on the 1st-stage turbine blades, a third parameter, $d_{r\ max}$, is useful and is defined as follows: the maximum positive difference between the measured and the desired circumferential average temperatures expressed as a percentage of the desired temperature rise at the same point. This parameter is quoted together with the percent span at which it occurs to indicate the location of the hottest region. However, d_{max} is the measure of temperature profile suitability and the goal for the SST engine is d_{max} = 10%. Figures 2, 3, and 4 show plots of ΔTVR, d_{max}, and $d_{r\ max}$ versus turbine inlet temperature for primary combustor assemblies that have been tested during Phase II-C development. The figures show a marked improvement in temperature profile as the turbine inlet temperature is increased. The projection of this trend indicates that the goal of d_{max} = 10% will be met.

The radial temperature profile of the first full-annular combustor tested in the JT4 engine is shown in figure 5. This figure shows (1) the overall average of the measured data, (2) the average measured at each radial position, (3) the maximum measured at each radial position, and (4) desired radial profile. Tabulated numerical parameters included in this figure provide comparison for evaluation of the temperature distribution. Modifications were then made to the primary combustor to improve durability and to reduce carbon formations. These modifications were tested in four additional schemes. The last configuration showed improved durability, decreased pressure loss, and increased combustion efficiency while still maintaining the good temperature distribution of the first configuration. The radial profile and isothermal plots showing the discharge temperature profiles are shown in figures 6 and 7.

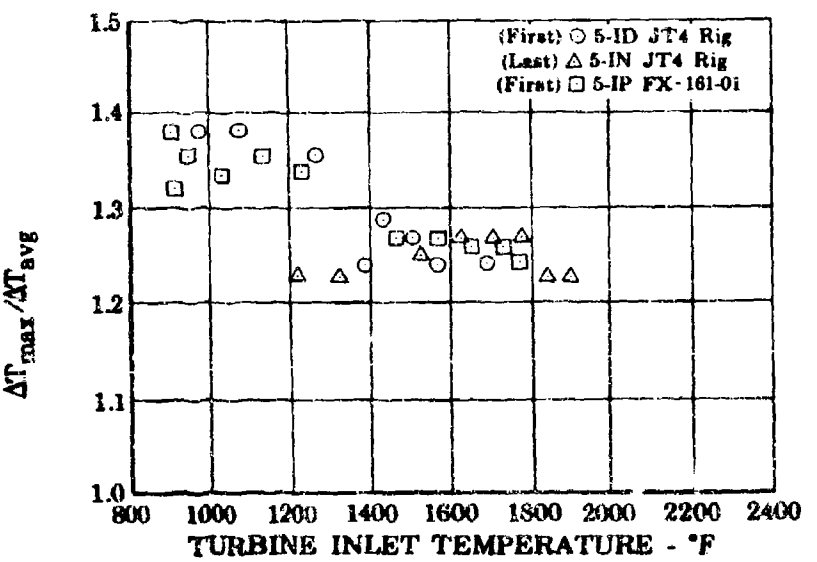

Figure 2. Turbine Inlet Temperature vs ΔTVR FD 16921 AIIIB

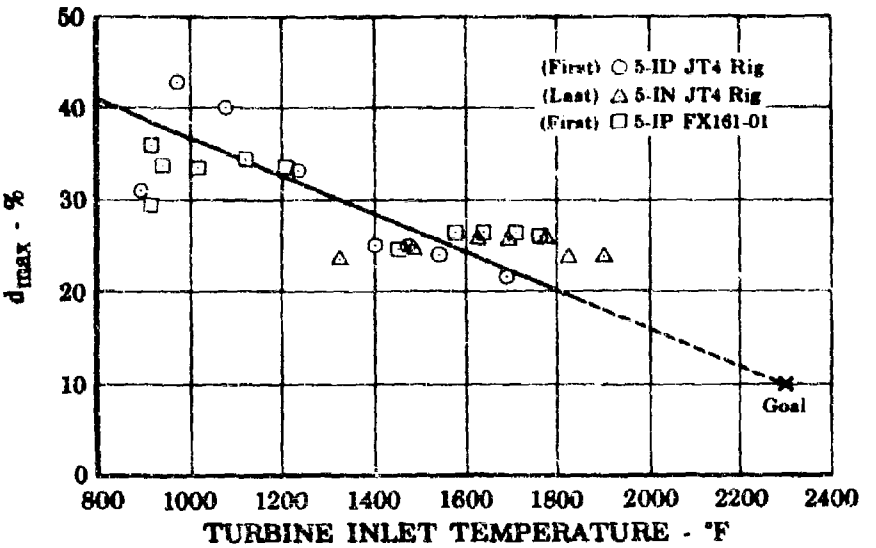

Figure 3. d_{max} vs Turbine Inlet Temperature FD 16922
AIIIB

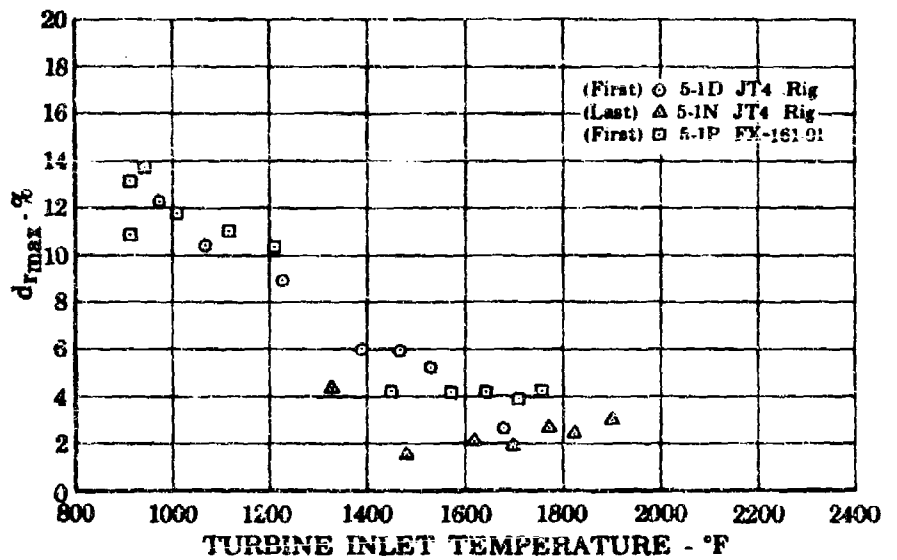

Figure 4. $d_{r\,max}$ vs Turbine Inlet Temperature FD 16923
AIIIB

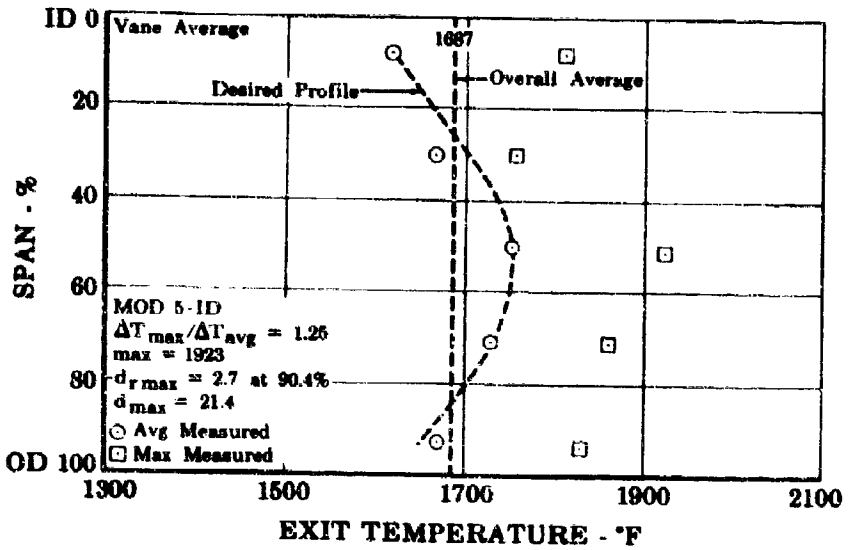

Figure 5. Radial Temperature Profile of First JT4 Combustor

FD 16924
AIIIB

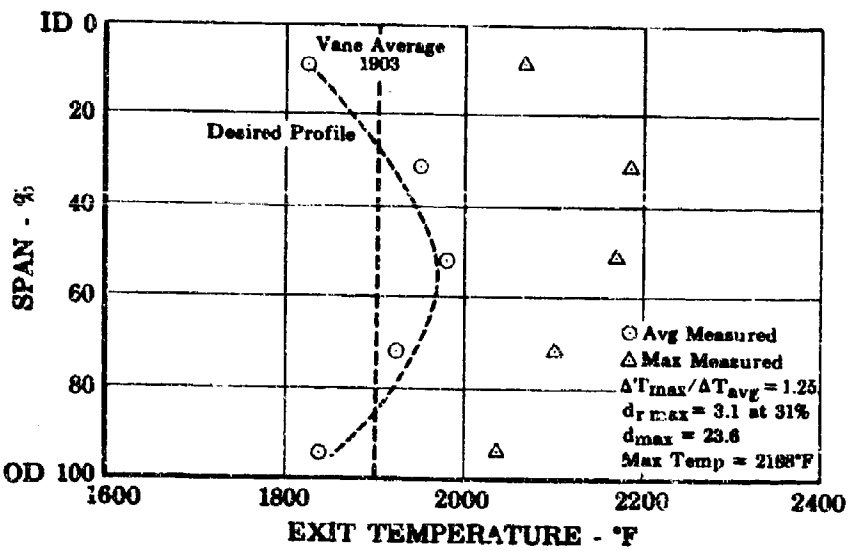

Figure 6. Radial Temperature Profile of Last JT4 Combustor

FD 16926
AIIIB

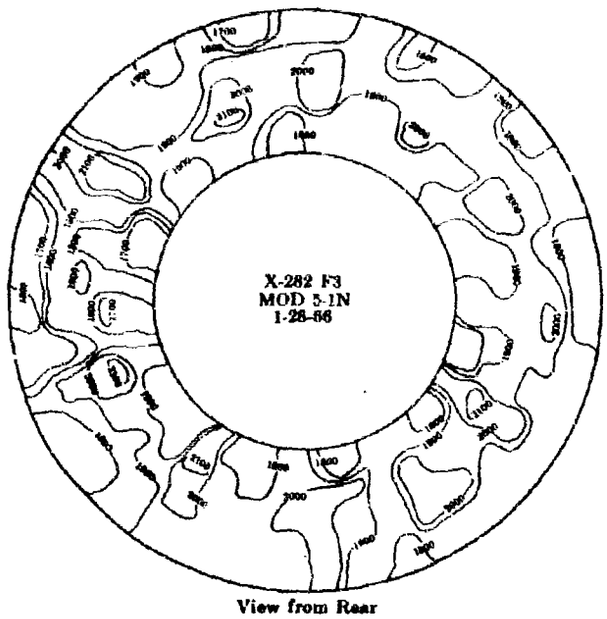

Figure 7. Turbine Inlet Temperature Distribution FD 16927
AIIIB

The best durability and performance features of the configurations tested in the JT4 engine were combined in the primary combustor for the first experimental JTF17 engine. The radial profile, circumferential profile, and isothermal plot of the primary combustor discharge temperature pattern are shown in figures 8, 9, and 10. The following tabulation of numerical parameters comparing the temperature distribution of the last two JT4 engine configurations with the first JTF17 experimental engine configuration shows excellent correlation.

Engine	Primary Combustor Configuration	Vane Avg, °F	ΔTVR	d_{max}, %	$d_{r\ max}$, %
JT4	Mod 5-1M	1901	1.28	28.5	4.4
JT4	Mod 5-1N (last)	1904	1.25	23.6	3.1
JTF17	Mod 5-1P (first)	1923	1.27	28.7	4.5

This demonstration of the ability to provide in the first build of an SST engine, the desirable burner features developed during rig testing is convincing evidence that the improved temperature profiles that have recently been developed in 120-degree sector burner rig tests can be readily incorporated in the engine and that the SST engine burner temperature profile goals will be met. Typical recent experimental data from 120-degree sector rig are tabulated below.

Vane Avg, °F	ΔTVR	d_{max}, %	$d_{r\ max}$, %
2132	1.09	10.2	1.6

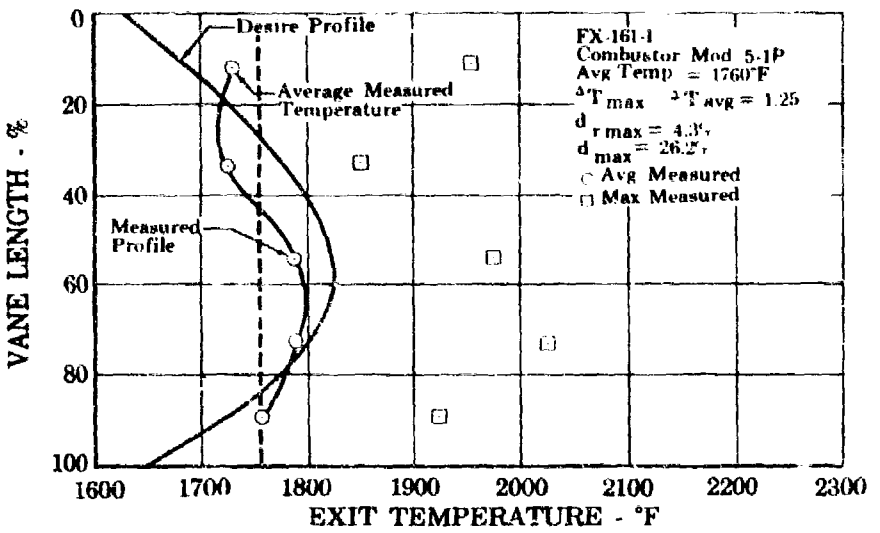

Figure 8. Radial Temperature Profile of the First JTF17 Combustor

FD 16928
AIIIB

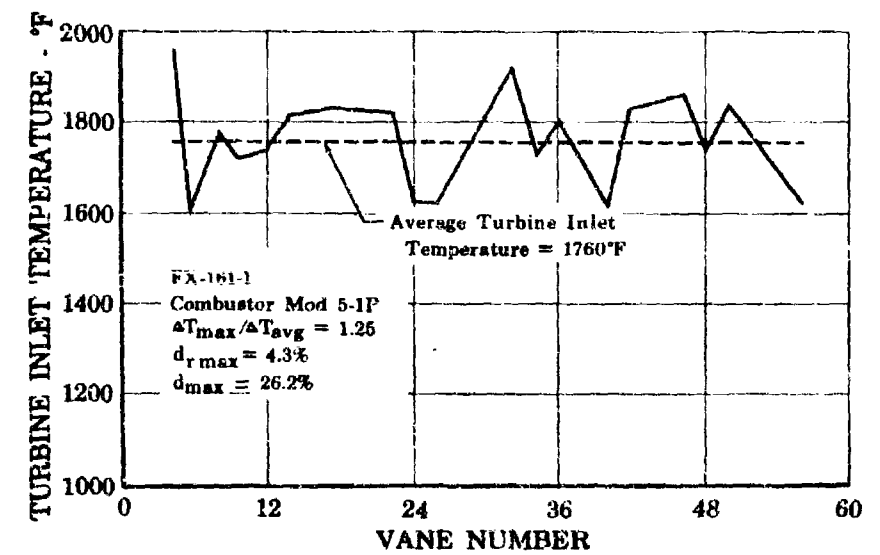

Figure 9. Mod 5-1P Circumferential Temperature Profile

FD 16929
AIIIB

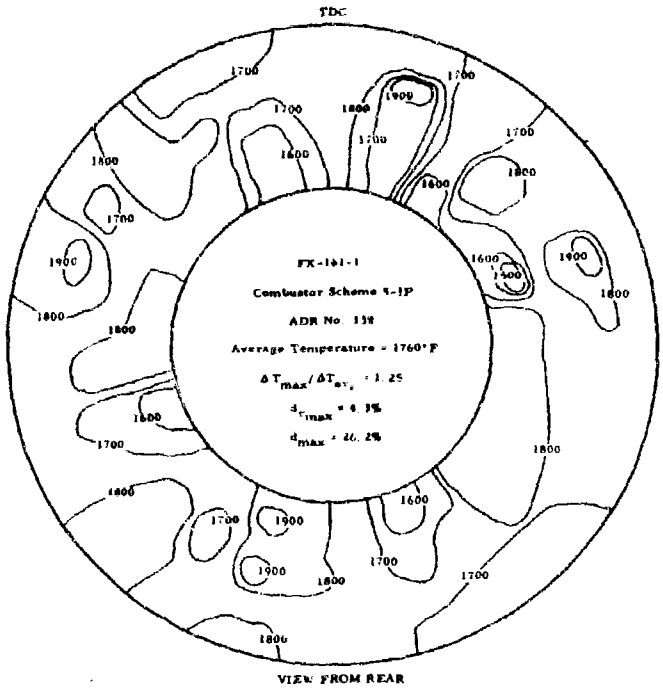

Figure 10. Mod 5-1P Turbine Inlet Temperature Distribution

FD 15552
AIIIB

b. Combustion Efficiency

The first annular primary combustor tested in the JT4 engine did not meet its combustion efficiency goal of 99.0%. In modifications to the design, the primary combustion zone air was redistributed and the outer annular wall was rotated to stagger the relationship of the OD and ID wall scoops. The results of subsequent testing demonstrate that the combustion efficiency of the ram-induction configuration is now above the SST engine goal of 99.0%, as shown in figure 11.

c. Cooling Air Effects

The 120-degree segment rig has been tested with changes in the percentage of air used for cooling the wall, and it was found that the combustor exit radial profile is affected. Figure 12 shows the result of tests with two different coolant airflows. These combustors were identical except for the change in wall cooling. This effect of wall cooling airflow rate is a useful tool for controlling the shape of the turbine inlet temperature profile. Testing of the JT4 engine and the experimental JTF17 engine indicates that the wall cooling airflow requirements of the primary combustor are compatible with the turbine inlet profile requirement.

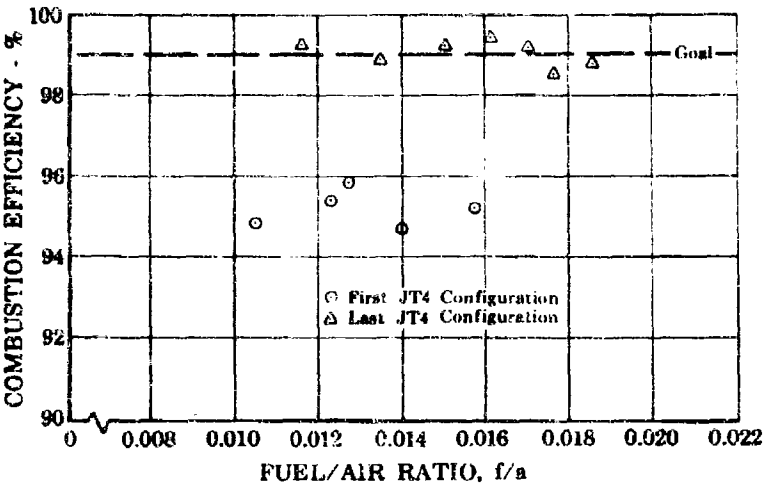

Figure 11. Primary Combustor Efficiency FD 16930
AIIIB

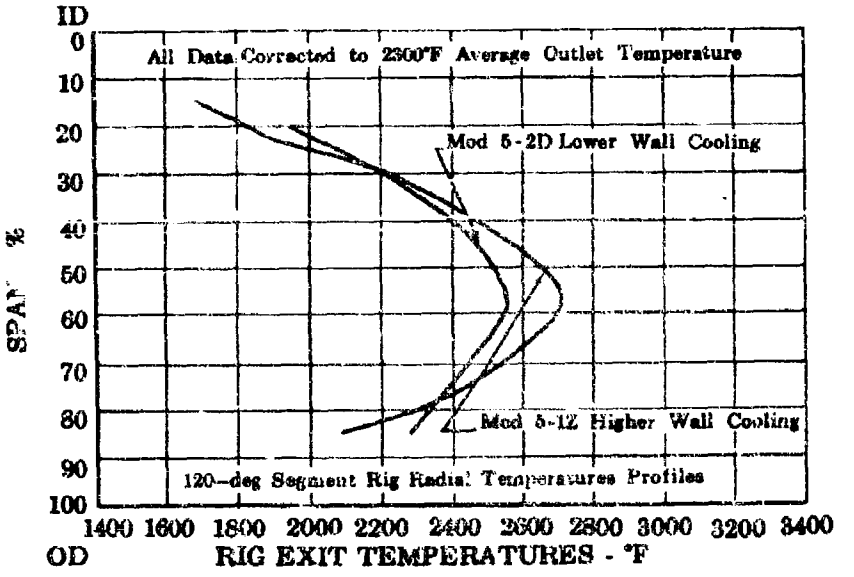

Figure 12. Simulated Sea Level Takeoff Condition FD 16931
AIIIB

CONFIDENTIAL

d. Pressure Loss

The two-dimensional water table analogy was used in the study of diffuser and scoop configurations prior to the completion of detailed drawings. Smooth, unseparated diffuser flow and high velocities through the scoops resulted from these studies and contributed to the low primary combustor pressure loss. Figure 13 shows a portion of the water table simulation testing, and figure 14 shows the overall airflow pattern of the primary combustor.

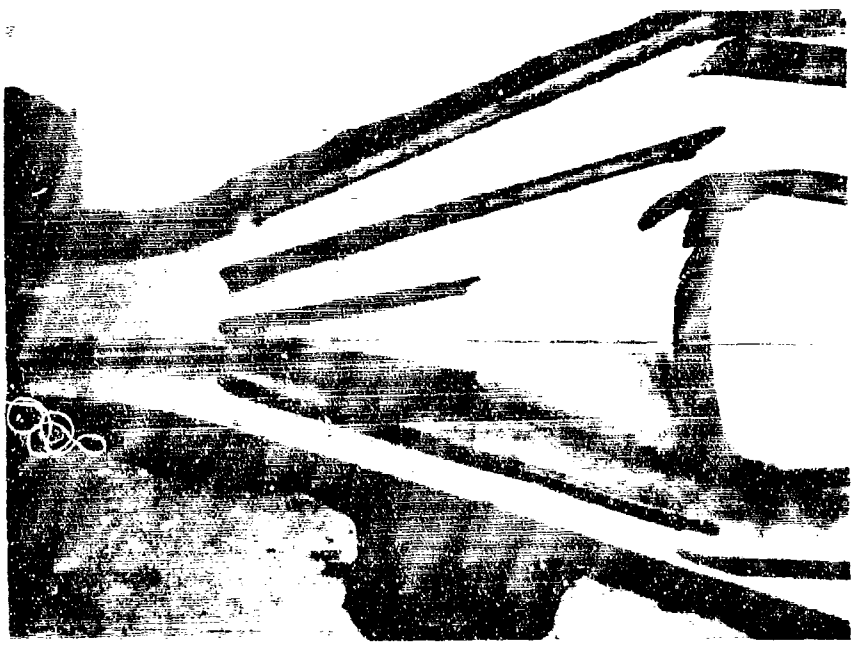

Figure 13. Primary Combustor Diffuser Water Table Testing. FE 52304 AIIIB

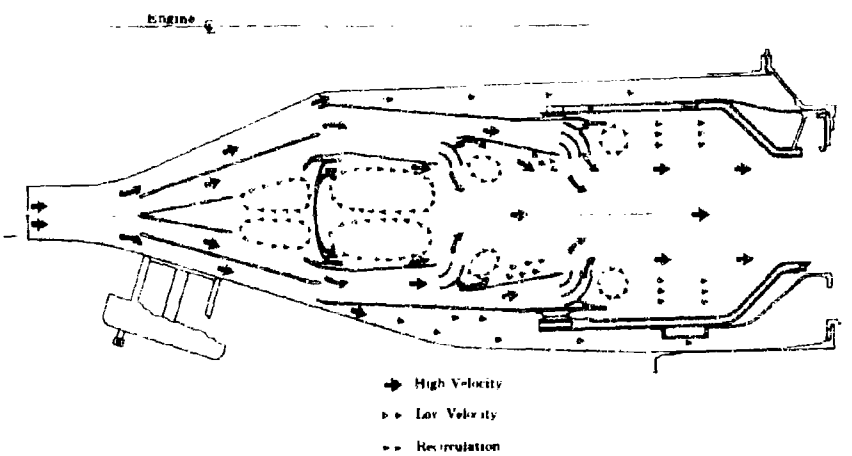

Figure 14. Water Table Evaluation of the Primary Combustor Airflow FD 13451B AIIIB

CONFIDENTIAL

The demonstrated pressure loss of the first and the last configurations run in the JT4 engine are shown in figure 15 along with the calculated increase for the higher heat release of the JTF17 at SLTO conditions. These test results and calculations show that the pressure drop for the primary combustor and diffuser will be substantially less than the maximum allowable 5.7%.

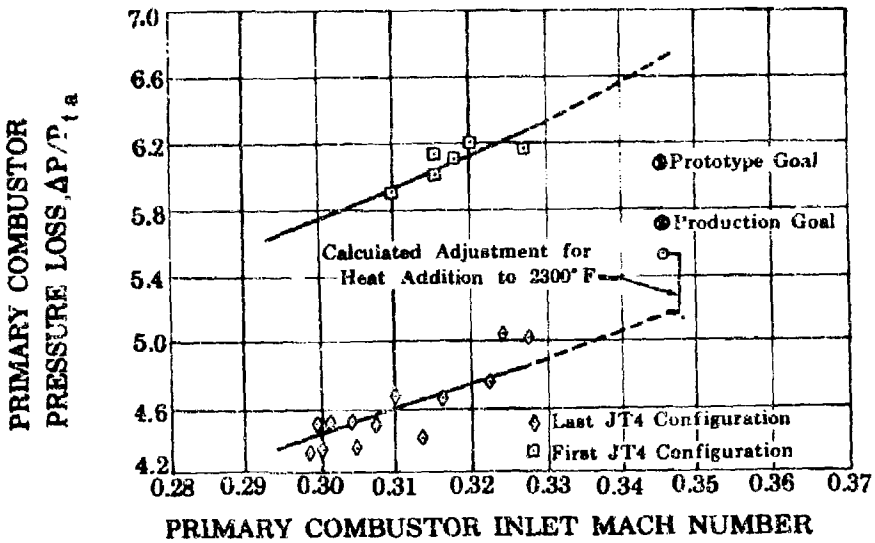

Figure 15. Comparison of Primary Combustor Pressure Loss

FD 16932
AIIIB

e. Volumetric Heat Release

The ram-induction combustor has demonstrated the high volumetric heat release rate required for the JTF17 engine in the experimental engine testing and in the 120-degree segment rig testing. The short-length, low engine cross-sectional area and low weight requirements result in a volumetric heat release rate requirement that is higher than that obtained from current can-annular burners. The comparison of requirements and experimental data is shown in table 1. In the development of the engine from the experimental JTF17 to the prototype JTF17, the volumetric heat release requirement has been reduced because of an increase in the primary combustor pressure level and a slight increase in the volume available.

Table 1. Primary Combustor Volumetric Heat Release Rates Btu/hr/ft^3/atm

Engine	Combustor Configuration	SLTO	Cruise
J58	Can-Annular	4.7×10^6	2.53×10^6
Experimental JTF17 Requirement	Annular Ram Induction	6.24×10^6	4.55×10^6
Prototype JTF17 Requirement	Annular Ram Induction	5.97×10^6	4.38×10^6
Phase II-C Demonstrated	120-Degree Segment Rig Annular Ram Induction	6.45×10^6	4.53×10^6
Phase II-C Demonstrated	Experimental JTF17 Engine	6.97×10^6	4.59×10^6

f. Turndown Ratio

The fuel/air ratio operating range of the primary combustor is from 0.002 to 0.027, and the ram-induction configuration has demonstrated stable operation over an even wider range. The 120-degree segment rig has demonstrated steady-state operation from 0.007 to 0.030 fuel/air ratio, and the annular duct heater rig, which is similar to the primary combustor in utilizing the ram-induction concept, has operated at a fuel/air ratio of 0.058, double that which is required for the primary combustor. Figure 16 shows the results of ignition tests on the 120-degree rig. These tests demonstrated rapid ignition down to a fuel/air ratio of 0.005, which is one-third of the expected sea level starting ratio. Both the JT4 engine and the experimental JTF17 engine tests have demonstrated this rapid ignition characteristic of the annular ram-induction combustor.

There have been no indications of any combustor stability problems in either the rig or engine testing over the range of operating conditions discussed in the previous paragraph. The JT4 annular burner rig has operated at a high rotor speed of 1800 rpm (approximately one-third the normal 5600 rpm at idle), and then accelerated without a problem. The trouble-free accelerations from ignition of the combustor to idle on both the JT4 engine and the experimental JTF17 engines have demonstrated the smooth combustion characteristics.

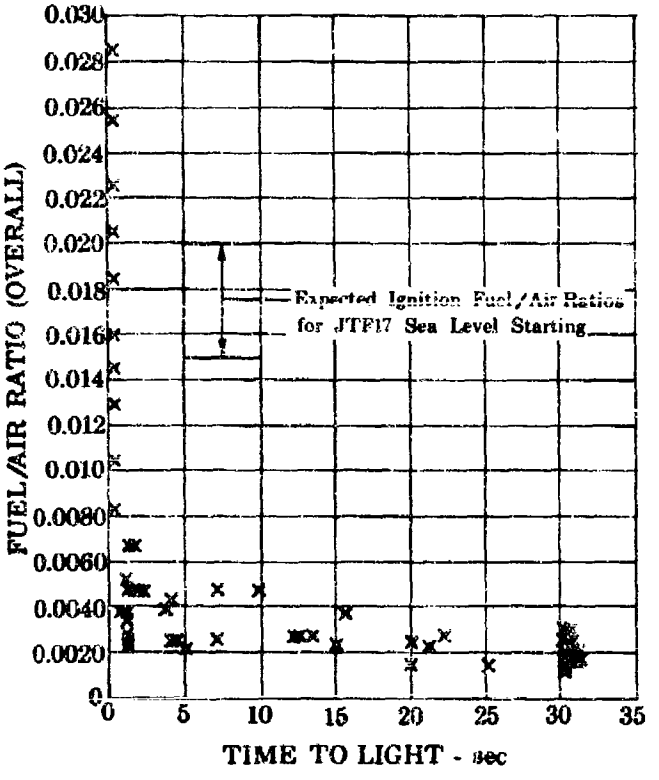

Figure 16. Mod 5-1C Combustor Sea Level Start Conditions

FD 16933
AIIIB

g. Acceptance of Airflow Profile Changes

The deflector in the primary combustor diffuser is effective in providing uniform airflow along both diffuser walls, even with changes in the diffuser inlet airflow profile. In the JTF17 prototype design, this deflector is a part of the primary combustor front end. The annular combustor configuration provides for the uniform division of the airflow around the complete circumference.

Tests have been run in 120-degree segment rig with uniform and distorted inlet airflow profiles simulating cruise conditions, as shown in figures 17 and 18. Comparison of data at 2200°F discharge temperature conditions does not show any significant effect on the average radial discharge temperature profile, as shown in figures 19 and 20.

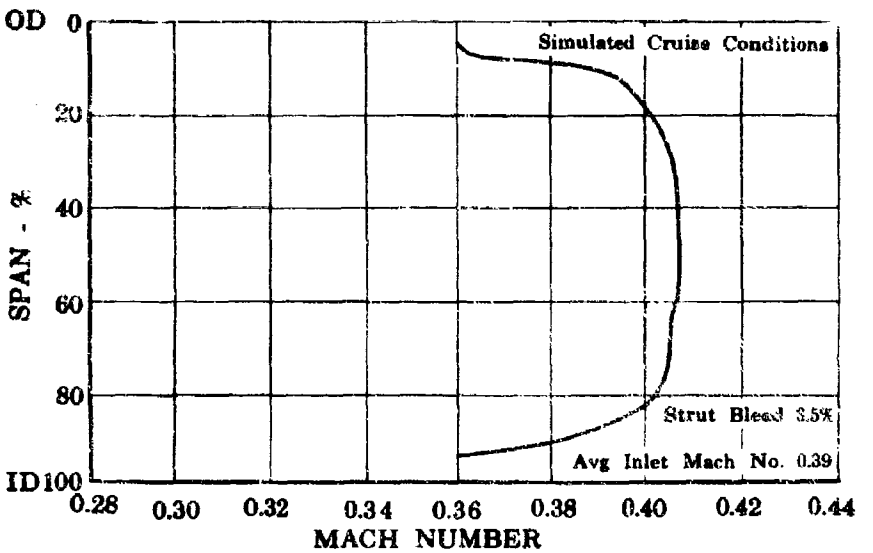

Figure 17. 120-deg Sector Rig Inlet Airflow Profile — FD 16934 AIIIB

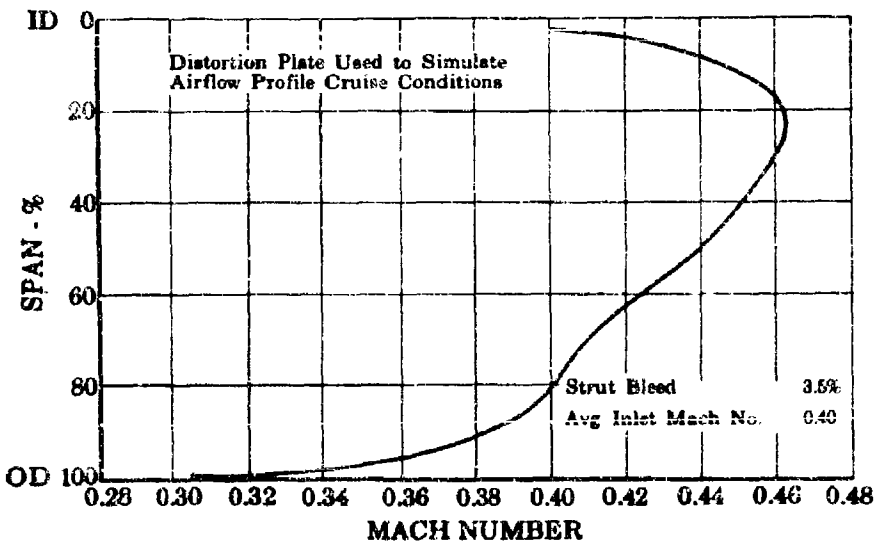

Figure 18. 120-deg Sector Rig Burner Inlet Airflow Profile — FD 16935 AIIIB

CONFIDENTIAL

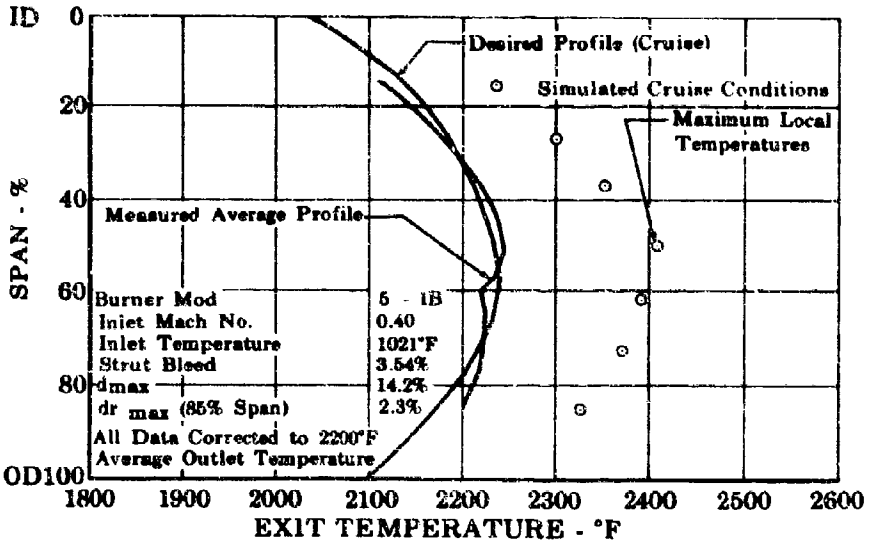

Figure 19. 120-deg Sector Rig Burner Outlet Radial Temperature Profile

FD 16936
AIIIB

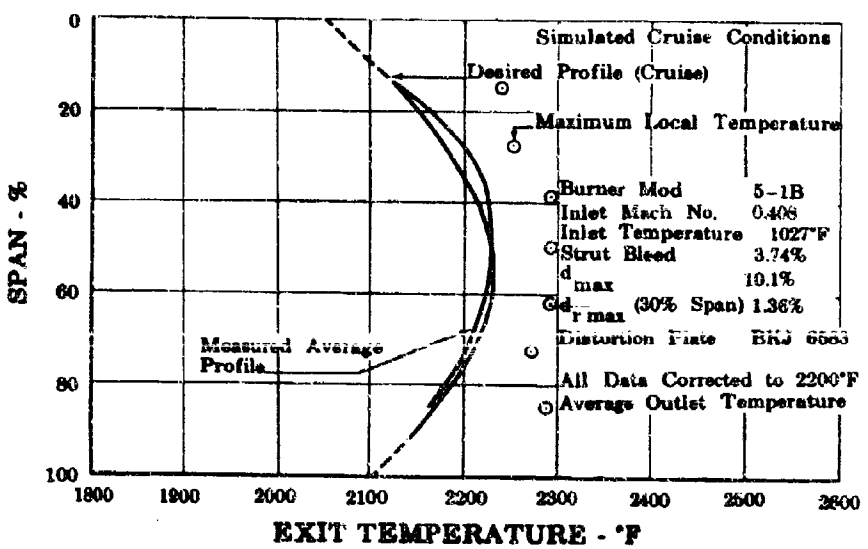

Figure 20. 120-deg Sector Rig Burner Outlet Radial Temperature Profile

FD 16937
AIIIB

h. Durability

The maintaining of high air velocities for efficient mixing in the ram-induction combustor also provides high heat transfer coefficients for cooling the metal surfaces. The initial testing in the annular JT4 engine showed effective cooling of the combustor walls with the exception of local scoop and wall edges, plus the heavy accumulation of carbon as shown in figure 21.

CONFIDENTIAL

A number of cooling louver additions and changes were effective in cooling the local scoops and walls, which had shown burning, and in reducing carbon accumulation. These changes were combined for the first primary combustor tested in the experimental JTF17 engine. Figures 22 and 23 show the combustor after testing, and clearly indicate the improvements made with the cooling air revision.

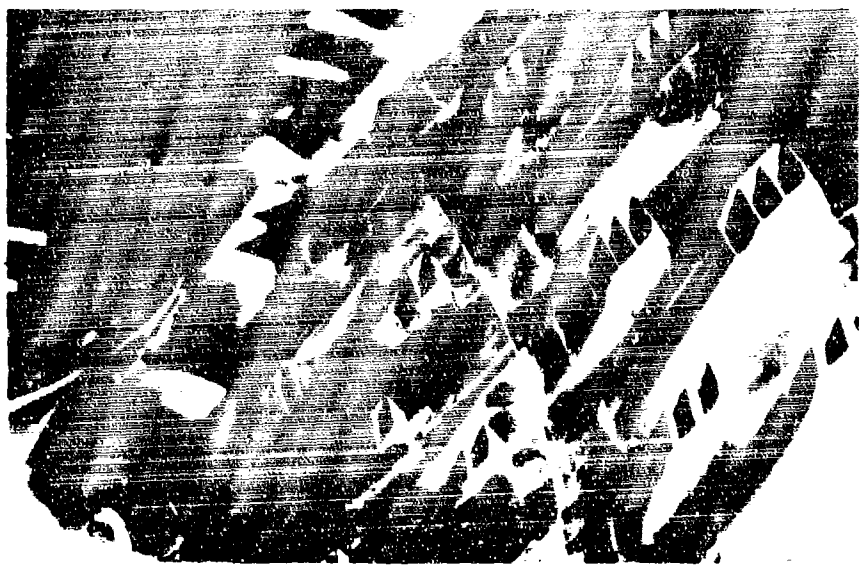

Figure 21. Mod 5-1D Primary Combustor Burnin and Carbon Accumulation — FE 55027 AIIIB

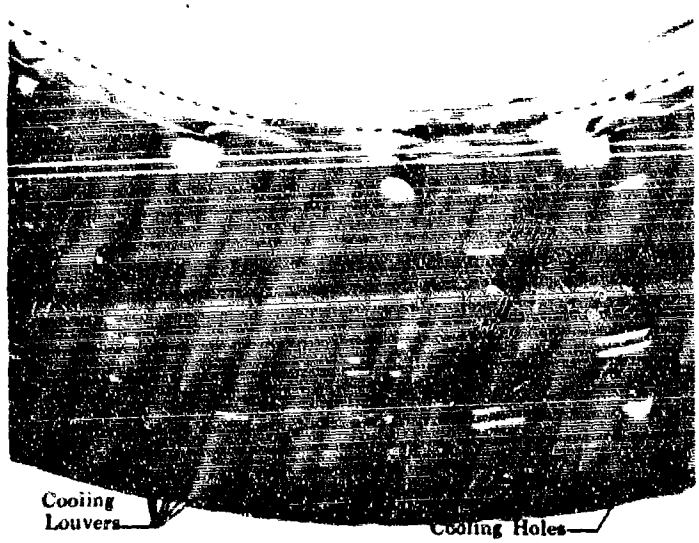

Figure 22. Mod 5-1P Primary Combustor After Testing on the JTF17 — FD 16707 AIIIB

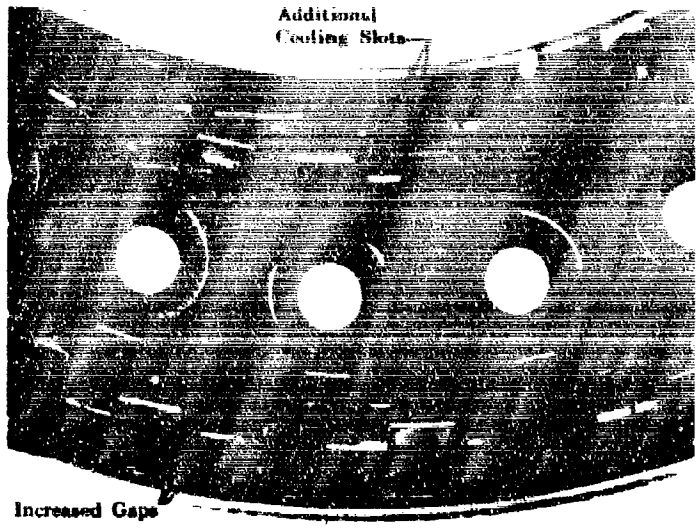

Figure 23. Mod 5-1P Primary Combustor After Testing on the JTF17 — FD 16708 AIIIB

Figures 24 and 25 show the metal temperatures of the primary combustor as measured in 120-degree segment rig, the JT4 engine and the experimental JTF17 engines at sea level conditions, and in the 120-degree segment rig for cruise conditions. The effective cooling of the high velocity airflow, coupled with the fact that the annular ram-induction combustor takes most of its structural load in walls that are not adjacent to the hot gas path, provides a long life and resistance to failure.

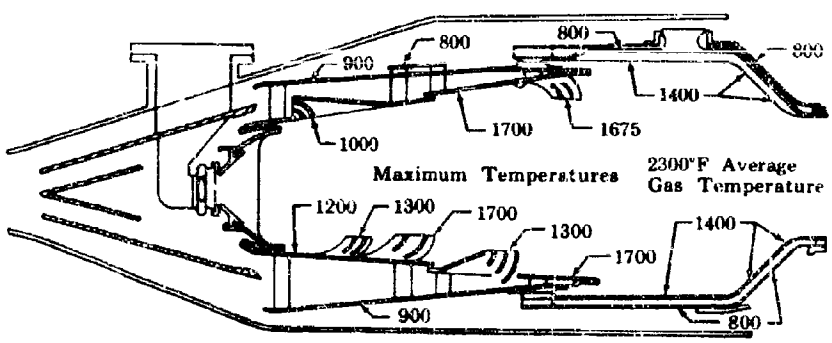

Figure 24. Combustor Section Metal Temperatures at SLTO — FD 16938 AIIIB

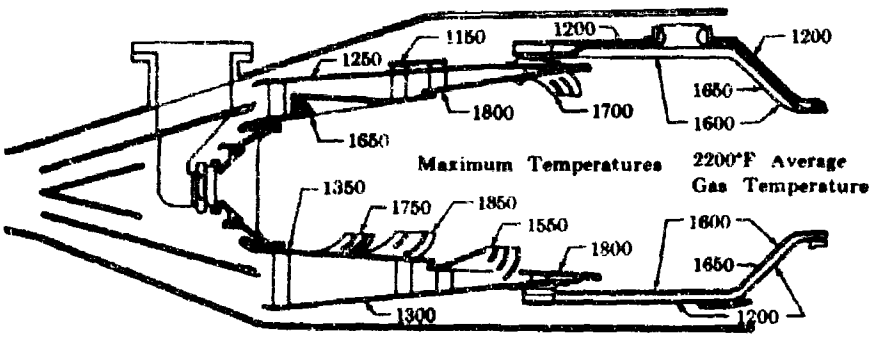

Figure 25. Combustion Section Metal Temperatures at Cruise

FD 16939
AIIIB

i. Smoke Generation

Although exhaust smoke density has not previously been a burner performance parameter, Pratt & Whitney Aircraft has had a full awareness of the potential problems of exhaust smoke. Sampling particulate matter from engine and component stands has been accomplished for many years and experience in the techniques required to measure smoke density has been accumulated.

The problem of smoke generation was considered early in the design and development of the JTF17 combustor. Exhaust sampling on the initial experimental engine shows good comparison with current commercial engines. The program has made use of comparative reflectance readings from engine exhaust samples using the Von Brand Smoke Meter. The data provided information enough for classification, or ranking, of the engines tested. An arbitrary scale of zero to one hundred is used to cover from clean to black. The following table will provide a comparison of current commercial engines with the JTF17 at maximum power conditions.

Table 2. Comparison of Current Engines With JTF17

Engine Type	Smoke Density
JT8D	45
JT3D	39
JT12	22
JTF17	17 to 21

During the many company development programs, experience has been accumulated on the variables which influence smoke generation. In general it appears that, with conventional burners, those that have leaner local fuel/air ratios at the front end of the combustion chamber produce less smoke.

j. Altitude Relight

During the SST Cruise performance demonstration tests, the experimental JTF17 engine has demonstrated an altitude start at 59,000 ft and 2.48 Mach number. This point may be seen on the windmilling restart envelope in figure 26. Additional engine relight data will be obtained during Phase II-C SST Cruise performance Tests

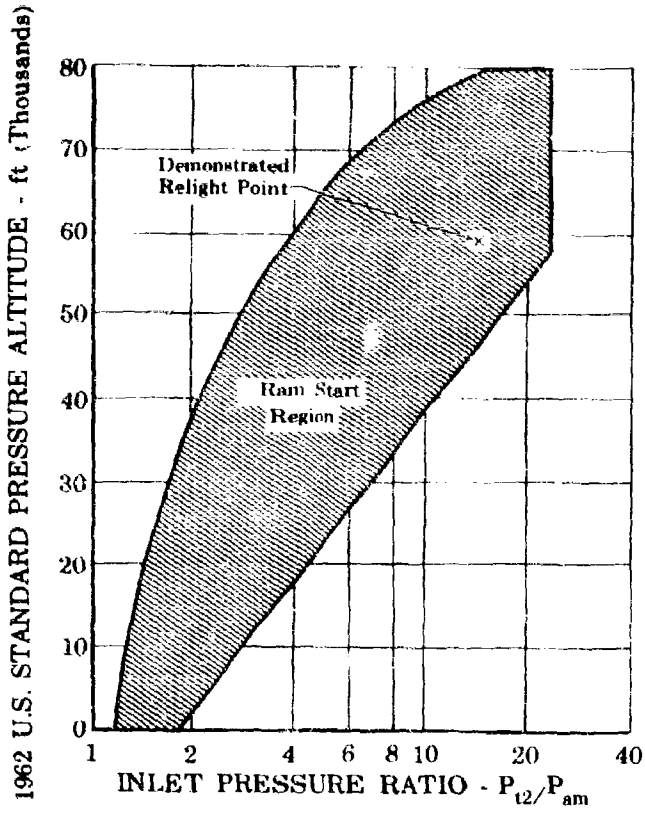

Figure 26. JTF17 Turbofan Engine Estimated Windmilling Restart Envelope Without Aerodynamic Braking

FD 17626
AIIIB

6. Fuel Nozzles

The fuel nozzle used for the Phase II-C program is a dual-orifice nozzle with a fixed primary orifice and a variable secondary orifice. This design allows the nozzle to operate satisfactorily over a flow range of 80 to 1, exceeding the burner requirement of 60 to 1, without requiring extremely high fuel pump discharge pressures. The spray characteristics of this nozzle are shown in figure 27. The nozzle provides a good atomization at low flows for ignition, and maintains a uniform pattern at all flow levels.

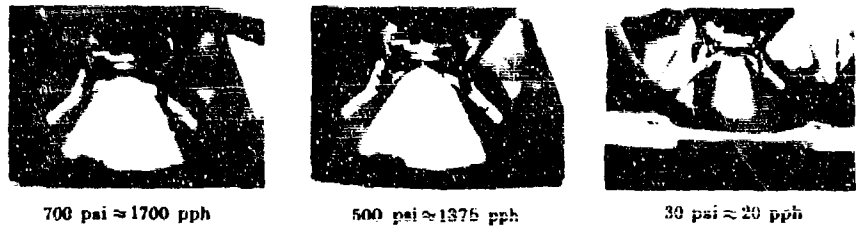

Figure 27. Spray Characteristics of Dual-Orifice Nozzle

FD 17569
AIIIB

A common nozzle tip for the metering of fuel flow is used in both the primary combustor and the duct heater with the only difference being the supports. Figures 28 and 29 show the total fuel flow schedule for the 24 primary combustor nozzles and the 40 duct heater nozzles.

Technology gained from the J58 program has been used in the design of these nozzles to provide the fuel flow range required with a minimum of maintenance and durability problems. These nozzles are designed to allow passage of relatively large contaminant particles and will be less susceptible to plugging than other designs. The results of nozzle testing in Phase II-C have been excellent, and this nozzle design will be used for continued development in Phase III. No problems have been encountered with these nozzles, and the flow schedules are repeatable after engine testing.

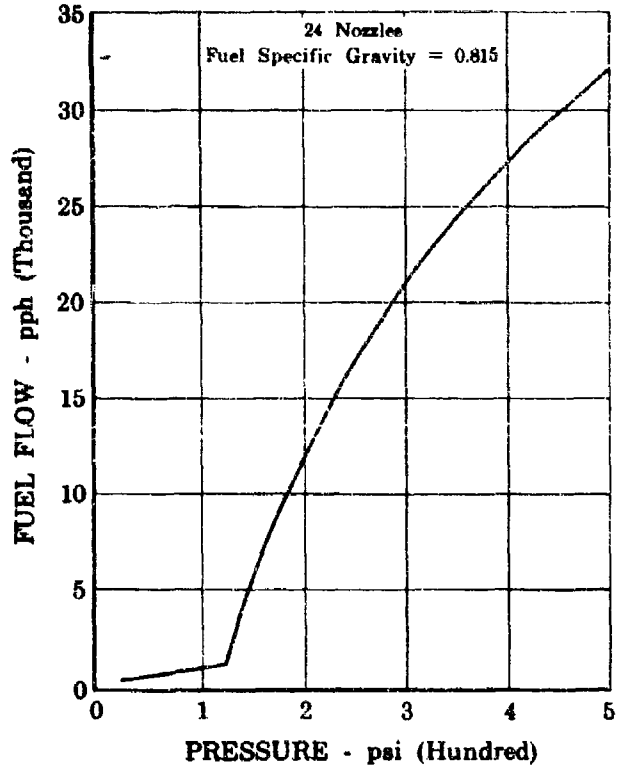

Figure 28. JTF17 Primary Combustor Nozzles FD 16940 AIIIB

CONFIDENTIAL

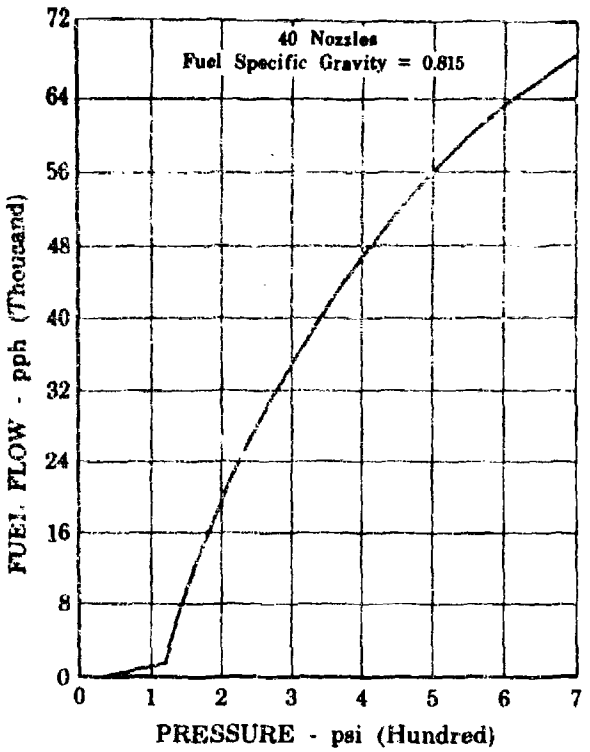

Figure 29. JTF17 Duct Heater Zone I Nozzles FD 16941 AIIIB

7. Summary

The important primary combustor characteristics of combustion efficiency and pressure drop have already met, or exceeded, the goals for the SST engine. In addition, substantial progress has been made in meeting the temperature profile goal in an engine, and the ability to apply rig test results to engine hardware successfully has been demonstrated. Thus, it is evident that continued development will result in a ram-induction burner that meets or exceeds all of the combustor goals set for the SST engine.

CONFIDENTIAL

C. TURBINE

1. Introduction

The high engine cycle performance, low engine specific weight, and high engine inlet temperature necessary in the supersonic transport aircraft require cruise operation at turbine inlet temperatures of 2200°F. Currently available turbine materials cannot operate at this temperature level and attain the long life required of a commercial engine, therefore cooling of the airfoils is required to reduce the metal temperature. The use of high compressor discharge air to cool the blades and vanes in the turbine introduces losses in turbine and overall cycle efficiencies. Consequently, it is necessary to establish the "cooling effectiveness" of the cooling method, or methods, to be employed in the various stages of the turbine to determine the cooling airflow rates and their associated losses. These must be known to accurately predict the cooled turbine efficiency. The following discussion includes, in addition to the aerodynamic and thermodynamic turbine performance and interstage leakage loss analyses, a description of the cooling methods and experimental results in terms of airflow requirements, resulting metal temperatures, and measured performance losses.

There are no differences between prototype and production engine turbine designs. The material in this section, therefore, applies to both engines. A summary of significant turbine design considerations and their effect on turbine performance is given below.

1. The turbine efficiency in a supersonic duct-burning turbofan engine has a relatively small effect on engine specific fuel consumption. Consequently, the turbine efficiency and weight tradeoff studies favor a lightweight turbine design with adequate turbine efficiency to meet the cycle requirements. These studies are not included in this report, but will be available for evaluation upon request.

2. For the reduced turbine velocity ratios chosen for the low spool turbine, the controlled vortex design provides a gain in turbine efficiency of 2 percentage points over that obtainable with a free vortex design. This advantage was used to reduce turbine diameters and weight, while maintaining the turbine efficiency required by the engine cycle.

3. The overall cycle efficiency cannot be improved by increasing turbine inlet temperature if this is accompanied by a proportional increase in cooling airflow. A gain in performance is attained by increasing the turbine exit temperature and pressure. Diluting the high temperature gas or causing higher turbine aerodynamic losses by further addition of cooling air can negate any gain or even cause a net loss in overall cycle efficiency. (See figure 1.) Therefore, it is important to minimize the amount of cooling air by employing the best high temperature materials and advanced cooling concepts to make the most efficient use of the cooling air.

4. The mode of cooling air discharge into the flow path, and disk and case cooling air leakage have significant effects on performance. Cooling air reentry parallel to the main gas stream and improved labyrinth seal systems have been employed to minimize these losses.

5. Complex methods of controlling the cooling air by separate cooling air lines and valves were unnecessary for performance or airfoil life reasons. The low cooling airflow allowed by the use of high temperature materials and high effectiveness cooling techniques reduce the performance penalties at the low temperature operating conditions where turbine cooling is not necessary.

6. Although the cooling effectiveness of film-cooled and convectively cooled airfoils are approximately equal at the low coolant flow rates required, the advanced convectively cooled airfoils are favored because the aerodynamic losses are considerably less for the trailing edge discharge type of convective cooling and because there is a most significant reliability and maintainability advantage for the solid exterior airfoil wall with regard to foreign object damage, low cycle fatigue life, structural integrity, coating application, and elimination of the possibility that the film cooling slots may become clogged. Results of the low cycle fatigue life testing will be made available for evaluation on request.

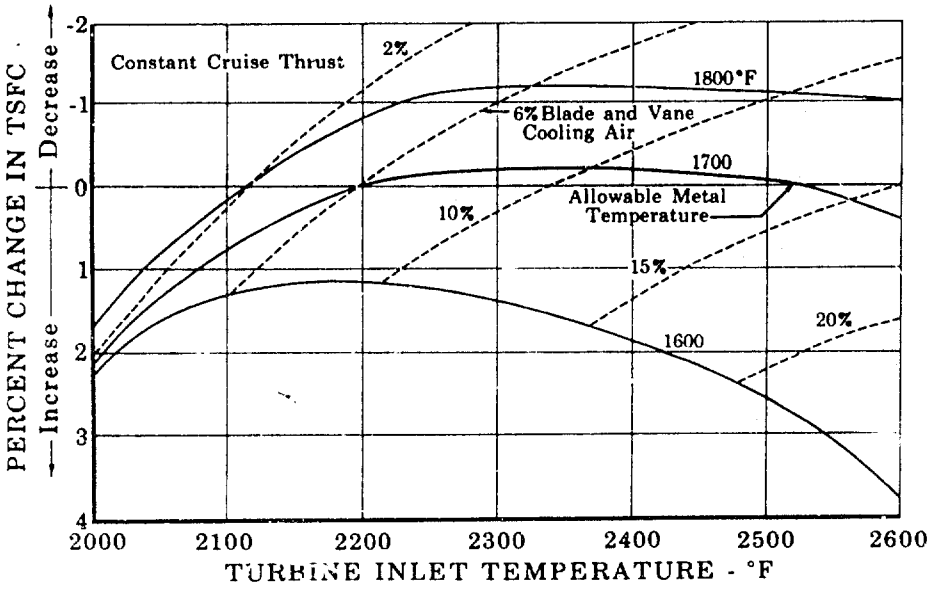

Figure 1. Percent Change in TSFC vs Turbine Inlet Temperature FD 17904 AIIIC

The predicted performance of the JTF17 turbine is based on the following principal factors.

1. Experimental verification of aerodynamic and thermodynamic effects of cooled airfoil air discharge into the turbine

2. The substantiated performance benefits obtained by the controlled vortex turbine design

3. Confirmation of the steady-state and transient airfoil metal temperature prediction system with measurements from engine and rig tests

4. Laboratory and engine tests of advanced high temperature materials and coatings demonstrating their high temperature strength and erosion and hot-corrosion resistance

5. Simulated engine environment rig tests demonstrating the level of cooling effectiveness attainable with over 20 advanced convective and film cooling configurations for 1st-stage airfoils

6. Refinement of a cooled airfoil low cycle fatigue (LCF) analysis system supported by substantiating test data.

The analytical procedures for the prediction of the JTF17 cooled turbine airfoil performance have been confirmed and substantiated by aerodynamic and thermodynamic testing of over 130 different cooled airfoil configurations.

The JTF17 turbine is a three-stage, axial flow reaction type that employs a controlled vortex flow pattern to attain high efficiency at low velocity ratios. A single high pressure stage drives the high compressor and two low pressure stages power the fan stages. The design objective was to design a low weight turbine with sufficient efficiency and power margin to attain an engine with a high thrust-to-weight ratio delivering high specific performance with a capability for future uprating. A three-stage turbine was selected as the result of optimization studies evaluating the weight, diameter, efficiency, cost and life trade factors necessary to set the flow path for the optimum engine. The results of these studies will be made available upon request. The metal parts are cooled where necessary by high compressor discharge air. The controlled vortex design was incorporated in all three stages to improve the blade root section reaction and turbine efficiency to the levels normally attained with larger diameter (and heavier) free vortex designs.

The performance of the turbine at the altitude design point is summarized in table 1 following.

CONFIDENTIAL

Table 1. JTF17 Turbine Performance Summary at Cruise

Stage		1		2		3	
Stage cooled efficiency		0.869		0.965		0.886	
Stage work, Btu/lb		112.38		61.87		51.85	
Stage flow rate entering,	lb/sec	117.06		119.48		121.29	
Airfoil		1Vane	1Blade	2Vane	2Blade	3Vane	3Blade
Cooling flow, %		1.9	2.0	1.0	0.5	0.3	0
Average Mid-Span gas temperature,	°F	2256	2011	1830	1721	1600	1509
Average metal temp,	°F	1700	1644	1617	1616	1543	1509
ΔT Cooling,	°F	556	367	213	105	57	0
Cooling effectiveness		0.48	0.421	0.31	0.18	0.12	0

$$\text{Cooling Effectiveness} = \frac{T_{gas} - T_{metal}}{T_{gas} - T_{cooling\ air}}$$

2. Cooling Requirements

Studies relating turbine inlet temperature, allowable airfoil metal temperature and engine cruise TSFC were performed to establish the effect that these paramters have on thrust specific fuel consumption. Figure 1 shows the results of this study. The important conclusions drawn are:

1. The selected 2200°F cruise turbine inlet temperature provides about the optimum TSFC for present turbine materials which are limited to approximately 1700°F airfoil metal temperature for the long life required for commercial service
2. Cruise operation above 2200°F turbine inlet temperature provides no significant improvement in fuel consumption for airfoil metal temperatures in the 1600-1800°F range, owing to the offsetting losses from the high percentages of cooling air required
3. A significant improvement in TSFC (1.2%) can be achieved by development of materials capable of long time operation at 1800°F metal temperature, because operation at higher turbine inlet temperature is then possible without an increase in cooling air requirements. Directionally solidified PWA 664 or single crystal PWA 1409 materials appear to have properties permitting this 1800°F capability for future engine growth.

CONFIDENTIAL

The JTF17 turbine incorporates cooling on all the airfoils except the 3rd-stage blades. Figure 2 is a sketch of the turbine showing the cooling flow distribution and amount used at the cruise point. Table 2 lists the percent cooling air and its effect on performance for takeoff, cruise, and idle descent for both standard and hot day conditions. The estimated overall loss in turbine efficiency due to cooling over the range of operating conditions is small, varying from 0.57% to 0.816%. Also, even though the predictions for cooling air requirements are believed to be accurate and well substantiated, it is comforting to note that a 50% increase in the required cooling air at cruise results in a further loss of only 0.366% in aerodynamic turbine efficiency.

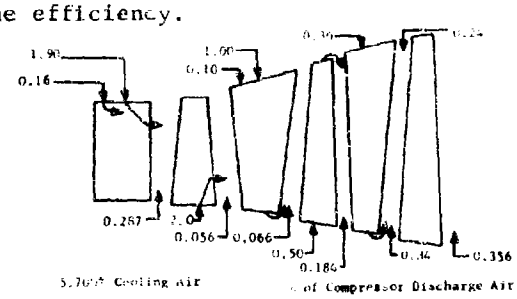

5.76% Cooling Air
1.68% Leakage Air
% of Compressor Discharge Air

	1st-Stage	2nd-Stage	3rd-Stage
Vane Cooling	1.90	1.0	0.30
Vane Platform Leakage	0.161	0.10	0.0
Disk Front Seal Leakage	0.267	0.066	0.034
Blade Cooling	2.00	0.50	0.0
Disk Rear Seal Leakage	0.056	0.184	0.336
Leakage Behind 2nd-Stage Vane	--	--	0.24
Stage Total C/A and L/A	4.403	1.850	0.930

Total Turbine Cooling and Leakage 7.153%

Leakage to Duct = 0.68%
Duct Fuel Pump Air = 1.00%
Total Bleed = 1.68%

Figure 2. Airfoil Disk and Case Cooling Flow Distribution at Cruise Design Point

FD 16765
AIIIC

Convective cooling is employed throughout the turbine. The 1st-stage airfoils operate in the hottest environment and require the high cooling effectiveness of the most advanced convective cooling technique to minimize the cooling air used. The 2nd-stage and 3rd-stage vane airfoils do not require such high cooling effectiveness, and consequently use current operational convective cooling techniques. The cooling effectiveness (ϕ) is the difference between the gas temperature and the cooled metal temperature divided by the difference between the gas and cooling air temperatures.

$$\phi = \frac{T_{gas} - T_{meta.}}{T_{gas} - T_{cooling\ air}}$$

Table 2. Turbine Efficiency Losses Due to Cooling Air

Condition	Alt	Mach No.	1st Stage		2nd Stage		3rd Stage		Overall Turbine
			% C/A	$\Delta\eta$	% C/A	$\Delta\eta$	% C/A	$\Delta\eta$	$\Delta\eta$
Cruise	65K	2.7	3.9	0.975	1.5	0.724	0.3	0.18	0.732
Cruise Hot Day	65K	2.7	3.58	0.894	1.38	0.666	0.27	0.162	0.671
SLTO	0.	0.	4.31	1.111	1.59	0.767	0.32	0.192	0.816
SLTO Hot Day	0.	0.	4.41	1.102	1.57	0.758	0.318	0.191	0.808
Idle Descent	65K	2.7	3.07	0.767	1.21	0.584	0.24	0.144	0.580
Idle Descent Hot Day	65K	2.7	3.03	0.756	1.195	0.576	0.235	0.141	0.572
Cruise 50% Increase C/A	65K	2.7	5.85	1.461	2.25	1.087	0.45	0.27	1.098
Subsonic Cruise	36150	0.9	4.00	1.00	1.52	0.734	0.31	0.186	0.759

% C/A - Percent Cooling Air

$\Delta\eta$ - Efficiency Loss Points

The cooling effectiveness has been measured in tests for several cooling methods, and the results are shown as a function of percent cooling air in figure 3. The results can be grouped in three general categories: current operational convective, advanced convective, and film cooled. The difference between the advanced convective and the current operational convective methods is the cooling heat transfer coefficient augmentation provided by impingement cooling and high coolant velocities on the inner wall. The high cooling efficiency of the 1st-stage airfoils is provided by the "thermal skin" type construction. This method of cooling has been particularly successful in the 1st-stage vane of the J58 engine for the last 4 years. Test data of figure 3 show that advanced convective cooling and film cooling have approximately the same cooling effectiveness in the region of 2% cooling airflow. Therefore, convective cooling was chosen for the following reasons.

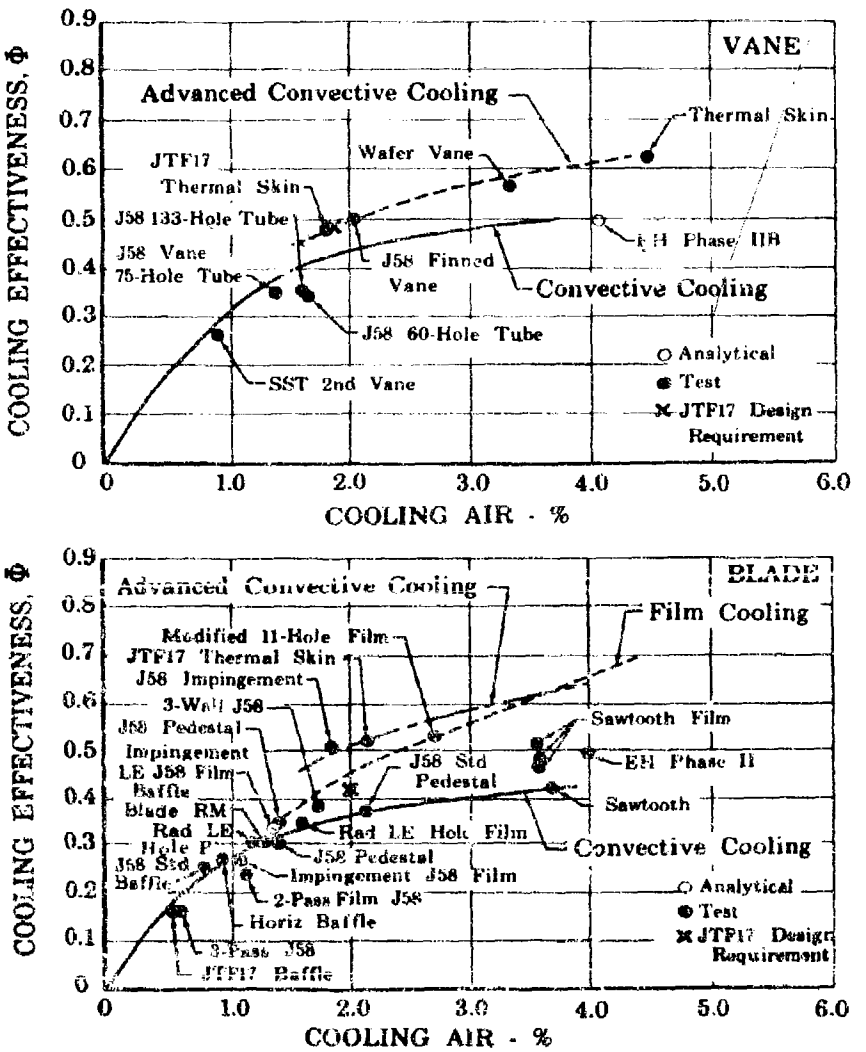

Figure 3. Blade and Vane Cooling Effectiveness FD 17093
AIIIC

1. The aerodynamic losses of the convective-cooled airfoils are lower than losses with film-cooled airfoils. All of the cooling air is discharged parallel to the main gas stream at the trailing edge where it serves to energize the wake and minimize losses. No cooling air is discharged into the flow passage between blades where it can disturb the main gas stream flow and boundary layer. Test data shown in figure 4 illustrate the change in turbine stage efficiency between the trailing edge discharge convective method and a film-cooled airfoil. An efficiency advantage of 1.2 points is shown for the trailing edge discharge method.

2. Foreign Object Damage Resistance - The leading edge of the airfoil is solid. Because of the superior cooling afforded by impingement cooling, film cooling slots that could clog or be closed by foreign object damage, are not needed on the airfoil.

3. Low Cycle Fatigue Life - The exterior wall has no stress risers or slots that can have severe temperature gradients across them.

4. Coatings can be stripped and renewed on a solid wall airfoil. An airfoil with a multitude of tiny slots creates a difficult recoating problem.

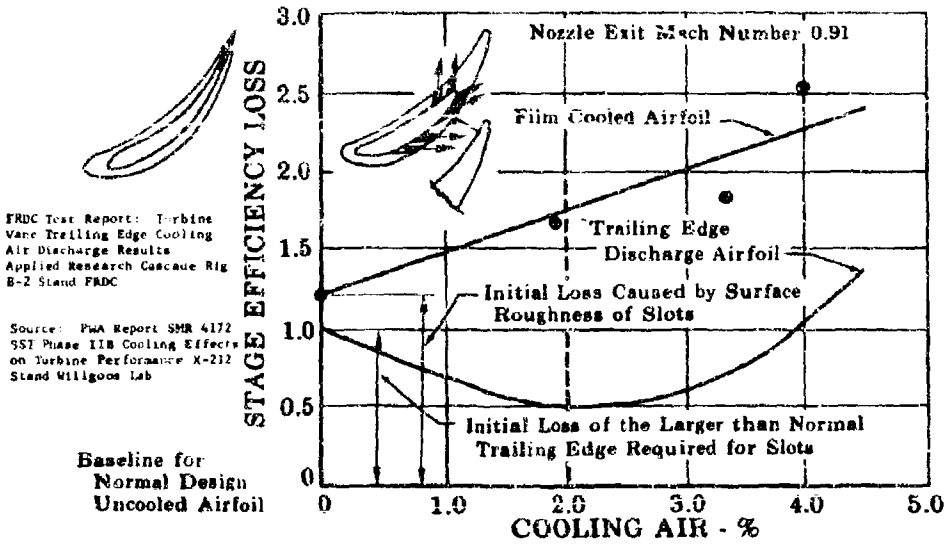

Figure 4. High Pressure Turbine Efficiency Loss vs Percent Cooling Air — FD 16369 A111C

a. Cooling Configuration of the 1st-Stage Turbine Vane

Figure 5 illustrates the 1st-stage turbine vane. The cooling air enters the center tube, travels radially to the leading edge impingement holes, reverses direction to pass between the tube and the outside wall, and discharges through the trailing edge. Effective cooling is accomplished at the leading edge by direct impingement, at the side walls by high velocity parallel flow, and at the trailing edge by high velocity air turbulated by pins. The center tube is removable to change the cooling air distribution if desired, during the development of the engine. This design develops a cooling effectiveness of 0.48 at the design cooling airflow rate of 1.9%.

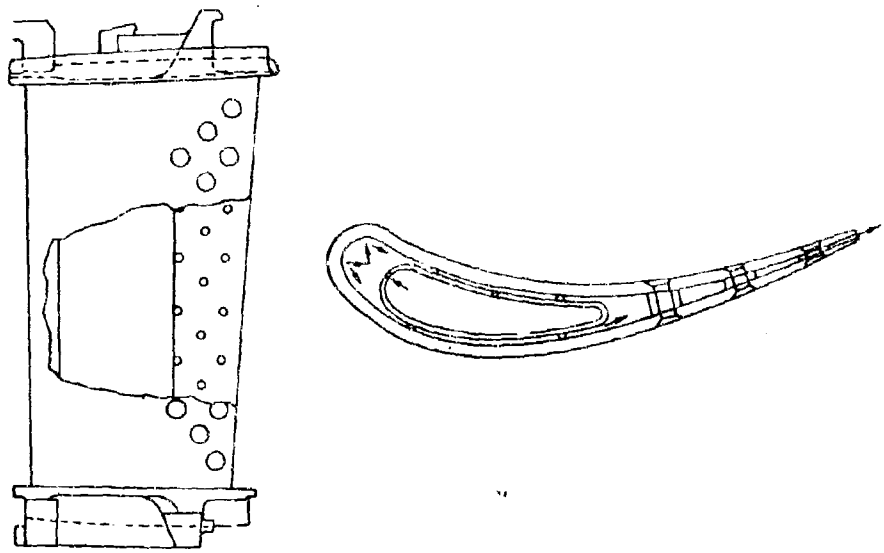

Figure 5. JTF17 1st-Stage Vane TD Nickel Sheet and Cast on Platform — FD 16774 AIIIC

b. Cooling Configuration of the 1st-Stage Turbine Blade

Figure 6 shows the 1st-stage blade cooling method. It is similar to the 1st-stage vane except that the center tube is an integral part of the blade casting. Air enters at the root and travels through the leading edge impingement holes, around the tube and exits at the trailing edge. The advantage of this design is its ability to place cool air at any span or chordwise location where it can best be used effectively to increase creep, erosion, or low cycle fatigue life at the critical sections. This airfoil also develops a cooling effectiveness of 0.42 with 2.0% cooling air.

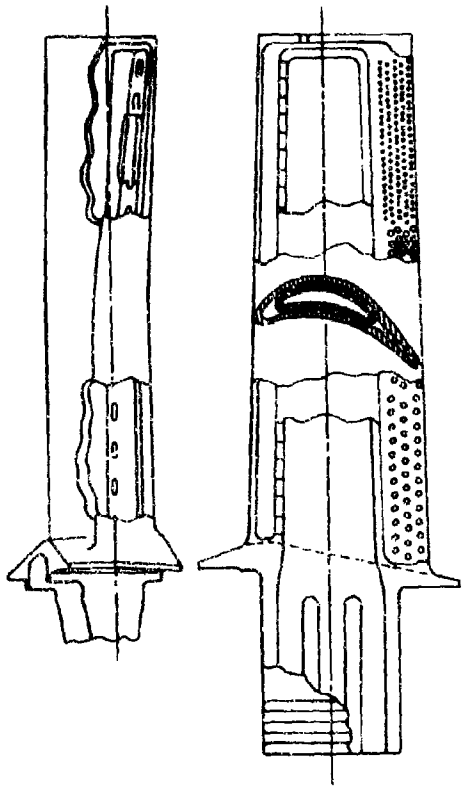

Figure 6. Four-wall 1st-Stage Turbine Blade Design FD 16773 AIIIC

An alternative method of manufacturing this cooled blade is being considered to reduce casting costs and improve the cooling effectiveness. The center cooling tube will be inserted from the tip and pinned to the root attachment. The tube and outside wall then become separate simple single wall castings with well controlled cooling air orifice sizes. Figure 9 in Report B, Section II, Paragraph C shows this blade configuration.

c. Cooling Configuration of the 2nd-Stage Turbine Vane and Blade, and 3rd-Stage Vane

Figures 7 and 8 present the cooling methods selected for the 2nd-stage turbine airfoils. These represent current operational cooling geometry, and no decided advantage exists to warrant selection of an advanced cooling scheme. The allowable metal temperature is attained with the low cooling effectiveness of 0.31, and savings in cooling air do not warrant the added cost of advanced cooling. The 2nd-stage blade also is a current operational cooling scheme and requires a cooling effectiveness of only 0.13 to attain its allowable metal temperature. Both airfoils have cooling air blowing radially through the hollow center chord and discharging at the vane root and the blade tip. The 3rd-stage vane cooling scheme is a duplicate of the 2nd-stage vane.

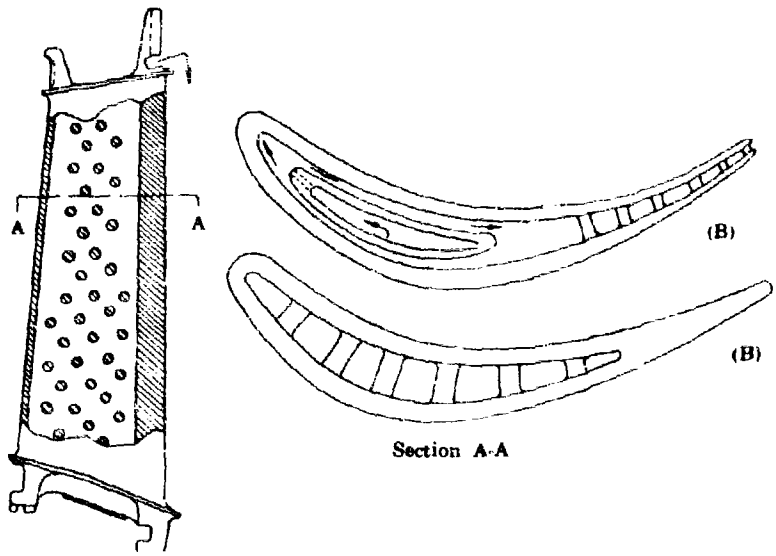

Figure 7. JTF17 2nd-Stage Vane

FD 16775
AIIIC

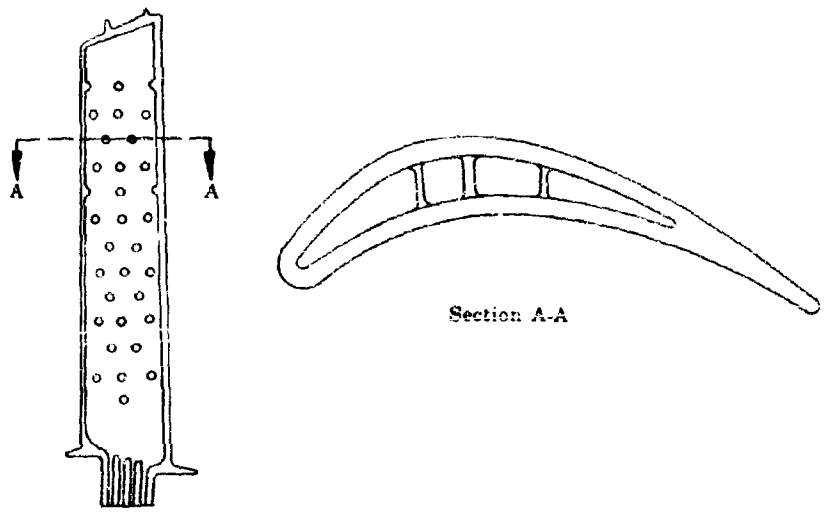

Figure 8. JTF17 2nd-Stage Blade

FD 16776
AIIIC

The 2nd-stage vane could be cooled by the same technique used in the 1st-stage if heating problems are encountered during development. However, at this time cost outweighs the advantages of increasing 2nd-stage efficiency 0.4 percentage points while reducing 2nd-stage blade gas temperature 10°F. With further casting development the cost of this type casting should be reduced to the point where inclusion of these performance improvements would be justified.

3. Cooling Losses

The turbine efficiency losses caused by cooling air for various flight conditions were previously tabulated in table 2. A breakdown of the losses at cruise for each airfoil is shown below:

Airfoil	1st-Stage Vane	1st-Stage Blade	2nd-Stage Vane	2nd-Stage Blade	3rd-Stage Vane	3rd-Stage Blade
Percent Cooling Air	1.9	2.0	1.0	0.5	0.3	0
Stage Efficiency Loss, Percentage Points	0.475	0.5	0.6	0.125	0.18	0

These losses are relative to an uncooled turbine, and are used to modify the uncooled mean line design. Cooling air losses were determined by cascade and rotating rig testing, and a high degree of confidence in the predicted losses has been achieved through the correlation of these data.

Figure 9 shows the stage efficiency loss as a function of percent cooling airflow for a turbine vane similar to the JTF17 1st-stage vane. The cooling air is discharged through a slot in the trailing edge. The point of minimum loss was found to be a function of the flow per unit area of both the cooling air and the mainstream. The tests show that minimum efficiency loss occurs when $(\rho V)_{\text{cooling air}}/(\rho V)_{\text{mainstream}}$ is between 0.4 and 0.5. Each JTF17 turbine airfoil with trailing edge discharge has been designed to achieve minimum loss with the design cooling flow. Figure 9 shows typical test data from a J58 1st-stage vane. This curve illustrates profile loss as a function of $(\rho V)_{\text{cooling air}}/(\rho V)_{\text{mainstream}}$. The low aerodynamic loss of the cooled vanes is the result of the pumping action of the trailing edge cooling air discharge energizing the trailing edge wake.

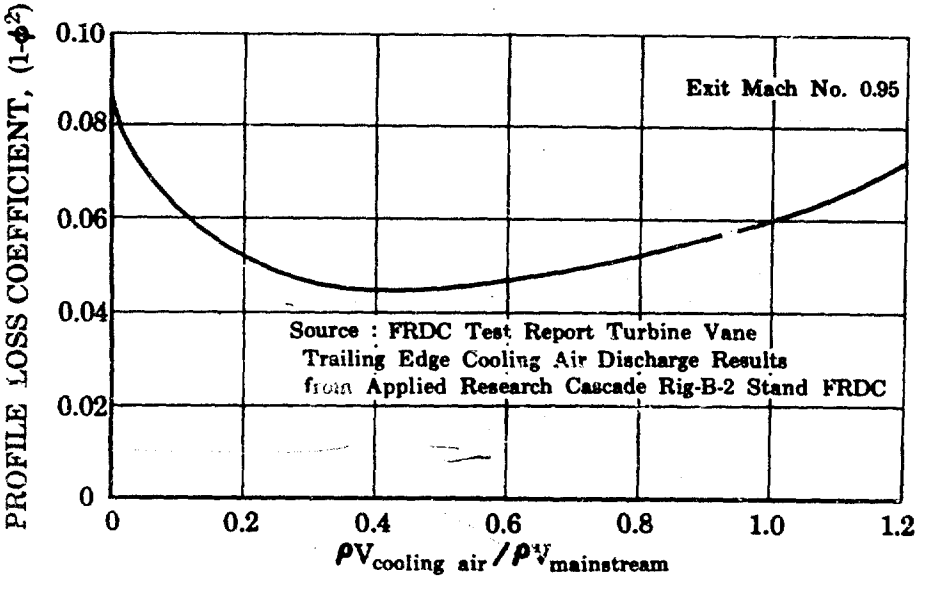

Figure 9. First Turbine Vane (J58) Profile Loss vs ρV Ratio for Trailing Edge Discharge of Cooling Air

FD 17523
AIIIC

Figure 10 illustrates the turbine stage efficiency variation for cooling air injection into the mainstream behind the vane root. The cooling air from the 2nd- and 3rd-stage vanes is discharged in this manner.

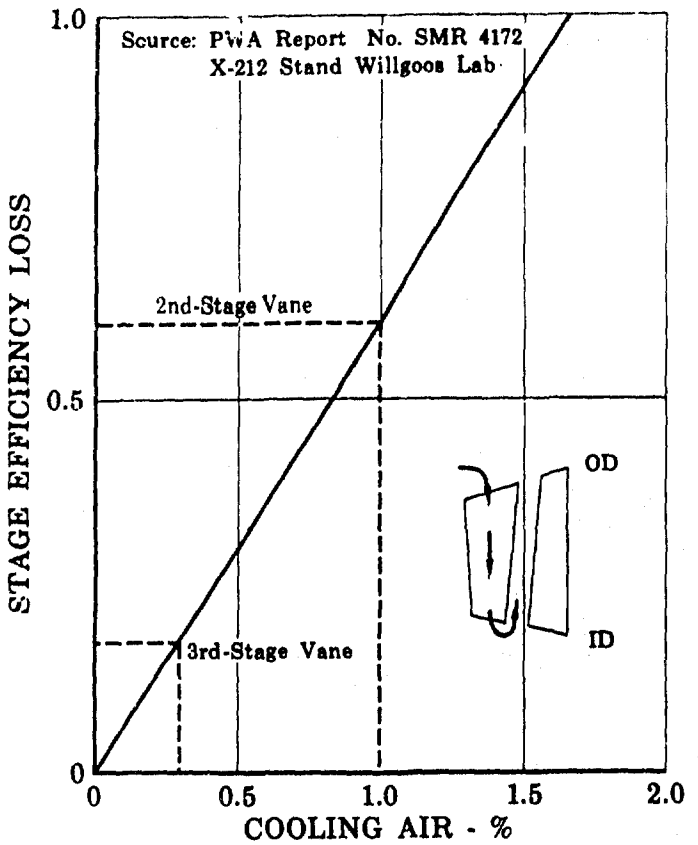

Figure 10. Turbine Efficiency Loss vs Cooling Air Injected Behind Vane Root (2nd- and 3rd-Stage Vanes)

FD 17530
AIIIC

Figure 11 shows the losses due to cooling air discharging from the blade tip. Since the flow of cooling air into the tip clearance space reduces the tip leakage loss, the efficiency loss due to the cooling air discharge is small.

4. Seal Leakage Losses

The JTF17 prototype engine will use segmented solid Waspaloy shrouds. The blade tip seal configurations are as follows:

1. The 1st-stage blade has no tip shroud. The cruise steady-state running clearance is 0.020 inch.

2. The 2nd-stage blade has a single-lip tip shroud to reduce vibratory stresses and leakage. The cruise steady-state running clearance is 0.030 inch.

3. The 3rd-stage blade has a double-lip tip shroud to reduce vibratory stresses and leakage. The cruise steady-state running clearance is 0.035 inch.

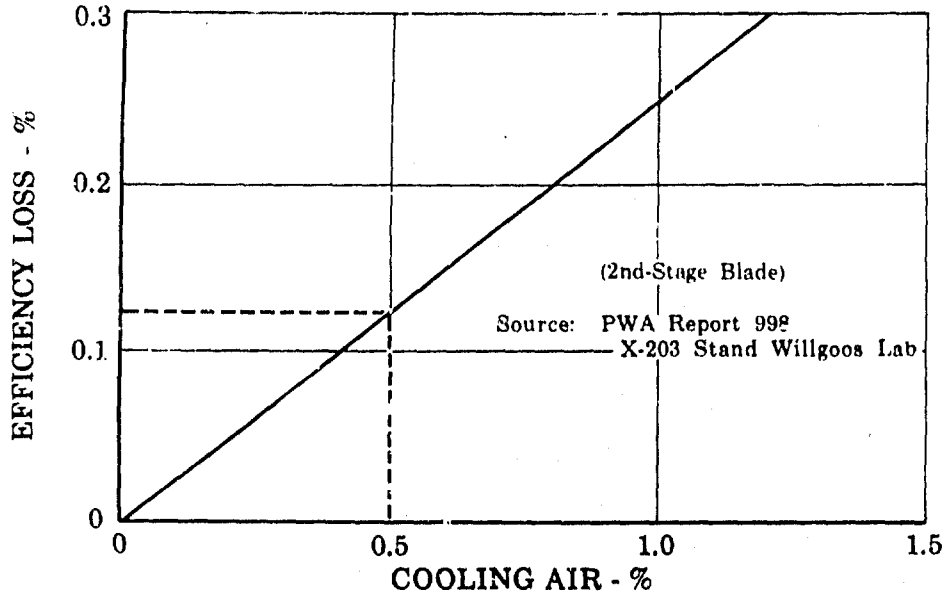

Figure 11. Turbine Efficiency Loss Due to Cooling Air Discharging From the Blade Tip — FD 16772 AIIIC

The gas that flows over the blade tips does no work in that stage and therefore causes an efficiency loss. Figure 12 shows the results of P&WA flow tests on various seal configurations. The leakage flow for a particular blade is calculated as a function of inlet static pressure and temperature, static pressure ratio, and seal geometry.

The blade tip leakage efficiency is defined as

$$\eta_L = \frac{\text{Mainstream flow - Leakage flow}}{\text{Mainstream flow}}$$

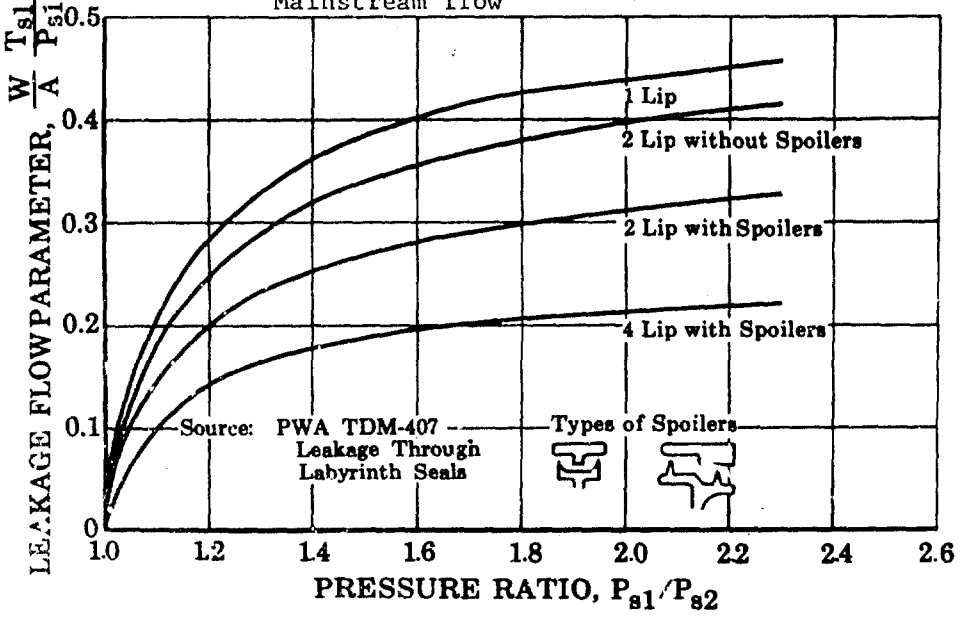

Figure 12. Flow Parameter vs Expansion Ratio for Various Seal Condigurations — FD 16766 AIIIC

The leakage efficiencies of the JTF17 turbine are as follows:

1st-Stage Blade	0.9918
2nd-Stage Blade	0.9948
3rd-Stage Blade	0.9957

These levels of running clearance and leakage efficiency are attained by the use of tip clearance control systems. Prevention of tip seal rub during the worst engine transient condition formerly set the amount of tip clearance at the steady-state running conditions. Simple and rugged tip clearance control systems are included in this design to limit the differential expansion between the case and rotor during the transient condition and allow tight steady-state clearances. These methods incorporated in the JTF17 raise turbine efficiency approximately 1.7 percentage points in the high- and 2.0 percentage points in the low-pressure turbine.

5. Aerodynamic Performance

a. Turbine Mean Line Design Program

The turbine mean line design program used to design the JTF17 is composed of the basic turbine equations and a well-developed loss calculation system. The loss calculation system includes the effects of airfoil camber, reaction, Mach number, incidence, secondary flow, Reynolds number, leakage flows, and cooling flows. Test results from many plane and annular cascades of turbine vanes and blades form the basis for the empirical loss coefficients used in this program. In addition to cascade data, single-stage rotating rig data and engine test data are continuously being acquired and used to modify the performance prediction system to assure a high degree of accuracy.

The predicted efficiency of the JTF17 turbines is summarized in table 3. The predicted efficiencies are based on the well substantiated free vortex design system with credits and debits being applied to this base efficiency for the effects of controlled vortexing, reduced tip clearances and cooling air losses.

Figure 13 compares turbine test efficiency with the predicted turbine efficiency. Note that agreement between the predicted and experimental free vortex turbine efficiencies is quite close. These turbines were free vortex, uncooled designs with typical running tip clearances. The base efficiency of the JTF17 was calculated using this free vortex system to preserve the previously established prediction reliability. Item (1) in table 3 presents this base efficiency.

Tests of controlled vortex turbine designs have shown test efficiencies considerably in excess of the free vortex designs. Figure 14 presents test data of controlled vortex gains over free vortex predictions. Conservative design values were used to ensure attainment of the design goals. These design values result in a 2.0% efficiency gain in the low pressure turbine and 0.0% in the high. These values are listed in table 3 item (2).

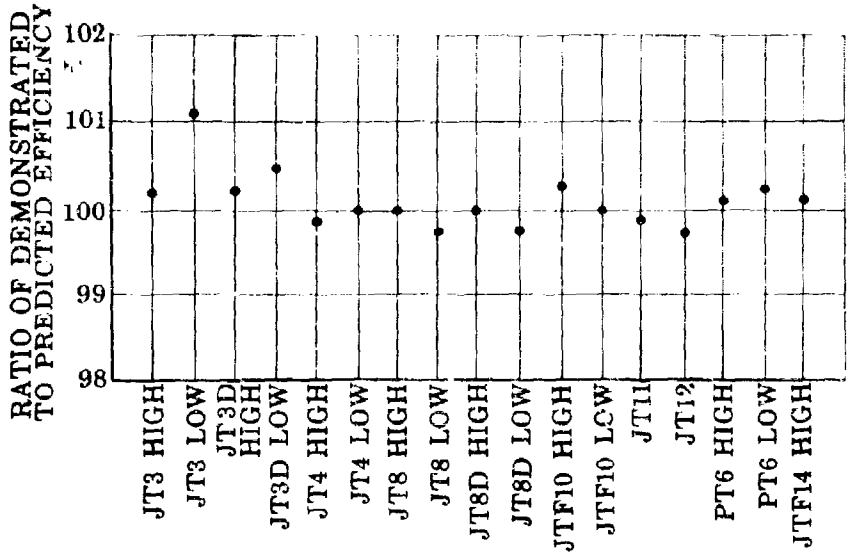

Figure 13. Accuracy of P&WA Turbine Design System Comparison of Demonstrated Turbine Efficiency With Predicted Efficiency

FD 17532
AIIIC

Table 3. JTF17 Turbine Efficiency Summary at Cruise Condition

	High Pressure Turbine	Low Pressure Turbine
(1) Base Turbine Efficiency Predicted by Free Vortex Design Methods and Normal Tip Clearances, %	86.2	84.5
(2) Turbine Efficiency Gain Predicted for Controlled Vortexing, %	0.0	+2.0
(3) Turbine Efficiency Gain Expected for Reduced Tip Clearances, %	+1.7	+2.0
(4) Efficiency Loss Due to Cooling Air Discharge Into Turbine Flow Path, %	-1.0	-0.5
Net Resultant Efficiency for a Controlled Vortex, Cooled Turbine With a Reduced Blade Tip Clearance Control System, %	86.9	88.0

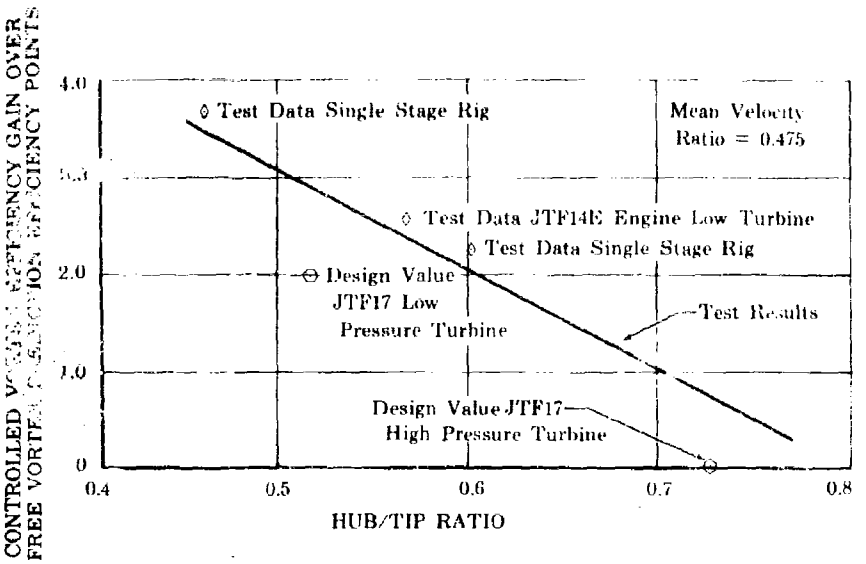

Figure 14. Efficiency Gains of Controlled Vortex Test Turbines Over Free Vortex Predictions

FD 17531
AIIIC

The use of reduced blade tip clearance control systems and its resultant gains in turbine efficiency are discussed fully in the Design Report (Report B) and also in paragraph D4 of this section. Potential efficiency gains of 3.4% in high turbine efficiency result from clearance reductions from 0.082 to 0.020 in. Similar clearance reductions in the low turbine reduce its leakage losses. Conservative design values of 1.7% gain in the high pressure turbine efficiency and 2.0% in the low were selected to ensure attainment of the required efficiency goals. Item (3) of table 3 lists this efficiency credit to the base efficiency of the uncontrolled tip clearance turbine.

The effect of cooling air and the test data substantiating the efficiency losses attributed to cooling air was discussed in paragraph D3 of this section. The resultant losses due to cooling air discharge into the turbine must be subtracted from the base uncooled turbine predicted efficiency. A 1% loss in high pressure turbine efficiency and 0.5% loss in the low pressure turbine efficiency are predicted. Item (4), table 3 lists this debit to the base efficiency.

The net resultant efficiency for the controlled vortex, cooled, reduced tip clearance turbines is 86.4% for the high pressure turbine and 88.0% for the low pressure turbine. The areas of performance improvement (i.e., controlled vortexing and reduced clearances) have been treated conservatively to assure the efficiency goals will be met or exceeded by the JTF17 turbine design.

The high pressure turbine is a high work, high hub/tip ratio stage. This type of stage benefits only a slight amount from controlled vortexing because of Mach number limitations and the small difference between the root and mean reaction levels. However, the low pressure turbine has

lower specific work levels and is not critical Mach number limited. Also, there is a considerable difference in the free vortex root and mean reaction level because of the low hub/tip ratio of these low pressure turbine stages. Controlled vortexing benefits these stages considerably by elevating the root reaction level close to that attained at the efficient mean diameter. Consequently the gain of 2% in low turbine efficiency over that attained by free vortex design methods is attributed to controlling the flow and stage reaction level over the entire span of the stage. These levels of efficiency have been substantiated by both rig and JTF14 engine turbine testing.

Cooling and leakage airflows contribute in two ways to stage efficiency losses. The first is an aerodynamic total pressure loss caused by cooling and leakage air disturbing the mainstream flow. The second loss is the decrease in enthalpy when cooling air mixes with the mainstream flow. This is treated as a temperature decrease at constant pressure. The first loss is accounted for by addition to the aerodynamic losses for each airfoil. To account for the second loss, a heat balance is run between each stage to correct the temperatures entering the following stage.

b. Solidity

The gap-chord ratios selected for the JTF17 turbine are 10 to 20% higher than previous designs. Recent P&WA test data (figure 15) show that the lowest drag-lift ratio is a function of foil turning and aerodynamic lift load coefficient. By designing to the optimum lift load coefficients, gains up to 0.4% in overall turbine efficiency can be obtained over previous designs. The increased gap-chord ratios allow the turbine to be designed with 8% fewer airfoils than previous P&WA turbines. The overall effect of designing to the optimum lift load coefficients is a lighter weight, more efficient turbine.

c. Aspect Ratio

The JTF17 turbine uses high aspect ratio blading for light weight and low aerodynamic losses. Significant weight savings are obtained from both the lower airfoil weights and the resulting lighter disks. Because of the lightweight construction, special care has been exercised to ensure normal vibration resonance margins. The design section discusses these margins. A comparison of blade aspect ratios is shown in table 4.

Table 4. Comparison of Blade Aspect Ratios

Stage	JTF17	STF200C	JT8D	TF-33	TF-30
1	3.07	3.37	2.77	2.61	2.56
2	4.94	4.43	3.62	3.54	3.85
3	5.61	6.10	4.97	4.68	5.11

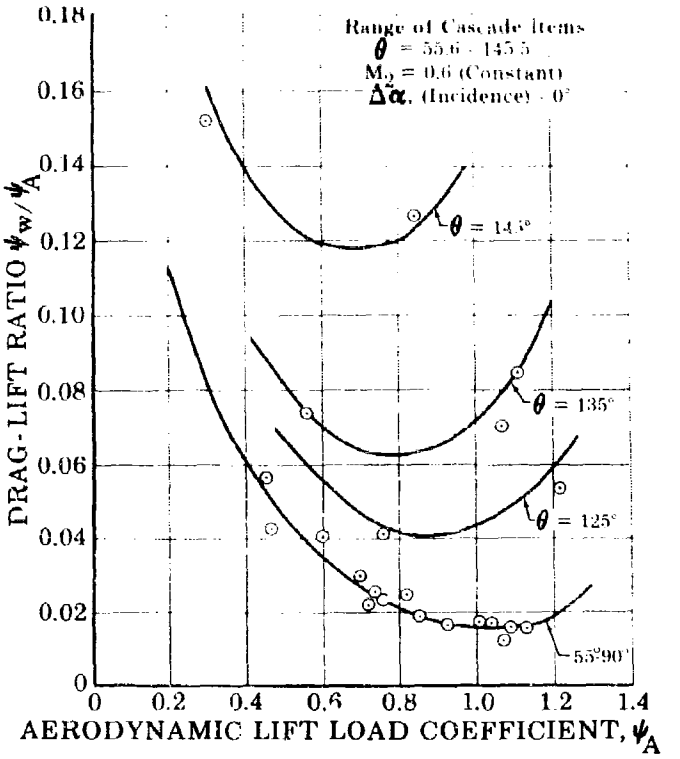

Figure 15. Drag-Lift Ratios of P&WA Turbine Planes Cascades as a Function of Zweifel's Lift-Load Coefficient

ID 16764
AIIIC

d. Work Distribution

The stage aerodynamic characteristics are defined by the distribution of work between the stages. The work distribution of the JTF17 turbine was chosen as follows: (1) high pressure first stage work was set by the high compressor power requirement, (2) 2nd- and 3rd-stage (low pressure turbine) work distribution (2nd-stage 53.8%, 3rd-stage 46.2%) was chosen to achieve optimum turbine performance giving consideration to the life of the blades, the airfoil Mach numbers, the overall turbine efficiency and absolute gas angle leaving the turbine.

From an aerodynamic efficiency standpoint, a 50-50 work split would be desired; however, by doing more work in the second stage, the required cooling air for the third stage is decreased, thus reducing cooling air losses. A lower work third stage gives a lower absolute exit Mach number and lower swirl velocity. Both these factors reduce the pressure drop across the exit guide vane.

After the work distribution was determined, the controlled vortex velocity triangles were determined for maximum performance within the established envelope. The velocity triangles were generated using a three-dimensional streamline analysis that is programed on an IBM 7090 computer. The program solves the equations of motion for axisymmetric, compressible flow and satisfies the energy and continuity equations at each turbine axial station (inlet and exit to blades and vanes, plus selected end points).

e. Controlled Vortex Turbine Design

Past experience at P&WA has shown that turbine efficiency can be significantly increased (2.0 to 3%) by modifying the root and tip velocity triangles from those given by a free-vortex flow pattern. "Controlled vortexing" results in a more constant radial distribution of airfoil flow path convergence. Thus, the blade root reaction and static pressure ratio is increased, while the blade tip reaction and static pressure ratio is decreased. This eliminates the tendency for the flow to separate at the root and reduces leakage around the blade tip. The JTF17 turbine has been designed for as much blade root and vane tip reaction as is possible without imposing: (1) a performance deficiency at the vane root, (2) an excessively high exit swirl angle, or (3) an unacceptable blade taper from lift coefficient and stress considerations. In summary, a high level of efficiency in the JTF17 turbine has been assured by designing for high reaction in the otherwise high-loss regions and by distributing the spanwise work to make maximum utilization of the most efficient sections of the airfoil. Figure 14 illustrates the efficiency gains possible by using a controlled vortex turbine.

f. Turbine Efficiency

The turbine efficiency is the total power output of the turbine divided by the total power available to the turbine. The total power available is determined by the gas conditions at the turbine inlet and the pressure at the exit.

The individual stage efficiencies are $\Delta h_1/\Delta h_1'$, $\Delta h_2/\Delta h_2'$, and $\Delta h_3/\Delta h_3'$. Since the constant pressure lines in figure 16 diverge with increasing entropy, the sum of the isentropic enthalpy drops of the individual stages is greater than the ideal enthalpy drop available to the whole turbine. The enthalpy drops are related by the reheat factor which is defined as:

$$R = \left[\Delta h_1' + \Delta h_2' + \Delta h_3'\right]/\Delta h'$$

From figure 15 the efficiency of the JTF17 turbine is

$$\eta_T = \left[\Delta h_1 + \Delta h_2 + \Delta h_3\right]/\Delta h'$$

The individual cooled stage efficiencies are presented in figures 17, 18, and 19 as a function of velocity ratio. Off-design performance is defined by these curves.

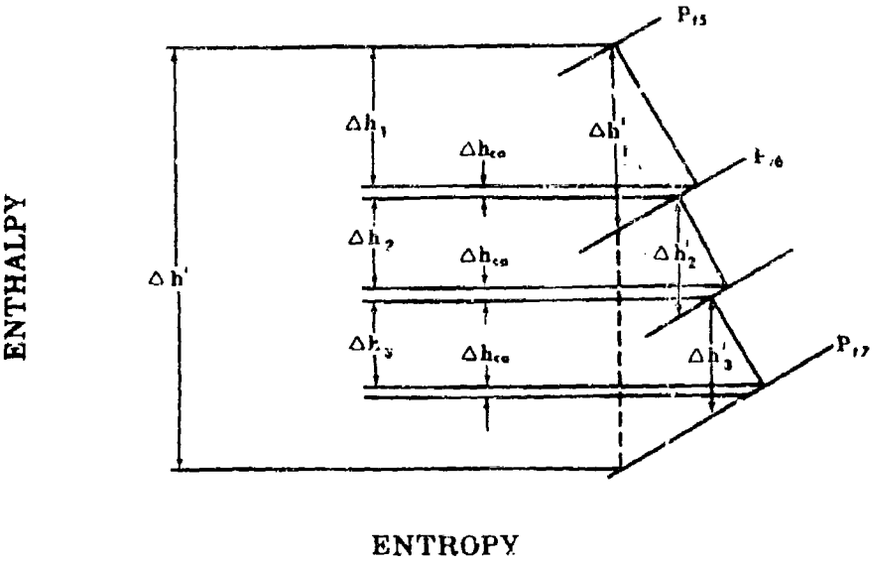

Figure 16. Constant Pressure Lines

FD 17527
AIIIC

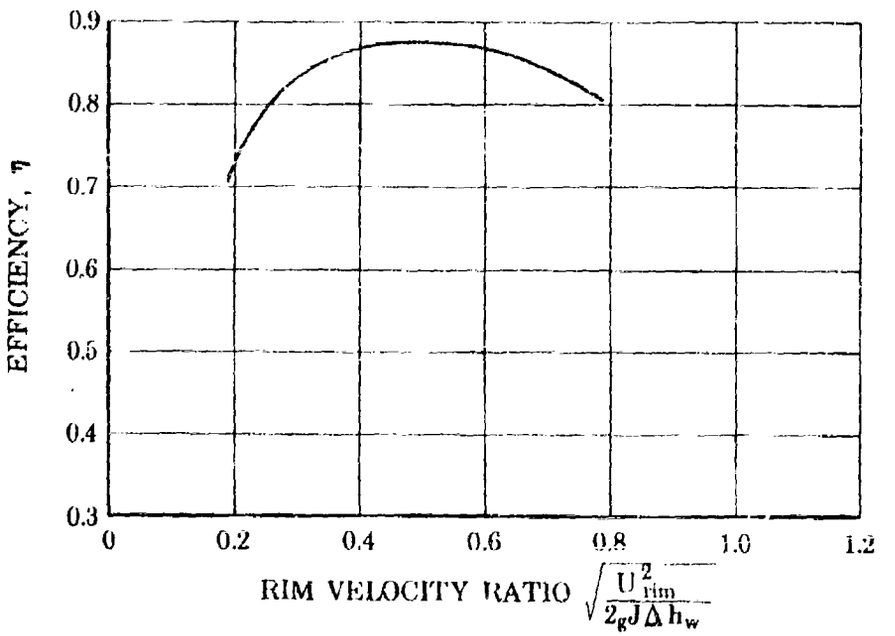

Figure 17. JTF17 Turbine 1st-Stage Efficiency vs Velocity Ratio

FD 17524
AIIIC

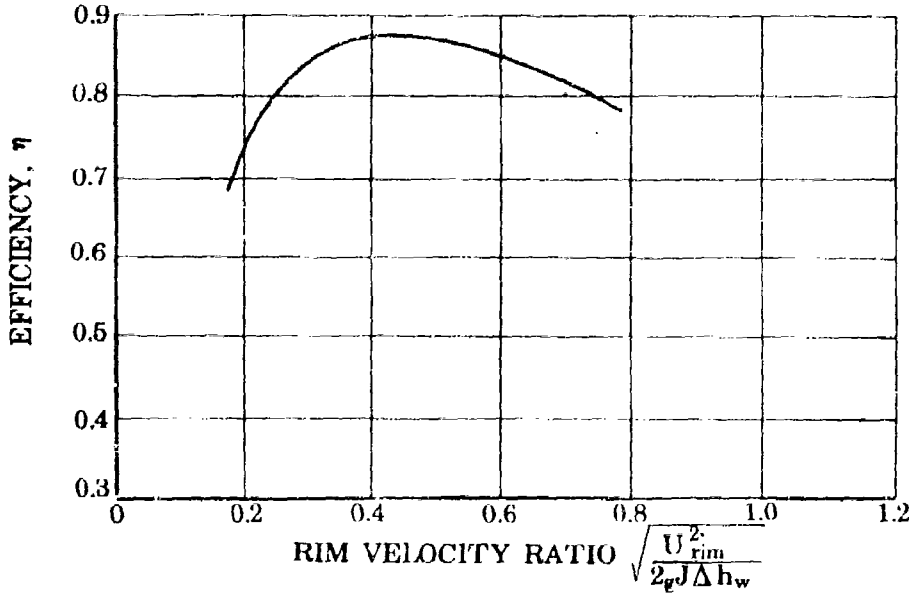

Figure 18. JTF17 Turbine 2nd-Stage Efficiency vs Velocity Ratio — FD 17525 AIIIC

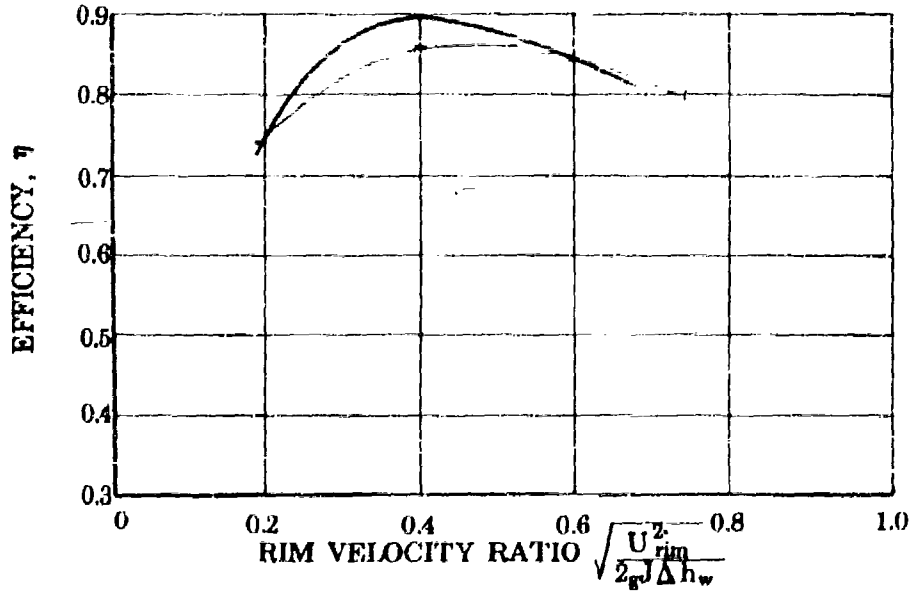

Figure 19. JTF17 Turbine 3rd-Stage Efficiency vs Velocity Ratio — FD 17526 AIIIC

D. DUCT HEATER

1. Introduction

Thrust augmentation is to be provided in the JTF17 engine by a duct heater that raises the temperature of the fan discharge air. Varying amounts of augmentation will be used over the major part of the aircraft flight envelope, as shown in figure 1. The duct heater performance will be most important to aircraft operation during:

1. Sea level takeoff
2. Transonic acceleration
3. Supersonic cruise.

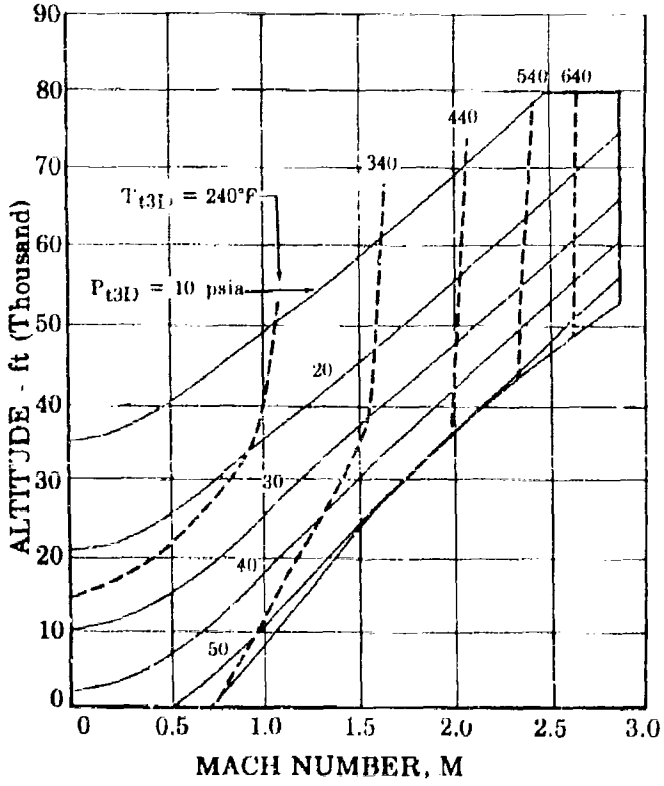

Figure 1. JTF17 Fan Discharge Conditions FD 16837 A111D

During sea level takeoff and transonic acceleration, maximum thrust augmentation and duct heater performance are required to achieve the required levels of engine thrust. Duct heater performance in supersonic cruise is most important to total engine fuel consumption due to the relatively long portion of the mission spent at this condition. The duct heater described in the following paragraphs is to be used for the production as well as prototype engines.

The duct heater (figure 2) consists of a diffuser, combustor, two-zone fuel injection system, cooling liners, and a variable area exhaust nozzle. The diffuser reduces the velocity of the fan discharge air from M = 0.5 to 0.6 to values suitable for the duct heater combustor (M = 0.25 to 0.30). Part of the fan air (10%) is bled through the inner wall of the diffuser to provide cooling for the inner liner (see figure 2). The duct heater utilizes two zones of combustion. The first zone is in the combustor, which (like the primary combustor) is an annular, ram-induction type. The second combustion zone occurs at the exit of the combustor. At low levels of augmentation, a portion (approximately 30%) of the fan air is burned in the combustor with fuel injected from the Zone I fuel nozzles. When high augmentation levels are required, fuel is also injected through the Zone II fuel system and burned with the combustor-bypass air and the Zone I combustion exhaust gases. Both fuel injection systems utilize variable-area dual-orifice nozzles to provide well atomized fuel over a wide flow range. The engine cases are protected from the hot combustion gases by the cooling liners (heat shields), which are cooled by bypass air. The air that cools the outer liners also cools the exhaust nozzle flaps.

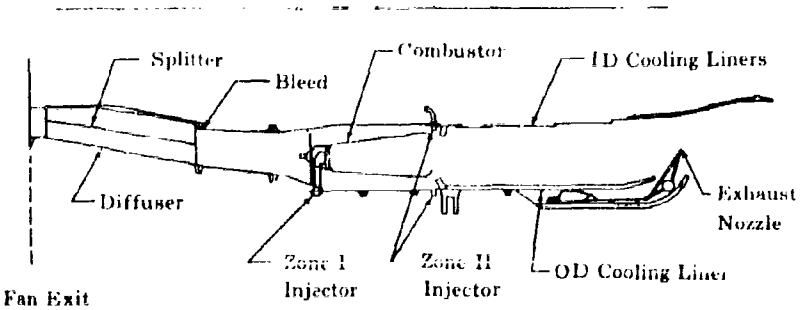

Figure 2. JTF17 Duct Heater Schematic FD 16838 AIIID

2. Requirements

a. General

To provide the required thrust augmentation effectively, the duct heater must (1) provide high combustion efficiency over a wide operating range, (2) offer low total pressure drop to the fan stream, (3) provide "soft" ignition and smooth acceleration characteristics, and (4) have durability for long life. These requirements are discussed separately below.

b. Combustion Efficiency

Combustion efficiency is by far the most important parameter of the duct heater performance. As shown in the engine performance section (Volume III, Report A, Section II), a 1.0% increase in combustion efficiency will decrease engine TSFC by 0.74% and result in a 1070 pound

increase in payload for a typical 4000 statute mile mission. In comparison, a decrease of 1% total pressure loss will decrease TSFC only 0.24% and increase payload 350 pounds. Based on these considerations, combustion efficiency will be the most important duct heater performance parameter during development.

To achieve the guaranteed thrust specific fuel consumption, the duct heater must achieve the following combustion efficiency goals:

$$97\%\ T_{t8} = 800^\circ \text{ to } 2500^\circ F$$

$$97\% \text{ to } 90\%\ T_{t8} = 2500^\circ \text{ to } 3600^\circ F$$

The maximum heat release rate of the duct heater is 8.1×10^6 Btu/ft^3 x Atm x hr. These performance goals are for a thrust equivalent combustion efficiency. As a result, the temperature and pressure profiles of the duct heater exhaust gases, which reflect the degree of mixing between the combustion products and the unburned air, as well as the chemical combustion efficiency are most important. This importance can be illustrated by use of figure 3, noting that the thrust calculated by using the mass-weighted average temperature (figure 3a) would be larger than the summation of the stream tube thrust (figure 3b). To achieve high thrust equivalent combustion efficiency, it is necessary to obtain very flat total pressure and temperature profiles as well as a near 100% chemical combustion efficiency.

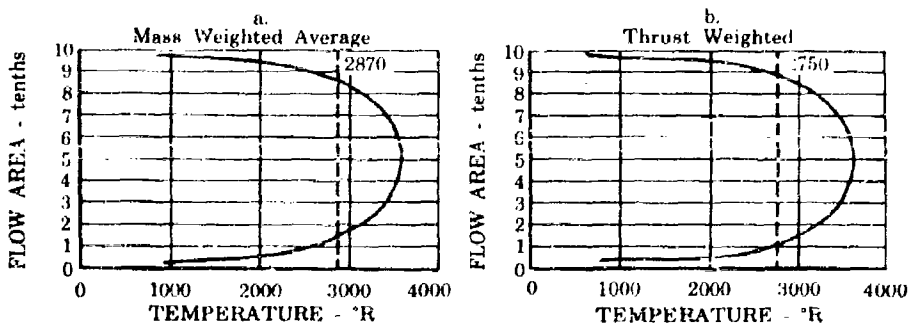

$$T_{t(mass)} = \frac{\Sigma \sqrt{T}\, T}{\Sigma \sqrt{T}}$$

$$T_{t(thrust)} = \frac{\Sigma (Fg)^2 T}{\Sigma\, Fg^2}$$

$T_{t(mass)} = 2870$ °R

$T_{t(thrust)} = 2750$ °R

Assumptions used in Calculations:
$P_{duct} = 45$ psia $F_{amb} = 15$ psia
$\gamma = 1.35$ Stream Tube Mass Flow = f(1/T)

Figure 3. Comparison of Chemical and Thrust Equivalent Combustion Efficiency — FD 16839 AIIID

In the full annular duct heater tests, chemical combustion efficiencies were measured and thrust equivalent combustion efficiency data were determined by using measured temperature profiles. Thrust equivalent combustion efficiency data were obtained more directly in the sector duct heater tests by using a choked nozzle at the rig exit, which permits a direct

computation of the thrust weighted temperature. Rig measurements and calculations are discussed in greater detail in the component development plan (Volume III, Report E, Section II).

c. Duct Heater Pressure Loss

To achieve the required engine performance goals, total pressure loss in the duct heater (without combustion) must be equal to or less than 4.7%to 8%, depending on the Mach number. (See figure 4.) The duct heater total pressure loss can be separated into the diffuser loss and the combustor loss. In addition to these losses, there is also a pressure loss due to heat addition. These losses are discussed in the following paragraphs.

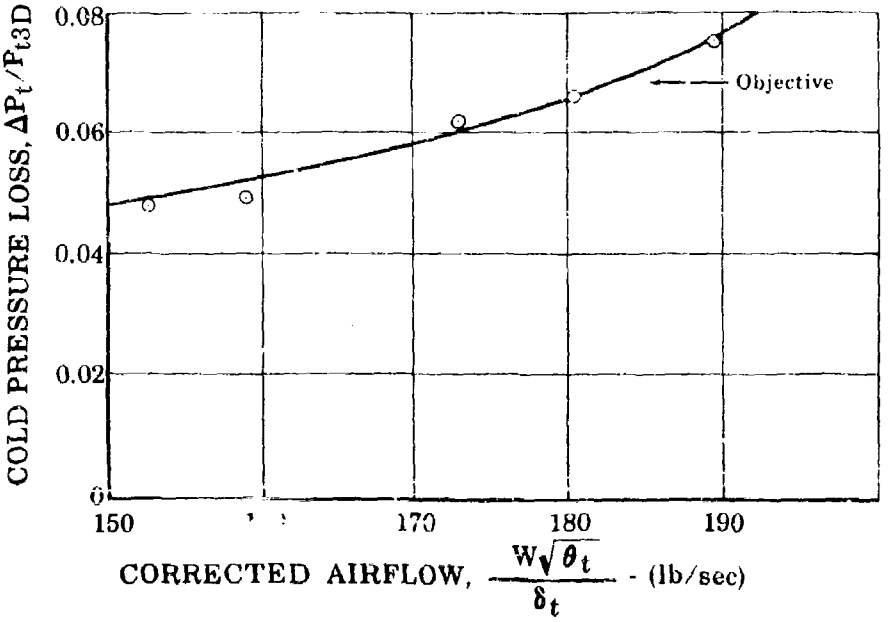

Figure 4. Cold Pressure Loss on Full Scale Annular Rig at Stations 3D to 8D — FD 16842 A111D

Control of the diffuser total pressure loss is accomplished by careful selection of divergence angle and area ratio to reduce the air stream Mach number without flow separation. In this respect, the duct heater-augmented turbofan engine has a definite advantage over an afterburning engine because a conservative (i.e., low angle) diffuser can be selected without increasing overall length of the engine (because the engine length is established by the length of the gas generator). This is not the case in the afterburning turbojet because the duct heater and gas generator are in series. A 6-degree angle diffuser having an area ratio of 1.95 is to be used for the JTF17 duct heater. This angle is conservative, as illustrated in figure 5, when compared to the design limit curve that has been established from extensive P&WA diffuser tests.

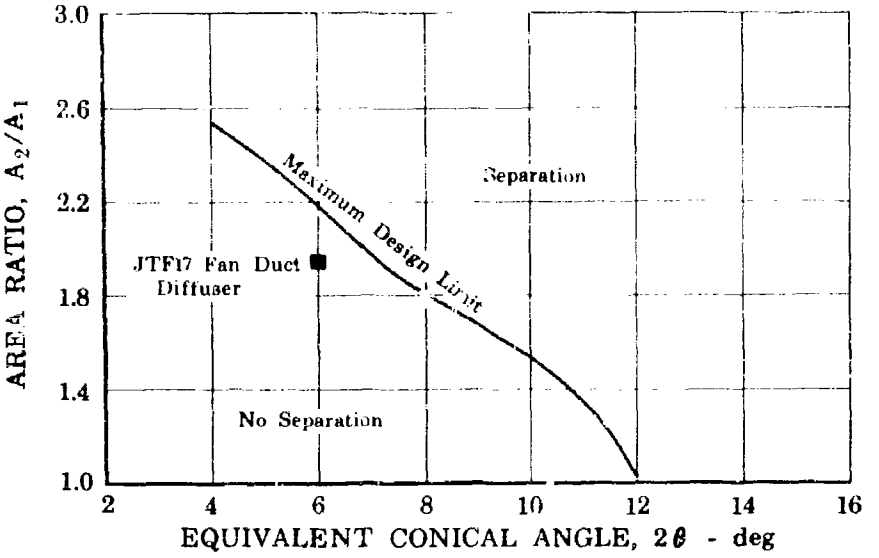

Figure 5. P&WA Diffuser Experience

FD 16840
AIIID

Because the total pressure or Mach number profile inlet to the diffuser can also substantially affect diffuser pressure drop, the achievement of "flat" fan-discharge flow profiles will be important in fan development (see Volume III, Report E, Section II).

The pressure drop through the combustor is minimized by using air entrances with high discharge coefficients and a combustor that has a low drag coefficient. The heat-addition pressure drop is minimized by achieving combustion in a low Mach number ($M < 0.1$) region of the combustor. The advantages of low-Mach-number heat addition is indicated in figure 6, which shows the relationship between total pressure loss (Rayleigh loss), inlet Mach number, and temperature rise ratio.

d. Ignition and Acceleration Characteristics

The duct heater must ignite and operate over the envelope shown in figure 1. Furthermore, the amplitude of the pressure perturbation caused by ignition must be (1) small enough to avoid unacceptable discontinuities in engine thrust, and (2) compatible with the fan or inlet operation. The engine must, however, be capable of rapid acceleration from an approach power setting to maximum augmentation.

e. Durability and Component Cooling

To achieve the required performance objectives, cooling air flow rates must be minimized, without jeopardizing the durability of engine parts. In the turbofan engine the temperature of the duct heater cooling air is approximately 1000°F lower than that of an afterburning turbojet. Adequate cooling and subsequent long life of the liners can be achieved with relatively small percentages of the total duct flow and low pressure drops. As a result most of the fan air is available for combustion, thereby minimizing potential thrust losses due to poor temperature profiles.

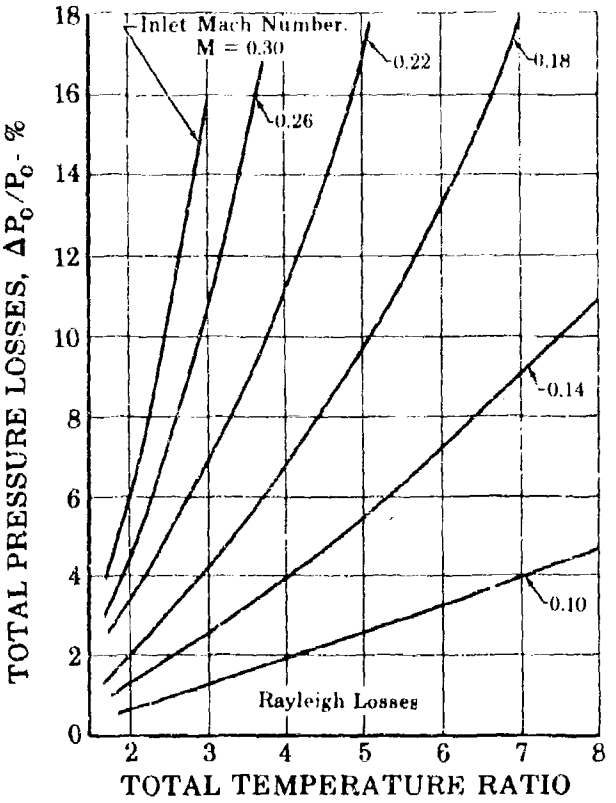

Figure 6. Total Pressure Loss Due to Heat Addition

FD 16841
ATTD

3. Substantiation

a. General

In general, the level of duct heater performance required for the proposed engine has either been closely approached or exceeded in the Phase II-C component development program. Table I summarizes the scope of the duct heater rig test programs accomplished during Phase II-C. A detailed description of the rigs and tests conducted appears in the component development section (Volume III, Report E, Section II) of the proposal. The results of the Phase II-C programs and how they substantiate the engine duct heater selection are discussed in the following pages.

Table 1. Summary of Duct Heater Rig Test Programs

Rig	Description	Data Acquired	Phase II-C Accumulated Hours
0.6-scale annular duct diffuser rig	0.6 simulation of engine duct passage from fan discharge to combustor forward cowl.	Diffuser total pressure loss. Static pressure recovery. Characteristics of flow.	96
Full-scale annular duct heater rig	Exact simulation of engine duct flow path from fan discharge to exhaust nozzle inlet.	Combustion efficiency. Total pressure loss. Ignition characteristics. Temperature distribution. Parts integrity.	45
Full-scale sector duct heater rig	Two-dimensional simulation (7-in. wide x 11-in. high) of duct heater.	Combustion efficiency. Combustor pressure loss. Ignition characteristics.	289
Large-scale annular jet flameholder rig	Annular duct heater rig sized for 600 pps engine used to evaluate jet flameholder duct heater.	Total pressure loss. Combustion efficiency. Bleed flow rate.	69

b. Total Pressure Loss

The duct diffuser of the prototype engine will be essentially the same as that tested in the duct diffuser rig and the annular duct heater rig.

The isothermal or "cold" pressure loss data obtained with the full-scale annular duct heater rig is presented in figure 4 as a function of the duct inlet Mach number (or corrected flow). The acceptable loss curve for the duct heater (established based on TSFC objectives) is also shown in this figure for comparison. The measured pressure-loss data are essentially equal to the acceptable-loss curve. The relatively low total pressure losses are attributed to the highly efficient duct diffuser. (A detailed description of the diffuser test results is presented in Volume III, Report F, Section II of the proposal.)

The pressure loss of the duct heater with combustion is shown in figure 7. The data in this figure were obtained with the full-scale duct heater rig. The loss due to heat addition is less than the predicted using the Rayleigh line and the average through (or reference) Mach

CONFIDENTIAL

number computed for the air duct without the combustor. These data indicate that the heat addition is occurring in the combustor where Mach numbers are lower than the reference Mach number.

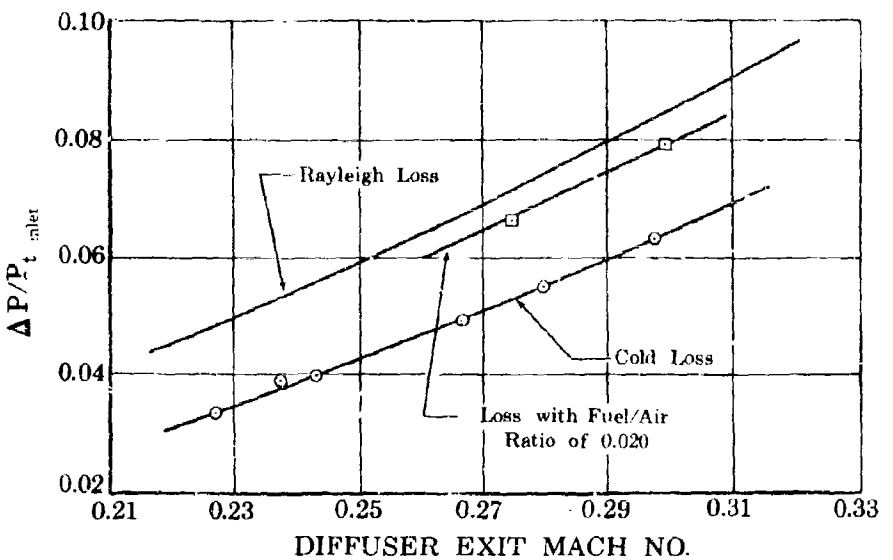

Figure 7. JTF17 Full-Scale Duct Heater Rig Overall Total Pressure Loss at Cruise Conditions — FD 17544 AIIID

c. Combustion Efficiency and Operating Range

A modified version of the full-scale annular duct heater design evaluated in Phase II-C rig tests will be used in the proposed engine. (See Volume III, Report B, Section II for a description of the engine duct heater.) This design proved to be very successful in the rig tests, producing high performance, and was operated successfully over a wide range of conditions. A summary of the conditions evaluated in the rig tests is given below:

Parameter	Maximum	Minimum
Combustor pressure, psi	40.0 (SL)	11.0 (80,000 ft)
Inlet temperature, °F	650	270
F/A ratio	0.058	0.001

In addition to the annular duct heater tests, several modifications and features of the duct heater were evaluated in the sector rig at inlet pressures down to 9 psia, temperatures as low as 200°F, and over a wide range of fuel-air ratios. These conditions are more severe than any in the operating envelope since the minimum required operating pressure is 10 psia. A summary of the operating range of representation duct heater configurations tested in the sector rig are shown in table 2.

CONFIDENTIAL

Table 2. Rich Blowout Limits at 9 psia and 200°F Inlet

Configuration	Zone I Only	Zone I and II
E3	0.011	No Zone II Ignition
K13*	0.020	No Zone II Ignition
J1	Unable to Burn	No Zone II Ignition
J6	0.025	Beyond Operating Limit (F/A > 0.05)
H7	0.015	Beyond Operating Limit (F/A > 0.06)
L12	0.013	0.030

*Configuration used in early experimental engines

The lean blowout fuel-air ratio was less than 0.002 for all the configurations except the J1, which could not be ignited at these conditions.

The performance obtained in the full annular and sector duct heater tests are compared with a curve reflecting goal performance in figure 8. Both thrust equivalent (shaded) and chemical (unshaded) combustion efficiency data are presented for the full-annular duct heater. Thrust equivalent data are presented for the sector duct heater. Thrust equivalent data are lower than the chemical data because the duct heater exit temperature profiles were not flat. In this respect it should be noted that flattening the profile during prototype engine development will improve performance (potentially by the amount represented by the difference between the chemical and thrust equivalent combustion efficiency data).

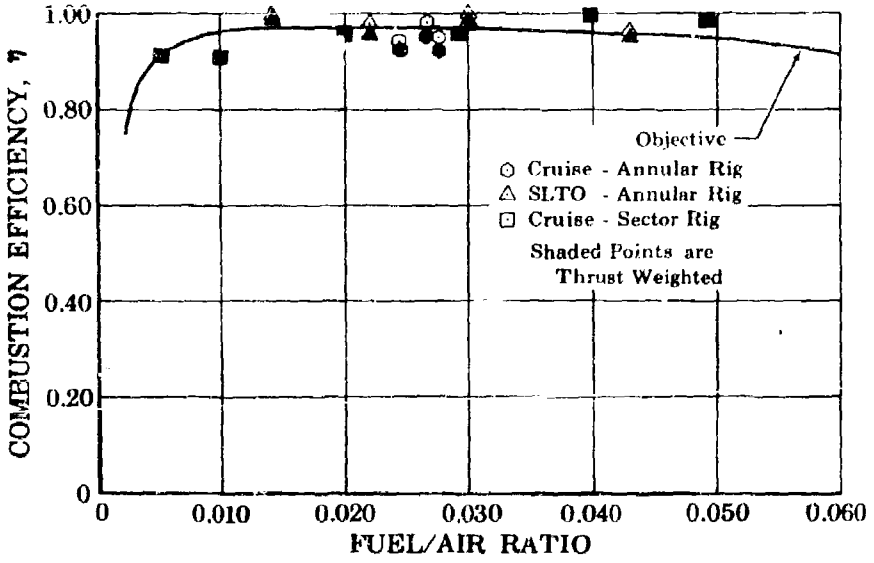

Figure 8. Duct Heater Combustion Efficiency FD 16844 AIIID

The combustion efficiency data in figure 8 indicate that the combustion efficiency goals for the JTF17 engine have been exceeded at SLTO and nearly met at cruise (65,000 ft, M = 2.7) conditions with both full-annular and sector duct heaters. In addition these data show that the two-stage combustion, ram-induction duct heater demonstrated high combustion efficiency over an extremely wide range of fuel-air ratios. The details of the Phase II-C rig component development program are discussed in Volume III, Report E, section II.

The outlet temperature and pressure distribution of the duct heater are shown in figures 9 and 10. In these figures, the curves denoted "maximum" and "minimum" are the profiles obtained at the maximum and minimum circumferential temperature (or pressure) locations. The average curve denotes the radial profile for the average circumferential conditions. These figures represent cruise and SLTO conditions, respectively. The radial temperature profile at cruise conditions (Zone 1 only) peaked near the center of the duct. Because of this peaked profile, the thrust equivalent combustion efficiency is 2.5% lower than the chemical combustion efficiency. The profile could be flattened considerably by improving the mixing between the air that bypasses the combustor and the combustor discharge gases. The radial temperature profile (figure 10) flattens considerably when Zone II fuel injection is used because the Zone II fuel is injected at the periphery of the combustor.

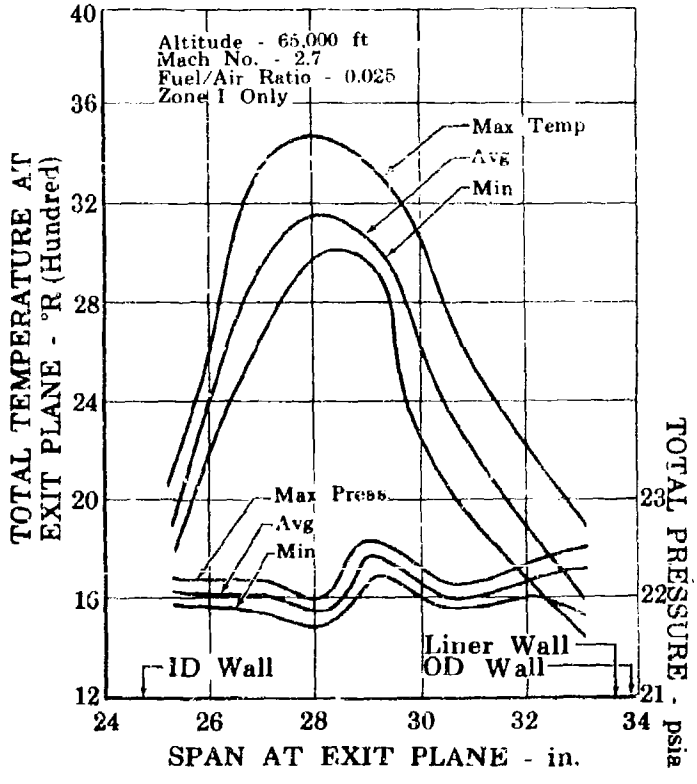

Figure 9. JTF17 Full-Scale Duct Heater Rig Radial Temperature Profiles at Cruise Conditions

FD 17019
AIIID

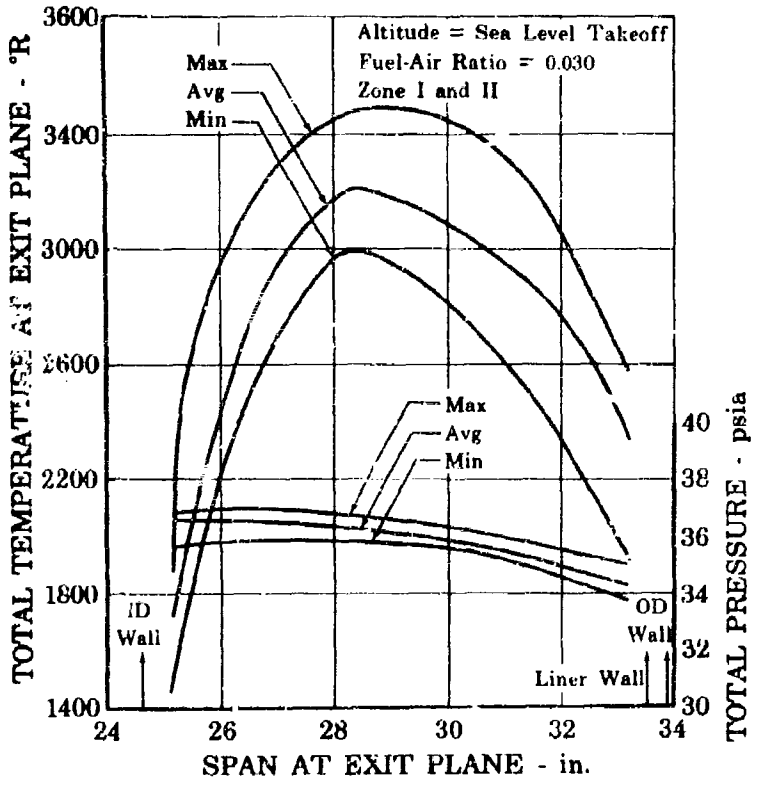

Figure 10. JTF17 Full-Scale Duct Heater Rig Radial Temperature Profiles at Sea Level Takeoff Conditions

FD 16846
AIIID

d. Ignition and Acceleration Characteristics

The later designs of the duct heater have been successfully ignited at all conditions tested in the annular and sector duct heater rigs using a 4-joule electrical ignition system similar to the one selected for the proposed engine. Successful ignition was obtained with duct heater fuel-air ratios from 0.0014 to 0.0048. Ignition was accomplished in all cases with a very slight rise in duct heater pressure, as shown in figures 11 and 12. Phasing-in of Zone II flow in incremental changes produced no pressure discontinuity (figure 13). These ignition results from the full-scale annular duct heater rig program have been incorporated in the engine transient simulations. The thrust and airflow transients due to duct heater operation are discussed in the controls design report (Volume III, Report B, Section III).

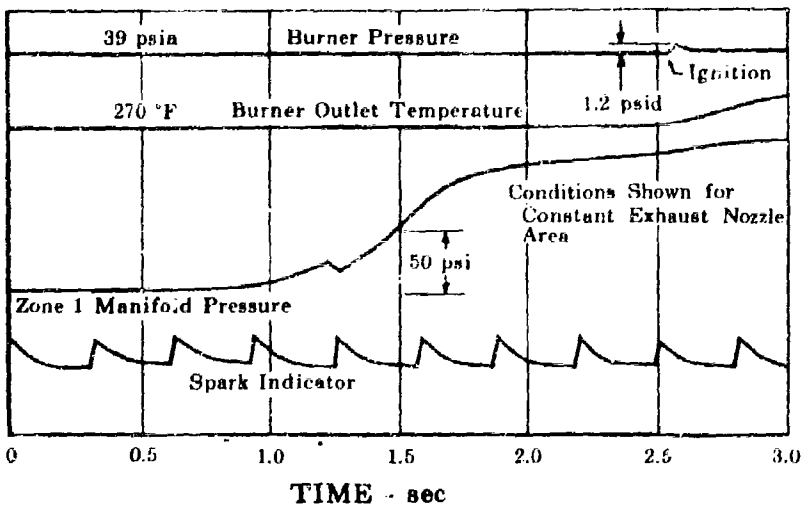

Figure 11. Full-Scale Annular Duct Heater Rig Sea Level Ignition Test Results

FD 15304B
AIIID

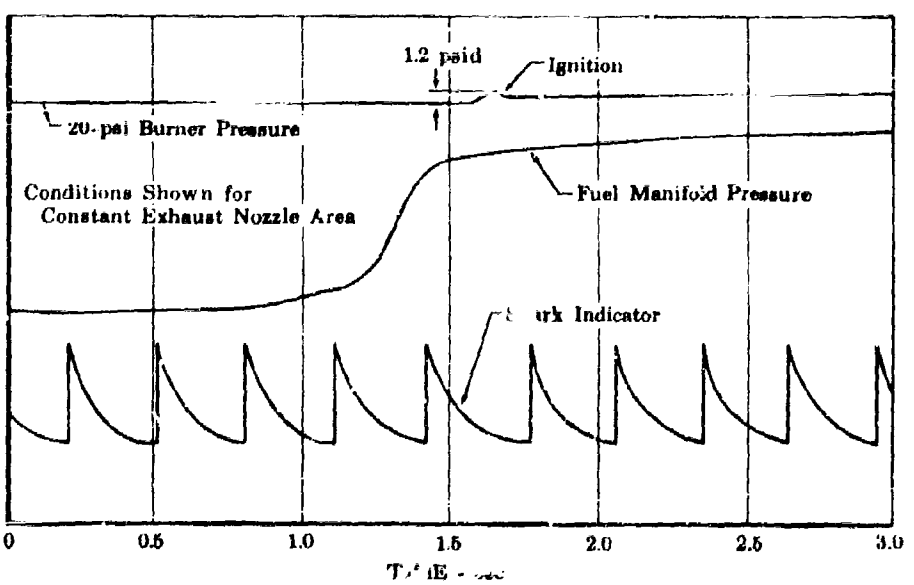

Figure 12. Full-Scale Annular Duct Heater Rig Mach 2.7, 65,000 Cruise Ignition Test Results

FD 15303B
AIIID

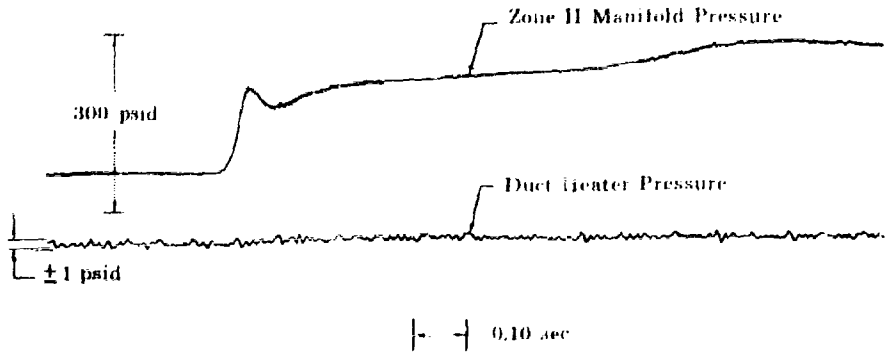

Figure 13. Rate of Duct Heater Pressure Rise With Addition of Zone II Fuel (Rig Data) FD 14605D AIIID

c. Component Durability and Cooling

The outer liners are to be cooled by approximately 7.5 to 11% of the fan air flow. Of this flow, 5 to 7.5% is discharged through the liner and mixed with the duct heater combustion gases. The remaining flow is injected on the nozzle flaps for film cooling. Adequacy of this coolant flow rate has been demonstrated in the rig tests. The maximum liner temperature measured during the annular duct heater rig program was 1550°F (at F/A = 0.058).

Of the 10% fan flow bled from the diffuser, approximately 6.0 to 8.5% is used to film cool the inner liner and reenters the combustion process. The remaining bleed flow is used to cool the inner plug. This flow rate is more than adequate to cool the inner liner, and therefore will probably be reduced during the engine development program. The highest observed metal temperature was 1400°F.

f. Summary

1. The duct heater combustor configuration selected for use in early experimental JTF17 engines exhibited excellent performance characteristics in the full-scale annular rig. The level of performance meets the objective of the proposed engine at SLTO conditions and nearly meets the objective at cruise conditions.

2. The duct heater has demonstrated excellent ignition characteristics over a wide range of temperature and pressure and at fuel/air ratios between 0.001 and 0.004. The duct pressure discontinuity associated with duct heater ignition is lower than anticipated and has caused no fan instability (see Volume III, Report D, Section II).

3. The condition of the duct heater parts was excellent after 45 hours of hot full-scale rig testing.

4. The Phase II-C tests results have demonstrated that the duct heater can be developed to operate over the required envelope of conditions while providing performance equal to or exceeding the goals necessary to meet JTF17 engine specifications of thrust and TSFC, and has the durability necessary for a long-life commercial aircraft engine.

E. EXHAUST SYSTEM PERFORMANCE

1. Introduction

Pratt & Whitney Aircraft has conducted a systematic program since 1959 to determine the best exhaust system for supersonic transport application. The exhaust system must be simple, lightweight, and capable of accomplishing the following major objectives: (1) control the expansion of the exhaust gases to achieve overall performance levels, (2) have an efficient method of reversing the exhaust gases to provide a high level of reverse thrust, and (3) effectively suppress engine exhaust noise. Results of this investigation led to the blow-in-door ejector nozzle concept proposed in Phase I. Comparison of the blow-in-door ejector with other exhaust nozzle schemes and reasons for its choice are given in Reference 1, Volume E-XI, "Ejector-Reverser" of the Phase II proposal. Early in Phase II, it became apparent that a variation in shroud geometry, in addition to the free floating blow-in doors and trailing-edge flaps, would be required to achieve the performance goals and operational modes required of the SST exhaust system. During Phase II-C two exhaust system concepts for accomplishing the proposed objectives resulted in the translating shroud and the rotating clamshell designs (the rotating clamshell design is also referred to as the reverser-suppressor). The translating shroud design was subsequently discarded in favor of the clamshell reverser-suppressor, shown in figure 1, because of life, size, and weight considerations as described in Volume III, Report B. All exhaust system models have been designed and tested at engine operating conditions corresponding to the Phase II-C 650 lb/sec engine to maintain a consistent basis for performance comparisons throughout the program. The small differences in operating conditions between the Phase II-C 650 lb/sec engine and the JTF17 687 lb/sec engine do not appreciably affect exhaust system performance levels or the mechanical design. There is no difference in the exhaust system design between the JTF17 production or prototype engines. However, the minimum exhaust system performance required to meet the prototype engine performance is less than for the production engine at the supersonic cruise and takeoff conditions as shown in the following table:

Exhaust System Gross Thrust Coefficient, C_{fp}

Corrected Secondary Airflow Ratio = 0.02

	JTF17 Production Engine	JTF17 Prototype Engine
Supersonic Cruise	0.999	0.997
Takeoff	0.982	0.980

The clamshell reverser-suppressor, designed for the Phase II-C 650 lb/sec engine, has demonstrated the Phase II-C performance goals shown in paragraph 4, Phase II-C Development Program.

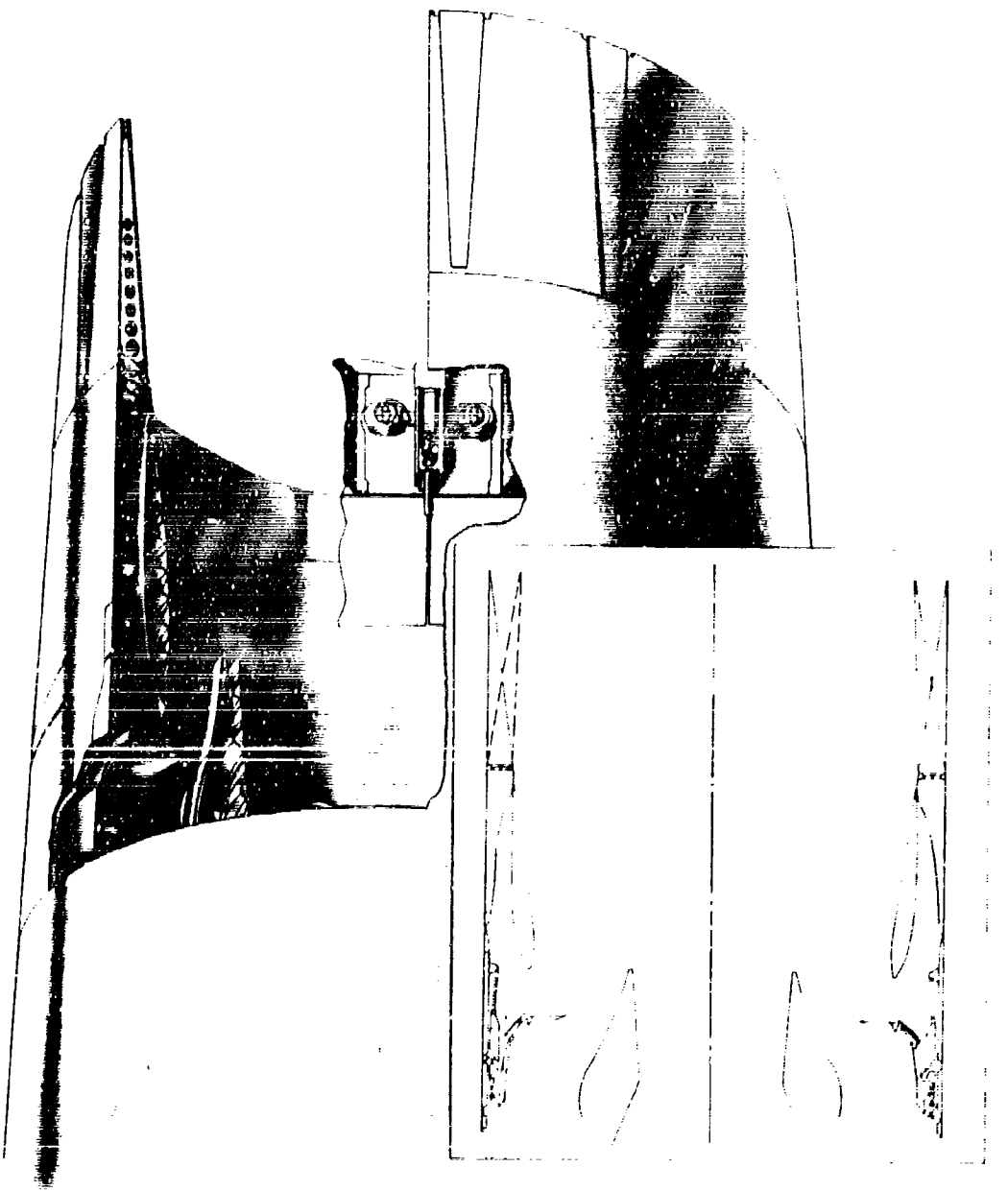

Figure 1. Clamshell Exhaust System

The reverser-suppressor mechanical design has proved to be simple and lightweight, and should provide a long-life exhaust system with minimum maintenance. In addition, the design concept, by virtue of the tertiary air induction system and rotating clamshell segments, allows reductions in exhaust noise, as discussed in Volume III, Report C, with small or no losses in performance.

The subsequent paragraphs provide a functional description of the clamshell reverser-suppressor and a discussion of the Phase II-C development program including results of the model test programs.

2. Symbols, Definitions, and Nomenclature

a. Symbols

Symbol	Item	Units
A_{base}	Engine plug base area	sq ft
A_{bleed}	Area between clamshells and trailing edge flaps at reverse	sq ft
A_{exit}	Reverser-suppressor exit area	sq ft
A_{jd}	Effective duct exhaust nozzle area	sq ft
A_{j9}	Effective gas generator exhaust nozzle area	sq ft
A_{rev}	Reverse flow area available through tertiary doors	sq ft
A_{max}	Exhaust system maximum cross-sectional area	sq ft
A_t	Tertiary door area	sq ft
B_1	Initial tertiary door angle	degrees
B_2	Final tertiary door angle	degrees
c	Clamshell maximum chord	inches
C_{fp}	Exhaust system gross thrust coefficient	
C_{fr}	Reverse gross thrust coefficient	
$C_{fp\ inst}$	Installed exhaust system performance coefficient	
$C_{fp\ mr}$	Exhaust system gross thrust coefficient accounting for the ram drag of the secondary air	
D_{exit}	Trailing edge flap exit diameter	inches
D_{dl}	Duct exhaust nozzle diameter	inches
D_{max}	Maximum reverser-suppressor diameter	inches
D_s	Reverser-suppressor minimum shroud diameter	inches

CONFIDENTIAL

Symbol	Item	Units
ΔC_{fp}	Incremental exhaust system gross thrust coefficient	
$\Delta C_{fp\ inst}$	Incremental exhaust system gross thrust coefficient due to installation effects	
ΔC_{fr}	Incremental reverse gross thrust coefficient	
ΔT_s	Temperature rise of secondary air from compressor inlet to exhaust system	^oR
K	Distance along centerline from leading edge of shroud to clamshells at reverse	inches
L	Distance from duct exhaust nozzle tip to end of trailing edge flap	inches
L_s	Exhaust system internal spacing; end of duct exhaust nozzle to minimum shroud location	inches
M	Flight Mach number	
M_L	Exhaust system external local Mach number	
P_{am}	Ambient pressure	psia
P_{td}	Total pressure at duct exhaust nozzle throat	psia
P_{ts}	Secondary total pressure at exhaust system - airframe interface	psia
P_{t2}	Engine inlet total pressure	psia
P_{t9}	Total pressure at gas generator exhaust nozzle throat	psia
Q_d	Duct exhaust nozzle flow coefficient	
Q_9	Gas generator exhaust nozzle flow coefficient	
t	Clamshell maximum thickness	inches
T_{td}	Total temperature at duct exhaust nozzle throat	^oR
T_{ts}	Secondary total temperature at exhaust system - airframe interface	^oR
T_{t2}	Engine inlet total temperature	^oR
T_{t9}	Total temperature at gas generator exhaust nozzle throat	^oR
W_{at}	Total engine inlet airflow	lb/sec
W_{g9}	Gas flow at the gas generator exhaust nozzle throat	lb/sec
W_{gd}	Gas flow at the duct exhaust nozzle throat	lb/sec
W_s	Actual secondary airflow	lb/sec

CONFIDENTIAL

Symbol	Item	Units
W_{sc}	Corrected secondary airflow ratio	
α	Engine plug throat angle; duct stream	degrees
β	Trailing edge flap boattail angle	degrees
δ	Duct-gas generator flow impingement angle	degrees
ζ	Clamshell angle of rotation from cruise position	degrees
η	Tertiary door angle during reverse operation	degrees
θ	Shroud internal divergence angle	degrees

b. Definitions and Nomenclature

(1) Exhaust System Thrust Coefficients

Exhaust system performance can be conveniently related to the performance of an ideal system. Several parameters may be used to describe the system and are explained below.

(a) Exhaust System Gross Thrust Coefficient - C_{fp}

The parameter used to present exhaust system performance is the exhaust system gross thrust coefficient, C_{fp}. C_{fp} is defined as the sum of the actual gross thrusts of the engine (i.e., gas generator plus duct), secondary, and tertiary streams minus the external pressure drags, minus all internal drags, and minus the induction drag of the tertiary stream, all divided by the ideal gross thrust of the engine stream. All drags, including any interacting effects between internal and external flow, and all internal thrust losses, are accounted for except the ram drag of the secondary air and the external skin friction of the exhaust system. Installation effects are not accounted for and the external skin drag is not included in the definition of C_{fp} by mutual agreement with the airframe manufacturers, because it can best be accounted for in the full airplane wind tunnel model tests conducted by the aircraft manufacturers.

In symbolic form, C_{fp} is given as:

$$C_{fp} = \frac{F_{g\ engine} + F_{g\ secondary} + F_{g\ tertiary} - D_{external\ pressure} - D_{internal} - D_{tertiary\ ram}}{F_{g\ ideal\ engine}}$$

Note that C_{fp} can be greater than 1.0 because the ideal thrust of the secondary flow is not included in the denominator, nor is the ram drag of the secondary subtracted in the numerator.

CONFIDENTIAL

(b) Exhaust System Gross Thrust Coefficient Accounting for the Ram Drag of the Secondary Air - $C_{f_{pmr}}$

C_{f_p} may be modified to account for the ram drag of the secondary air to yield another thrust coefficient, $C_{f_{pmr}}$. This coefficient may be used to establish the efficiency of the exhaust system, including the ram drag of any secondary air. $C_{f_{pmr}}$ is defined as the sum of the actual gross thrusts of the engine, secondary, and tertiary streams minus the external pressure drags, minus all internal drags, minus the induction drag of the tertiary stream, and minus the ram drag of the secondary stream, all divided by the ideal gross thrust of the engine stream.

In symbolic form:

$$C_{f_{pmr}} = \frac{F_{g\ engine} + F_{g\ secondary} + F_{g\ tertiary} - D_{external\ pressure} - D_{internal} - D_{tertiary\ ram} - D_{secondary\ ram}}{F_{g\ ideal\ engine}}$$

or

$$C_{f_{pmr}} = C_{f_p} - \frac{F_{g\ secondary} - D_{secondary\ ram}}{F_{g\ ideal\ engine}}$$

(c) Exhaust System Reverse Gross Thrust Coefficient - C_{f_r}

The exhaust system reverse thrust coefficient is used to establish the efficiency of the reverser. It is defined as the engine reverse gross thrust, plus all exhaust system drags taken parallel to the exhaust system centerline divided by the ideal gross thrust of the engine stream.

In symbolic form:

$$C_{f_r} = \frac{F_{g\ reverse\ engine} + D_{all}}{F_{g\ ideal\ engine}}$$

(d) Gas Generator and Duct Exhaust Nozzle Flow Coefficients - Q_g and Q_d

The exhaust nozzle flow coefficient is defined as the ratio of the actual flow rate to the ideal one-dimensional flow rate for either the gas generator nozzle or duct nozzle throat areas. The nozzle flow coefficients determined for reverse operation may be compared with the forward flight flow coefficients to establish the effect of the reverser on engine flow characteristics. A reduction in the coefficient during reverse operation from the value for forward flight can be used to indicate a suppression of engine flow during reverse operation.

(e) Installed Exhaust System Performance Coefficient - $C_{f_{p\ inst}}$

The installed exhaust system performance coefficient includes the effect of the aircraft-engine installation on nozzle performance. The thrust coefficients defined above do not include installation effects. These effects

CONFIDENTIAL

must be obtained for a particular airframe-engine installation, and the correction applied, to obtain the installed performance. Normally, these effects are significant only at transonic and low supersonic flight conditions when the nozzle tertiary doors are open and the trailing edge flaps are closed.

In symbolic form:

$$C_{f_{p\ inst}} = C_{f_p} + \Delta C_{f_{p\ inst}}$$

(2) Exhaust System Secondary Airflow Characteristics

Secondary airflow is normally required for exhaust system performance and cooling. It is necessary, therefore, to describe the quantity, pressure, and temperature level of the flow required. One parameter chosen to define the quantity of secondary air is the corrected secondary airflow ratio, W_{sc}, defined as the product of the ratio of secondary airflow to engine (i.e., gas generator plus duct) gas flow and the square root of the secondary stream total temperature divided by the result of mass weighting the total temperature of the gas generator flow and the duct flow.

In symbolic form, W_{sc} is:

$$W_{sc} = \frac{W_s}{W_{g9} + W_{gd}} \sqrt{\frac{T_{t2} + \Delta T_s}{\left[\frac{(T_{t9})(W_{g9}) + (T_{td})(W_{gd})}{W_{g9} + W_{gd}}\right]}}$$

(a) Actual Secondary Airflow Ratio - W_s/W_p

The actual secondary airflow ratio is defined as the ratio of actual secondary airflow to the engine inlet airflow minus any customer bleed air.

(b) Secondary-to-Duct Total Pressure Ratio, P_{ts}/P_{td}

The secondary pressure required to supply a given secondary flow rate is normally specified as a fraction of duct total pressure, i.e., P_{ts}/P_{td}. Duct pressure is used because it is the duct flow that aerodynamically restricts the secondary passage. The secondary pressure may also be ratioed with compressor inlet total pressure, P_{t2}, for a specified inlet ram recovery, for ease of presentation.

(3) Exhaust System Tertiary Airflow

The tertiary airflow for a blow-in-door nozzle is normally used only by the exhaust system, and its gross thrust and ram drag are both included in the gross thrust coefficient. Therefore, definition of the quantity or pressure level of tertiary flow is not required other than to specify that in the absence of installation effects the flow be at free stream conditions just ahead of the tertiary door entrance.

CONFIDENTIAL

3. Exhaust System Description and Operation

a. General

Aircraft operating at high Mach numbers develop elevated ram pressure ratios. As a result, there is a high level of available energy in the engine exhaust stream. Therefore, some form of convergent-divergent (i.e., not simply convergent) exhaust nozzle is required to convert this available energy into thrust. Because operation of the aircraft at supersonic cruise conditions occurs for a large portion of the overall mission, efficient conversion of this energy to thrust is essential. In addition, because the aircraft must also take off, climb and fly at other conditions, efficient operation at off-design conditions must also be considered. Selection of an exhaust system configuration for an aircraft must be based upon several considerations such as aircraft configuration, aircraft mission, inlet characteristics, and engine noise requirements.

The clamshell exhaust system provides a high level of performance over the entire flight envelope and consequently high engine thrust and low fuel consumption. Mechanical simplicity and light weight are also inherent in the design concept due to the multifunctional capability of the reverser clamshells and the tertiary air doors.

Aircraft jet noise requirements are also an important factor affecting the selection of a particular exhaust nozzle system. The tertiary door, rotating clamshell concept provides reductions in jet noise as described in Volume III, Report C. All these considerations serve as the basis for the selection of the clamshell reverser-suppressor design for the commercial supersonic transport exhaust system.

b. Reverser-Suppressor Operation

Figure 2 shows the clamshell reverser-suppressor in its three basic modes of operation. The nozzle employs both physical and aerodynamic means of reducing the over- or under-expansion performance losses associated with off-design operation.

During low speed operation (figure 2a), the tertiary-air doors are open and external (tertiary) air is drawn into the nozzle along with any available secondary airflow to aerodynamically reduce overexpansion losses. The clamshells are rotated to the proper angle to facilitate admission of the tertiary air. The pressure-actuated trailing edge flaps are closed, due to pressure loading, and physically reduce overexpansion losses by reducing the exit area. At high subsonic Mach numbers, the closed trailing edge flaps produce external pressure drag, and so a compromise must be reached between the quantity of tertiary air induced and the minimum exit setting of the trailing edge flaps.

As the aircraft continues to accelerate to transonic flight Mach numbers, the tertiary doors will close due to increased internal pressures. The trailing edge flaps will continue to reduce overexpansion losses by providing small exit areas. At higher flight Mach numbers, the trailing edge flaps move outward to the cruise configuration shown in figure 2b.

CONFIDENTIAL

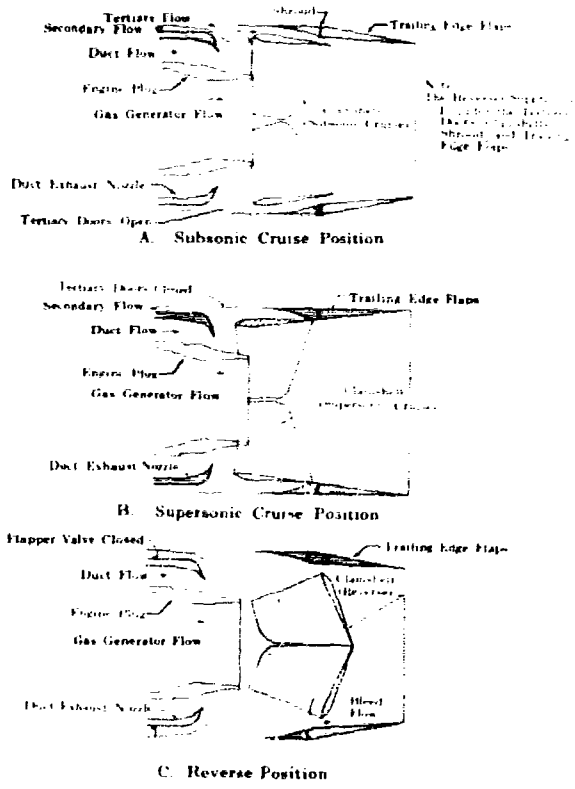

Figure 2. JTF17 Exhaust System With Clamshell Reverser-Suppressor

FD 17039
AIIIE

The near-ideal performance level demanded of the reverser-suppressor for supersonic cruise operation requires a specific shroud geometry. If this geometry were fixed to provide maximum cruise performance, the tertiary air passage would be blocked by the clamshells, and little or no tertiary air would be admitted during doors-open operation with a resultant performance loss. Consequently, the clamshells have been designed to serve several functions.

1. Provide the optimum expansion contour for cruise operation
2. Rotate to facilitate admission of tertiary air to ensure high off-design performance
3. Rotate further to form the blocker doors for reverse operation.

The tertiary-air doors also serve several functions. During subsonic and low supersonic operation, the doors open to admit tertiary air and reduce performance losses. During high supersonic and cruise operation the tertiary doors close to provide a cylindrical no-drag outer contour. During reverse operation, the reverse gas is exhausted through the tertiary-air doors at the desired angle. (See figure 2c.)

The pressure-actuated trailing edge flaps help to provide high off-design performance through a compromise between external boattail drag losses, internal overexpansion losses, and tertiary air induction drag losses.

c. Secondary Air System

Secondary air is required for cooling the reverser-suppressor during tertiary-air doors closed operation and to control the expansion of the exhaust stream to maintain maximum performance. During tertiary doors open operation, secondary air is not required for cooling, but will give small performance benefits if available. The minimum required secondary-to-engine flow ratio is defined in the Engine Model Specification.

The variation of the exhaust system gross thrust coefficients, C_{fp}, and $C_{f_{pmr}}$, with corrected secondary flow ratio is given in figure 3. Note the more rapid decrease of C_{fp} below flow ratios of 0.02 especially at supersonic cruise conditions. This is due to loss of control of the initial expansion of the duct stream and subsequent shock systems set up as the flow impinges on the nozzle shroud. The variation of $C_{f_{pmr}}$ at supersonic cruise conditions indicates that a corrected secondary airflow ratio of 0.02 gives maximum cruise performance. This occurs because, above 0.02, the ram drag of the secondary air is greater than the thrust attainable from it. During transonic operation, however, increased secondary flows provide additional nozzle performance by reducing nozzle overexpansion losses and external pressure drag, in addition to the thrust attained from the increased airflow. The exhaust system and inlet will be matched in cooperation with the airframe manufacturer to provide best utilization of the secondary air.

Routing of the secondary air passage from the inlet can be accomplished by either of two methods, a duct system or a pressurized nacelle. The pressurized nacelle system allows direct flow of the secondary air over the outer engine case and components, whereas the duct system contains the flow and allows the nacelle to be vented to ambient pressure. In either case, valving in the inlet itself or in the duct passage is required to control the quantity of secondary air. A flapper valve, or similar valving is also required to prevent flow of the reverse gases up the secondary air passage and into the nacelle. A detailed description of the secondary air systems for the Boeing and Lockheed installations is given in the Design Report.

d. Tertiary-Air System

Tertiary air is required to provide high exhaust nozzle efficiencies during off-design operation. The tertiary doors also provide reverse discharge area. The tertiary-air passage is sized to achieve maximum low-Mach-number performance through a compromise between external pressure drag losses, internal overexpansion losses, and tertiary-air induction drag losses. Consideration must also be given to obtaining the required reverser area for maximum reverse performance.

During tertiary-air doors open operation, there is an interaction between exhaust system internal and external performance. In this proposal, these effects are not separated; rather, the combined internal-external flow interaction and its effect on exhaust nozzle performance is presented. Tests and analytical studies have been conducted during Phase II, and will continue to be pursued, to investigate the tertiary airflow characteristics.

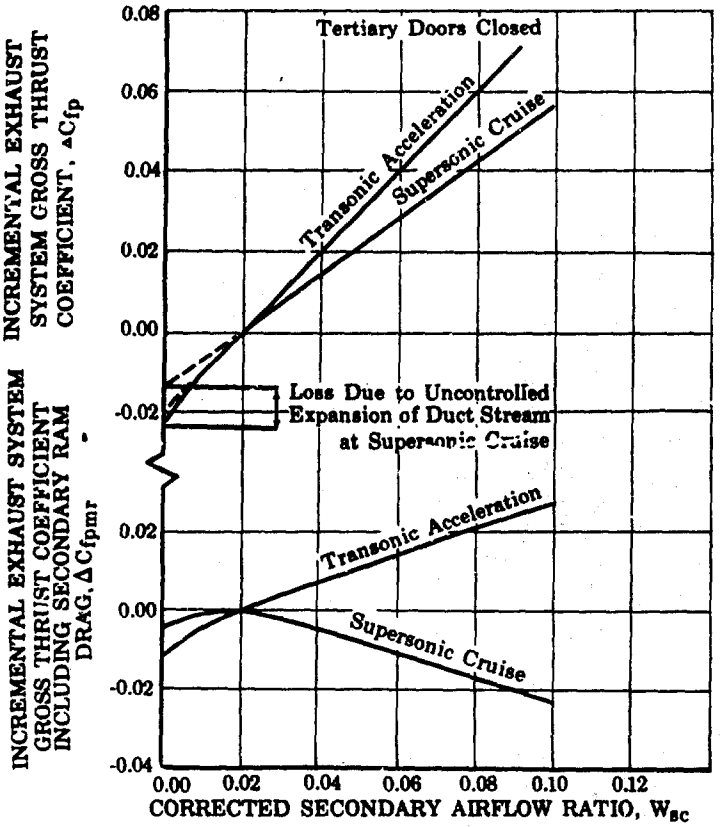

Figure 3. Variation of Exhaust System Gross Thrust Coefficient With Corrected Secondary Airflow Ratio

FD 17040
AIIIE

4. Phase II-C Development Program

a. Summary

The Phase II-C reverser-suppressor model test program was directed toward development of the exhaust system to obtain flow geometry consistent with good mechanical design and to verity the goal performance objectives at critical flight conditions. The performance objectives have been demonstrated with several model configurations. Inasmuch as the exhaust system configuration must be varied with flight condition, consideration must be also given to obtaining the best mechanical design as well as high performance. The exhaust system development program for Phase II-C has resulted in a sound mechanical design which can meet or exceed the performance goals. The development effort will be continued into Phase III to ensure the best overall exhaust system design.

CONFIDENTIAL

The scale model exhaust systems for the SST were tested in facilities of the United Aircraft Research Laboratories. The facilities used included a static test stand, a continuous-flow interchangeable subsonic-transonic wind tunnel, and a 17-inch by 17-inch transonic-supersonic blow-down wind tunnel. All have a three-flow balance that splits, meters, and throttles three concentric flows.

Tests of 1/20-scale models were conducted to maximize performance by a systematic variation of exhaust system geometry. Variations in the geometry of the tertiary doors, shroud, clamshells, and engine plug configurations were investigated at the following critical flight conditions:

Mach 0.0	Takeoff
Mach 0.9	Cruise
Mach 1.2	Acceleration
Mach 2.7	Cruise
Mach 0.0	Reverse

The wind tunnel test periods and areas of investigation are shown in figure 4. Approximately 1600 hours of wind tunnel test time, directed toward establishing the optimum reverser-suppressor configuration consistent with good mechanical design, light weight, and high performance, have been completed as of August 1966. Detailed results of these tests are discussed later in this section. As is subsequently developed, based on the results of these tests, the design of the exhaust system configuration for the JTF17 engine meets or exceeds the performance goals. Development of this configuration will be continued during the remainder of Phase II-C and in Phase III.

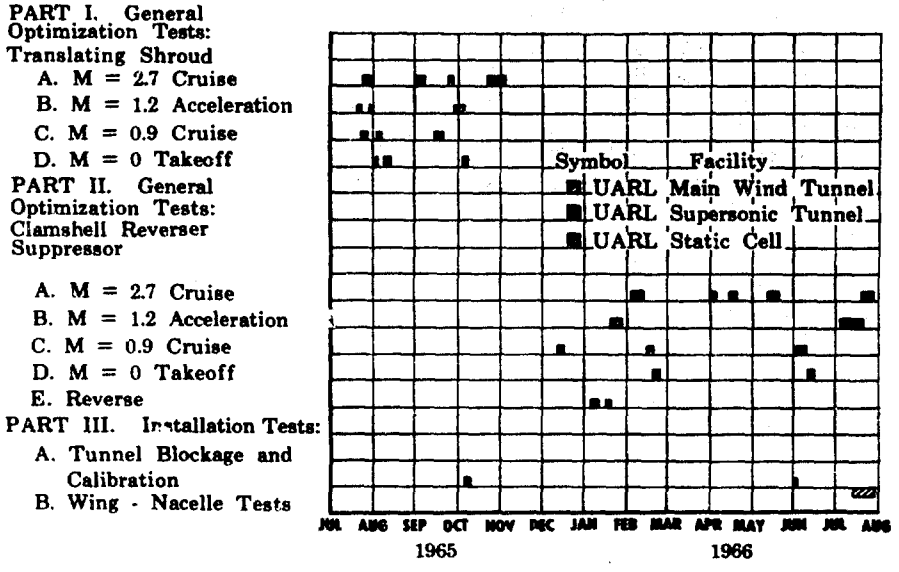

Figure 4. JTF17 Exhaust System Phase II-C Model Test Program

FD 17041
AIIIE

CONFIDENTIAL

Tests have also been conducted to establish preliminary installation effects. Approximately 230 hours of testing with a wing-mounted installation have been completed as of August 1966. The effect of the installation on exhaust system performance during subsonic operation has been determined. Initial results presented later in this section indicate that the installed model performance meets the subsonic cruise performance goal. The installation effects during transonic acceleration will be investigated during Phase III. No installation effects are expected at supersonic cruise conditions for the cylindrical nacelle configuration investigated. However, if other nacelle configurations are required P&WA will investigate these configurations in conjunction with the airframe manufacturer.

Test programs and analytical studies have also been conducted to investigate exhaust-system trailing-edge flap stability, hot flow effects, and advanced exhaust system design concepts. The results of these studies are also discussed in this section.

b. Computer Programs

An analytical representation of the exhaust system is incorporated in the engine performance computer decks to investigate and determine exhaust system performance. The calculations are based on a balance of the gas generator, duct, and secondary gas streams at the minimum shroud diameter and exit plane to establish the nozzle flow conditions and performance for operation with the tertiary doors closed. Performance with tertiary doors open is determined from a correlation of extensive wind tunnel test results obtained over many years of blow-in-door ejector nozzle model testing. The engine performance supplied to the airframe contractors incorporates exhaust nozzle performance determined with this calculation procedure.

A three-flow computing deck utilizing the method-of-characteristics has also been formulated to permit detailed analytical design and performance analysis of nozzle configurations. The program is especially useful for supersonic cruise performance determination and optimization. This program is currently being extended to include the effects of off-design operation, such as oblique shocks in the flow streams. This will permit additional analytical design and investigation to reduce the number of model tests required and thereby save wind tunnel test time and reduce costs. Future studies will investigate the effect of mixing between the secondary and duct streams.

Several other computing decks are available and have been used to perform calculations such as external boattail drags to aid in determining overall nozzle performance, and jet wake characteristics to determine jet wake profiles and flow properties. These decks will be improved and updated as required.

c. Performance Objectives

Mission analysis studies of the supersonic transport have shown that aircraft performance is extremely sensitive to exhaust system efficiency, and that high overall exhaust system performance is essential to economical aircraft operation. For example, one percent in nozzle efficiency at super-

CONFIDENTIAL

sonic cruise conditions is equivalent to 1450 pounds in engine weight. This corresponds to 5800 pounds of aircraft payload or 130 statute miles in aircraft range.

Exhaust system performance goals for the Phase II-C 650 lb/sec engine and the 687 lb/sec JTF17 production and prototype engines are given in table 1 for the critical flight conditions. The performance goals are based on the exhaust system performance calculation deck previously mentioned. The exhaust system calculation procedure has been adjusted to provide performance judged by past experience to be near the maximum attainable for a flight exhaust nozzle at the critical flight conditions. All exhaust system models have been designed and tested for the Phase II-C 650 lb/sec engine operating conditions to maintain a consistent basis for performance comparisons throughout the Phase II-C program. The small differences in operating conditions between the 650 lb/sec and the 687 lb/sec engines do not appreciably affect exhaust system performance levels or the mechanical feasibility of the design. There is no difference in the exhaust system design between the JTF17 production or prototype engines. However, the minimum exhaust system performance required to meet the prototype engine performance is less than for the production engine at supersonic cruise and takeoff conditions as shown in table 1.

Table 1. Exhaust System Performance Goals

Mach Number	Flight Condition	Exhaust System Gross Thrust Coefficient, C_{fp}, with 2% Corrected Secondary Airflow for Forward Flight, (Zero Secondary Airflow for Reverse Operation)		
		687 lb/sec JTF17 Engine		Phase II-C 650 lb/sec Engine
		Production	Prototype	
0.0	Takeoff	0.982	0.980	0.980
0.9	Cruise	0.923		0.922
1.2	Acceleration	0.967		0.965
2.7	Cruise	0.999	0.997	0.999
0.0	Reverse	40% of Maximum Nonaugmented Thrust Corresponding to $C_{f_r} = 0.47$		40% of Maximum Nonaugmented Thrust Corresponding to $C_{f_c} = 0.50$

The Pratt & Whitney Aircraft exhaust system goals have been established to be compatible with guaranteed engine performance. Because the exact levels of secondary flow may vary with design changes, the performance goals are based on 2% corrected secondary airflow ratio, W_{sc}, at all flight conditions except reverse, where no secondary airflow is allowed. The engine operating conditions for the critical flight conditions are listed in table 2.

CONFIDENTIAL

Table 2. Estimated JTF17 Engine Operating Conditions and Design Criteria Nacelle Dia - 80 in.

Mach No.	Flight Condition	Gas Generator Pressure Ratio P_{t9}/P_{am}		Duct Nozzle Pressure Ratio P_{td}/P_{am}		Effective Duct Exhaust Nozzle Area sq ft		Trailing Edge Flap Boattail Angle - degrees	Reverser-Suppressor Exit Area A_{exit} - ft^2
		Phase II-C 650 lb/sec Engine	JTF17 Production Engine	Phase II-C 650 lb/sec Engine	JTF17 Production Engine	Phase II-C 650 lb/sec Engine	JTF17 Production Engine		
0.0	Takeoff	2.3	2.2	2.4	2.6	8.8	8.6	11.0	23.5
0.9	Cruise	2.8	2.6	3.3	3.4	4.3	4.3	11.0	23.5
1.2	Acceleration	5.6	5.4	5.7	6.3	9.5	8.9	4.8	29.9
2.7	Cruise	15.6	14.8	28.7	29.3	5.4	5.5	0.0	34.9
0.0	Reverse	1.9	1.9	2.2	2.2	4.3	4.3	----	----

CONFIDENTIAL

Model tests conducted during Phase II-C have demonstrated the exhaust system goal performance levels for the Phase II-C 650 lb/sec engine. The subsonic configuration test model shown in figure 5 depicts the important model parts. The models are composed of a forebody that supports the tertiary doors and shroud assembly. The shroud assembly includes the fully variable clamshell segments and removable trailing edge flaps. The supersonic cruise test configuration installed in the 17-inch by 17-inch supersonic wind tunnel test section is shown in figure 6. A diagram of the exhaust system for the JTF17 engine is given in figure 7, with the important design parameters listed in table 2. The test data presented in figures 8 through 12 for the five critical flight conditions show that goal performance has been achieved. The test models have exceeded the supersonic cruise goal performance for the prototype exhaust system and achieved the required level for the production engine.

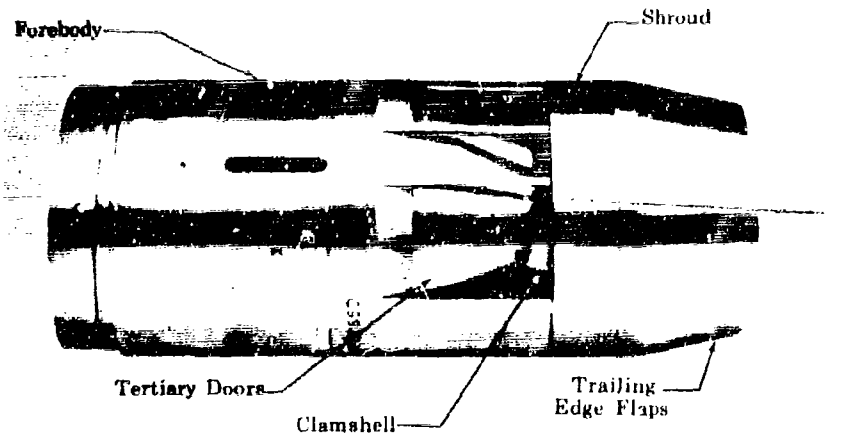

Figure 5. JTF17 Exhaust System Wind Tunnel Model— Tertiary Doors Open FD 16916 A111E

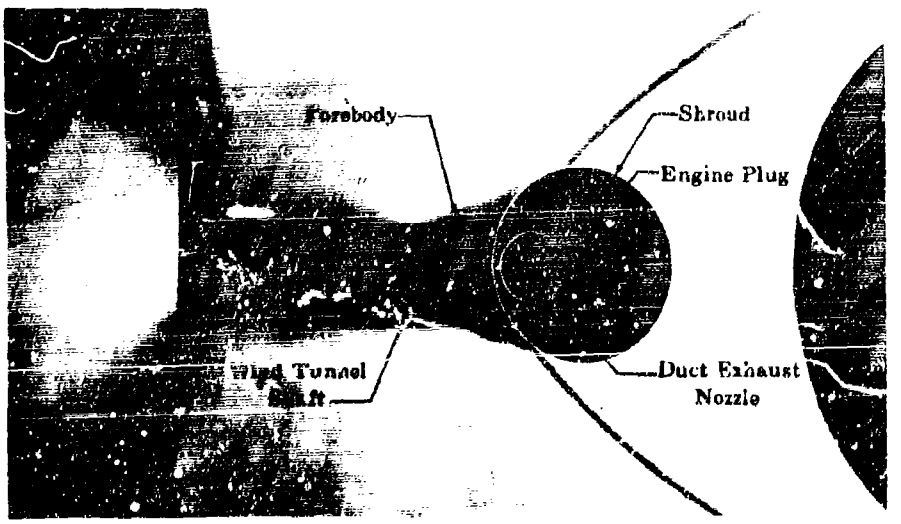

Figure 6. JTF17 Exhaust System Wind Tunnel Model— Supersonic Cruise Configuration Installed in Wind Tunnel FD 16873 AIIIE

CONFIDENTIAL

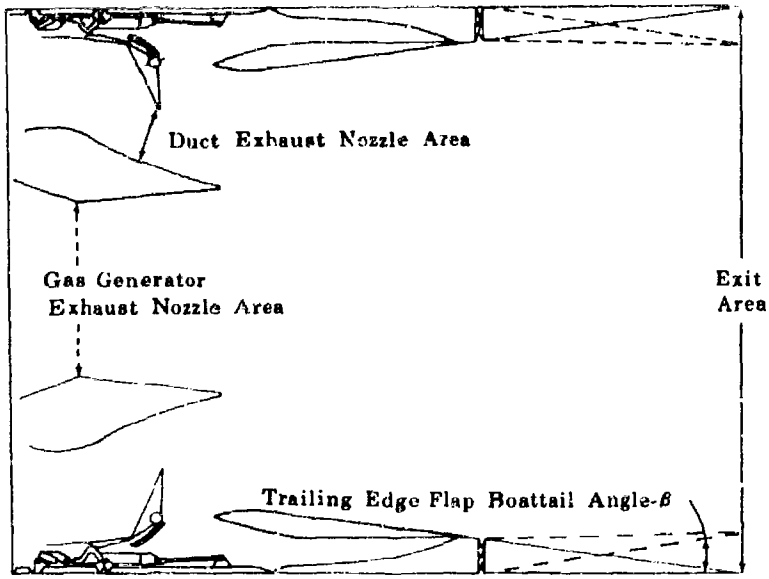

Figure 7. JTF17 Exhaust System FD 7042
AIIIE

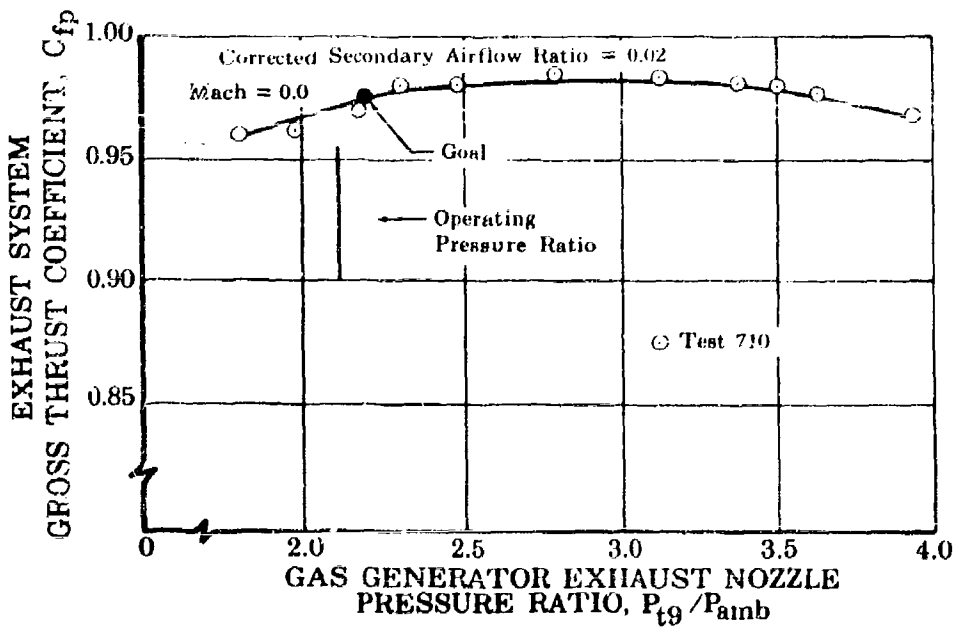

Figure 8. JTF17 Exhaust System Model Performance FD 17043
AIIIE

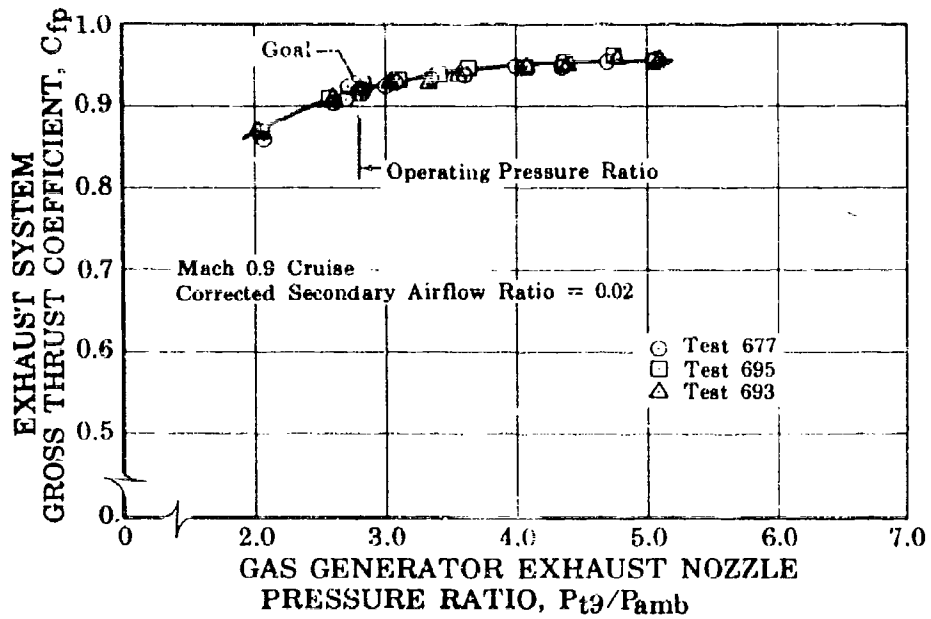

Figure 9. JTF17 Exhaust System Model Performance FD 17044 AIIIE

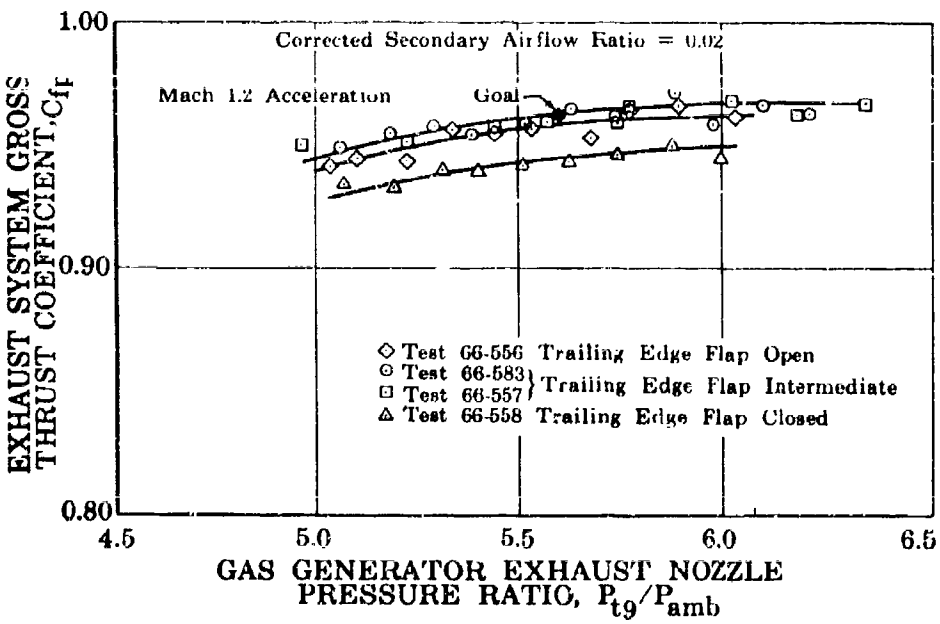

Figure 10. JTF17 Exhaust System Model Performance FD 17045 AIIIE

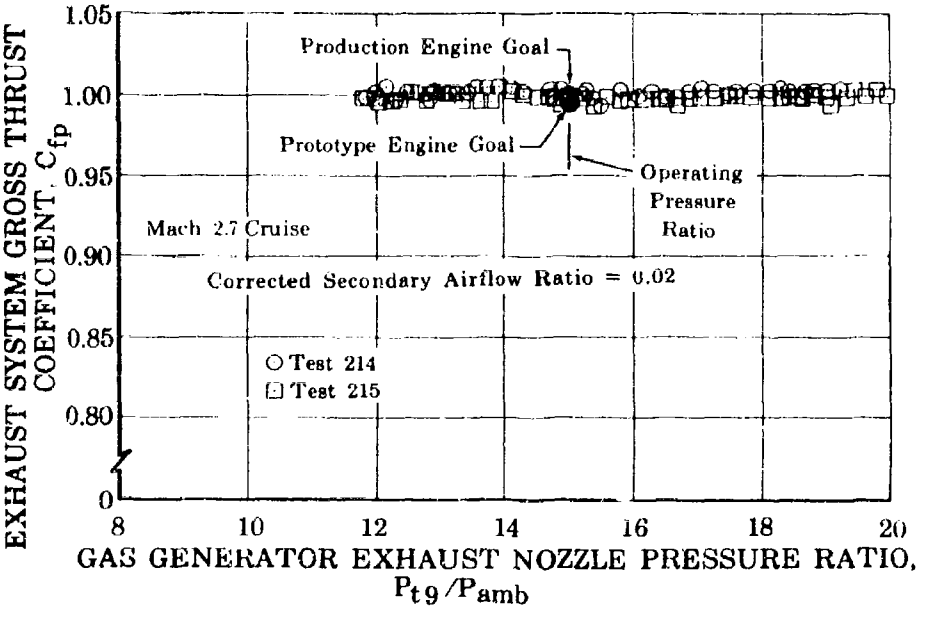

Figure 11. JTF17 Exhaust System Model Performance FD 17097
AIIIE

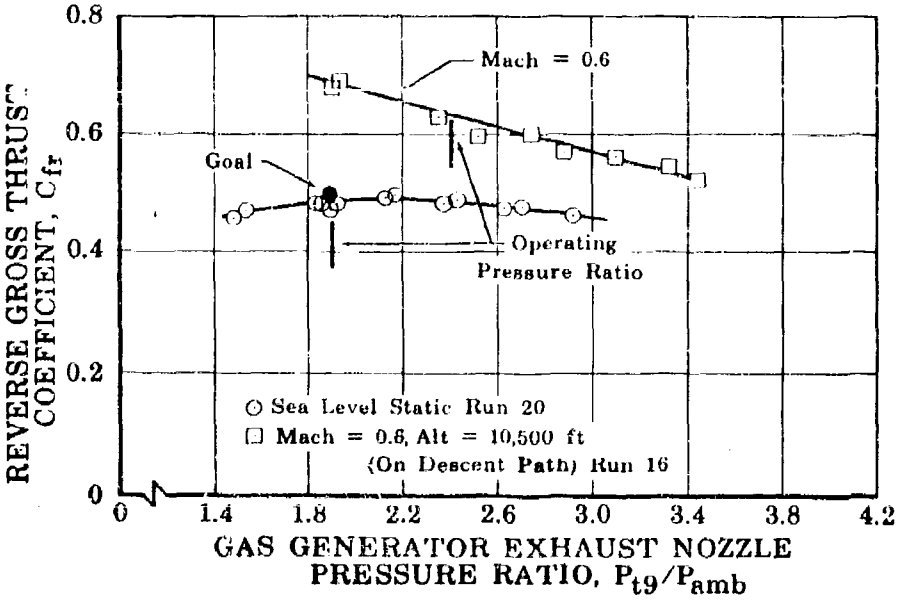

Figure 12. JTF17 Exhaust System Model Reverse Performance - Clamshell Data Run FD 17098
AIIIE

Past experience with blow-in-door exhaust nozzles similar to the JTF17 has shown that flight exhaust nozzle performance with full-scale hardware can be predicted from scale model tests. Figure 13 shows a comparison of predicted nozzle performance with that measured during flight tests of the YF12A airplane for tertiary doors open and closed operation. The in-flight performance was obtained by pressure area integration of pressure tap data obtained from an instrumented blow-in-door ejector nozzle. The performance of the flight hardware is higher than performance predicted from the scale model tests except for small performance decrements in the transonic region due to installation effects. A discussion of installation effects is given in paragraph 4f of this section.

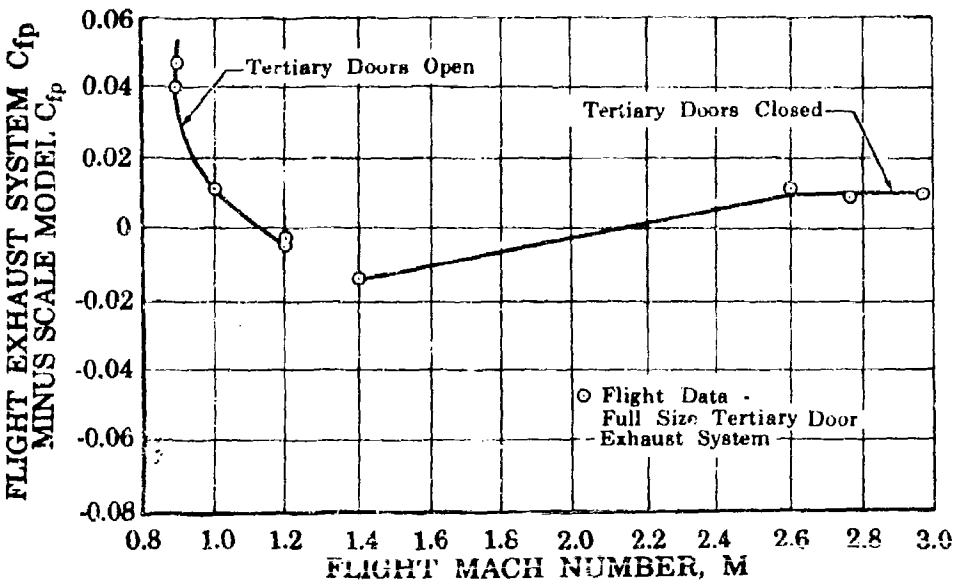

Figure 13. Performance Comparison of Flight and Scale Model Exhaust Systems — FD 17100 AIIIE

d. Correlation of Predicted Reverser-Suppressor Performance With Test Results

A comparison of model test data with exhaust nozzle performance theoretically predicted from the one-dimensional three-flow calculation deck is presented in figures 14 through 16. Figure 14 presents predicted nozzle gross thrust coefficient, C_{fp}, for maximum duct heat engine operation along a typical supersonic transport climb path and at cruise operation. Model test data at takeoff and Mach 1.2 acceleration and cruise conditions show good agreement with predicted values. Figures 15 and 16 present curves of theoretically predicted gross thrust coefficient versus engine power setting for the subsonic and supersonic cruise conditions, respectively. Model test data at the engine power required to cruise at these conditions, as determined from mission studies, compare favorably with these predictions, thereby validating the predicted exhaust nozzle performance levels supplied to the airframe companies.

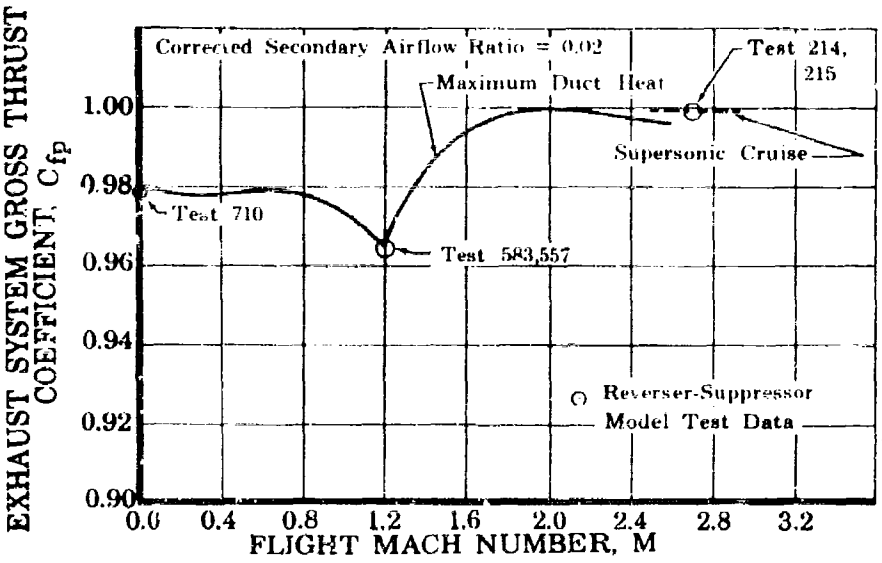

Figure 14. Comparison of Predicted JTF17 Exhaust System Performance with Model Test Data — FD 17101 AIIIE

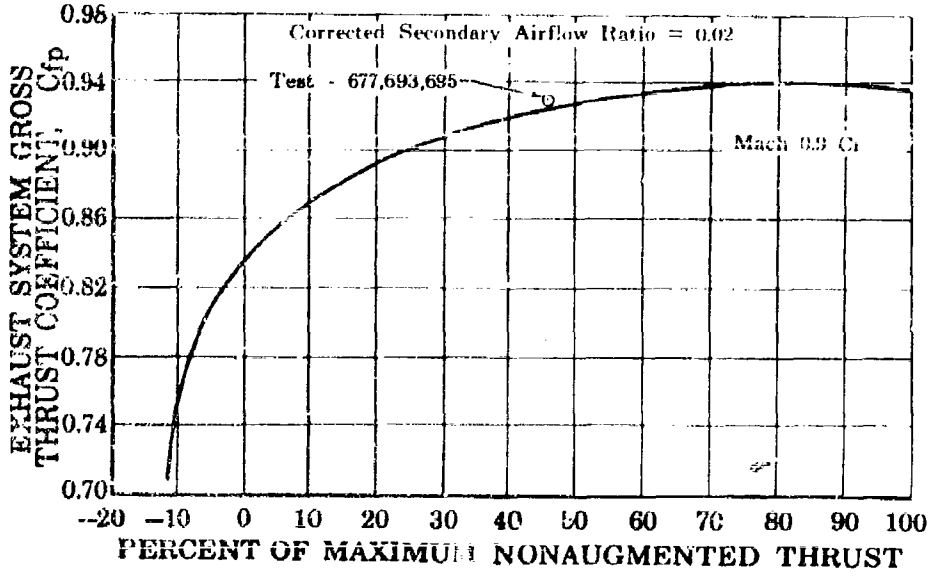

Figure 15. Comparison of Predicted JTF17 Exhaust System Performance with Model Test Data — FD 17102 AIIIE

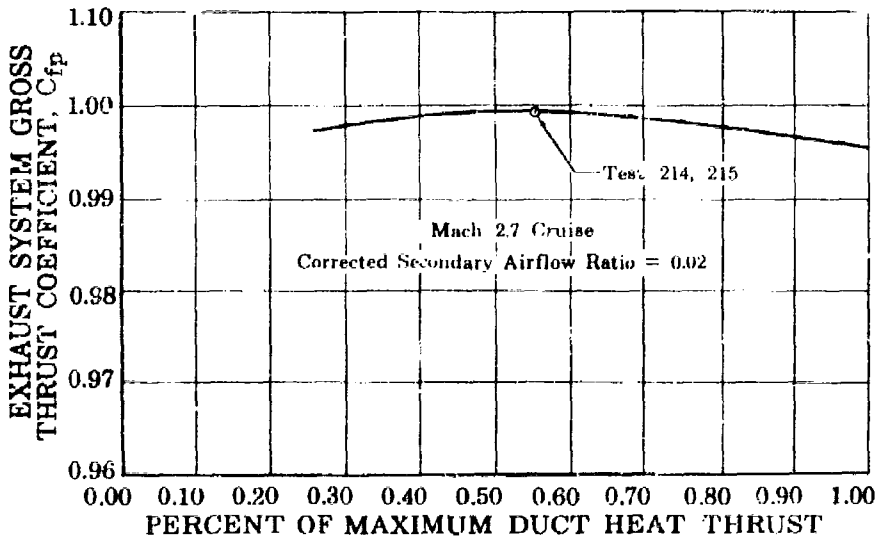

Figure 16. Comparison of Predicted JTF17 Exhaust System Performance with Model Test Data — FD 17103 AIIIE

e. Effect of Reverser-Suppressor Geometry on Performance

Extensive wind tunnel tests were conducted to determine the effect of various geometric variables on performance levels to ensure the best performance-mechanical design trade-off possible. The results of these tests are discussed in the following paragraphs.

(1) Exhaust System Tertiary-Door-Closed Design Variables

(a) Supersonic Cruise

A nonmixed-flow turbofan engine requires consideration of both gas generator and duct gas streams in the exhaust system design to ensure maximum cruise performance. The design variables that must be taken into account for cruise and associated high Mach number operation are shown in figure 17. The multitude of various combinations of these design variables required extensive wind tunnel testing to establish the effect of each parameter. The following discussion presents the effect of each variable or exhaust nozzle performance levels.

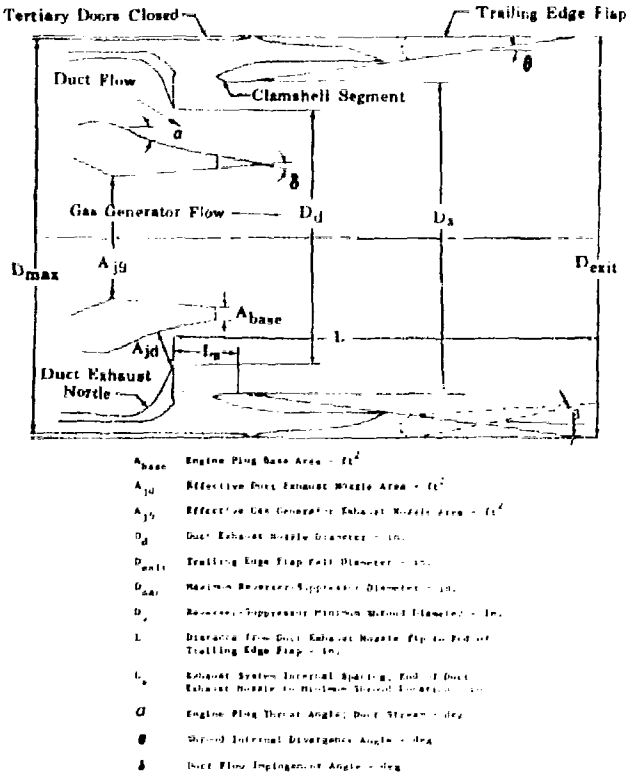

A_{base} Engine Plug Base Area - ft^2

A_{jd} Effective Duct Exhaust Nozzle Area - ft^2

A_{j9} Effective Gas Generator Exhaust Nozzle Area - ft^2

D_d Duct Exhaust Nozzle Diameter - in.

D_{exit} Trailing Edge Flap Exit Diameter - in.

D_{max} Maximum Reverser-Suppressor Diameter - in.

D_s Reverser-Suppressor Minimum Internal Diameter - in.

L Distance from Duct Exhaust Nozzle Flap to End of Trailing Edge Flap - in.

L_n Exhaust System Internal Sparing, End of Duct Exhaust Nozzle to Minimum Shroud Diameter - in.

α Engine Plug Throat Angle; Duct Stream - deg

θ Shroud Internal Divergence Angle - deg

δ Duct Flow Impingement Angle - deg

Figure 17. Exhaust System Design Variables - Tertiary Doors Closed

FD 16619
AIIIE

Nozzle Sizing

The reverser-suppressor maximum diameter, D_{max}, is sized at supersonic cruise conditions based on aircraft cruise drag determined from mission analyses. The exit area is sized close to the area required for complete expansion for all streams so that over or underexpansion losses are negligible at cruise conditions. The dotted line in figure 18 presents the performance variation as a function of nozzle diameter. Typical SST aircraft mission studies indicate that 145 pounds in engine weight is equivalent to approximately one-tenth of one percent of nozzle gross thrust coefficient. With this approximation, plus an estimate of nozzle weight versus diameter, it is possible to calculate the dashed curve of figure 18. The combination of the data represented by the dotted and dashed curves produces the resultant weight-performance curve of figure 18. The maximum diameter should be chosen at the peak of this weight-performance curve unless this diameter is less than the minimum allowable physical nacelle diameter for clearance around the engine case. The test results shown in figure 12 indicate that the exhaust system has been properly sized and over or underexpansion losses are negligible, since the cruise operating pressure ratio occurs near the peak of the nozzle gross thrust coefficient curve.

CONFIDENTIAL

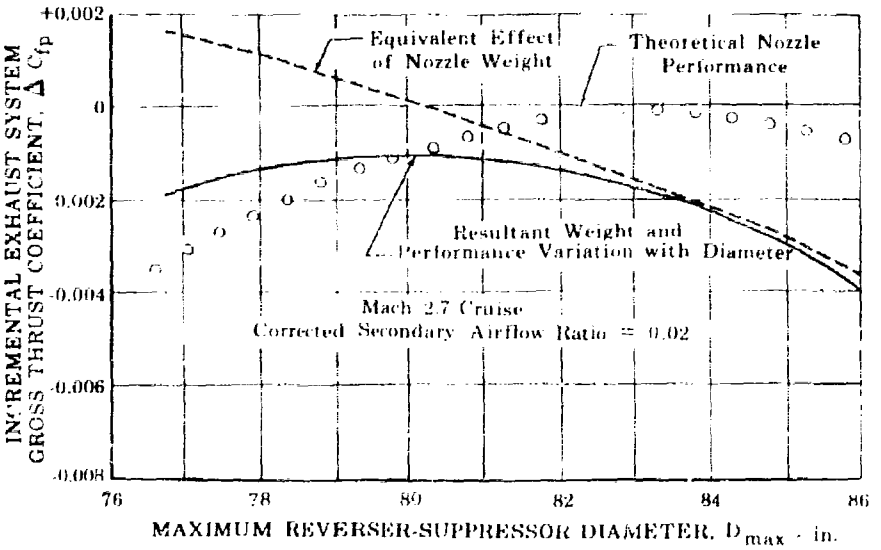

Figure 18. JTF17 Reverser-Suppressor Sizing FD 17104 AIIIE

The shroud length, L, for maximum performance can be determined from the peak of the curve of nozzle performance versus length as shown in figure 19. The effect of shroud length on performance was determined from test results as well as theoretically from the method-of-characteristics performance deck. Cruise performance is relatively insensitive to small variations of shroud length from the optimum, thus permitting shorter nozzle lengths and light weight.

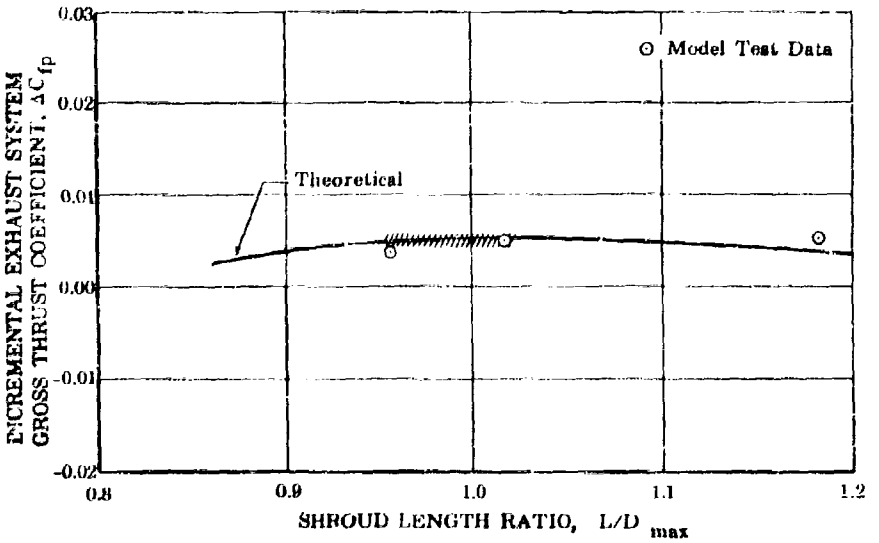

Figure 19. Variation of Incremental Exhaust System Gross Thrust Coefficient With Reverser-Suppressor Shroud Length FD 17105 AIIIE

CONFIDENTIAL

Shroud Geometry Effects on Performance

The location of the reverser-suppressor minimum shroud point relative to the duct exhaust nozzle is important at supersonic cruise conditions. That point is defined in figure 17 by the minimum shroud diameter, D_S, and its distance from the end of the duct exhaust nozzle, L_S. There is a pronounced interaction between L_S, D_S, and the engine plug that forms the duct stream expansion surface. This is to be expected because the minimum shroud point and plug, and their relative positions, determine the duct stream expansion and the secondary-to-duct total pressure ratio. Also, the duct expansion surface determines the duct exhaust nozzle diameter (D_d in figure 17) necessary to obtain the required duct nozzle throat area. Parametric studies have shown that the effect of the minimum shroud location can best be studied if L_S and D_S are ratioed to D_d. In effect, D_S/D_d is equivalent to an annular area or diameter ratio, and L_S/D_d is equivalent to a spacing ratio. The engine plug is designed with an isentropic contour so as to balance the static pressure and direction of the duct and gas generator flows at the plug tip.

Extensive wind tunnel tests were made to determine the interaction of these parameters and their effect on performance. The results of these tests are shown in figures 20 through 22, which give the variation of C_{fp} with L_S/D_d and D_S/D_d for 0, 10, and 20-degree conical plugs. Similar results for isentropic contoured engine plugs having throat angles of 20 to 30 degrees are presented in figure 23. These figures indicate that the performance trends are similar for the various engine plugs but the island of maximum performance occurs at slightly different L_S/D_d and D_S/D_d ratios. The design region selected for the JTF17 exhaust system is shown in figure 23.

For the exhaust system area ratios under consideration, an isentropic contoured shroud can achieve the same performance levels as a conical shroud with shorter length, and consequently lighter weight. However, the contoured shroud may suffer more off-design performance losses due to the larger area and consequently additional overexpansion losses at the trailing edge flap hinge plane. The final determination of shroud shape depends upon weight, performance, and fabrication considerations.

The effects of L_S/D_d and D_S/D_d on secondary pressure requirements are illustrated in figure 24. It can be seen that variations in D_S/D_d have a much larger effect on secondary pressures than variations in L_S/D_d. Consideration in shroud design should be given to utilizing as much secondary pressure as available in the installation to ensure high levels of nozzle performance.

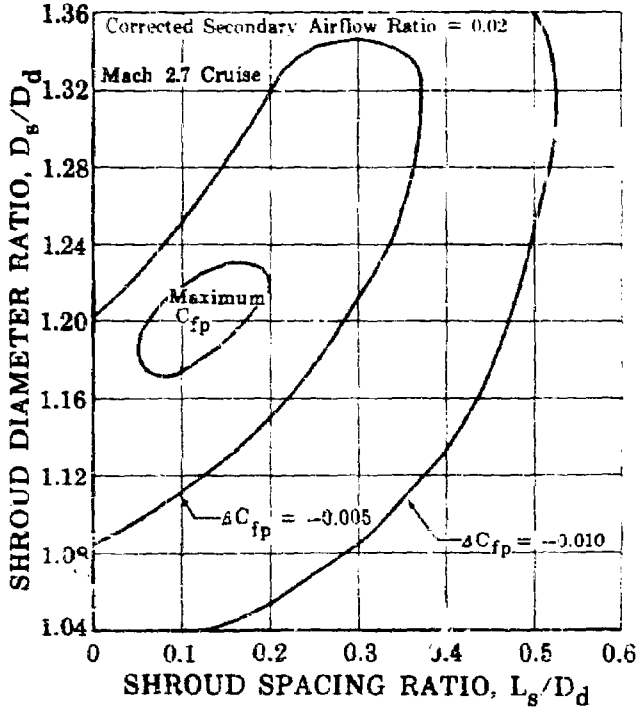

Figure 20. Variation of Exhaust System Performance With Shroud Geometry-Zero Degree Conical Engine Plug

FD 17106
AIIIE

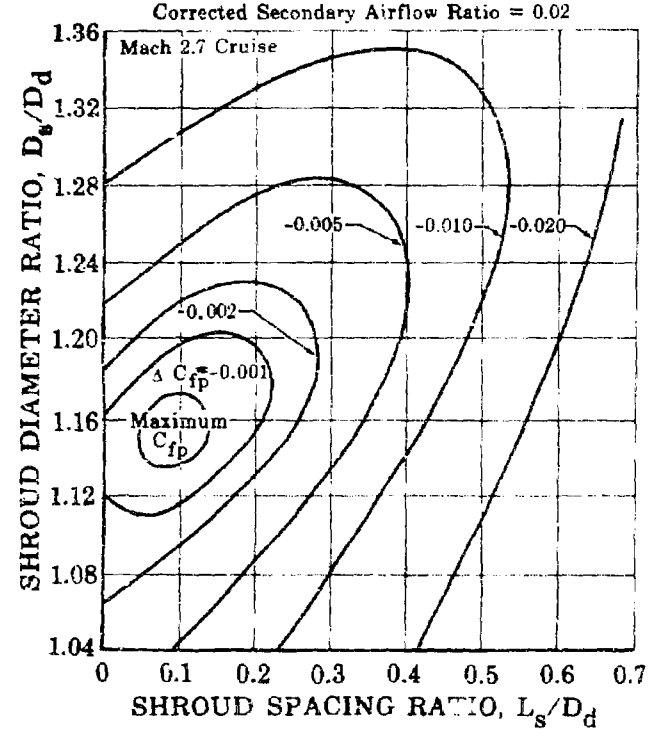

Figure 21. Variation of Exhaust System Performance With Shroud Geometry-10 Degree Conical Engine Plug

FD 17107
AIIIE

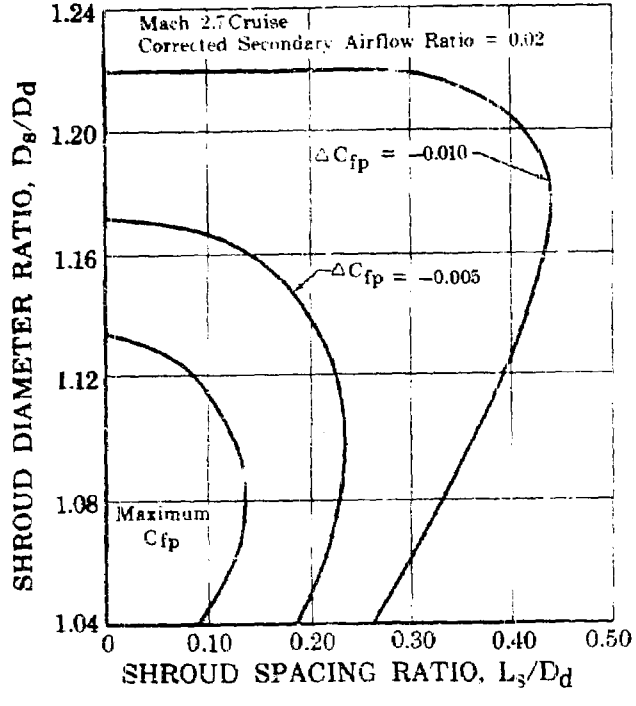

Figure 22. Variation of Exhaust System Performance With Shroud Geometry 20 Degree Conical Engine Plug

FD 17108 AIIIE

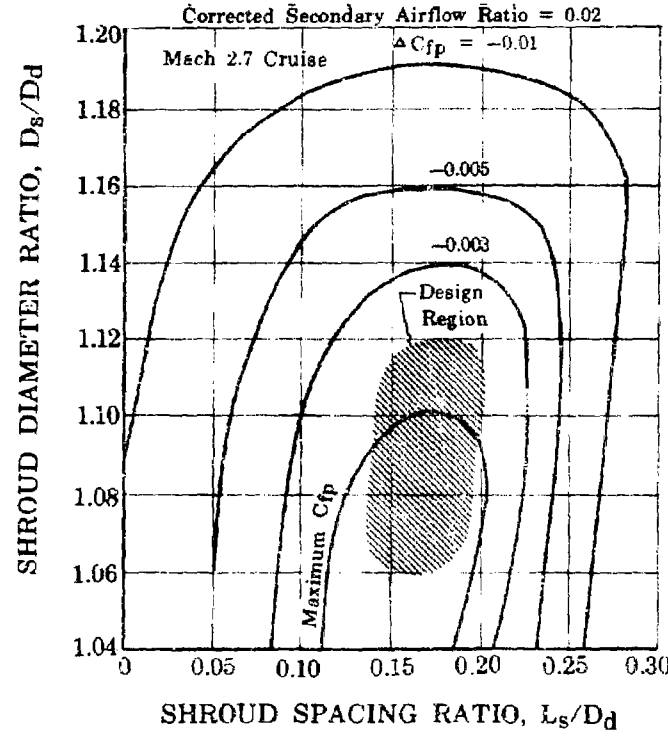

Figure 23. Variation of Exhaust System Performance With Shroud Geometry 20 to 30 Degree Contoured Engine Plug

FD 17109 AIIIE

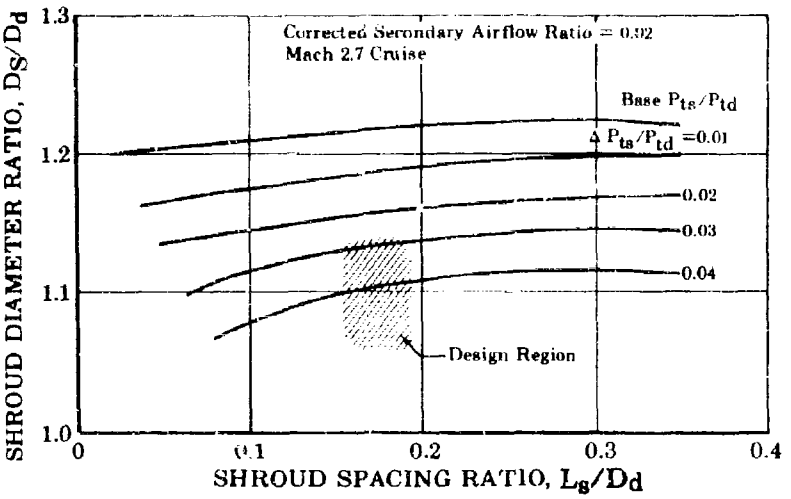

Figure 24. Typical Variation of Exhaust System Secondary to Duct Total Pressure Ratio With Shroud Geometry

FD 17657
AIIIE

Engine Plug Geometry Effects on Performance

Proper design of the plug geometry is required to obtain supersonic cruise performance levels. The duct expansion surface should be designed so as to provide a static pressure and flow direction balance with the gas generator flow. This can be accomplished with both conical and isentropic contoured plugs.

A plot of nozzle performance data versus plug throat angle, for conical and isentropic contoured plugs, is shown in figure 25. Photographs of the plug configurations tested are shown in figure 26. The performance trend shown in figure 25 is explained in the following paragraph.

The 0-degree plug does not perform as well as the 10-degree plug because a smaller duct nozzle diameter is required for a given duct nozzle throat area. This requires a smaller minimum shroud diameter to maintain the optimum D_S/D_d ratio. This, in turn, increases the shroud divergence angle for a given shroud length, and consequently additional performance losses are present. On the other hand, the 20-degree conical plug can maintain the optimum D_S/D_d ratio with small shroud divergence angles. However, the flow impingement angle, δ, between the duct and gas generator streams becomes large as plug angle increases, causing oblique shocks with subsequent performance loss. The isentropic contoured plugs give high performance at intermediate throat angles because the impingement angles can be kept quite low. However, as the throat angles increase, the expanding flow does not billow sufficiently to maintain high secondary pressures or optimum expansion contours, and performance losses result. These data indicate that maximum performance levels can be obtained with an isentropic contoured plug designed with the method-of-characteristics to balance static pressures at the impingement point with a throat angle of approximately 25 degrees.

Figure 27 gives the variation of performance with plug base area and flow impingement angle, and indicates that the optimum base area and impingement angle is zero for a typical plug with no base bleed. However, performance losses associated with low impingement angles are small and consequently low angle conical plugs can give near maximum performance.

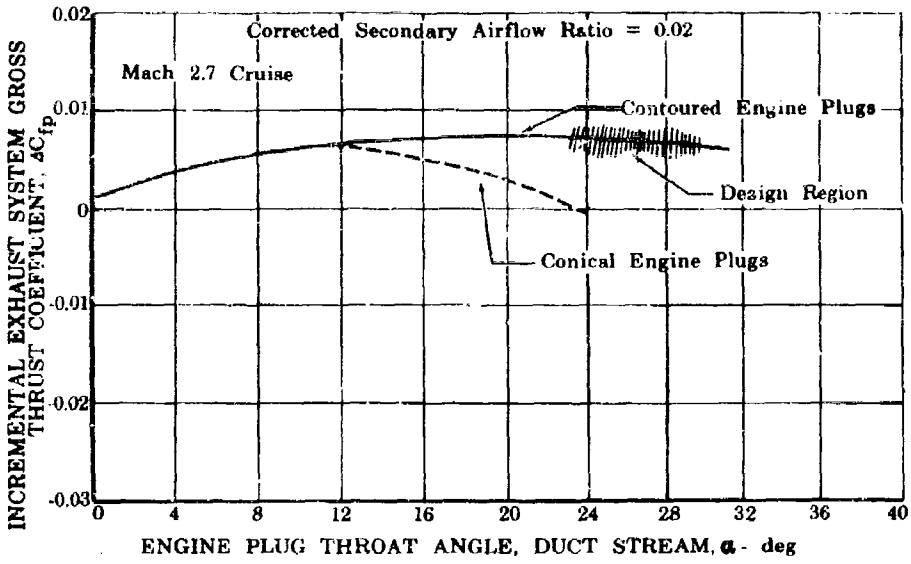

Figure 25. Variation of Exhaust System Performance With Engine Plug Throat Angle

FD 17111
AIIIE

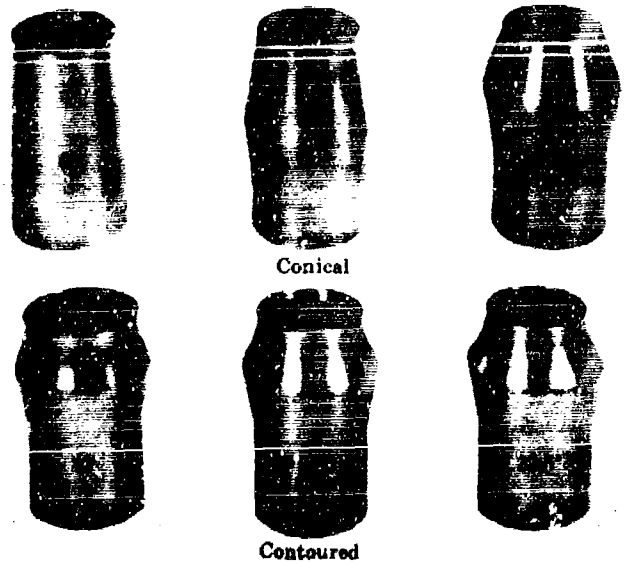

Figure 26. Exhaust System Model Engine Plugs

FD 16907
AIIIE

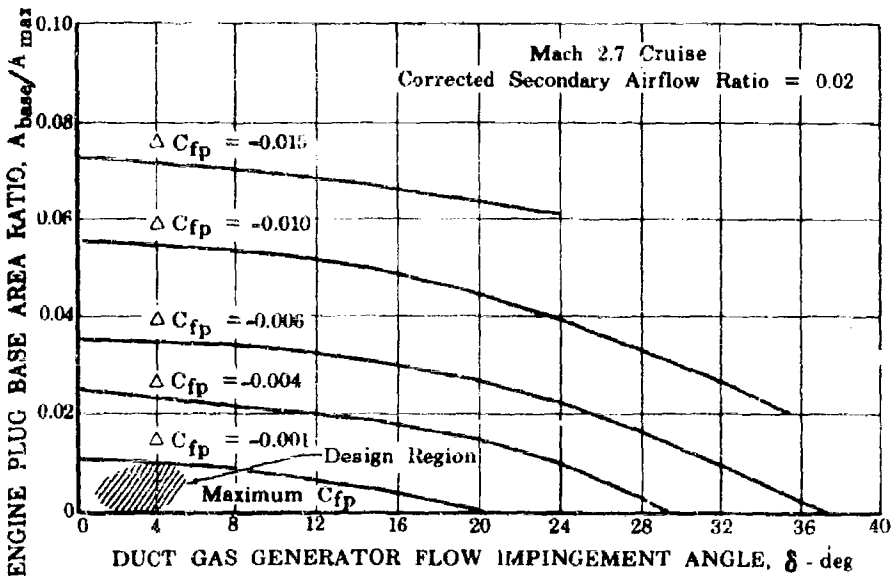

Figure 27. Typical Variation of Exhaust System Performance With Engine Plug Base Area — FD 17112 AIIIE

(b) Acceleration - Tertiary Doors Closed

As previously discussed, it is necessary to size the reverser-suppressor for maximum performance at Mach 2.7 cruise conditions. However, high performance at off-design conditions such as Mach 1.2 acceleration and subsonic cruise is also required. The JTF17 reverser-suppressor has been designed to provide the off-design performance goal while remaining consistent with the configuration necessary to meet the cruise performance goal.

The critical parameters affecting operation during acceleration conditions are tertiary door position, trailing edge flap boattail angle, and clamshell position. Wind tunnel tests at M = 1.2 were conducted to determine the effect of these parameters on performance. Photographs of typical models tested are shown in figures 28 and 29. Results of these model tests are presented in figures 30 and 31 for tertiary doors closed and open, respectively. These figures show the interrelationship between trailing edge flap boattail angle and clamshell position and their effect on performance. Analytical studies comparing the internal and external pressure distributions over the free floating tertiary doors indicate that the tertiary doors will be closed at Mach 1.2 during aircraft acceleration. Model tests were conducted to investigate both tertiary doors open and closed conditions but performance estimates are based on doors closed operation. Figure 30 shows the optimum clamshell angle to be zero degrees for transonic acceleration operation (with tertiary doors closed), which is also the supersonic cruise position. Figures 30 and 31 also show that the optimum trailing edge flap boattail angle for Mach 1.2 acceleration is approximately 5 degrees. This is confirmed by analytical studies conducted using the one-dimensional, three-flow internal performance prediction deck and the method-of-characteristics boattail drag deck, as shown in figure 32. However, as discussed in the next paragraph, a trailing edge flap angle maximum setting of 5 degrees

provides too large an exit area for subsonic operation for the shroud lengths under consideration so that overexpansion losses would result. Consequently, the minimum exit area is sized for the subsonic cruise condition since analytical studies indicate the flaps will be floating at an intermediate exit area during Mach 1.2 acceleration operation.

(2) Exhaust System Tertiary-Doors-Open Design Variables

When cruise exhaust system geometry consistent with peak performance levels and good mechanical design has been determined, the configuration required to obtain high performance during subsonic cruise conditions, i.e., tertiary doors open, must be established.

The geometric variables affecting subsonic cruise operation are tertiary door area (A_t), initial and final tertiary door angle (B_1 and B_2), exit diameter (D_{exit}), trailing edge flap boattail angle (β), clamshell angle (ζ), and clamshell thickness ratio (t/c). These parameters are illustrated in figure 33. Tertiary-doors-open models with fully variable clamshells were tested at Mach 0.9 cruise conditions to establish the effect of these variables on doors-open performance.

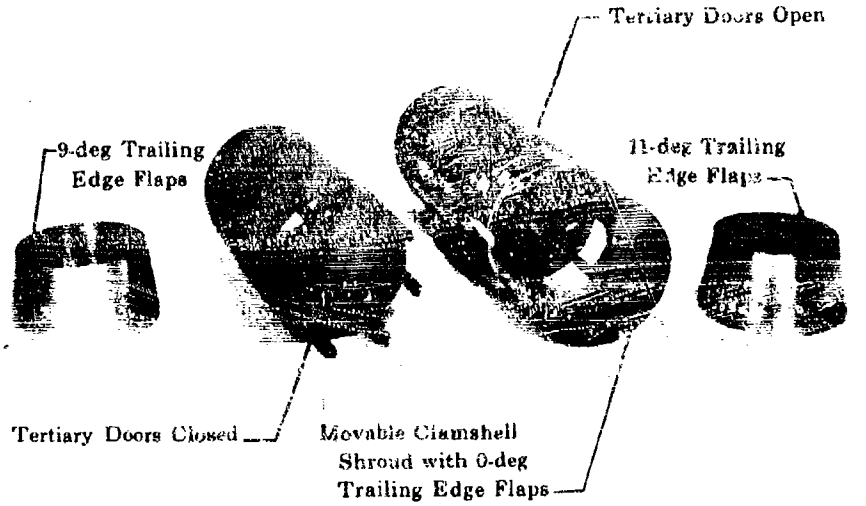

Figure 28. JTF17 Exhaust System Wind Tunnel Model. FD 16874 AIIIE

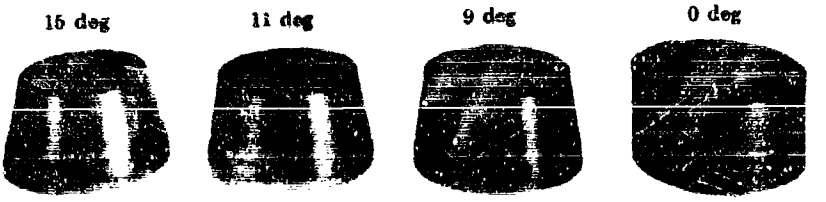

Figure 29. JTF17 Exhaust System Wind Tunnel Model Trailing Edge Flaps FD 16875 AIIIE

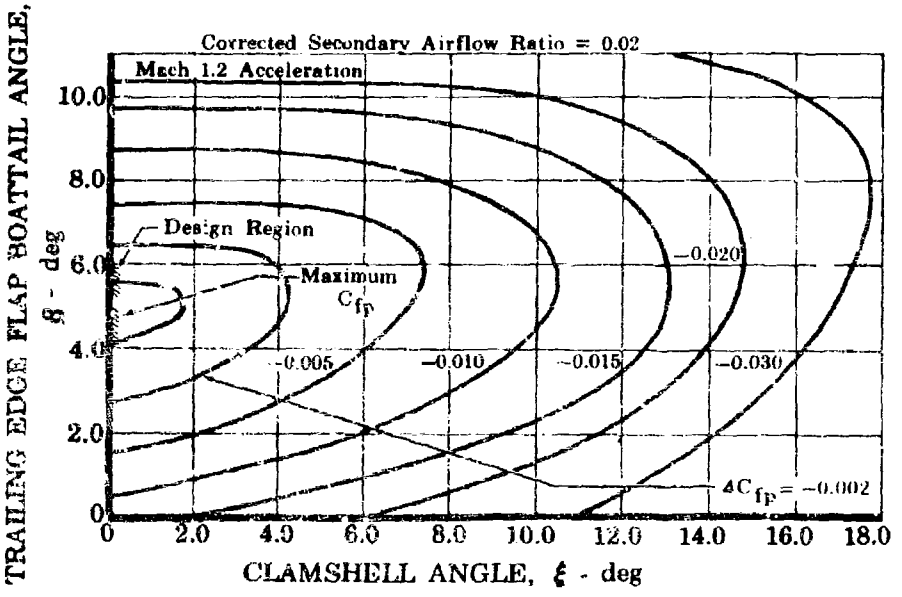

Figure 30. Variation of Exhaust System Performance with Reverser-Suppressor Geometry - Tertiary Doors Closed

FD 17113
AIIIE

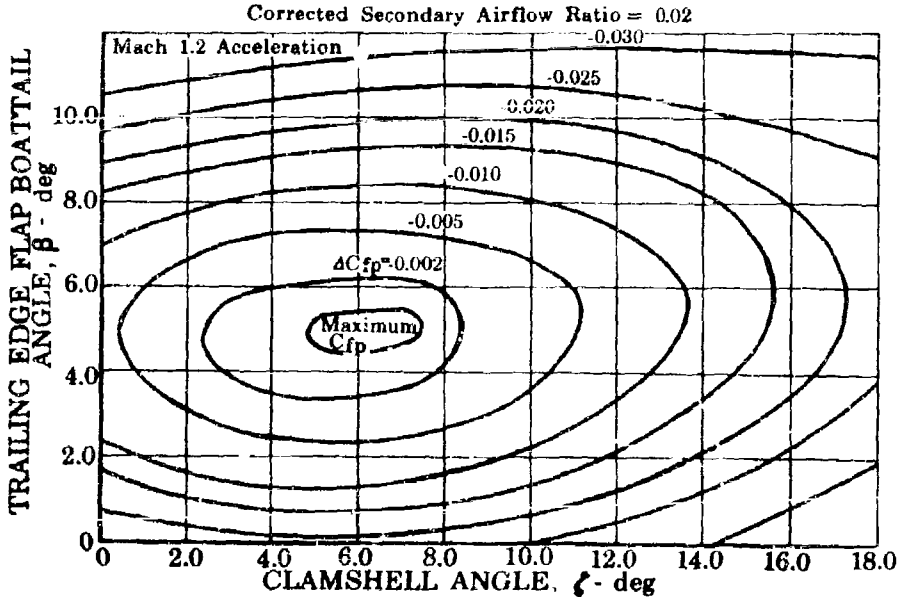

Figure 31. Variation of Exhaust System Performance With Reverser-Suppressor Geometry - Tertiary Doors Open

FD 17114
AIIIE

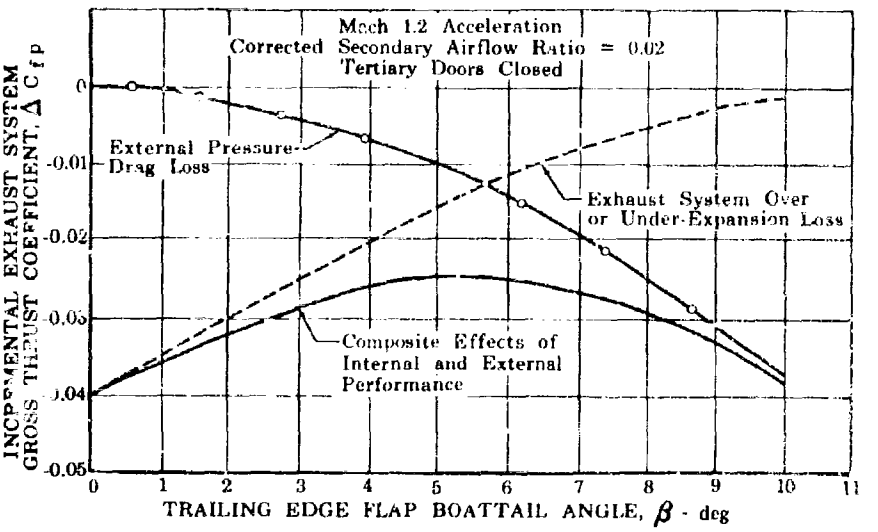

Figure 32. Theoretical Determination of Reverser-Suppressor Optimum Trailing Edge Flap Position

FD 17115
AIIE

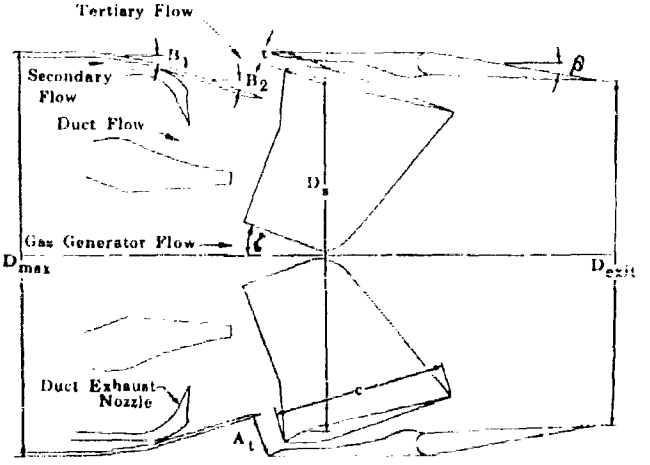

Figure 33. Exhaust System Design Variables Tertiary Doors Open

FD 17004
AIIIE

CONFIDENTIAL

Tertiary Door Area and Trailing Edge Flap Angle Effects on Performance

The effect of tertiary door area and trailing edge flap angle on nozzle performance is illustrated in figure 34. A compromise between overexpansion losses, external pressure drags and tertiary air induction drags must be made to obtain maximum performance levels. An increase in tertiary area gives increased performance up to the point where overexpansion losses are minimized and tertiary induction drag losses become large. The actual door area selected should be less than optimum, since resulting performance losses are relatively small and the mechanical design becomes increasingly complicated and heavy to achieve large areas.

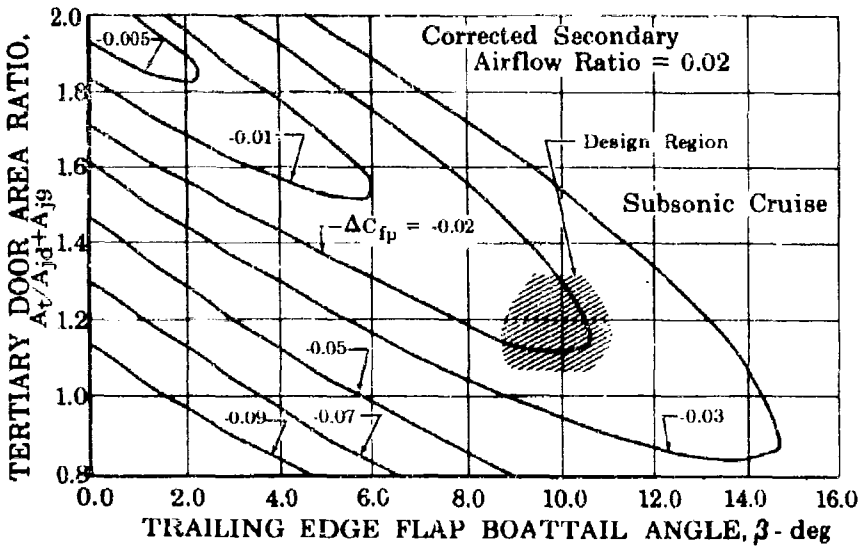

Figure 34. Variation of Exhaust System Performance With Tertiary Door Area and Boattail Angle

FD 17116
AIIIE

Clamshell Angle Effects on Performance

Rotation of the clamshells during tertiary-doors-open operation is required to facilitate the admission of tertiary air. An investigation was carried out to determine the angle of clamshell rotation required to give maximum performance. Figure 35 indicates that a clamshell angle between 15 and 20 degrees provides peak performance levels. At lower angles, the clamshells block the tertiary passage and restrict the admission of tertiary air. Above 20 degrees, the passage behind the clamshells is restricted and sufficient flow is not provided to fill the drag-producing base areas generated by the clamshells. The clamshells need only be approximately located within the 15 to 20 degree band because the performance peak is relatively flat.

CONFIDENTIAL

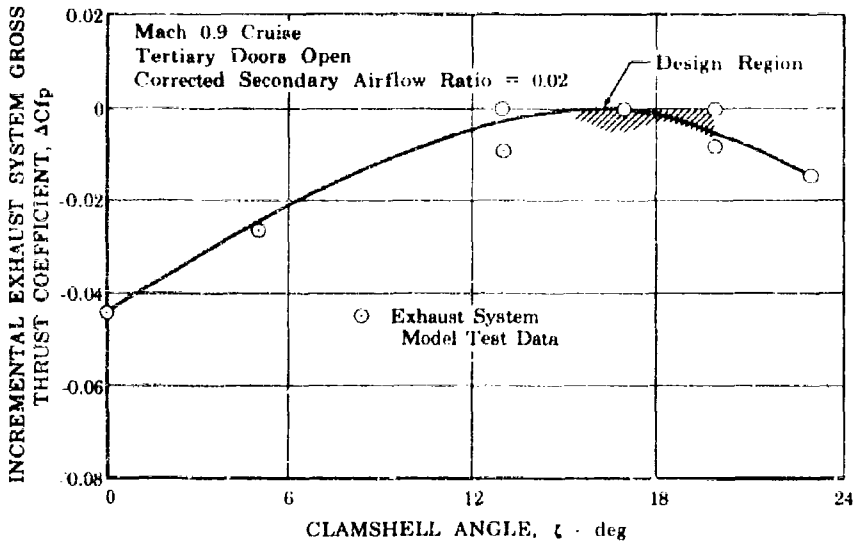

Figure 35. Variation of Performance With Reverser-Suppressor Clamshell Angle

FD 17117
AIIIE

Clamshell Fineness Ratio Effects on Performance

The effect of clamshell thickness on performance was investigated. No appreciable difference in performance was observed for fineness ratios ranging from 0.03 to 0.10.

Tertiary Door Configuration

Several mechanical schemes to obtain the required tertiary and reverser door areas have been investigated and the relative performance of each determined by model tests. The configurations tested included steep-angle and shallow-angle double-hinged tertiary doors, scoops, pop-out doors, and tandem tertiary doors. The configurations and their relative performance are presented in figures 36 and 37. Deep, double-hinged tertiary doors with shallow angles give the best subsonic cruise performance and consequently were selected for the reverser-suppressor design. Consideration must also be given to the required reverse area because the tertiary doors also serve as the reverse flow passage. The reverser requirements are covered in the following section.

(3) Reverser Design Variables

Figure 38 illustrates the design variables associated with reverser operation: reverser discharge area (A_{rev}), bleed area (A_{bleed}), circumferential blockage (degrees), spacing ratio (K/D_{max}), and tertiary doors reverse angle (?).

The effect of these variables was established by scale model tests at static and subsonic flight Mach numbers. A photograph of the clamshell reverser model with the clamshells in the reverse configuration is shown in figure 39.

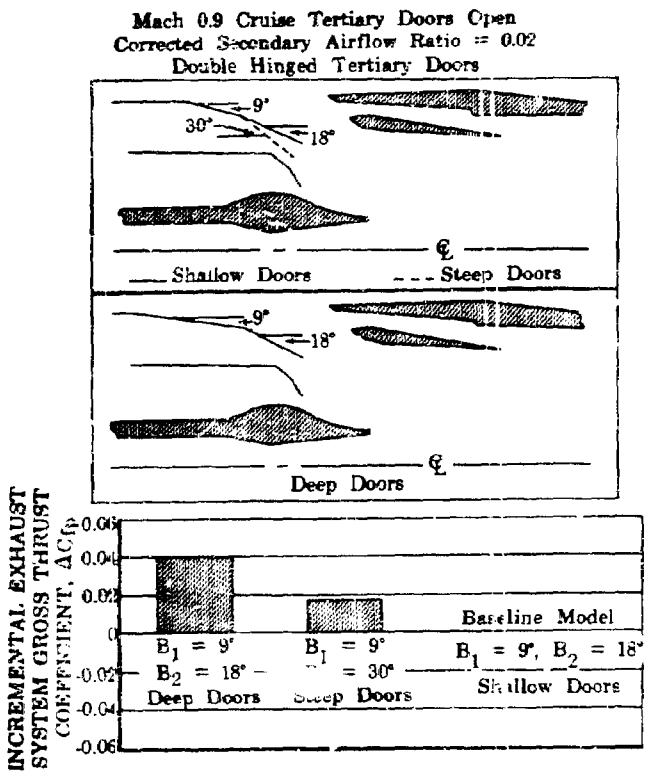

Figure 36. Variation of Exhaust System Performance With Tertiary Door Configuration

FD 17118
AIIIE

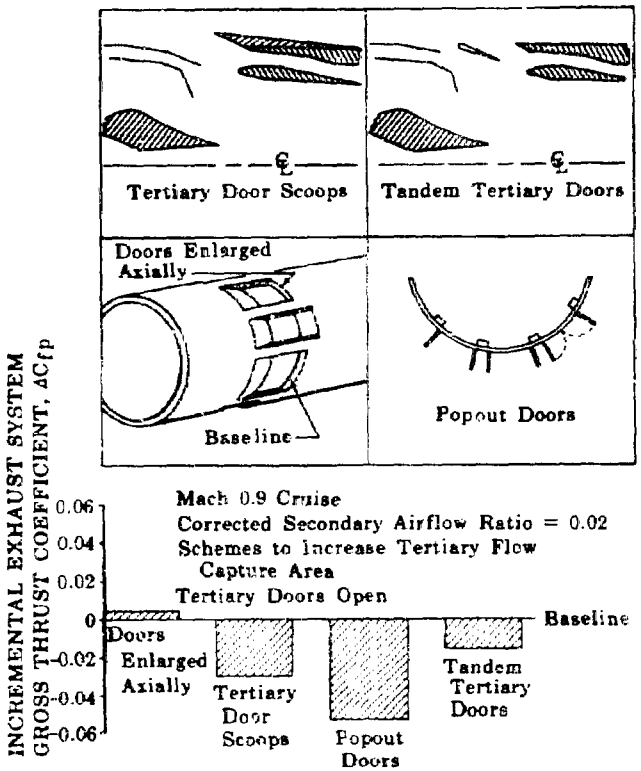

Figure 37. Variation of Exhaust System Performance With Tertiary Door Configuration

FD 17119
AIIIE

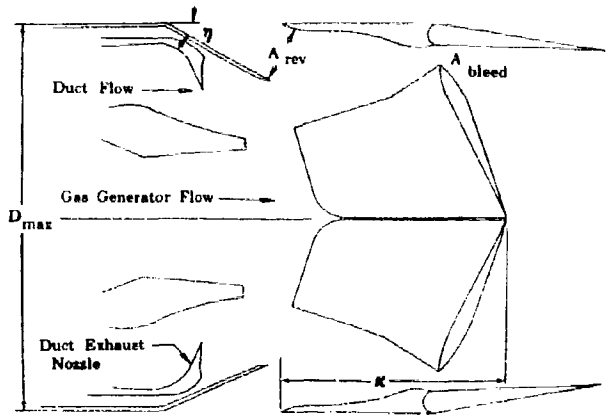

A_{bleed} Area Between Clamshells and Trailing Edge Flaps at Reverse - ft^2

A_{rev} Reverse Flow Area Available through Tertiary Doors - ft^2

D_{max} Maximum Reverser-Suppressor Diameter - in.

K Distance Along Centerline from Leading Edge of Shroud to Clamshells at Reverse - in.

η Tertiary Door Angle During Reverse Operation - deg

Figure 38. Exhaust System Design Variables - Reverse Configuration

FD 17003
AIIIE

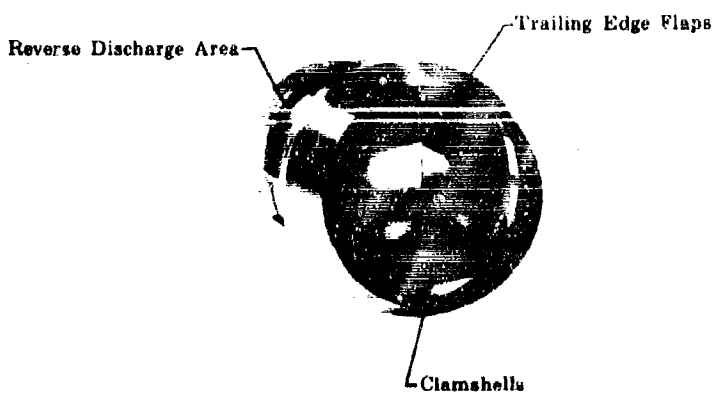

Figure 39. JTF17 Reverser-Suppressor Wind Tunnel Model - Reverse Configuration

FD 16906
AIIIE

Reverser Discharge Area and Bleed Area, Effects on Reverser Performance

Figure 40 shows the variation of reverser performance with reverser discharge area and bleed area for static sea level reverse operation. Figure 41 shows the variation of gas generator and duct flow coefficients with discharge and bleed area. Selection of a reverser design is based on a compromise between the required reverse thrust coefficient, avoidance of engine air flow suppression, and mechanical limitations in obtaining the reverse area. The goal, reverse thrust level of 40% of the maximum nonaugmented static sea level thrust, can be obtained with minimum weight by sizing the reverse-to-engine area ratio, $A_{rev}/(A_{jd}+A_{j9})$, equal to 1.2 to 1.3 with approximately 10% to 20% bleed flow area. No appreciable gas generator or duct flow suppression is evident for this configuration, as shown in figure 41. The reverse thrust requirement is based on an engine power setting of approximately 80% which corresponds to a gas generator discharge total temperature of 1250°F and a total temperature at the duct nozzle throat of approximately 240°F. These temperatures permit extensive use of titanium in the reverser-suppressor with resultant light weight, and requires a reverse thrust coefficient, C_{fr}, of approximately 0.5 to obtain the goal value of 40% of the maximum nonaugmented static sea level forward thrust. A discussion of the materials used in the reverser design is given in Volume III, Report B, Section IIF.

Reverse Circumferential Blockage, Effects on Performance

Circumferential blockage of the reverse gas flow can affect reverser performance as shown in figure 42. The decrease in reverse thrust coefficient, C_{fr}, with a decrease in reverser circumferential flow is due to an increase in reverse gas angle as the area of each reverse door is enlarged to maintain the required total reverse discharge area. Close coordination will be maintained with the airframe manufacturer to ensure a circumferential reverse gas flow consistent with airframe targeting requirements

Clamshell Spacing Effects on Reverser Performance

The effect of reverser clamshell spacing is shown in figure 43. Because the variation of reverse thrust coefficient is relatively insensitive to small changes in spacing, the importance of this parameter lies in its effect on engine flow suppression characteristics. The range of spacing ratios under consideration for the reverser system is shown by the abscissa of figure 43 and indicates little or no engine flow suppression.

Tertiary Door Reverse Angle Effect on Reverser Performance

The tertiary door reverse angle, η, can affect the mean reverse gas discharge angle and consequently reverser performance. The variation of reverse thrust coefficient with the mean reverse discharge angle is shown in figure 44. An analytical solution obtained by taking the cosine of the reverse discharge angle is shown for comparison and indicates good agreement.

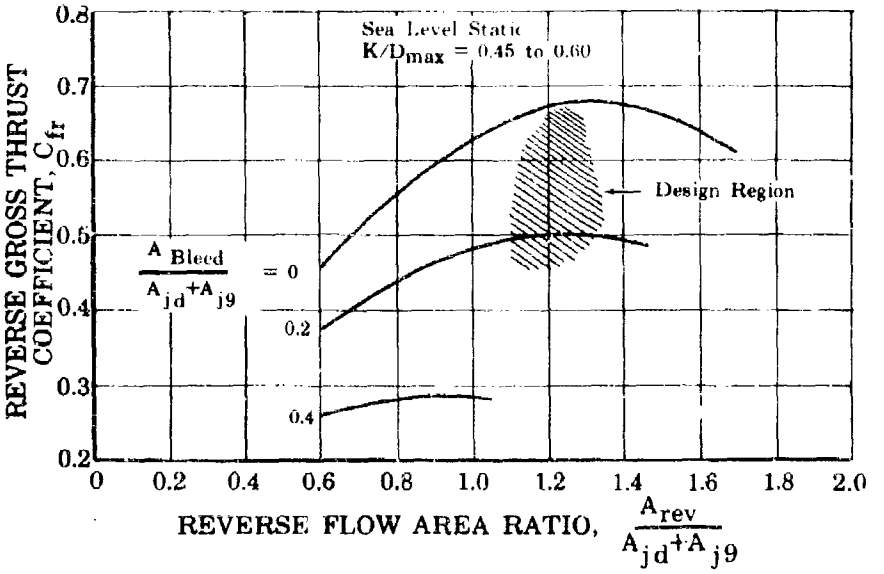

Figure 40. Variation of Exhaust System Performance With Reverse Flow Area and Bleed Area - Approx 200 Degree Circumferential Discharge

FD 17120
AIIIE

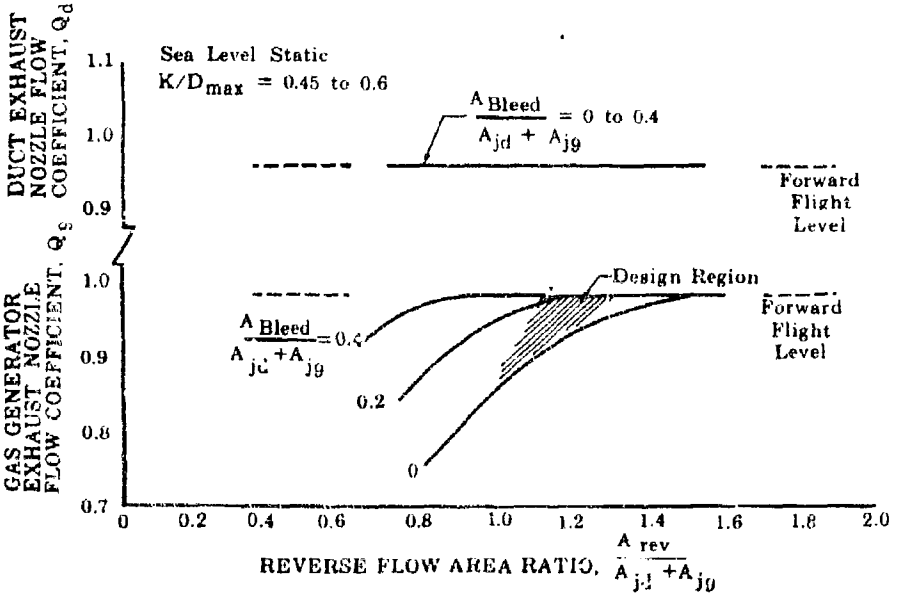

Figure 41. Variation of Flow Coefficient With Reverse Flow Area and Bleed Area

FD 17121
AIIIE

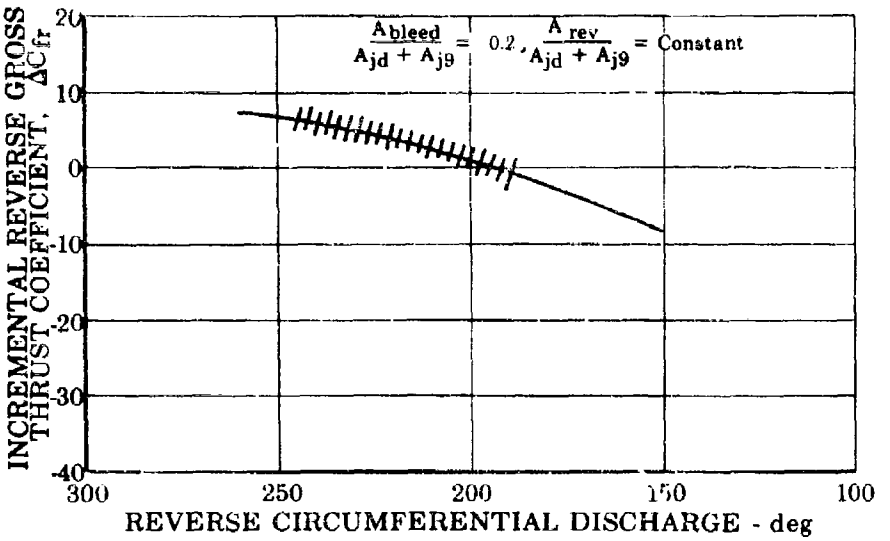

Figure 42. Variation of Reverse Performance With Circumferential Discharge — FD 17665 AIIIE

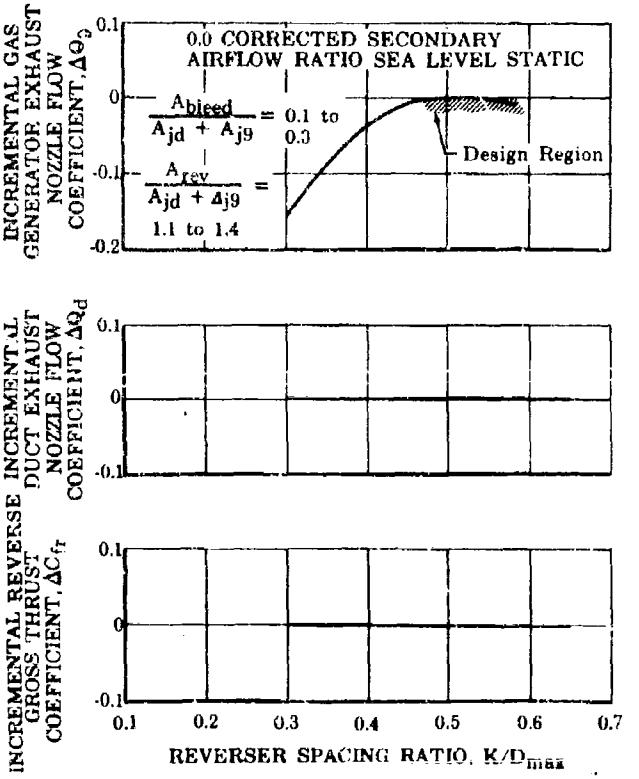

Figure 43. Variation in Exhaust System Reverse Performance With Reverser Spacing — FD 17122 AIIIE

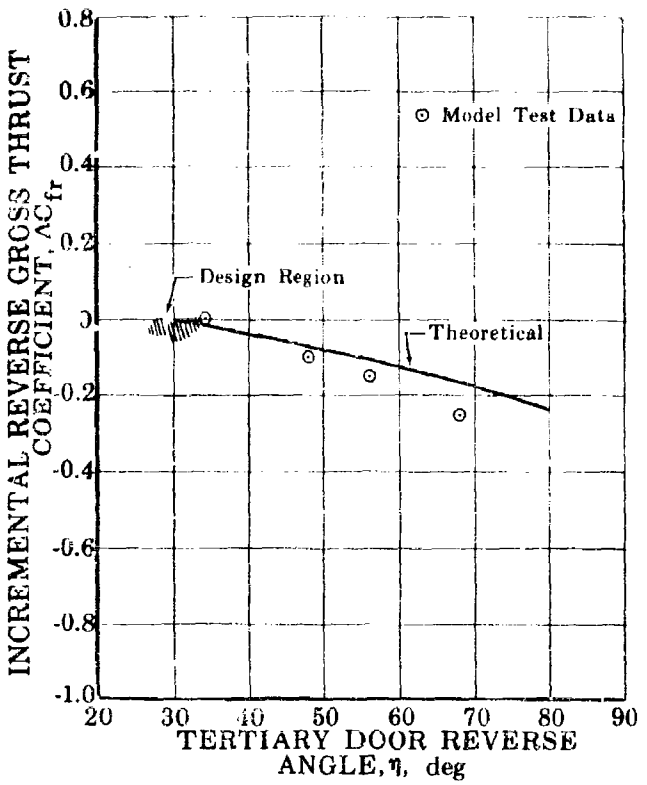

Figure 44. Variation of Reverse Performance With Tertiary Door Reverse Angle

FD 17123
AIIIE

The tertiary door reverse angle also affects the separation and attachment characteristics of the reverse gas flow. Flow studies conducted with scale model reversers in isolated flow fields indicate that the reverse gas flow will be separated from the nacelle at tertiary door reverse angles of approximately 20 degrees above forward flight speeds of approximately 75 knots. Tuft board pictures at 0, 75 and 150 knots forward velocity indicate the onset of separation at 75 knots as shown in figure 45. Separation characteristics for an actual installation may vary from the isolated case, and installed reverser tests will be conducted during Phase III.

Time to Achieve Maximum Reverse Thrust from Idle

The time required to achieve maximum engine reverse thrust from idle power is limited by the time required to accelerate the engine rotor to maximum rotor speed, which is approximately 6 seconds. The net engine thrust variation during this time period depends not only on the engine rotor speed but also on the angle of clamshell rotation. When the clamshell angle is small, engine thrust is positive or forward. When the clamshells approach the full closed position, engine thrust is negative or reverse. Complete rotation of the clamshells takes approximately one second and provides a smooth and continuous variation of engine thrust. A more detailed discussion of reversal times is given in the Design Report.

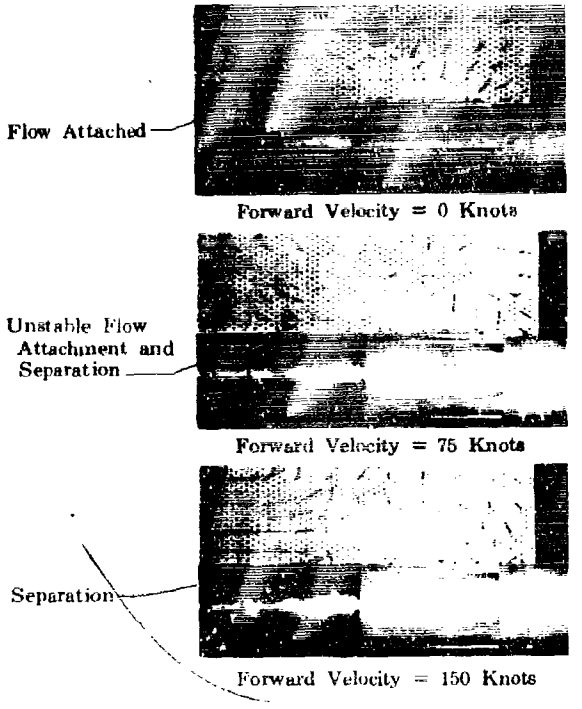

Figure 45. Reverse Flow Field Investigation
20° Reverse Door Angle

FD 17740
AIIIE

f. Installation Effects

The selection of the exhaust nozzle configuration for the JTF17 engine was based upon trade-off studies involving three different nozzle configurations. Although not the only criterion, the sensitivity of the nozzle to installation effects was an overriding factor in the evaluation of candidate nozzles. Such trade-off studies rely heavily on experience of service aircraft for evaluation criteria, and the initial evaluation was made utilizing the excellent service experience of the blow-in-door ejector in the YF12 aircraft. When data became available from the less favorable F-111 installation, these trade-off studies were repeated to assure data from the less favorable installation received proper consideration.

Three configurations, the plug nozzle, the long variable flap nozzle and the blow-in-door ejector were included in the study. Detail results of these studies can be made available upon request; however, in summary the plug nozzle was rated very low because of its relatively high sensitivity to performance loss from flow field variations. The blow-in-door ejector and long variable flap nozzle were rated about equal for performance loss due to installation effects during the initial evaluation and again during the reevaluation. The final choice of the blow-in-door ejector was then made on the basis of its overall performance, better sealing, less complexity and weight, and better noise attenuation characteristics. Like the long variable flap nozzle, the blow-in-door nozzle can suffer from installation effects due to variations of the aircraft local flow field. Proper design

of the nozzle and installation can minimize these losses. Model tests, summarized in figure 46, have shown that tertiary door open nozzle performance is dependent upon providing the required quantity of tertiary flow regardless of the amount of door blockage. Performance is directly related to tertiary flow quantity as indicated in figure 46 and adverse local flow fields can be compensated for by increasing tertiary door area. An exhaust system placed relative to the aircraft such that it operates in a uniform flow field with minimum deviation from free stream conditions will exhibit little or no installation effect. Both airframe manufacturers are aware of this, and have provided wing-mounted installations that should produce minimum deviations of the nozzle local flow fields from free stream conditions.

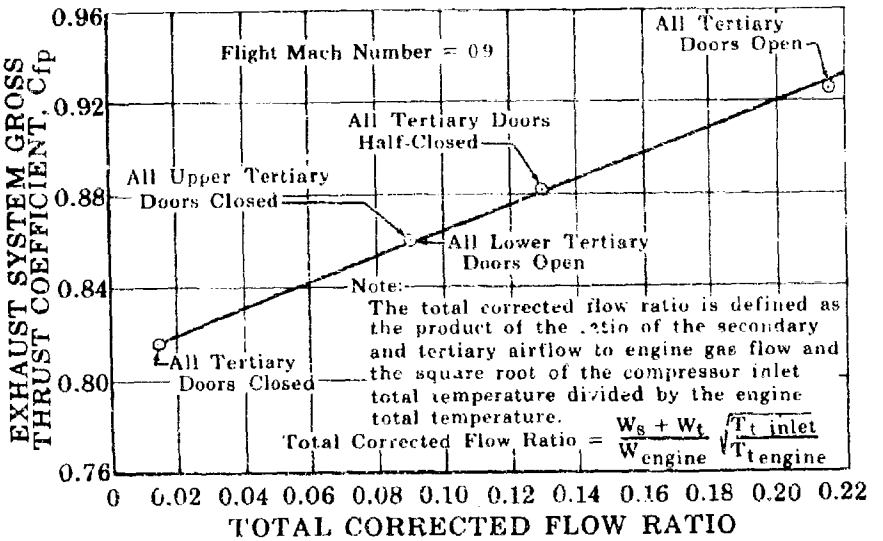

Figure 46. Variation of Exhaust System Performance With Total Corrected Flow Ratio — FD 17124 AIIIE

The JTF17 exhaust system is being designed to compensate for variations in local flow conditions when they occur, thereby minimizing installation effects. The local flow field approaching the exhaust nozzle may vary from isolated test conditions due to the effect of the wing and adjacent bodies, overboard bleed flows upstream of the nozzle, and differences in model and full-scale boundary layers. The difference between free stream Mach number and the local Mach number around the nozzle can affect nozzle performance by changing the tertiary air inlet conditions and the external pressure drags. High local Mach numbers, and consequently low local static pressure fields, may also cause the pressure-actuated tertiary doors to close prematurely and thereby produce overexpansion losses in the nozzle. The local pressure field can also affect the position of the trailing edge flaps, which can produce overexpansion losses in the nozzle if the flaps float to a larger exit area. A variation of boundary layer height between the installed and isolated test conditions will also affect the tertiary flow and internal performance. The isolated transonic wind tunnel investigations of the JTF17 exhaust system are conducted in a free stream flow field with 4-inch diameter models. The models are mounted on a shaft approximately 7 feet long that protrudes from a streamlined strut located just ahead of

the test section. Calculations indicate that the relative boundary layer heights between the isolated scale model tests and the actual aircraft (approximately 11 inches full-scale) are similar. In the absence of large quantities of overboard bleed and large variations in boundary layers, installation effects are primarily a function of the local Mach numbers produced by the aircraft. Experience has shown that differences in nozzle performance occur in the transonic flight region where the tertiary doors are open and the trailing edge flaps are closed. At cruise Mach numbers, nozzle performance is not affected by the aircraft flow field.

(1) Previous Experience

Installation effects have been thoroughly investigated in the Pratt & Whitney Aircraft J58 engine installation in the YF12 aircraft. Wing-nacelle model test programs and full-scale flight investigations have been conducted in conjunction with the airframe manufacturer. Results of these programs show that installation effects are predictable and that the exhaust system can be designed to minimize these effects. The magnitude of these effects can be obtained from figure 13 where small performance decrements, due to the installation effects, are evident in the transonic flight range.

J58 experience has shown that an approximation of installation effects for a wing-mounted nacelle can be made by testing isolated scale models at the local Mach number of the aircraft flow field. For example, a simulation of the conditions at a flight Mach number of 1.05 could be made by testing at approximately Mach 1.2. This type of test would simulate both the lower pressure air entering the tertiary doors as well as the increment in boattail pressure drag caused by the aircraft flow field. This test would not, however, show the effect of low pressures caused by the boattail on aircraft surfaces. A similar investigation has been carried out for the JTF17 exhaust system installation in the Lockheed aircraft, as discussed in the next paragraph.

(2) Prediction of JTF17 Exhaust System Installation Effects

Chordwise static pressure distributions have been measured for the inboard and outboard nacelles on the Lockheed wing. Average local Mach numbers in the vicinity of the tertiary doors have been calculated from these data and a comparison is shown in the following table:

Freestream Mach Number	0.9	1.3
Average Local Mach Number	0.92	1.31

Isolated models have been tested over a range of Mach numbers for transonic acceleration and subsonic cruise engine operating conditions. Figures 47 and 48 indicate the estimated performance increments as a function of local Mach numbers for the JTF17 nozzle during subsonic cruise and transonic acceleration, respectively. No appreciable installation effect is estimated from either figure with the maximum ΔC_{fpinst} of 0.004 occurring during subsonic cruise operation. During operation at acceleration conditions, exhaust system throat areas and pressure ratios are larger than for subsonic part power, and installation effects will be less than at part power conditions.

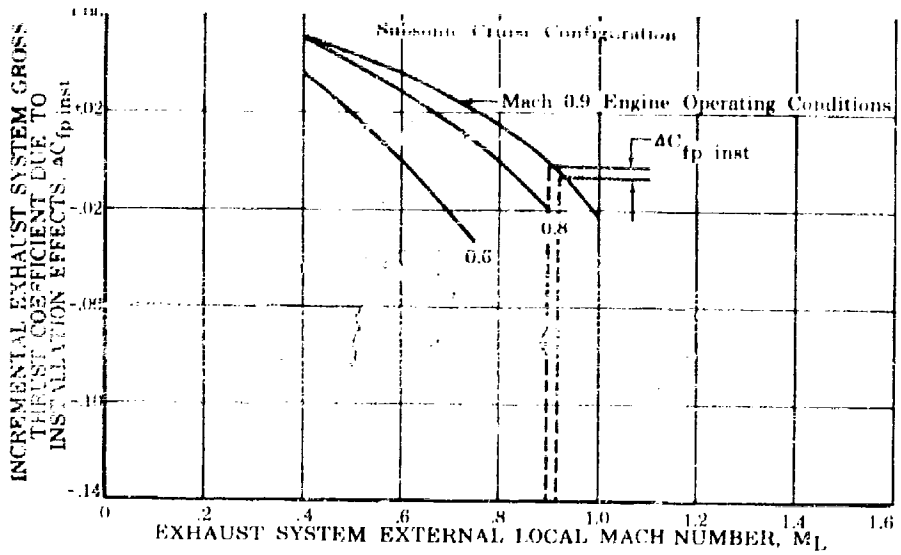

Figure 47. Estimated JTF17 Exhaust System Installation Effects - Lockheed Installation

FD 17125
AIIIE

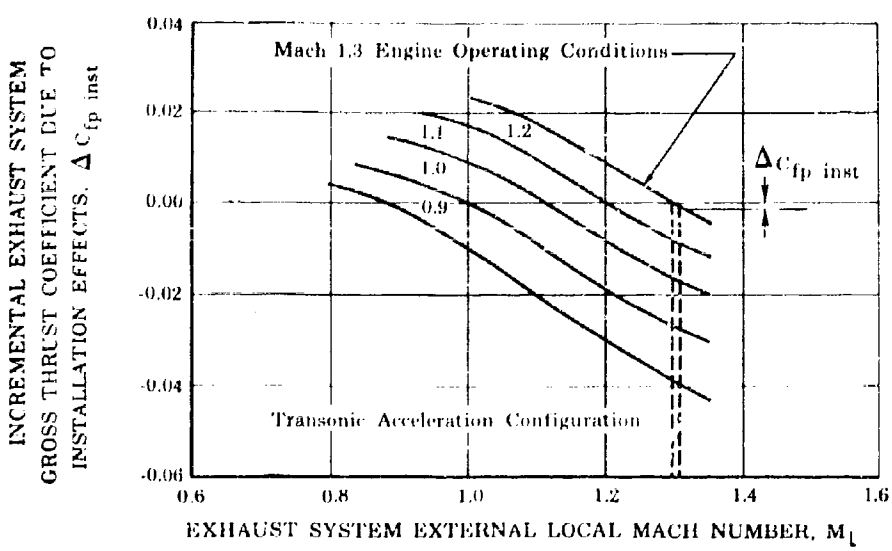

Figure 48. Estimated JTF17 Exhaust System Installation Effects - Lockheed Installation

FD 17126
AIIIE

(3) JTF17 Installation Tests

During Phase II-C the first of a series of tests with a JTF17 exhaust system wind tunnel model representing the Lockheed installation were conducted in the United Aircraft Research Laboratories main wind tunnel to investigate installation effects on exhaust nozzle performance. The complete test series, to be continued into Phase III, will investigate the effects of angle of attack, exhaust system trailing edge flap variation eleven deflection angle, and exhaust system axial location. The initial tests established the effects of the Lockheed installation on the performance of the JTF17 exhaust system during subsonic part power operation and investigated the wing and exhaust system local flow field pressure and Mach number distributions.

The 1/20th-scale installation model consists of a metric flowing nacelle with the JTF17 exhaust system and a nonmetric half wing of cropped-delta plan form with an open channel dummy nacelle as shown in figure 49. The metric flowing nacelle consists of a 4-inch outside diameter shaft that extends 7 feet downstream of the trailing edge of a streamlined fairing. The upstream end of the shaft is attached to a three-flow force balance and the exhaust system is attached to the downstream end.

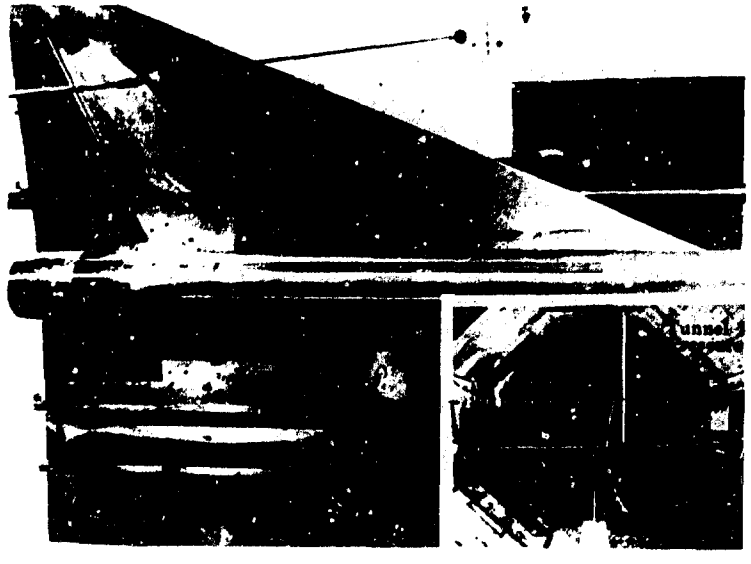

Figure 49. Exhaust System Installation Model - Tests - Lockheed Configuration FD 16905 AIIIE

The nonmetric half wing consists of a cropped-delta plan form with a modified double wedge section and a 10 degree tip droop. A half wing model is representative of the installation and should establish preliminary effects since a splitter plate at the wing root divides the flow field and the flowing nacelle is located four nacelle diameters away from the centerline. P&WA recognizes that a half installation model may not completely duplicate the aircraft flow field and full model tests will be conducted in cooperation with the airframe manufacturer during Phase III. An open channel dummy nacelle simulates the inboard propulsion package. Replaceable

flaps are available to simulate various trim positions but were not tested during this initial test program. The flowing nacelle shaft was set at a negative incidence of 2 degrees relative to the wing chord and the tests were conducted at angles of attack of 2 degrees and 5 degrees. The wing was mounted on edge in the test section on the wing root plate and two support struts.

The test instrumentation consisted of the following:

1. A three-flow balance to record exhaust system gross thrust coefficients.

2. Three static pressure pipes running the length of the tunnel test section and located three feet from the upper wing surface, three feet from the lower wing surface, and 3 inches off the wing tip.

3. Tunnel wall static pressure plates mounted on the upper wing surface side of the tunnel and on the lower wing surface side of the tunnel.

4. A tunnel spanning static and total pressure "T" rake. Readings from this rake were taken just upstream of the plane of the ejector tertiary doors.

5. The lower surface of the wing was instrumented with 35 static pressure taps and the upper surface with 18 taps.

6. The exhaust nozzle had four static taps circumferentially spaced just ahead of the tertiary doors.

7. Two one-inch high boundary layer pressure rakes were mounted on the nacelle just ahead of the tertiary doors above and below the wing.

Preliminary results of these tests are shown in figure 50. The isolated and installed performance should be compared only at Mach 0.9 since the data were accumulated over a range of Mach numbers at a gas generator pressure ratio corresponding to Mach 0.9 operation. The installed model meets the subsonic cruise performance goal as shown in figure 50 with a 1/2% performance decrement due to the installation. Note that this represents only the effect of the installation on the exhaust system and does not include the effect of the nozzle on the aircraft. Angle of attack has little effect on the installed performance. The excellent agreement between the theoretical and test results indicates that installation effects for the JTF17 exhaust system are predictable and that the nozzle design can be modified when necessary to minimize these effects.

The initial test program was limited to subsonic flight Mach numbers because of wind tunnel limitations. Wind tunnel flow field investigations conducted with both Boeing and Lockheed wings (no exhaust nozzles) indicated that satisfactory flow fields could be established for subsonic Mach numbers only. However, a wind tunnel modification incorporating a perforated wall test section to permit transonic Mach number testing is planned. This facility should be available for use early in Phase III.

No exhaust system flow field information has been obtained from the Boeing Company at this writing. A similar investigation will be conducted for the Boeing installation when this information becomes available.

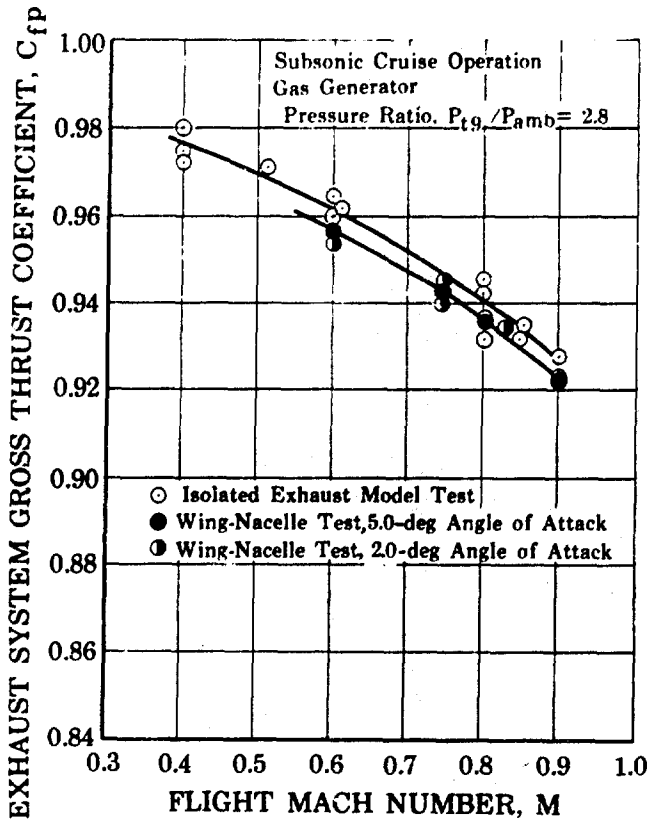

Figure 50. JTF17 Exhaust System Wing, Nacelle Test - Lockheed Installation

FD 17127
AIIIE

g. Hot Flow Effects

Performance predictions for full-scale exhaust systems are normally determined by cold-flow, small-scale,model tests. The effect of a hot flow on exhaust system thrust coefficient and secondary pressure and flow characteristics has been the subject of much speculation. Full-scale test data indicate that errors in predicting exhaust system secondary pressure requirements from cold flow model tests can occur unless heat transfer to the secondary stream is accounted for. However, no errors in nozzle thrust coefficient are apparent from the full-scale tests. A literature and information search conducted in cooperation with an airframe manufacturer revealed similar findings by two NASA Reports (references 3 and 4). However, the magnitude of the effects or a method for correcting the cold flow data was not suggested.

In the absence of any usable test data an investigation was initiated to establish a theoretical method for correcting the cold flow data, and a hot flow model test program was planned to verify the theory.

The following discussion outlines the theory and gives a procedure that can be used to correct for hot flow effects. A brief description of the test program and its results is also included.

(1) Theory

The theory developed here applies to a typical exhaust system and refers to parameters subscripted by "p" or primary and "s" or secondary. In these instances, the discussion is based on a single mainstream-type exhaust such as one for a turbojet engine, and the following special nomenclature will be used:

A = Area
G = Gravitational Constant
k = Specific Heat Ratio
M = Mach number
P = Pressure
R = Gas Constant
T = Temperature
V = Velocity
W = Flow Rate
ρ = Density

and the subscripts are:

* = Designates choked flow
s = Secondary stream
p = Primary stream
t = Total

Secondary flows and pressures are normally determined as a function of primary pressure ratio, as shown in figure 51. Model tests are conducted using cold (approximately 70°F) air for both the secondary and primary flows. As shown in this figure, P_{ts}/P_{tp} becomes constant above a certain primary-to-ambient pressure ratio, for a given W_{sc}. This corresponds to the pressure ratio at which the secondary flow chokes due to the formation of an aerodynamic throat. The relationship between secondary pressure and secondary flow can be written as:

$$\frac{W_s}{W_p} = \frac{\rho_s A_s V_s}{\rho_p A_p V_p} = \frac{\frac{P_s}{R_s T_s} A_s M_s \sqrt{k_s G R_s T_s}}{\frac{P_p}{R_p T_p} A_p M_p \sqrt{k_p G R_p T_p}} \qquad (1)$$

Introducing total temperatures and total pressures,

$$\frac{W_s}{W_p} = \frac{\frac{P_{ts}\left[1 + \frac{k_s - 1}{2} M_s^2\right]^{\frac{k_s}{1 - k_s}}}{R_s T_{ts}} \left[1 + \frac{k_s - 1}{2} M_s^2\right] A_s M_s \sqrt{k_s G R_s} \sqrt{\frac{T_{ts}}{\left[1 + \frac{k_s - 1}{2} M_s^2\right]}}}{\frac{P_{tp}\left[1 + \frac{k_p - 1}{2} M_p^2\right]^{\frac{k_p}{1 - k_p}}}{R_p T_{tp}} \left[1 + \frac{k_p - 1}{2} M_p^2\right] A_p M_p \sqrt{k_p G R_p} \sqrt{\frac{T_{tp}}{\left[1 + \frac{k_p - 1}{2} M_p^2\right]}}} \qquad (2)$$

In the small scale cold flow tests

$$k_s = k_p$$

$$R_s = R_p$$

$$T_{ts} = T_{tp} ,$$

which reduces equation (2) to:

$$\frac{W_s}{W_p} = \frac{P_{ts}}{P_{tp}} \frac{A_s}{A_p} \left[\frac{\text{function } (M_s)}{\text{function } (M_p)} \right] \tag{3}$$

When both the secondary and primary streams are choked,

$$\frac{W_s}{W_p} = \frac{P_{ts}}{P_{tp}} \frac{A_s^*}{A_p^*} \tag{4}$$

Therefore, for a given nozzle geometry, i.e., A_s^* and A_p^*, a unique relation between W_s/W_p and P_{ts}/P_{tp} exists, as shown in figure 51, because both streams are choked on the flat portion of the curve.

In the actual flight condition,

$$k_s \neq k_p$$

$$T_{ts} \neq T_{tp}$$

and equation (2) for choked primary and secondary streams becomes

$$\frac{W_s}{W_p} = \frac{P_{ts} \sqrt{T_{tp}}\, A_s^* \left[1 + \frac{k_s - 1}{2} \right]^{\frac{k_s}{1 - k_s}} \left[1 + \frac{k_s - 1}{2} \right]^{\frac{1}{2}} \left[k_s \right]^{\frac{1}{2}}}{P_{tp} \sqrt{T_{ts}}\, A_p^* \left[1 + \frac{k_p - 1}{2} \right]^{\frac{kp}{1 - kp}} \left[1 + \frac{k_p - 1}{2} \right]^{\frac{1}{2}} \left[k_p \right]^{\frac{1}{2}}} \tag{5}$$

This may be written as:

$$\frac{W_s}{W_p} \sqrt{\frac{T_{ts}}{T_{tp}}} = \frac{P_{ts}}{P_{tp}} \frac{A_s^*}{A_p^*} \frac{\text{function } (K_s)}{\text{function } (K_p)} \tag{6}$$

which is denoted as W_{sc} (corrected secondary airflow ratio).

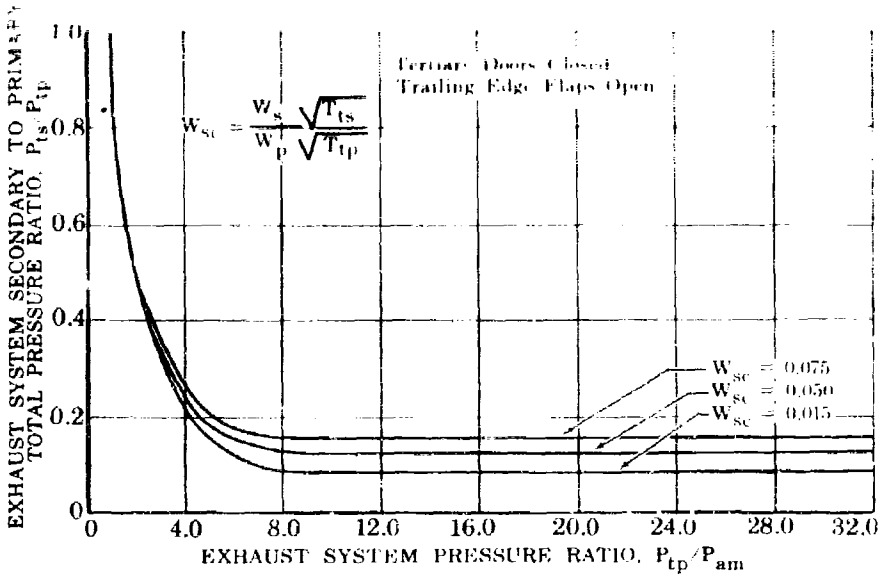

Figure 51. Typical Exhaust System Secondary Pressure Variation

FD 17128
AIIIE

From equation (6) it can be seen that for a given corrected secondary flow ratio, nozzle geometry, and specific heat ratio for both sonic streams, there is a unique value of P_{ts}/P_{tp}.

This discussion indicates that tests of a cold model that is geometrically similar to the full-scale nozzle, when corrected for hot flow specific heat ratios, can be used to predict the full-scale secondary flow relations.

Figure 52 presents a comparison of the secondary stream total pressures measured during actual exhaust system flight tests, ratioed to the secondary pressures predicted from cold flow model tests. A correction for the differences in specific heat ratio between the hot and cold tests has been made to the cold flow data using the one-dimensional calculation program previously discussed. The magnitude of this correction is small as shown in figure 53. However, figure 52 indicates that a higher secondary pressure is required to force a given flow under hot primary conditions than under cold conditions.

In both the scale model tests and the actual flight tests, the secondary total temperature is defined as the secondary stream total temperature at the entrance to the exhaust nozzle. Equation (5) indicates that the secondary stream parameters should be denoted where the secondary stream chokes. Static pressure tap data and method-of-characteristic calculations show that the secondary stream chokes slightly downstream of the ejector minimum shroud point. Temperature measurements taken from nozzle wall thermocouples in flight show that minimum shroud wall temperatures are higher than the secondary total temperature at the nozzle entrance. This indicates that the secondary total temperature at the secondary choke point (T_{ts}*) is considerably greater than that used in the definition of the corrected flow. Heat transfer and mixing effects between the primary stream and the secondary stream has become an important consideration in determining secondary pressure and flow characteristics.

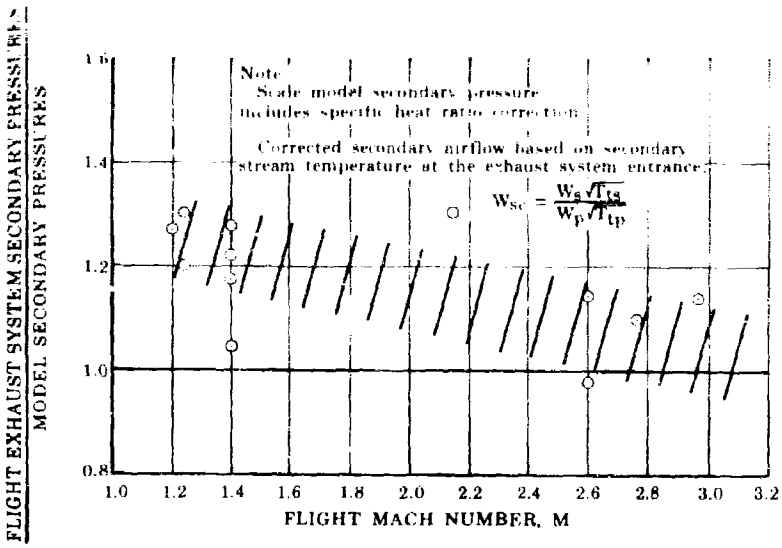

Figure 52. Comparison of Flight Exhaust System and Model Secondary Pressures

FD 17130
AIIIE

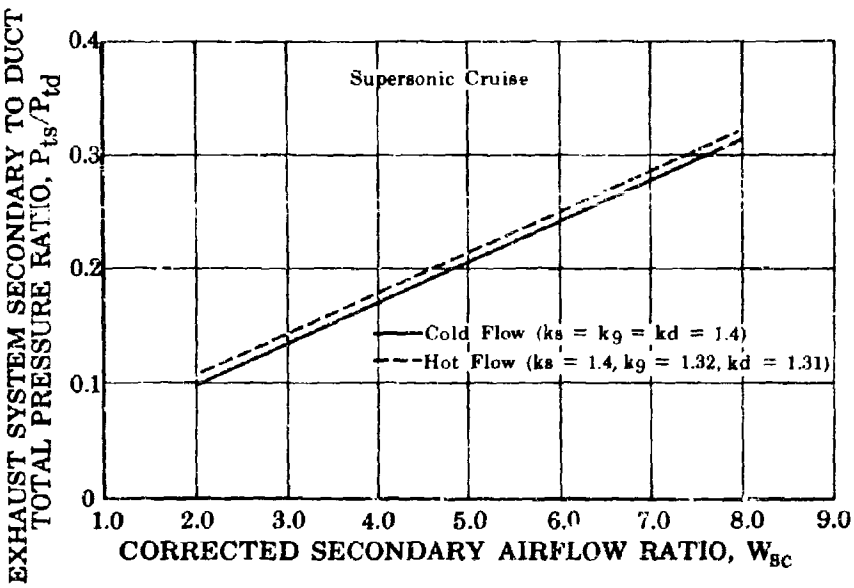

Figure 53. Effect of Specific Heat Ratio on Secondary Pressure

FD 17129
AIIIE

(2) Hot Flow Test Program

An experimental test program was conducted to obtain secondary pressure and flow characteristics, and nozzle wall temperatures and pressures for a scale model exhaust system. Existing Pratt & Whitney Aircraft FRDC test stand facilities, including a slave engine for air supply, furnished the necessary flexibility to conduct the tests over a range of flows, temperatures, and pressures. Primary and secondary stream pressures were controlled by a series of valves. Primary stream temperatures were varied with an air preheater mounted upstream of the test rig. Hot secondary flow was supplied by the slave engine. Cold secondary temperatures were obtained by passing the secondary air through a water-cooled heat exchanger. For intermediate temperatures, the hot and cold streams were mixed.

All data were read and recorded manually. Normal pressure and temperature measurement methods were employed. The primary flow was measured with an ASME venturi with a 4.600-inch throat diameter and the secondary flow was measured with a 2.209-inch diameter ASME orifice.

The test models consisted of two exhaust system configurations, one scaled for transonic flight operation and the other for cruise flight operation. The program consisted of a series of test runs with a minimum of four (4) corrected secondary weight flow ratios tested for each flight configuration. Primary stream temperature and pressure were held constant for each test.

Results of the tests support the theory presented previously. Figure 54 shows the increase in secondary pressure requirements as the primary-to-secondary stream temperature ratio is increased. The test facility was not capable of obtaining the high primary-to-secondary temperature ratios possible with the actual flight exhaust system. However, over the temperature range tested, the hot model data agree with the flight data.

The hot model tests allow the determination of the correct secondary temperature (T_{ts}*) to be used in the calculation of the corrected secondary airflow ratio, W_{sc}. The nozzle wall temperature in the region of the secondary choke point can be used to approximate T_{ts}*. Replacing T_{ts} with T_{ts}* in the definition of W_{sc}, figure 52 can be converted to figure 55 and corrects the cold model data to agree with the flight pressures.

No variation in exhaust system thrust coefficient due to hot flow effects was evident from the tests. Consequently no corrections to the exhaust system gross thrust coefficient need be applied to cold flow model data.

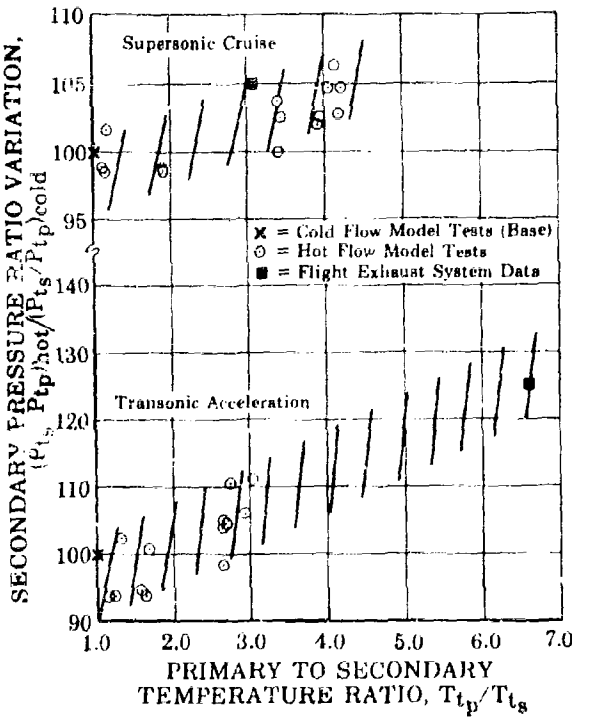

Figure 54. Variation of Secondary Pressure With Primary Temperature

FD 17664
AIIIE

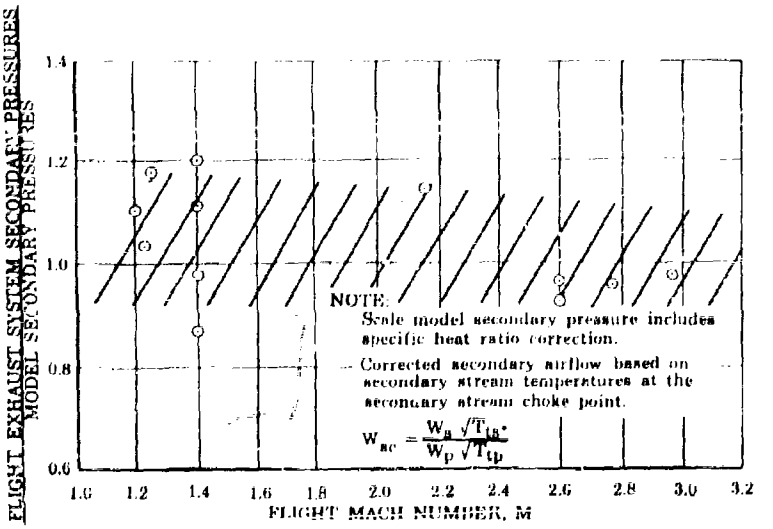

Figure 55. Comparison of Flight Exhaust System and Model Secondary Pressure

FD 17131
AIIIE

h. Trailing Edge Flap Stability

Any variable flap convergent-divergent exhaust nozzle can experience flow instability when operating at off-design conditions. Flap instability problems have been encountered on both the long variable flap nozzle and the blow-in-door exhaust system.

Flow, and consequently mechanical system instability can occur for several basically different reasons. One familiar stability problem, first encountered during early flights of the B-58 and reported in Reference 2, is the unstable flow separation phenomena in overexpanded convergent-divergent nozzles with no stabilizing or cushioning air to force flow separation. The stabilizing airflow ensures a stable normal-shock-location in the diverging portion of the nozzle. This phenomenon occurs at the low nozzle pressure ratios associated with subsonic engine operation when the main flow stream is overexpanded. This type of instability is not experienced in an exhaust system where large quantities of tertiary air are introduced and variable trailing edge flaps are provided to reduce the nozzle area ratio.

A second type of stability problem common to exhaust nozzles with variable geometry operating at off-design conditions is low-area-ratio instability. A variable converging-diverging nozzle may, during off-design operation, have an inner contour as shown in figure 56. During operation at nozzle pressure ratios where a normal shock stands at or near the maximum area, an unstable flow condition can result. Slight fluctuations in the nozzle pressure ratio can cause the shock to move to a new position along the nozzle or out of the nozzle completely, causing sudden changes in loading on the trailing edge flaps. Schlieren photographs of this phenomena taken with an exhaust nozzle model having transparent walls are shown in figure 57. The indicator dial shows the nozzle supply gage pressure in psi. Note the large movement in the normal shock position from inside the nozzle on the trailing edge flaps to slightly downstream of the exit plane with only a slight change in nozzle supply pressure. The rapid shock movements cause rapid fluctuations in the flap pressure loading and consequently flap movement. This interaction between the trailing edge flaps and the shock can cause the trailing edge flaps to become unstable and "flutter".

Experience with the F-111 aircraft indicates that a nozzle designed such that the shock system is not located on the trailing edge flaps will eliminate the flutter problem. Mechanical damping schemes have also been successfully applied as in the case of the YF12 aircraft. Both methods are being investigated for use with the JTF17 nozzle. Schlieren photographs of the JTF17 exhaust system, shown in figure 58, taken during Mach 0.9 cruise exhaust system tests, indicate that the shock system is located downstream of the trailing edge flaps and should not cause a stability problem. In addition, several mechanical damping designs are being investigated for backup.

In the final analysis, actual hardware tests at the engine operating conditions are required to resolve the possibility of trailing edge flap instability. These tests will be conducted during Phase III.

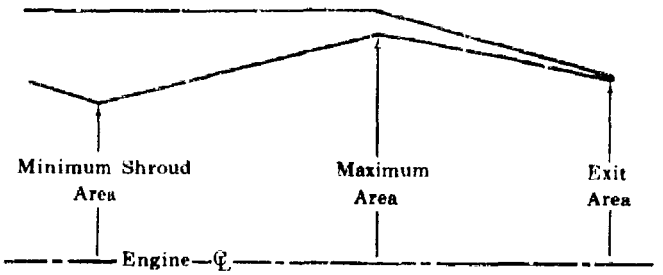

Figure 56. Typical Ejector Nozzle Contour Off - Design Operation

FD 17132
AIIIE

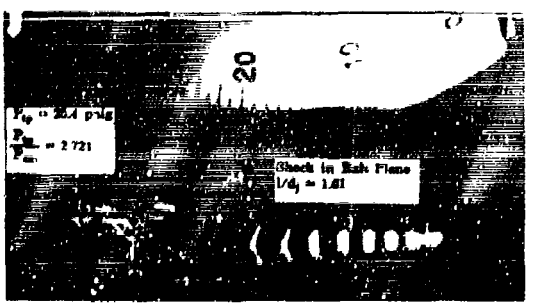

Figure 57. Shock System Behavior in a Typical Exhaust System

FD 17511

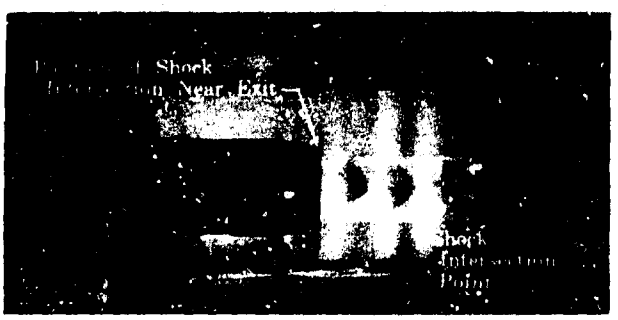

Figure 58. JTF17 Exhaust System - Tertiary Doors Open at Subsonic Cruise

FD 16917
AIIIE

i. Advanced Design Concepts

A continuing effort is being made to improve the performance and mechanical design of the exhaust system for the supersonic transport. A split flow nozzle, shown in figure 59, designed to utilize high secondary pressures was investigated during Phase II-C. This nozzle has shown excellent cruise performance potential. The maximum cruise performance levels obtained with this configuration are given in figure 60 and indicate a 0.3% increase in nozzle thrust coefficient over performance levels obtained with nozzles capable of using only low secondary pressure levels. The split nozzle design has proved capable of utilizing a secondary-to-duct pressure ratio, P_{ts}/P_{td}, of at least 0.4 compared with 0.15 to 0.20 in most other coannular models tested to date. A performance increase of approximately 0.5% may ultimately be possible by the use of even higher secondary pressures, and by proper contouring of the nozzle walls. The shorter lengths possible with this nozzle may provide overall weight reductions. The investigation of this nozzle concept will continue in order to establish its full performance potential and to study the mechanical problems associated with off-design and reverse operation.

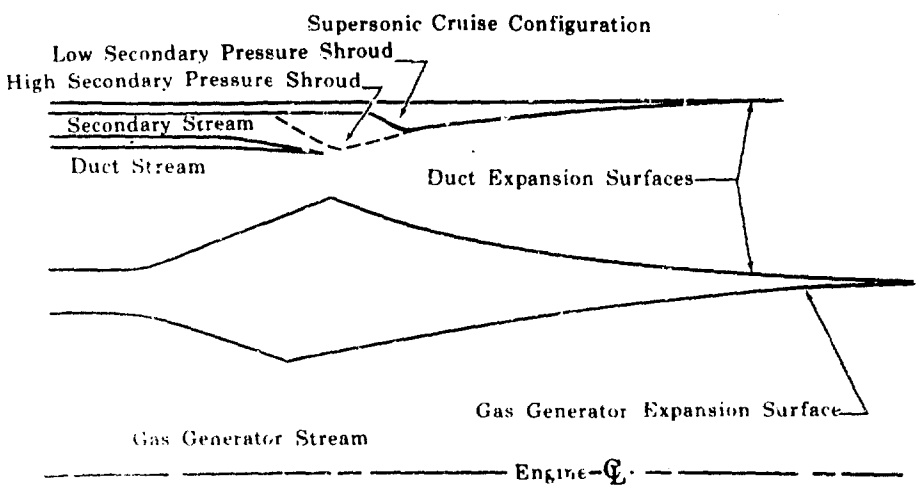

Figure 59. Split Flow Nozzle

FD 17133
AIIIE

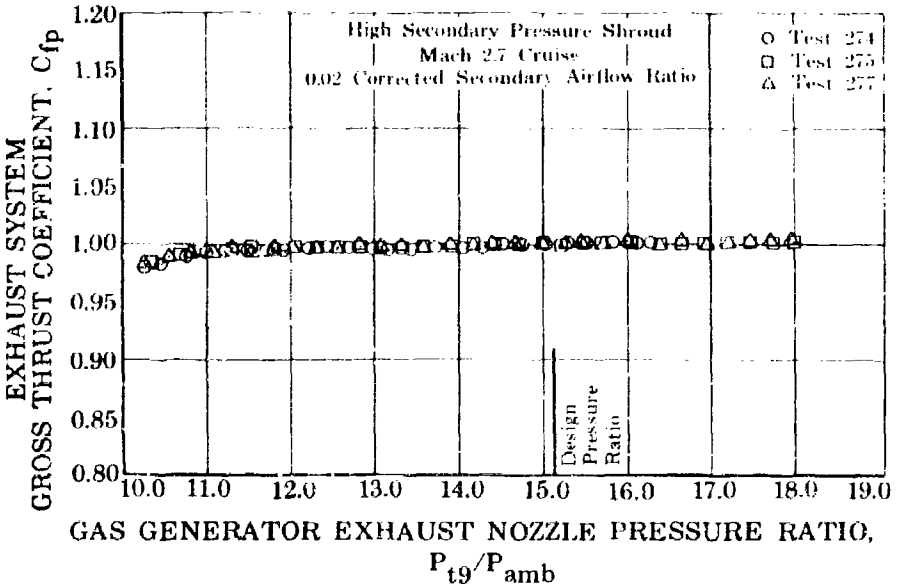

Figure 60. Split Flow Nozzle Performance

FD 17076
AIIIE

5. References

1. Volume E-XI, "Exhaust System for the Commercial Supersonic Transport," Phase II Proposal, Pratt & Whitney Aircraft.

2. AIAA Preprint 64-247, "Aerodynamic Stability Considerations of High-Pressure Ratio, Variable-Geometry Jet Nozzles," by J. S. Alford and R. P. Taylor.

3. NACA RM E9E16, "Effect of Temperature on Performance of Several Ejector Configurations," by H. D. Wilsted, S. C. Huddleston, and C. W. Ellis (1949).

4. NACA RM E51J04, "Full-Scale Investigation of Cooling Shield and Ejector Nozzle for a Turbojet Engine Afterburner Installation," by L. E. Wallner and E. T. Jansen (1951).

SECTION IV
WEIGHT

A. INTRODUCTION

Engine weight is the common denominator for all performance objectives. The relative merit of design concepts and of specific design features must, therefore, be measured against this exacting criterion. The direct effect of engine weight on overall system performance includes magnification by aircraft structural considerations relative to engine mounting. Each pound of added engine weight (per engine) would result in approximately 20 pounds of added gross takeoff weight (per aircraft) to maintain constant payload. At constant gross weight, engine weight and payload are traded pound for pound. Section I of this report provides a discussion of the interaction of weight, thrust and TSFC as they relate to the significant mission characteristics such as range and payload. It is in this context, along with consideration of cost, maintainability and reliability, that weight influences design decisions on the JTF17 program.

The measured weight of the initial demonstrator engine has provided a base for projection of production engine weight. Although heavier due primarily to test considerations and manufacturing time concessions such as material substitutions and unfinished machining, all features pertinent to performance have been included in the demonstrator engines. Precise design differences which derive the production engine weight are included in this report.

The following paragraphs describe the engine design in terms of a complete weight breakdown. Substantiation of the weight includes a comparison of production engine design to the actual weight of the initial test engine. Substantiation further relates to previous engine weight experience and to comparison of calculated and actual part weights.

Finally, production engine design features are discussed as they relate to weight considerations which were involved in the design decisions. A description of the weight control organization and procedures, along with a summary of specific Phase III tasks are shown in Volume IV, Report F, Section VII.

B. WEIGHT STATEMENT

1. Specification Weights

The JTF17 production engine specification weights, i.e., that total weight guaranteed in the Engine Model Specification, are tabulated below. Basic engine and special installation weights are quoted separately in order to accurately evaluate engine weight against engine function. Special installation items serve specific airframe requirements rather than basic engine objectives.

	Basic Engine Weight, lb	Special Installation Weight, lb	Total Weight, lb
Boeing	9910	730	10,640
Lockheed	9860	387	10,247

Specification weight for the JTF17 prototype engine is 3% higher than the weights listed above.

2. Engine Weight Description

These basic engine weights are broken down by engine section in table 1. The sections are defined by the exploded engine cross section of figure 1. These weights correspond to the detailed production engine design description of Report B. The 50-lb basic engine weight difference between Boeing and Lockheed versions is due to operating envelope differences. Special installation features peculiar to the Boeing and Lockheed installations are listed in tables 2 and 3, respectively.

C. WEIGHT SUBSTANTIATION

Confidence that the above quoted weight breakdown accurately represents the detailed design description of Report B is based on the three basic factors: (1) test engine actual weight, (2) previous engine weight experience, and (3) actual vs calculated engine part weight comparison described below.

1. Initial JTF17 Test Engine Weight

The weight of the initial test engine was calculated at 10,615 lb prior to engine build (FX-161). The actual engine weight was 10,565 lb (table 4), or 50 lb from the calculated weight. Production engine specification weights of 9910 lb and 9860 lb, for Boeing and Lockheed respectively, are then derived from the 10,565 lb actual test engine weight by reference to calculated weight differences between test and production engine designs. Table 5 itemizes these changes in a section-by-section breakdown.

This measured weight of the initial demonstrator engine is approximately 2250 lb heavier than the production engine weight when corrected to the same configuration. Approximately 360 lb of this are due to test engine requirements such as variable 3rd and 7th stage compressor stators. Another 1425 lb is assignable to manufacturing shortcuts such as material substitutions and unfinished machining. The remaining 465 lb are derived from detail design refinements not included in the first engines.

Table 1. Weight Breakdown

	Weight, lb	
	TBC	LCC
Fan Rotor	500	500
Fan Stator and Front Mount	420	410
Intermediate Section including No. 1 and No. 2 Bearing Compartment	640	640
High Compressor Rotor	730	710
High Compressor Stator including Start Bleed System	235	230
Diffuser and Primary Combustor including No. 3 Bearing Compartment	825	825
High Turbine Rotor	255	255
Low Turbine Rotor and Fan Drive Shaft	580	580
High and Low Turbine Stator and Case	550	550
Turbine Exhaust Section including No. 4 Bearing Compartment and Gas Generator Exhaust Nozzle	440	440
Duct Heater Section including Duct Diffuser, Heater and Case	1510	1500
Variable Area Nozzle	425	420
Controls and Plumbing including All External Basic Engine Accessories	1250	1250
Reverser-Suppressor	1550	1550
Total Basic Engine	9910	9860

CONFIDENTIAL

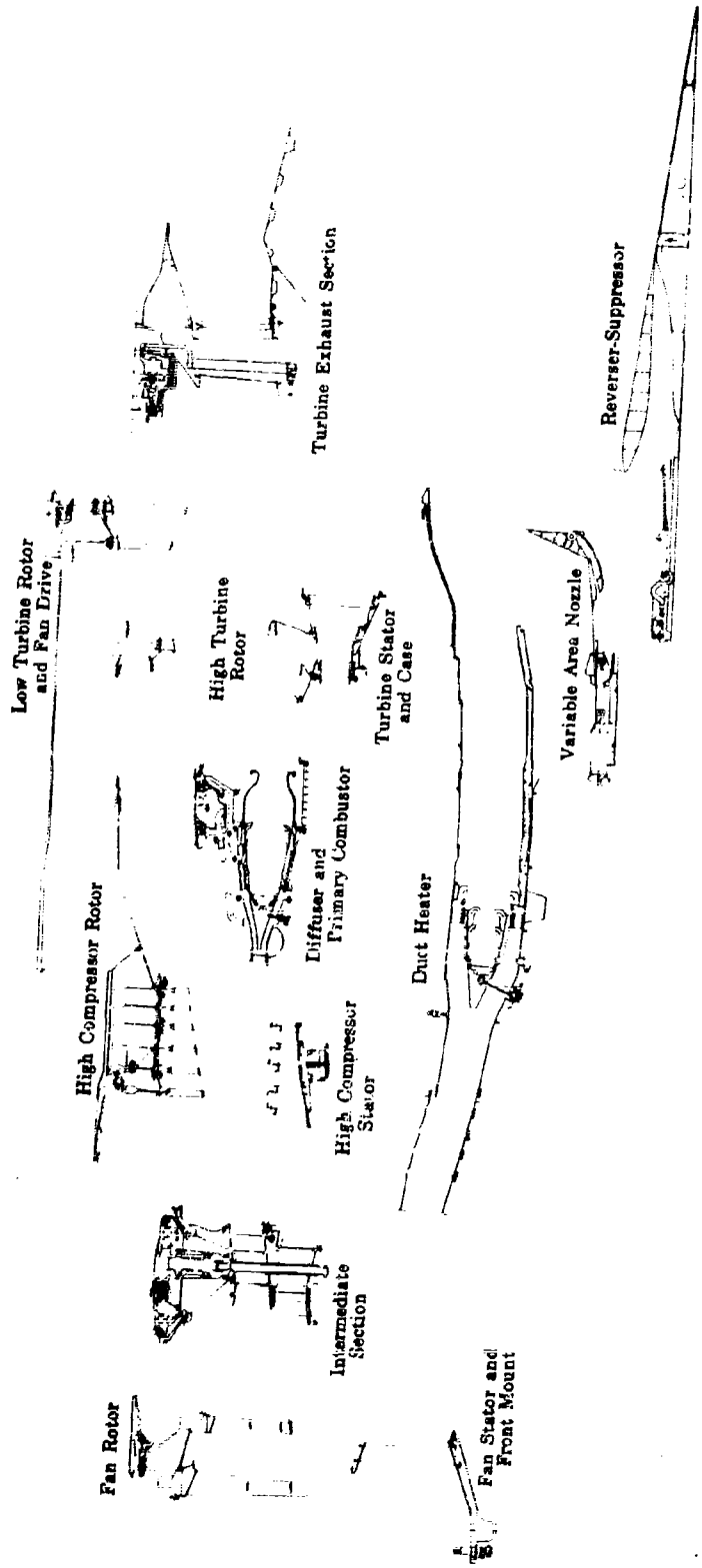

FD 16999

Figure 1. Engine Sectional Breakdown

CONFIDENTIAL

Table 2. TBC Special Installation Features

Common fuel inlet manifold

Ducts for secondary air, fire seal

Beef-up mount and cases for inlet

6-1/2-degree Canted Engine Exhaust

Added tower shaft

PTO gearbox

Anti-icing bleed port and line

Oil tank remote filler, oil level provisions, and oil filter pressure differential provisions

Duct heater fuel pump air discharge duct

Cabin bleed manifold

Conical suppressor-reverser

Power lever adaptation

Front hub spinner

Drain tank mounting and tubes

Special ground handling

Table 3. JTF17 LCC Special Installation Features

5-degree Cant Angle (Cent Bend)

Additional Towershaft

PTO Gearbox

PTO Gearbox Decoupler

Interchangeable Mounting Right or Left

Radially Loaded Rear Mount

Front Mounts Located 52-degree from Top Centerline

Outer Skin Forward of Suppressor-Reverser

Plumbing, Engine to Interface (Common)

Inlet Splitter Attachment

ECS Compressor Drive

Duct Heater Fuel Pump Air Discharge Duct

Table 4. Verification of Estimated Test Engine Weight

Initial Test Engine Weight	Weight, lb
Total scale reading of FX-161, Build 1	11,140
Deduct the following non-engine equipment:	
1. Lead weights to counteract moment due to left side components	-240
2. Rear mount links, swaybar, bolts and nuts	-50
3. Thrust mount plate and bolts	-151
4. Transport mount plate and bolts	-49
5. Instrumentation wires and fittings	-50
6. Non-parts-list brackets and hardware	-22
7. Nonchargeable PTO gearshaft parts	-13
Initial Test Engine Weight (no Suppressor-reverser)	10,565
Estimated Test Engine Weight with Adjustments for FX-161 Special Features	10,615
Actual Weight Below Estimated Weight	50

Table 5. JTF17 Production Engine Weight Based on Initial Test Engine Weight

Engine Section and Design Differences	Initial Test Engine Weight	Boeing Weight Change	Lockheed Weight Change	Boeing Weight	Lockheed Weight
FAN ROTOR	525			500	500
1. Design changes including increased inlet temperature		+25	+25		
2. Design revision of 1st- and 2nd-stage disks with integral titanium front hub replacing steel hub.		-55	-55		
3. Respace fan blading for reduced noise		+5	+5		
FAN STATOR AND FRONT MOUNT	935			420	410
1. Revised front mount ring and inlet case incorporating the following changes:					
a. Hollow front mount ring replaces solid unfinished ring on test engine		-385	-395		
b. Finish machining of inlet case and instrumentation bosses forward of mount ring		-75	-75		
2. Replace steel 1st-stage vanes with titanium vanes		-55	-55		

Table 5. JTF17 Production Engine Weight Based on Initial Test Engine Weight (Continued)

Engine Section and Design Differences	Initial Test Engine Weight	Boeing Weight Change	Lockheed Weight Change	Boeing Weight	Lockheed Weight
INTERMEDIATE CASE AND FRONT BEARING COMPARTMENT	1020			640	640
1. Fully machined titanium intermediate case replaces unfinished nickel alloy case		-270	-270		
2. Titanium fan exit guide vanes replace steel vanes on test engine		-58	-58		
3. Titanium aerodynamic brake replaces steel design in test engine		-20	-20		
4. Bearing compartment revised and hydrostatic seals replace test engine carbon seals		-20	-20		
5. Remove low spool tachometer drive and gears		-12	-12		
HIGH PRESSURE COMPRESSOR ROTOR	850			730	710
1. Titanium blades replace steel blades on stages 3 through 5		-24	-24		
2. Integral spacer arms on stages 3, 5, and 7 replace flanged spacers on test engine		-35	-35		
3. Eliminate extended necks on blade attachments		-30	-30		
4. Thinner disks due to lower temperatures with revised cooling scheme, improved material properties, and 3rd-5th stage titanium blades with lower pulls		-55	-75		

Table 5. JTF17 Production Engine Weight Based on Initial Test Engine Weight (Continued)

Engine Section and Design Differences	Initial Test Engine Weight	Boeing Weight Change	Lockheed Weight Change	Boeing Weight	Lockheed Weight
HIGH PRESSURE COMPRESSOR ROTOR (CONTINUED)					
5. Remove air seal forward of 3rd-stage disk		-14	-14		
6. Add removable knife-edge seals between stages		+15	+15		
7. Add bore tube and anti-vortex tubes		+35	+35		
8. Revised rear hub with seal change		-12	-12		
HIGH PRESSURE COMPRESSOR STATOR	400			235	230
1. Fixed stators replace variable geometry stators on stages 3 and 7 and redesign case		-165	-170		
2. Titanium vanes and cases replace steel on stages 3 and 4		-25	-25		
3. High compressor cases thinned due to lower stresses with supported gas generator		-25	-25		
4. Add manifolds for start bleed and seal pressurization air		+20	+20		
5. Transfer 8 start bleed valves from primary diffuser case to high compressor case		+30	+30		

Table 5. JTF17 Production Engine Weight Based on Initial Test Engine Weight (Continued)

Engine Section and Design Differences	Initial Test Engine Weight	Boeing Weight Change	Lockheed Weight Change	Boeing Weight	Lockheed Weight
PRIMARY COMBUSTOR AND NO. 3 BEARING COMPARTMENT	1075			825	825
1. Unfinished diffuser case on initial test engine replaced by fully machined case		-70	-70		
2. Add cabin air bleed tubes not on test engine		+12	+12		
3. Remove 12 start bleed valves from diffuser case		-55	-55		
4. Segmented burner with lightweight fuel nozzles		-82	-82		
5. Shortened, segmented transition duct		-35	-35		
6. Burner cases with axially-split outer case and diffuser-burner case interface moved forward		+40	+40		
7. Lightweight combustor inlet fairing		-40	-40		
8. No. 3 bearing compartment revised; hydrostatic seals replace carbon seals and scavenge pump removed from compartment		-20	-20		

Table 5. JTF17 Production Engine Weight Based on Initial Test Engine Weight (Continued)

Engine Section and Design Differences	Initial Test Engine Weight	Boeing Weight Change	Lockheed Weight Change	Boeing Weight	Lockheed Weight
TURBINE ROTORS AND SHAFTING	860			835*	835*
1. Multi-faired blades replace straight line faired test engine blades		-35	-35		
2. Integral hub on 1st-stage turbine disk		-15	-15		
3. Turbine disks with increased life and low cycle fatigue requirements		+25	+25		
*Now separated as high rotors, 255 lb, and low rotor, 580 lb					
TURBINE STATOR AND CASE	640			550	550
1. Single turbine case replaces front and rear cases on test engine		-30	-30		
2. Fabricated 1st-stage vane, paired vanes on lightweight platforms, reduced vane solidity, and simplified inner vane supports and seal diaphragms		-60	-60		

Table 5. JTF17 Production Engine Weight Based on Initial Test Engine Weight (Continued)

Engine Section and Design Differences	Initial Test Engine Weight	Boeing Weight Change	Lockheed Weight Change	Boeing Weight	Lockheed Weight
TURBINE EXHAUST AND NO. 4 BEARING COMPARTMENT	550			440	440
1. Remove workhorse turbine exhaust nozzle with provisions for changing throat contour and replace with increased diameter, high temperature nozzle		-90	-90		
2. Turbine exit guide vanes brazed to case replace bolted initial test engine design		-10	-10		
3. Revised No. 4 bearing compartment with hydrostatic seals replacing carbon seals		-10	-10		
DUCT BEARER	1995			1510	1500
1. Revised duct heater including aft scoop section removal		-90	-90		
2. Add gas generator supports		+50	+50		
3. Revised outer ducts and liners for balanced-flap nozzle system		-140	-140		
4. Add secondary air bulkhead		+35	+25		
5. Lightweight fuel nozzles		-75	-75		
6. Titanium duct diffuser replaces steel diffuser in test engine		-155	-155		

Table 5. JTF17 Production Engine Weight Based on Initial Test Engine Weight (Continued)

Engine Section and Design Differences	Initial Test Engine Weight	Boeing Weight Change	Lockheed Weight Change	Boeing Weight	Lockheed Weight
DUCT HEATER (CONTINUED)					
7. Thinned inner rear duct nozzle		-20	-20		
8. Burne. support struts made of titanium and beefed to support gas generator replace steel test engine design		-40	-40		
9. Revised inner liner with Z stiffeners replacing hat sections		-50	-50		
VARIABLE AREA NOZZLE	345			425	420
1. Balanced flap nozzle design replaces test engine pivoted flap design		+80	+75		
CONTROLS, PLUMBING AND HARDWARE	1370			1250	1250
1. Controls designed for prototype replace breadboard controls and plumbing on test engine. Includes addition of reverser interlock system and reverser actuator plumbing		-120	-120		
REVERSER-SUPPRESSOR	----			1550	1550
No reverser-suppressor on initial test engine					
TOTAL WEIGHT	10,565			9910	9860

2. Previous Engine Weight Experience

Previous experience on production status commercial engine weight has shown weight predictability within ± 10 lb or approximately ± 0.2% at the time of initial delivery engine build. This high degree of accuracy is accomplished by a system of incorporating actual part weights into calculated weight summations as they become available. The J58 project advanced this procedure by predicting engine weights several months into the future by scheduling engineering change weights. In the case of the active J58 development and weight reduction programs, this left large portions of the predicted weight unsubstantiated by actual part weights. The curve of figure 2, drawn from a J58 weight report indicates an accuracy of ± 18 lb or 0.3% for engine weights predicted 5 months in advance.

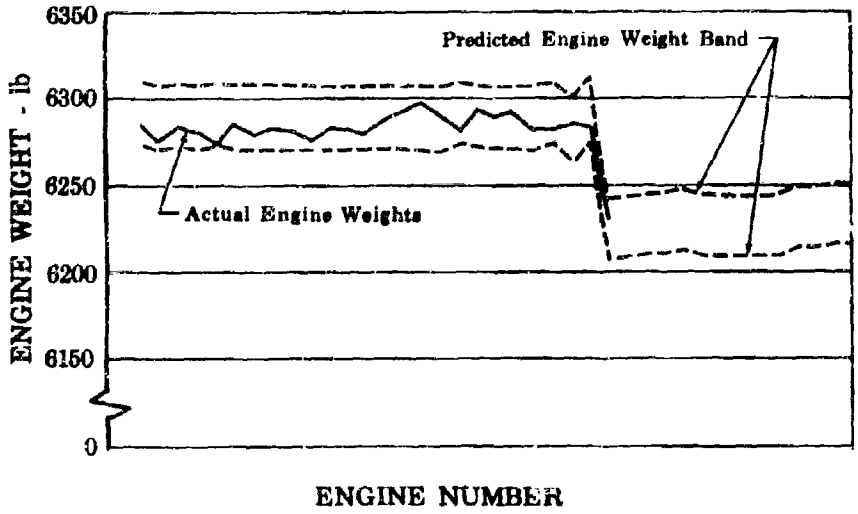

Figure 2. J58 Engine Weight FD 17046

3. Actual vs Calculated Part Weight Comparison

Further substantiation of JTF17 weight is obtained by weighing each part and component at the time it is received in "Finished Stores." This procedure applies to all parts, not just the first of each that becomes available. Each weight is then compared with its corresponding calculated weight and with previous actual weights to reveal, not only inaccuracies in calculations, but also manufacturing trends toward one end of the dimensional tolerance bands. Discrepancies are, of course, investigated and corrected. Experience has shown most calculated weight within the tolerance band.

D. WEIGHT-DESIGN JUSTIFICATION

Weight trades have been involved in JTF17 design since the choice of cycle. Trade studies have been continued as the production engine design has progressed. Examples of weight considerations involved in the current design are discussed below. References are made to the more detailed discussions of the appropriate design description section.

1. Fan Rotor

Maximum usage of the best available titanium is the key to minimum weight in the fan design. Material-weight trades were made in detail and considered the particular operating conditions of each part. For instance, AMS 4928 was chosen for the first-stage disk because of greater resistance to low cycle fatigue than PWA 1202 and a subsequent 3-pound weight advantage. The higher temperature second stage, with a less severe, LCF producing, thermal gradient is PWA 1202 because of a 20-pound weight advantage relative to AMS 4928. Weight was also the primary consideration in arriving at the structural configuration of the fan rotor. As described in Volume III, Report B, Section IIA, the current design includes a titanium 1st-stage disk, front hub combination with rim stiffness derived from the stage 1 to 2 rim spacer. This design replaces a "box" disk design with nickel alloy hub at a weight saving of 55 pounds. An earlier study had considered a non-box 1st-stage disk but with a nonintegral nickel alloy hub and no rim spacer. This design was eliminated by a 30-pound weight penalty.

2. Fan Stator and Front Mount

The key to minimum weight in this section is the optimum utilization of material for mount stiffness and blade containment. Mount loads are distributed back into the case by local shear sections which also help supply blade containment. By use of this technique the weight required for fan blade containment has been held to 50 pounds. The variable cross section mount ring design, locating stiffness where it is needed for local loads, was incorporated because of a 30-pound saving relative to an original uniform stiffness configuration.

3. Intermediate Section

A large percentage of the engine weight is concentrated in the intermediate case and No. 1 and No. 2 bearing compartments. Specific weight control recommendations related to relieving bending moment on the case by supporting the gas generator through the duct burner support struts have been incorporated into the design. This was accomplished, along with the change from nickel alloy to titanium, for a weight saving of 200 pounds. The bearing compartment was redesigned to effect a weight saving of 20 pounds. This was accomplished by a rearrangement of the bearing compartment and an increase in the use of titanium. A weight-function trade study revealed that the incorporation of the front end bearing removal feature cost 5 pounds and individually replaceable fan exit vanes cost another 5 pounds. Revised flange arrangement at the rear ID of the intermediate case was a specific weight control recommendation accomplished at a saving of 5 pounds.

4. High Compressor

Significant weight savings in the high compressor resulted from rerouting of thrust balance air. The original design filled the compressor bore with compressor discharge air, necessitating rim heating during descent to keep disk thermal gradients and consequently disk LCF life at an acceptable level. The present scheme utilizes a compressor

bore tube to guide the much cooler 4th-stage air through the bore, resulting in lower metal temperatures and consequent higher allowable stresses and less severe LCF inducing thermal gradients. The net weight saving due to directly associated design changes is 75 pounds. The net weight penalty for LCF relative to a stress limited design is now 95 pounds with weight reduction efforts still underway to reduce this number further.

Though titanium is used in blades through stage 5, its strength-to-weight ratio did not merit use in disks due to creep limits. Creep properties that would be attractive for compressor disk design have been given to the Materials Development Laboratory to guide future material development efforts. Weight effect was also determined for predicted properties of several other advanced alloys such as U-630 nickel alloy and PWA 1209 titanium alloy, again for the purpose of directing material development efforts. The current integral spacer configuration was selected instead of a comparable separate spacer design with a net weight saving of 35 pounds.

Early consideration was given to the optimum number of high compressor stages. A weight trade study showed a 200-pound weight advantage for the present 6-stage design relative to a 5-stage design at a larger diameter and higher wheel speed. The effect of compressor exit diameter on main and duct combustor weight was included. Other weight studies which have influenced the present design are:

Weight vs blade and vane chord

Weight vs rotor-stator spacing

Weight vs exit diameter

Weight vs exit Mach number

Weight vs disk bore diameter

Weight comparison between various methods for mounting compressor stator vanes.

5. Diffuser and Primary Combustor

The basic design concept of the ram-induction burner has the inherent weight advantages of:

1. Less engine length due to reduced diffusion required
2. Low pressure loading due to low static pressure air entry
3. Effective convection cooling due to high velocity air.

The weight effective design seeks to exploit these features to their maximum potential by close attention to detail design. The inherent length saving and its effect on critical speed was further exploited in reduced shaft weight. A sheet metal combustor inlet air fairing design replaced an earlier forged design at a weight saving of 40 pounds. Similarly, fuel nozzle supports were revised with considerable thinning to save 10 pounds. Comparison of several segmented transition duct designs saved 30 pounds relative to the previous nonsegmented convectively cooled design. This reduction was due primarily to design finesse as was a 20-pound reduction in the No. 3 bearing compartment.

6. Turbine

Weight-affecting variables which have figured in turbine design include material choice, damping method and blade chord and solidity. Earlier design phases considered the weight effect of number of stages and diameter.

A disk material comparison showed Astroloy 20 pounds lighter than Waspaloy. Tip shroud damping on stage 2 blades was chosen because of its 10-pound weight advantage relative to an extended root design. Chord and solidity optimization utilized weight trends which included the effects on disk weight and engine length. Multiple faired blade design was incorporated on the basis of a 35-pound weight advantage relative to the previous 2-section fairing. Vane pairing, which eliminates the need for mechanical foot retention was incorporated on the basis of a 60-pound weight reduction. Brazed foot turbine exhaust vanes resulted from a weight study showing a 10-pound weight saving.

7. Duct Heater Section

Weight optimized material selection has resulted in titanium duct diffuser and duct heater support struts and case. Use of titanium in the rear mount ring was eliminated because of secondary air space limitations. Titanium in cases aft of the mount ring would theoretically save weight on a strength-to-weight basis but a trade study revealed that the requirement for extra flanges more than counteracted this strength-to-weight advantage.

Major weight reductions in the duct heater section have been the removal of rear combustor segments at -65 pounds and redesign of fuel nozzle supports at -75 pounds. Noise suppression liners have been incorporated at minimum weight penalty (15 pounds) by integrating them as structural members.

The catenary segment liner design with membrane loading saves 30 pounds relative to the alternative cylindrical design with its buckling limit criteria.

8. Exhaust Section

A net weight reduction of 725 pounds was the purpose for replacing the sliding shroud, blow-in-door, ejector-reverser with the present clamshell design. A further weight reduction has resulted from the more extensive use of titanium in stings and outer cases. The present design has also realized a substantial weight advantage by utilizing the reverser clamshell as the inner nozzle throat contour, thereby eliminating the need for additional structure and variable mechanism.

E. WEIGHT REDUCTION

It is recognized that an active weight reduction program will be required to keep pace with the usual development increases and ensure a certification engine that meets or betters specification requirements. The extensive weight reduction program now underway will be extended through Phase III. Many previously generated ideas, not included in the current design, await test verification. Others are being generated by studies currently in work. The weight control system which is supporting this effort is described in detail in Volume IV, Report F, Section VII, along with a summary of specific Phase III tasks.

SECTION V
THRUST INDICATING SYSTEM

A. REQUIREMENTS

There are two requirements for developing a thrust indicating system. After takeoff brake release, the flight crew must have verification that engine thrust exceeds the takeoff safety requirements. This thrust measurement must be available within seconds after the engines have accelerated.

During the remainder of the mission, after takeoff, thrust indication is needed as a measure of engine health and of inter-engine thrust differences. The system must be highly reliable, and well adapted to flight crew operating procedures.

The following characteristics describe the mission requirements for the system:

1. Takeoff - Takeoff thrust consistent with aircraft gross weight and ambient conditions should be set within ± 2% (± 3 standard deviations).

2. Initial Climb - During noise abatement following takeoff, thrust must be set at an initial level which will then be adjusted to give the desired climb rate.

3. Climb and Acceleration - Climb power and inter-engine thrust levels should be set within ± 2%.

4. Supersonic Cruise - At start of cruise, thrust must be set at an initial desired level and then adjusted to maintain cruise Mach number and/or altitude. Inter-engine thrust must be balanced for best performance.

5. Flight Idle - Accurate thrust setting is not required.

6. Subsonic Cruise - During subsonic cruise required thrust and inter-engine balance should be set to ± 2%.

7. Approach - An initial value of thrust will be set and then adjusted to maintain a desired sink rate.

Since the Supersonic Transport will incorporate an independently controlled inlet ahead of the engine, the output of the propulsion system will depend on the combined performance of the inlet and engine. Inlet performance is particularly significant at cruise conditions. However, in order that proper corrective action can be taken to achieve desired thrust levels, the performance of the two must be monitored separately. If the engine were trimmed to a predetermined absolute thrust level when the inlet pressure recovery is low, it would result in either turbine overtemperature or an undesirably high duct heater fuel flow. Engine in-flight performance should, therefore, be referenced to engine inlet pressure and temperature.

B. PHASE II-B SYSTEM

During Phase II-B, the feasibility of using a small, lightweight computer to calculate thrust from measured engine thermodynamic parameters was pursued. Reference PWA-2600, pages 1-23, 24. The precision achieved by this system was marginal at takeoff and acceleration (± 3% and 4% respectively), and unacceptable at cruise (± 12%).

C. PHASE II-C SYSTEMS

The use of engine pressure ratio (EPR) as the basic power-setting parameter has proven highly successful on both turbojet and turbofan engines with fixed gas generator nozzle discharge areas. In the case of the P&WA duct heating turbofan, EPR serves exactly the same function for the gas generator, but an additional function is required for monitoring the fan duct thrust. The following parameters were investigated for the additional function:

1. Duct nozzle area and total pressure
2. Duct fuel flow
3. Total fuel flow

Figure 1 shows the variation in net thrust with EPR for these three additional parameters.

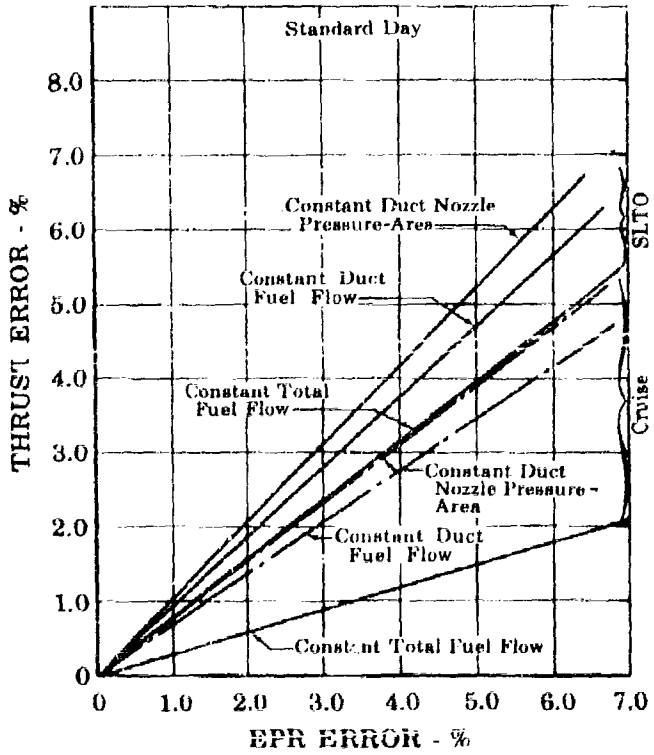

Figure 1. Variation in Net Thrust With Variations in EPR at a Constant Total Fuel Flow, Duct Fuel Flow or Duct Nozzle Pressure Area

FD 17722 AV

1. Duct Nozzle Area and Total Pressure

The most direct approach is to use a combination of duct nozzle total pressure and area; however, because of the high temperature that exists in the duct heater, it is not feasible to measure nozzle total pressure. Although a special water-cooled traverse probe has proven to be a successful development tool, its use in an aircraft installation is not practical. Duct nozzle total pressure can be determined indirectly by two means: (1) the total pressure in the duct at the fan discharge can be measured and a correction factor applied to account for the pressure losses that occur (this pressure loss correction can be determined as a function of duct jet area to account for variations in duct Mach number and heat addition losses giving an error of ± 2%); and (2) the static pressure in the duct upstream of the nozzle can be measured. Because the duct nozzle operates choked, this static pressure and the ratio of areas can be utilized to determine the duct total pressure upstream of the nozzle. This pressure can be corrected for losses giving an error of ± 2%.

Under operational conditions, duct nozzle area measurement to 2 to 3% is the best that can be anticipated. The error in determining the product of the duct nozzle total pressure and area is the root-sum-square of these errors, or ± 3.6%. Figure 2 shows the variation in thrust with variations in this product while holding EPR at the scheduled value.

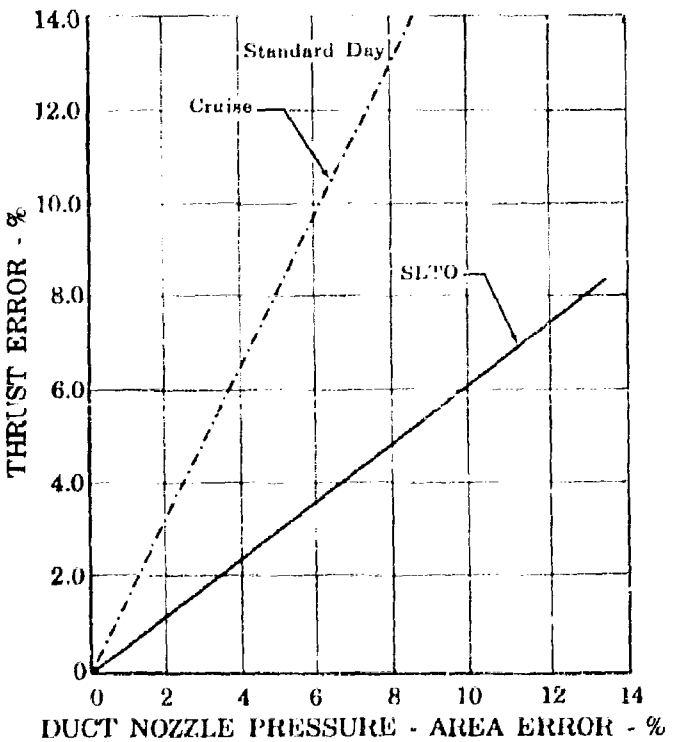

Figure 2. Variation in Net Thrust With Variations in Duct Nozzle Pressure Area - EPR Constant

FD 1/723 AV

2. Fuel Flow

Fuel flow can be measured more precisely than duct nozzle area and total pressure. In current jet transports it is sometimes used to set and balance engine power during cruise. Figure 3 shows the variation in net thrust with variations in duct fuel flow while holding EPR at the desired value.

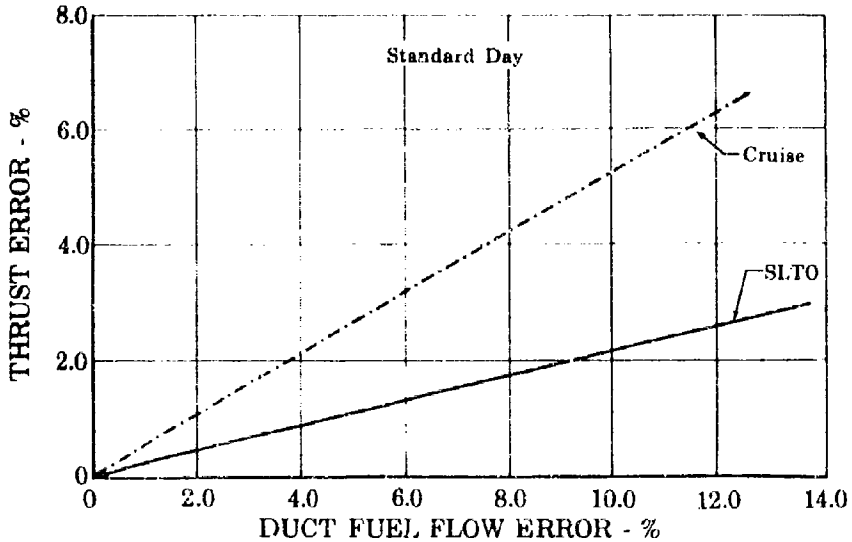

Figure 3. Variation in Net Thrust With Variations in Duct Fuel Flow - EPR Constant FD 17724 EV

Figure 4 shows the variations in net thrust with variations in total fuel flow while holding EPR at the desired value.

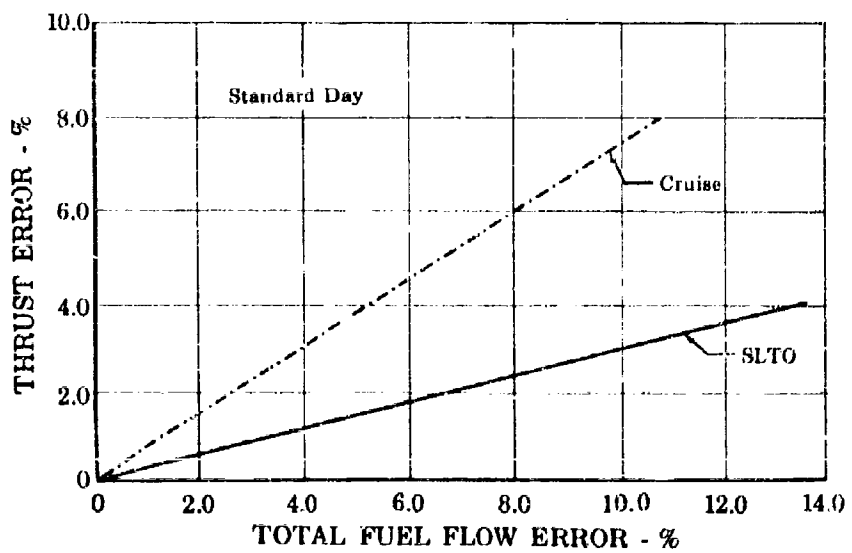

Figure 4. Variation in Net Thrust With Variain Total Fuel Flow - EPR Constant FD 17725 AV

Table I presents a comparison of thrust setting error estimates for the three different systems involving EPR. Based on these total error estimates, total fuel flow is the best additional parameter for EPR thrust setting systems on the JTF17. Total fuel flow is more advantageous than duct fuel flow because holding it at a given value largely compensates for small changes in thrust caused by slight variations in EPR and inlet total pressure.

To evaluate the resulting thrust setting errors, a comparison was made between the JTF17 and the JT8D engines. Figure 5 compares the variation in thrust with EPR for these two engine models at cruise and sea level takeoff. The JTF17 engine is much less sensitive to EPR changes since both the airflow and total fuel flow remain constant while both vary on the JT8D engine. Using these variations and expected errors in setting EPR and total fuel flow, estimates of the thrust setting errors were made. These estimates, presented in table II, show a slight improvement over current precision. The setting errors in EPR and fuel flow are based on instrument precision received from the airframe manufacturers during discussions with them on this subject. There are instruments under development which may result in better precision, but these have not yet been developed for flight operation.

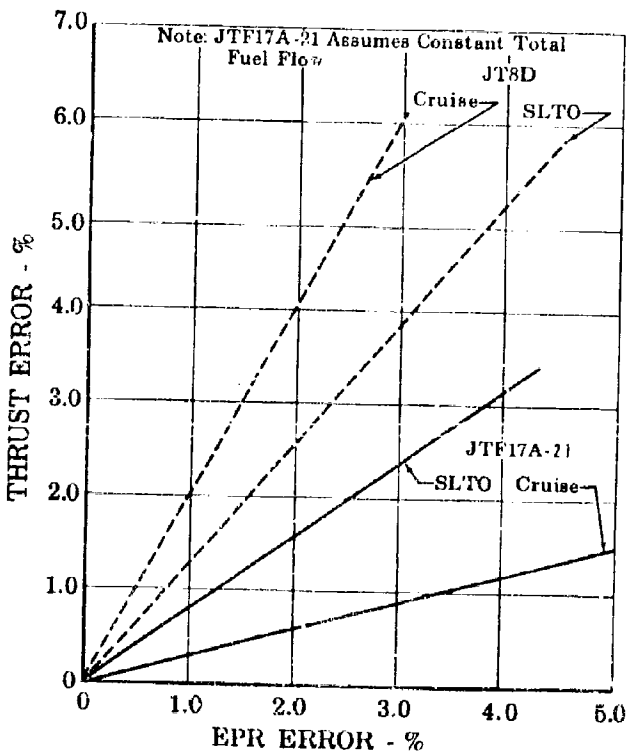

Figure 5. Thrust Errors Resulting From EPR Errors

FD 1//26
AV

Table I. Error Estimates for Three EPR Systems

Function Setting Error Estimate	Thrust Setting Error Estimates - Percent					
	SLTO			Cruise		
	Duct Nozzle Pressure-Area	Duct Fuel Flow	Total Fuel Flow	Duct Nozzle Pressure-Area	Duct Fuel Flow	Total Fuel Flow
± 3.6% Error in Duct Nozzle Pressure Area*	± 2.20	-	-	± 5.90	-	-
± 1.0% Error in Duct Fuel Flow**	-	± 0.25	-	-	± 0.60	-
± 1.0% Error in Total Fuel Flow**	-	-	± 0.30	-	-	± 0.75
± 0.5% EPR**	± 0.53	± 0.45	± 0.40	± 0.38	± 0.33	± 0.15
(± 1.6% EPR)***	(± 1.70)	(± 1.50)	(± 1.25)	(± 1.23)	(± 1.10)	(± 0.48)
Total Error Estimates						
±0.5% EPR	± 2.26	± 0.52	± 0.50	± 5.92	± 0.69	± 0.77
(±1.6% EPR)	(± 2.78)	(± 1.52)	(± 1.29)	(± 6.02)	(± 1.25)	(± 0.89)

* Based on root-sum-square of duct nozzle total pressure (±2.00%) and duct nozzle area (±3.00%) errors
** Based on instrument precision received from airframe manufacturer
*** Based on root-sum-square of turbine discharge total pressure (±1.00%) and compressor inlet total pressure (±1.25%) errors (Phase II-B)

Table II. Thrust Setting Error

Setting Error	Thrust Error - Percent JT8D	JTF17A-21
At SLTO		
0.5% error in setting EPR	0.65	0.4
1% error in setting total fuel flow		0.3
Total thrust error**	0.65	0.50
At Cruise	M = 0.8, 45000 ft	M = 2.7, 65000 ft
0.5% error in setting EPR	1.0	0.48*
1% error in setting total fuel flow		0.75
Total thrust error**	1.0	0.89

* Based on 1.6% error in setting EPR because of the low absolute level of EPR at this condition.
**Root-sum-square of the individual errors.

All of these systems require a set of standards that can be used to define the desired engine thrust setting and to indicate any deficiency in the performance of an engine. Exhaust gas temperature (EGT) required to achieve the EPR rating serves as an indication of the health of the gas generator and as a redundant check on EPR. Duct nozzle area performs this function for the duct heater; a degradation of either duct heater efficiency or pressure loss will be reflected in duct nozzle area. A duct nozzle area indication may be obtained from monitoring duct nozzle actuator position and would provide a redundant function for checking total fuel flow. The EGT-EPR and fuel flow-duct area functions would either be in tabular and curve form, as currently used, or if space is available, they could be stored in a computer. If they are computerized, some of the inputs, such as altitude, Mach number, T_{t2} and P_{t2} could be automatic.

3. Cockpit Simulator

To evaluate these thrust setting methods and the required flight crew operating procedure at all flight conditions, an analog simulation of the system has been constructed. This simulator includes a flight crew console, shown in figure 6, and a general purpose analog computer. The analog portion provides an analytical model of the engine operation from full reverse to maximum augmentation over the simulated operating range of the aircraft. Airframe characteristics and inlet performance are also included over the mission envelope from takeoff to landing. Engine pressure ratio, exhaust gas temperature, total fuel flow, duct nozzle area, fan and high compressor rotor speeds, and duct fuel flow are displayed on the console in a form similar to an airframe cockpit. The cockpit also

contains engine power levers and trim switches for engine pressure ratio and bypass door position. At present this console contains the displays for one engine; however, it is now being expanded to accommodate four engines. To orient the flight crew during takeoff and landing simulations, aircraft position is displayed on a model runway at the top of the console. During the aircraft flight, Mach number and altitude are displayed on a conventional X-Y recorder. A time history recorder is also used so that the results of the flight can be analyzed later. Using this analog simulation, the thrust indicating and trimming methods have been evaluated for their steady-state precision and the dynamic interaction between the flight crew and the propulsion system. As an example, this simulation has shown that the dynamic interaction between the duct nozzle area and engine pressure ratio makes it impractical to rapidly set engine thrust using these parameters. There are no adverse interactions between total fuel flow and engine pressure ratio.

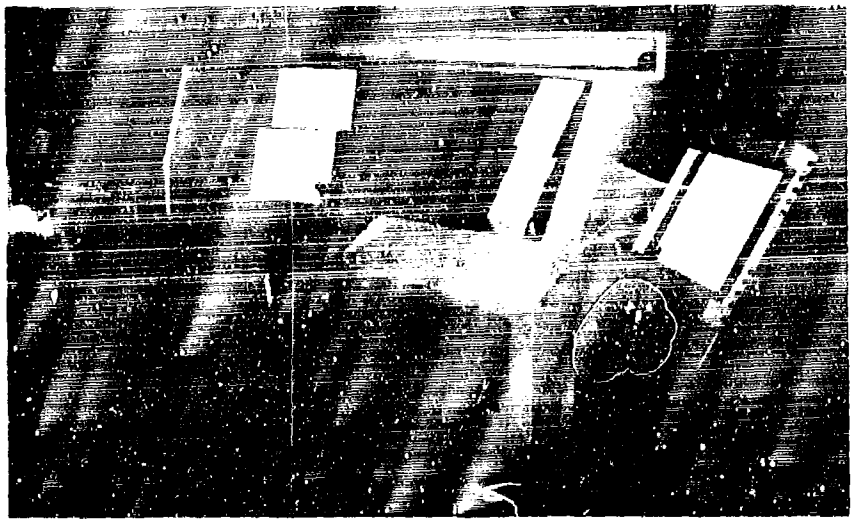

Figure 6. Cockpit Simulator FC 13433
AV

4. Direct Thrust Measurement

All of the methods discussed above are indirect measurements of thrust. Their weakness is that no measured effect of the exhaust system is included. A direct method of measuring thrust would not suffer from this disadvantage.

A system using a load cell designed as an integral part of the engine mount system is feasible and would include the effects of the exhaust system as well as the inlet pressure effects. It would be quite satisfactory for takeoff. However, at supersonic cruise a large percentage of the net thrust is generated by the inlet. Unless the inlet thrust is transmitted to the aircraft through the engine thrust mount, this system could not be used for setting inflight thrust. The problem of attaching the inlet to the engine to meet this requirement is formidable. Whenever the aircraft is being accelerated or decelerated or when the thrust axis is not horizontal, the inertia of the engine mass will lead to erroneous results. An accelerometer aligned to read along the thrust axis would be needed to compensate the load cell reading for non-steady-state, non-horizontal flight.

Based on the assumptions that the load cell system can be made to withstand the temperature cycle (special load cell or externally-cooled conventional load cell) and all the engine thrust is transmitted through a single mount, the estimated SLTO thrust setting accuracy would be in the range of ± 0.5 to ± 1.0%.

During Phase III, this method of providing a positive indication of takeoff thrust will be tested for precision and durability by incorporating load cells into the experimental engine test stand mounting system for comparison with the test stand thrust indication during development and endurance testing.

D. SUMMARY

The EPR plus total fuel flow system satisfies the requirement for a simple and precise method of setting thrust. This method is an extension of the current commercial techniques and, based on results of analog simulations, is well suited to flight crew procedure. Detailed thrust setting procedures are outlined in Volume III, Report B, Section III, Paragraph B. It may be desirable to supplement this method with a direct thrust measurement at takeoff.